



Lou, Chengwei (2022) *Flexible power distribution technique and P2P energy trading in active distribution networks*. PhD thesis.

<https://theses.gla.ac.uk/83008/>

Copyright and moral rights for this work are retained by the author

A copy can be downloaded for personal non-commercial research or study, without prior permission or charge

This work cannot be reproduced or quoted extensively from without first obtaining permission in writing from the author

The content must not be changed in any way or sold commercially in any format or medium without the formal permission of the author

When referring to this work, full bibliographic details including the author, title, awarding institution and date of the thesis must be given

Enlighten: Theses

<https://theses.gla.ac.uk/>
research-enlighten@glasgow.ac.uk



University
of Glasgow

**Flexible Power Distribution Technique and P2P Energy
Trading in Active Distribution Networks**

Chengwei Lou

Submitted in fulfilment of the requirements for the
Degree of Doctor of Philosophy (Ph.D.)

James Watt School of Engineering
College of Science and Engineering
University of Glasgow

February 2022

Copyright © Chengwei Lou

Abstract

With the increasing severity of the greenhouse effect, the depletion of fossil fuels, and the deterioration of human living environment, the development, and continuation of society are facing unprecedented crises. Energy issues are inextricably linked to global economic and social development, as well as the development of an ecological civilisation. The traditional alternating current (AC) power distribution network was a passive system with conventional operation, control, and management, making it difficult to meet the increasing demand for high-reliability electricity supply, active energy management, and flexible and open energy market. To address the three critical issues of ecological sustainability, market openness, and energy security in the energy industry, flexible power distribution techniques and distributed localised energy solutions, such as Soft Open Points (SOPs), AC/DC hybrid electricity network, and peer to peer electricity trading have emerged as new research topics. These emerged technologies are aimed at creating a power distribution network with high intelligence, robustness, and reliability to adapt to access requirements from large-scale distributed energy resources (DERs).

In this thesis, SOPs are used to achieve adaptive service restoration and improve the three-phase imbalance in ADNs. The impact of faults of varying duration on the network with SOPs at distribution levels is investigated, followed by potential solutions of network reconfiguration using SOPs to improve the three-phase imbalance. The potential of SOPs is first explored via a new method of connection, entitled phase power transfer, also known as phase-changing SOP (PC-SOP). Based on the proposed two-terminal PC-SOP, an optimised operational strategy is proposed for unbalanced ADNs based on different types of SOPs (SOP with bifurcation connection and multi-terminal SOP). It is also attempted to employ AC/DC hybrid networks and optimal ESSs dispatch to decrease the three-phase four-wire imbalances while improving the operational efficiency of active distribution networks (ADNs). Finally a new P2P market architecture is designed based on the dynamic power flow tracing technique. The complete potential of the P2P market is investigated where the analogy of a "cocktail-layered" energy market is utilised to illustrate market segmentation.

Acknowledgements

I would like to thank my PhD supervisor, Dr. Jin Yang, for his ongoing assistance with my research. His advice has been invaluable to me throughout this research and thesis writing process. I'd like to thank Dr. Eduardo Vega-Fuentes, Dr. Nand K. Meena, and Dr. Jingli Guo for their assistance with my writing and research skills.

Thank for China Scholarship Council (Reference: CSC201806350260) and the University of Glasgow for supporting my PhD study. Thanks are also due to the Department of Electronics and Electrical Engineering for support in academic visits, in particular Dr. Jin Yang.

In addition, I'd want to thank all of my Aston University and the University of Glasgow colleagues. They provide me a lot of joy throughout my PhD period, and I hope they all do well in the future.

At last, I would like to express my deepest appreciation to my parents for their love and support.

Contents

Abstract	i
Acknowledgements	ii
Contents	iii
List of Tables	vi
List of Figures	viii
Abbreviations and Nomenclature	x
Chapter 1 Introduction	1
1.1 Motivation and Knowledge Gaps	1
1.2 Research Objectives	5
1.3 Organisation of the Thesis	7
Chapter 2 Background and Literature Survey	11
2.1 Development of Active Distribution networks	11
2.1.1 Service restoration in distribution networks	14
2.1.2 Three-phase imbalance in distribution networks	15
2.2 Review of Soft Open Point and AC/DC Hybrid Network	17
2.2.1 Soft open point	17
2.2.2 AC/DC hybrid network	20
2.3 Review of Convex Optimisation of Power Flows in ADNs	23
2.4 Review of P2P Electricity Market Research	26
Chapter 3 Service Restoration Strategy with SOPs	31
3.1 Introduction	31
3.2 Modelling of Service Restoration Distribution Network with SOPs	32
3.2.1 Control mode of SOP and the adaptive service restoration strategy	32
3.2.2 Modelling of service restoration of distribution network with SOP	34
3.3 Second-Order Cone Transforming	38
3.3.1 Second-order cone transforming of objectives	38
3.3.2 Second-order cone transforming of constraints	39
3.4 Methodology: Design of the Experiment	40
3.5 Case Studies	42
3.5.1 Comparison of different scenarios	42

3.5.2	Comparison of different cases	45
3.6	Conclusion	47
Chapter 4	Phase-Changing SOP	49
4.1	Introduction	49
4.2	Unbalanced Three-Phase Optimal Operation Problem Formulation in Three-Phase Four-Wire Distribution Networks	50
4.3	Second-Order Cone Transforming and Algorithm Process	58
4.4	Methodology: Design of the Experiment	60
4.5	Case Studies	61
4.5.1	Active power controlled by the PC-SOP	67
4.5.2	PV curtailment and ESS utilisation	68
4.5.3	Reactive power compensation and voltage profile	70
4.5.4	Algorithm validation	71
4.6	Conclusion	74
Chapter 5	Adapting AC Lines for DC Power Distribution	76
5.1	Introduction	76
5.2	Strategy of Adapting AC Lines for DC Power Distribution	77
5.3	Modelling of AC/DC Hybrid Networks with PVs, VSCs and ESSs	79
5.4	Second-Order Cone Transforming	85
5.5	Methodology: Design of the Experiment	86
5.6	Case Studies	87
5.7	Conclusion	92
Chapter 6	Bifurcation PC-SOP and Multi-terminal PC-SOP	93
6.1	Introduction	93
6.2	Unbalanced Optimal Operation Problem Formulation	95
6.2.1	Principles and Modeling of Different SOPs	96
6.2.2	Optimisation Modeling of Three-phase ADNs with PVs, SOPs and Voltage Regulators	98
6.3	Symmetrical SDP Transforming	102
6.4	Methodology: Design of the Experiment with Bifurcation PC-SOP	104
6.5	Case Study with Bifurcation PC-SOP	106
6.6	Methodology: Design of the Experiment with Multi-terminal PC-SOP	108
6.6.1	Design of the experiment with three-terminal PC-SOP	108
6.6.2	Design of the experiment with four-terminal PC-SOP	109
6.7	Case Studies with Multi-terminal PC-SOP	111
6.7.1	Case Study with three-terminal PC-SOP	111
6.7.2	Case Study with four-terminal PC-SOP	113
6.7.3	Algorithm validation	116
6.8	Conclusion	118
Chapter 7	Power Flow Traceable P2P Electricity Market	120
7.1	Introduction	120
7.2	Dynamic Power Flow Tracing	122

7.2.1	Dynamic Power Flow Tracing Model	122
7.2.2	Loss Allocation Based on Power Flow Tracing	126
7.3	Market Segmentation and Modeling	128
7.3.1	Market Segmentation Principle	129
7.3.2	Market Segmentation Model	131
7.3.3	Individual Market Loss Allocation Model	134
7.3.4	Individual DER Pricing Strategy Model	134
7.3.5	Model Implementation	135
7.4	Methodology: Design of the Experiment	138
7.5	Case Studies	140
7.5.1	Market Segmentation Result	140
7.5.2	Individual Market Sharing Result	142
7.5.3	Market Pricing Results	144
7.5.4	Modeling Details	148
7.6	Conclusion	149
Chapter 8 Conclusions and Future Work		151
8.1	Conclusions	151
8.2	Future Work	154
Appendix A		156
Appendix B		173
Appendix C		181
Bibliography		185
Publications		207

List of Tables

2.1	Comparison of Existing Research on SOPs	18
2.2	Comparison of AC and DC in distribution networks	20
2.3	Comparison of existing designs of three typical types of P2P Market Structure	28
3.1	Control modes of VSC-based SOP	33
3.2	Priorities and controlling types of the loads	41
3.3	Locations and capacities of ESSs	42
3.4	Comparison of power recovery results under different scenarios	43
3.5	DER outputs and loads during the service restoration	43
3.6	Results of service restoration	44
4.1	Comparison of different connection ways of PC-SOP	61
4.2	Spot loads of the IEEE 34-node test feeder	62
4.3	Distributed loads of the IEEE 34-node test feeder	63
4.4	Optimisation results comparison	65
4.5	Computation information of the four cases and performance comparison between the proposed method and IPOPT	72
4.6	Optimisation results of the four scenarios with IEEE 123-node test feeder	72
5.1	Active power and reactive power demand at all buses of the test system (Cells in red represent the highest bus load of one phase; Cells in green represent the highest total load among three phases)	87
5.2	Optimization results of network loss, PV output, average voltage deviation and ESSs	91
6.1	Optimisation results comparison	106
6.2	Optimisation Result Comparison of the IEEE 13-Node Test Feeder Network	112
6.3	Optimisation result comparison of the IEEE 123-Node test feeder	114
6.4	OPF solution time and voltage error on various test feeders	117
6.5	Nodal voltages for the IEEE 13-node test feeder	118
7.1	Transaction Breakdown	127
7.2	24-hour power flow tracing results for the IEEE 33-Node test network	142
7.3	Active power market-entry limitations of DERs	143
7.4	Loss Function Parameters	144
7.5	P2P Price and DER Output Results	145
7.6	Consumers' Cost Reductions and DERs' Income Increases	146
A1	Regulator data of the IEEE 13-node test feeder	156

A2	Shunt capacitors of the IEEE 13-node test feeder	157
A3	Line segment data of the IEEE 13-node test feeder	157
A4	Overhead line configurations (Config.) of the IEEE 13-node test feeder	157
A5	Distributed loads of the IEEE 13-node test feeder	157
A6	Spot loads of the IEEE 13-node test feeder	158
A7	Transformer data of the IEEE 13-node test feeder	158
A8	Underground cable configurations (Config.) of the IEEE 13-node test feeder	158
A9	Regulator data of the IEEE 34-node test feeder	161
A10	Shunt capacitors of the IEEE 34-node test feeder	161
A11	Transformer data of the IEEE 34-node test feeder	161
A12	Line segment data of the IEEE 34-node test feeder	162
A13	Overhead line configurations (Config.) of the IEEE 34-node test feeder	162
A14	Spot loads of the IEEE 34-node test feeder	162
A15	Distributed loads of the IEEE 34-node test feeder	163
A16	Regulator data of the IEEE 123-node test feeder	165
A17	Line segment data of the the IEEE 123-node test feeder	166
A18	Spot loads of the IEEE 123-node test feeder	167
A19	Overhead line configurations (Config.) of the IEEE 123-node test feeder	168
A20	Transformer data of the IEEE 123-node test feeder	168
A21	Underground line configuration (Config.) of the IEEE 123-node test feeder	168
A22	Three phase switches of the IEEE 123-node test feeder	168
A23	IEEE 33-node test feeder	172
B1	SOP and PC-SOP active power outcome (kW)	173
B2	ESS active power outcome (kW)	174
B3	The maximum and minimum voltage of three phases of Case 1 (kV)	175
B4	The maximum and minimum voltage of three phases of Case 2 (kV)	176
B5	The maximum and minimum voltage of three phases of Case 3 (kV)	177
B6	The maximum and minimum voltage of three phases of Case 4 (kV)	178
B7	Three-terminal PC-SOP active power outcome (kW)	179
B8	Four-terminal PC-SOP active power outcome (kW)	180
C1	24-hour power flow tracing results of load proportion	181

List of Figures

1.1	Development process of new SOP technologies in power systems applications.	2
2.1	Geographical information of Angle-DC between Isle of Anglesey and North Wales [84]	22
2.2	A hierarchy of convex optimisation problems and convexity of OPF problems	24
3.1	Back-to-back VSC-based SOP	33
3.2	Flow chart of the proposed adaptive recovery strategy	34
3.3	Schematic of the control mode of SOP under fault condition	36
3.4	A modified IEEE 33-node test feeder with DERs and SOPs	41
3.5	Load and DER output levels of the 4 typical scenarios	44
3.6	Active power balance during service restoration	45
3.7	Reactive power balance during service restoration	46
3.8	Optimal energy dispatch during service restoration	47
4.1	The new ways of connection of the SOP (PC-SOP)	50
4.2	Flow chart of the applied solving process with the proposed model and algorithms	59
4.3	(a) The topology of the modified IEEE 33-node test feeder; (b) Residential Area and Commercial Area profiles; (c) Individual PV generation profile	60
4.4	The concept of using SVCs to replace the SOP with the same capacity	62
4.5	(a) PC-SOP active power outcome; (b) SOP active power outcome; (c)PC-SOP average active power outcome; (d) SOP average active power outcome	64
4.6	Actual PV outputs.	65
4.7	ESS output profiles	66
4.8	The maximum and minimum voltage of three phases - (a) Case 1; (b) Case 2; (c) Case 3; (d) Case 4	66
4.9	Reactive power outcomes - (a) PC-SOP reactive power of Case 1; (b) SOP reactive power of Case 2; (c) SVC reactive power of Case 3	69
4.10	Comparison of active power outputs of SOP and PC-SOP	73
5.1	The process of adapting AC lines to DC power distribution	77
5.2	AC and DC systems linked by two VSCs	79
5.3	(a) The map of the area of the modified system; (b) The topology of the test system ;(c) Single-phase load profiles; (d) Individual PV generation profile	88
5.4	The maximum and minimum voltages of three phases of the original network for 24 hours	89
5.5	The neutral-wire voltage profiles of the original network	89

5.6	The maximum and minimum voltages of three phases for 24 hours after adapting AC lines to DC power distribution	90
5.7	The neutral-wire voltage profiles after adapting AC lines to DC power distribution	90
5.8	(a) Upgrade solution by SOP; (b) Upgrade solution by adapting AC lines to DC power distribution	91
6.1	Illustration and comparison of different SOPs.	95
6.2	Comparison of conventional SOP with PC-SOP and normal connection with bifurcation connection	95
6.3	Test network with IEEE 13-node topology and profiles.	105
6.4	IEEE 13-Node test feeder with three-terminal PC-SOP	108
6.5	Test network with IEEE 123-node topology.	110
6.6	Actual PV outputs.	112
6.7	SOP power flows outcome (kVA).	115
7.1	Benchmark circuit for demonstrating the DN-PFT energy transaction model.	122
7.2	Proposed dynamic power flow tracing algorithms based on DFS.	123
7.3	Market segmentation based on dynamic power flow tracing.	130
7.4	Flow chart of the implementation process with the proposed P2P market model, functions and algorithms.	135
7.5	IEEE 33-node test feeder and PV, wind generation and load profiles.	139
7.6	Loss functions of DERs in different markets.	141
7.7	Pricing strategy and total income functions of DER 1 and DER 2.	143
7.8	Graph matrix of 24-hour market.	148
8.1	IEEE 13-node test feeder impedance	159
8.2	IEEE 34-node test feeder impedance	164
8.3	IEEE 123-node test feeder impedance	169

Abbreviations and Nomenclature

AC	Alternating Current
ADN	Active Distribution Network
B2B	Back-to-Back
CIGRE	International Council on Large Electric Systems
CP	Cone Programming
DC	Direct Current
DER	Distribution Energy Resource
DLC	Direct Load Control
ESS	Energy Storage System
FiT	Feed-in Tariff
HV	High Voltage
ICT	Information and Communication Technology
LBC	Loop Balance Controller
LP	Linear Programming
MINLP	Mixed-Integer Non-Linear Cone Programming
MISOCP	Mixed-Integer Second-Order Cone Programming
MMC	Modular Multilevel Converter
MV	Medium Voltage
MVdc-link	MV direct current (dc) link
OPF	Optimal Power Flow
P2P	Peer-to-Peer
PC-SOP	Phase-changing Soft Open Point
PV	Photovoltaics
QP	Quadratic Programming
SDP	Semidefinite Programming
SMOP	Soft Multi-state Open Point

SOCP	Second-Order Cone Programming
SOP	Soft Open Point
SSSC	Static Synchronous Series Compensator
UPFC	Unified Power Flow Controller
VSC	Voltage Source Converter

Parameters

$Price^{Grid}$	Electricity price from the substation
\overline{VUF}_m	Maximum allowable voltage unbalance factor at bus m
\underline{V}_i	Minimum allowable steady-state voltage magnitude at node i
E_i^{ESS}	Energy storage capacity at node i
$[M]$	$l \times n$ connection matrix
$[Y]$	$n \times n$ nodal admittance matrix
γ^{VSC}	Loss index of voltage-source converters (VSCs)
\overline{I}_{ij}	Current limit of branch connecting nodes i and j
\overline{V}_i	Maximum allowable steady-state voltage magnitude at node i
\overline{v}_i	Upper limit for second-order decision variable of voltage at node i
\underline{v}_i	Lower limit for second-order decision variable of voltage at node i
B_{ij}	Branch conductance
G_{ij}	Branch susceptance
$P_{i,t}^{load}$	Active power of load at node i at time t
P_i^{load}	Active power of load at node i
$P_{i,t}^{DER,max}$	Maximum active powers of DER at node i at time t
$P_{i,t}^{DER,min}$	Minimum reactive powers of DER at node i at time t
$P_i^{DER,max}$	Maximum active powers of DER at node i
$Q_{i,t}^{load}$	Reactive power of load at node i at time t
Q_i^{load}	Reactive power of load at node i
$Q_{i,t}^{DER,max}$	Maximum reactive powers of DER at node i at time t
$Q_{i,t}^{DER,min}$	Minimum reactive powers of DER at node i at time t
R	$l \times 1$ vector containing all branch resistances
R_{DC}	$l_{DC} \times 1$ vector containing all branch resistances of DC system
R_{ij}	Branch resistance from node i to node j
S^{VSCx}	Capacity of VSCx
SOC_{max}	Maximum state of charge

SOC_{min}	Minimum state of charge
V_n^φ	Nominal network voltage at phase φ
$V_{n,i}$	Nominal voltage at node i
$V_{nominal,DC}$	$n \times 1$ vector containing DC nominal voltages at each node
$V_{nominal}$	$n \times 1$ vector containing nominal voltages at each node
X_{ij}	Branch reactance from node i to node j
Y_i	Nodal admittance at node i
y_i	Nodal shunt capacitance of node i
Y_{ij}	Element of the admittance matrix from node i to node j
Y_i^{DER}	Element of the admittance matrix from node i to DER
z_{ij}	Branch resistance from node i to node j

Variables

$P_i^{DER-load_a}$	Active power from DER at node i to $load_a$
$P_i^{Grid-load_a}$	Active power from substation at node i to $load_a$
$\eta_i^{DER,share}$	Market share of DER at node i
$Price^{DER}$	Electricity price from the DER
I_i	Current injected in node i
$I_i^{DER_g}$	Current injected in node i from DER at node g
$I_i^{load_y}$	Current injected in node i from load at node y
$P_{loss_{ij}}^{DER_g}$	Active power loss consumption of line ij of DER at node g
$P_{loss}^{DER_g}$	Active power loss consumption of DER at node g
$P_i^{DER_{noloss}}$	Active power output from DER at node i except for its accounts for the losses.
P_{lk}^{loss}	Losses in line lk
$P_i^{DER,cp}$	Critical points of DER outputs
α_{ij}	Boolean variable, referring to the switch status between node i and node j
β_{ij}	Auxiliary Boolean variable
$\eta_i^{DER,share}$	Market share of DER at node i
$\gamma_{ij}^{DER_g}$	Proportions of power of line ij provided by DER at node g
$\gamma_{load_j}^{DER_g}$	Proportions of power provided by DER at node g to load j
$\gamma_{loss_{lk}}^{DER_g}$	Proportions of power loss of line lk provided by DER at node g
$\gamma_{ij}^{load_y}$	Proportions of power of line ij of load at node y

γ_{lk}^{load}	Proportions of power of line lk provided by load at node y
$\vec{V}_{t,DC}$	$n_{DC} \times 1$ vector containing DC voltages at each node at time t
\vec{V}_t	$n \times 1$ vector containing DC voltages at each node at time t
$d_{i,t}^+$	Positive penalty variable at node i at time t
$d_{i,t}^-$	Negative penalty variable at node i at time t
$E_{i,t}$	Energy storage present state at node i
$I_{branch,imag,t}$	Imaginary part of $I_{branch,t}$
$I_{branch,real,t}$	Real part of $I_{branch,t}$
$I_{branch,t}$	$l \times 1$ vector containing all branch currents at time t
$I_{ij,t}$	Branch current vector from node i to node j at time t
I_{ij}	Branch current vector from node i to node j
$I_{inj,t}$	$n \times 1$ vector containing all currents drawn or injected into the network at time t
$I_{inj,t}^{DER,SOP or ESS}$	Current contribution from DER, SOP, or ESS
$I_{inj,t}^{load}$	Current drawn by load at time t
$l_{branch,DC}$	Second-order decision variable vector of DC current
$l_{ij,t}$	Second-order decision variable of current from node i to node j at time t
$P_{i,t}^{DER}$	Active power of DER at node i at time t
P_i^{DER}	Active power of DER at node i
$P_{i,t}^{DER,SOP or ESS}$	Active powers of DER, SOP, or ESS at node i at time t
$P_{i,t}^{ESS,c}$	Energy storage charging power limit at node i at time t
$P_{i,t}^{ESS,d}$	Energy storage discharging power limit at node i at time t
$P_{i,t}^{ESS}$	Energy storage charging power or discharging power at node i at time t
P_{ij}	Branch active power vector from node i to node j
P_i	Active power injection at node i
P_k	Active power of lost loads at node k
$P_t^{VSCx,\varphi,loss}$	Active power loss of VSCx at phase φ at time t
$P_t^{VSCx,\varphi}$	Active power of VSCx at phase φ at time t
$Q_{i,t}^{DER}$	Reactive power of DER at node i at time t
Q_i^{DER}	Reactive power of DER at node i
$Q_{i,t}^{DER,SOP or ESS}$	Reactive powers of DER, SOP, or ESS at node i at time t
Q_{ij}	Branch reactive power vector from node i to node j
Q_i	Reactive power injection at node i

$Q_t^{VSCx,\varphi}$	Reactive power of VSCx at phase φ at time t
s_i	Nodal injection at node i , i.e. either loads or the net injection of a distributed energy resource
$S_{ij,t}$	Second-order decision variable of power from node i to node j at time t
$V_{m,t}^\varphi$	phase φ voltages at bus m at time t
V_0^{ref}	Nodal voltage vector at the source node
v_0^{ref}	Second-order decision variable at the source node
$V_{i,imag,t}$	Imaginary part of $V_{i,t}$
$V_{i,real,t}$	Real part of $V_{i,t}$
$V_{i,t}$	Nodal voltage vector at node i at time t
$v_{i,t}$	Second-order decision variable of voltage at node i at time t
V_i	Nodal voltage vector at node i
v_i	Second-order decision variable of voltage at node i
$VUF_{m,t}$	Voltage unbalance factor at bus m at time t

Indices and sets

*	Conjugate transpose
α	Phasor rotation operator, $1\angle 120^\circ$
α_k	Important degree of node k
ϕ_i	Set of the head nodes from the system whose terminal node is i
ψ_i	Set of the terminal nodes from the system whose head node is i
Ω_b	Set of all network branches
Ω_d	Set of all disconnected DERs
Ω_l	Set of all network power out nodes
Ω_n	Set of all network nodes
Ω_{bDC}	Set of all DC network branches
Ω_{nf}	Set of all network head nodes
Ω_{nDC}	Set of all DC network nodes
φ	Phase A, B or C (a, b, or c)
H	Hermitian transpose
L	Set of power loss load
l	Number of branches
M	Penalty index
m	Number of buses, each bus have phase A, B, C and neutral nodes
N	Collection of neutral nodes

n	Number of all nodes
n_{DC}	Number of all DC nodes
T	Set of time
VSC_x	VSC1, VSC2 (VSC3, VSC4 for multi-terminal SOP)
012	Symmetrical components
abc	Phase components

Chapter 1

Introduction

1.1 Motivation and Knowledge Gaps

Traditionally, the electric system has been highly centralized, with enormous power plants connected by transmission networks, which feed power to loads via distribution networks. Power electronics technology and demand for distributed energy resources (DERs), such as wind and sun, because of environmental concerns have resulted in the installation of a great number of power electronics-based DERs in distribution networks over the last few years. It is this transition from passive distribution networks to active distribution networks (ADNs).

As an example of power electronic devices, soft open points (SOPs) are important parts of ADNs to provide ADNs with additional controllability and flexibility. With these relatively new devices, ADNs can achieve flexible closed-loop operations (e.g. DC-link inside SOPs). There are two characteristics when ADNs are under flexible closed-loop operations: (i) VSC based devices, like SOPs, can supply reactive power independently which is an opened-loop and transfer active power which is a closed-loop.; (ii) power electronic devices, like SOPs,

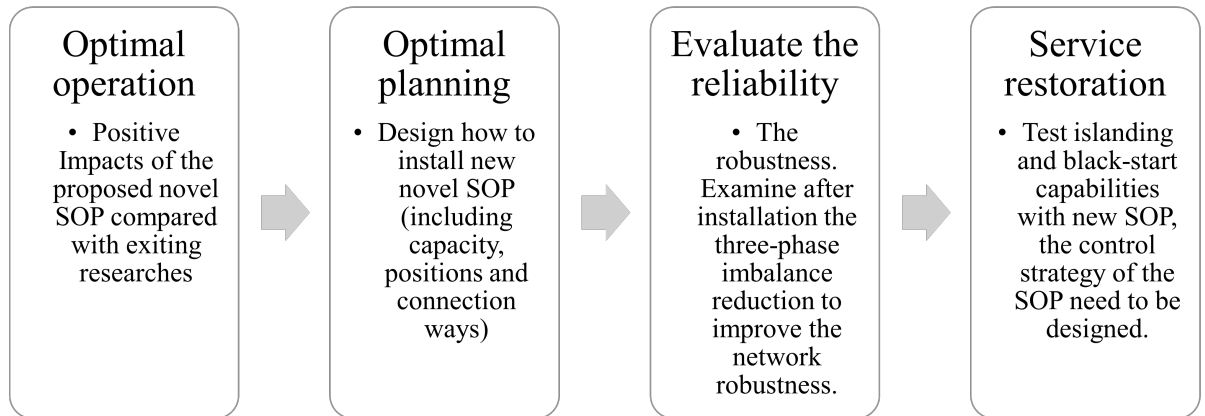


Figure 1.1: Development process of new SOP technologies in power systems applications.

have the capability to adjust power flows of multiple branches for multi-direction. Therefore, power flows within the whole distribution system are influenced by the installed power electronic devices. The meshed operation can improve network reliability and stability, for example, SOPs provide an external link to replace traditional switches. For network robustness, short-time blackouts can be avoided or reduced because loads are supplied from multi-terminal connections linked by power electronic devices when overhauls on assets or faults in the network happen. For network intelligence, flexibility of power electronic devices can improve the adaptability of the network which is influenced by DERs' output fluctuation. Therefore, from network operators' point of view, power electronic devices can increase the network adjustment ability to face the challenges of high DER penetration.

New technologies or devices for ADNs would normally experience in four development stages before installation and commission, as shown in Figure 1.1.

- Optimal operation: to prove new devices, SOPs and AC/DC hybrid network (or technologies, Peer to Peer Trading) can improve system performance.

- Optimal planning: to find a balanced solution between technical performance and economic costs, SOPs installation investment or customer and prosumer benefits during P2P trading.
- Evaluate the reliability: The security is the most important issue of power systems. Both the reliability of the new devices and the reliability of the system including new devices should be evaluated such as SOP fault rates.
- Service restoration: to assess how new devices contributes to the resilience of power systems. After installing SOPs, networks are provided extra reactive power sources and active power links. Therefore, service restoration strategies should be redesigned.

These four steps of the process are highly related to two basic power system calculations: power flows and stability calculation. However, with the development of power electronic technology and deeper understanding of customer demand, power system analysis (including the above calculations) and further optimisation require new techniques hence novel application potentials. SOPs are the new type of power electronic device to replace traditional tie switches in distribution networks. SOPs can control active power transmission and reactive power supply. Therefore, it provides a possible solution for the above two issues in distribution networks by installing individual SOPs. Further to that, by adapting AC lines for DC power distribution, the DC section of a network can be regarded as a regional "SOP" which can achieve SOP functionality for the rest AC network. The transactions of retail energy between several independent parties are referred to as peer-to-peer (P2P) energy trading. In most cases, extra energy generated by local solar panels or wind generators was transmitted to upstream grid with fixed feed-in-tariffs (FiTs). P2P energy trading gives customers additional options of choosing who they buy power from and who they sell it to.

This thesis will focus on these three topics for ADNs including SOPs, AC/DC hybrid network

and Peer to Peer Trading. Linked to these, knowledge gaps are investigated: (iii) how to design a P2P electricity marketing architecture with physical network power flow proofs for P2P transactions and network usage quantification.

Knowledge gap i: Transformers and switches that are currently in use are nearing or have exceeded their design life span. Therefore, their replacement must be made. The SOP provides both an alternative to traditional switches as well as a way to defer replacement of assets. How to utilise DERs more effectively to achieve service restoration when faults happen in a network with SOP under high DER penetration is the first knowledge gap.

Knowledge gap ii: There is no doubt that the installation of expensive assets including SOPs and PC-SOPs into a distribution grid, would almost certainly be investigated should be case-by-case in detail rather than on a single-case basis. The purpose of this work is to replace the detailed studies with different network operation situations, different scales of networks and different types of renewable generation. Distribution network planners or operators are directed towards which implementation options are suitable for PC-SOP applications to handle network imbalance due to unbalanced DER installations.

Knowledge gap iii: In existing P2P electricity market studies, non-traceable transactions (those that do not consider the path covered by electricity) cannot be correlated to physical power transfers and therefore do not reflect the utilization of assets in the physical network. It results in two problems: an oversimplified loss allocation process and unjustified aggregation of participants without consideration of their shared interests.

1.2 Research Objectives

This PhD research aims to explore above three topics to integrate distributed renewable energy (e.g. wind and/or solar) into energy systems in both the physical layer and commercial layer.

With SOPs or PC-SOP proposed in this thesis, objective is to keep technologies updated, meet the growing needs of our customers and improve power quality (harmonic distortion, reliability, voltage stability, three-phase imbalance reduction etc.). In this regard, implementation of guidelines and procedures of SOP or PC-SOP installation can serve as an alternative to potentially undesirable alternatives, such as traditional network reinforcement, reconfiguration of networks with traditional switches and participation of power-site developers in generation curtailment schemes. It should be noted that these options are not incompatible with SOP or PC-SOP implementation. In the thesis, it will be demonstrated that these techniques may be used in conjunction to further enhance network performance.

Quantifying the benefits of the proposed PC-SOP is also hoped the studies will help manufacturers design devices that are suitable for a wide variety of industrial practices. In order to quantify the benefits of SOP and PC-SOP, a techno-economic analysis of their performance is conducted in a number of scenarios. There are a number of research objectives that these studies seek to achieve such as: which service restoration strategies are suitable for a particular network fault situation, which topology or connection way can reduce three-phase imbalance, and how many DC loads converted from AC are needed to achieve a certain level of benefit. The authors also examine several different schemes for deploying SOPs, as well as individual SOP deployments, in order to demonstrate how the use of SOP with many other network devices can be accomplished. DNOs with responsibility for large-scale distribution networks have the ability to make better planning and operation decisions when it comes to SOPs and

PC-SOPs.

The design of a peer-to-peer energy trading system based on flow-tracing arrangements in distribution networks need to be explored. In this respect, a novel energy transaction model based on tracing the dynamic flow of power is proposed in order to investigate peer-to-peer bidding between peers during the bidding time period. This energy transaction model enables the bridge between P2P energy trading and network operations. This dynamic power flow analysis can identify the actual power transfers present in the physical network. It can also determine the losses by quantifying the power flows reaching the load nodes from each source. The electricity transaction prices are established using graph-based modelling which measures each transaction's network consumption with allocated losses in order to maximize the benefits of both consumers and DERs. It is believed that multiple markets segmented by power flow can create more opportunities for profits in comparison to the current centralised market with unified incentives, both for DER owners and consumers. FiTs are more lucrative for DER owners; customers also benefit from lower bills. By using second-order cone programming (SOCP), these newly defined critical points can be identified with the minimum absolute value of the specified branch active power. In an analogy based on power flow tracing, market segmentation could be compared to a layered cocktail with a sequentially filled character. As with the inter-layer liquid interfaces in a cocktail, critical points are similar. According to the above P2P market segment model, customers' (minimize their electricity purchase costs) and DERs' (maximize their total income) objectives are mirrored within the real-world power flow outcome.

The implementation of SOP (AC/DC hybrid network seems as a general concept of SOP) and P2P electricity trading are further guided by considerations at an interdisciplinary level, such as electrical vehicles, multi-energy system interconnection options, and demand-response

options. Meanwhile, a revolutionary P2P energy market model is developed that incorporates dynamic power flow tracing over distribution networks in tandem with an optimised market segmentation strategy based on dynamic power flow tracing.

1.3 Organisation of the Thesis

The remaining parts of this thesis are organised as follows:

Chapter 2 - Background and Literature Survey

There are a series of SOP research that have been considered for distribution network planning, optimisation scheduling, operation control, and fault recovery. An overview of the AC/DC hybrid network is provided in this chapter in order to justify studies performed later in the thesis. An analysis of optimal power flow studies is equally crucial to this study, so a description and review of the literature on optimization are also presented in this chapter. In addition, there are several studies to explore P2P electricity trading in lieu of the rest existing market.

Chapter 3 - Adaptive Service Restoration Strategy of Distribution Networks with Distributed Energy Resources and Soft Open Points

This chapter examine the impacts of faults of varying durations on the distribution level of networks with SOP. A suitable optimisation objective (involving least load weight, minimum DER curtailment and minimum network losses) is established. Combining scenarios with control models of SOPs are conducted for different network situations. System lines and other control devices modelling with different features are proposed based on the mixed-integer SOCP. The results indicate that ESSs, SOPs, and network reconfiguration can be combined to

minimise power losses, restore more lost loads to minimise customer interruptions and loss of customer minutes.

Chapter 4 - A New Phase-Changing Soft Open Point and Impacts on Optimising Unbalanced Power Distribution Networks

In this chapter, we extend the model from one-phase to three-phase from the last chapter. This chapter describes a novel way of SOP connection known as phase-changing SOP (PC-SOP). For unbalanced three-phase four-wire distribution networks, an optimised operating approach based on PC-SOPs is presented to minimise operational losses, three-phase imbalance when DER penetration levels rising. The OPF of the system's three-phase active and reactive power is obtained by optimising the operations of the PC-SOP and ESSs, according to the case study results and analyses. The PC-SOP improves the unbalanced state and reduces operating losses as compared to the standard SOP and SVCs in both the IEEE 34-node and 123-node test feeders.

Chapter 5 - Adapting AC Lines for DC Power Distribution to Reduce the Power Imbalance in Three-Phase Four-Wire Systems

As an alternative to reducing three-phase four-wire imbalance, AC/DC hybrid networks with flexible DC links should also be considered. This chapter presents an optimised operating approach for AC/DC hybrid networks and optimal ESSs dispatch in order to decrease three-phase imbalance while improving ADNs' operational efficiency. The SOCP is used to solve the relaxed model of AC/DC hybrid network OPF problem fast and accurately. Case studies on a modified 415V three-phase four-wire system in the UK indicate that using an AC circuit for DC power distribution improves unbalanced loading circumstances and decreases power losses considerably.

Chapter 6 - Bifurcation Phase-Changing Soft Open Point and Multi-terminal Phase-Changing Soft Open Point SDP Modeling for Imbalance Mitigation in Active Distribution Networks

In the case of multi-region or single-phase wire connections, conventional two-terminal SOPs and two-terminal DC networks will not be sufficient. Therefore, bifurcation PC-SOPs as well as multi-terminal PC-SOPs deserve further investigation. This chapter investigates an SOP with a bifurcation connection for connecting single-phase and two-phase wires, and a multi-terminal SOP to replace more than one SOP installed in the system. This research is based on the PC-SOP proposed in Chapter 3. To reduce operational losses in unbalanced three-phase networks with increasing DER penetration, optimal operational strategies are proposed for the above SOPs based on different connection methods. The IEEE 13-node test feeder is used as the test network to implement and validate the models of bifurcation PC-SOP and multi-terminal PC-SOP model. The scalability of the optimum multi-terminal operation in large-scale ADNs under severe unbalanced circumstances is further verified by the IEEE 123-node test feeder.

Chapter 7 - Power Flow Traceable P2P Electricity Market Segmentation and Pricing

In terms of performance, both PC-SOP and AC/DC hybrid networks can be beneficial. In this chapter, research will be conducted on how to increase customer engagement and transfer the benefits of the network to consumers. This chapter builds a new P2P energy market model supported by dynamic power flow tracing in power distribution networks. An improved market segmentation strategy is suggested based on the identification of power transactions. A graph-based modeling is applied to the pricing and maximisation of electricity transactions by measuring the network use of each transaction with assigned losses by both DERs and

consumers. Optimisation findings based on the IEEE 33-node test feeder show profitability potential for individual DER owners as well as customers across multiple power flow tracking segregated markets in comparison to the already centralised market with unified motivation.

Chapter 8 - Conclusions and Future Work

Descriptions of the primary research outcomes and contributions of the thesis are presented, as well as the conclusions and recommendations for future research.

Chapter 2

Background and Literature Survey

The key to power system industrial development is to enhance renewable energy supply stability. There are two main directions related to that: the first is by building long-distance, large-capacity, and low-loss cross-regional transmission networks, especially ultra-high voltage transmission to dispatch renewable energy in large area; the second is by optimal scheduling of distribution networks and customers' demand to utilise available renewable energy locally. Compared with the first, the second has its advantages in short building cycle, low investment, and flexible operations. Therefore, developing distribution networks can improve low-carbon engagement as an addition to the transition of transmission networks [1].

2.1 Development of Active Distribution networks

In traditional distribution networks, power normally flows from up-stream substations to load bus in one direction. The operational principles of this are clearly understood. However, due to increasing penetration levels of distributed energy resources (DERs), e.g., photovoltaic solar cells, distribution systems face additional challenges during operations: (i) power quality is

deteriorated such as voltage fluctuation and power flicker because of intermittency and volatility of DERs' output [2]; (ii) DERs cannot be grid-tied because of overvoltage issues caused by instantaneous high DER outputs [3]; (iii) the dynamic adjustment ability of traditional distribution networks is not enough to adjust DERs on time with network regulation requirements ; (iv) increasing short-circuit capacities [4]. These challenges need joint effort from the network operators, customers as either consumers, generation owners, and prosumers.

These issues are not fully considered in the traditional distribution network. Also, the traditional distribution networks hardly meet demand with thorough consideration of low-carbon economics. Based on that, in the 18th International Conference on Electricity Distribution (CIRED), the concept of active distribution networks (ADNs) was firstly proposed [5]. ADNs can support more DG installations than traditional distribution networks hence improve the utilisation of local renewable energy resources.

Compared with microgrids which mainly focus on customer premises, ADNs are up for the public distribution networks managed by electricity distribution companies. Based on smart distribution network technologies, a new and open distribution network structure is designed for ADNs with functions such as DER management, power factor correction management, automatic on-load tap changer adjustment, network reconfiguration, flexible load (demand management and response, e.g. electric vehicle charging and discharging) [6, 7].

According to the ADNs definition made by International Council on Large Electric Systems (CIGRE) C6.11 working group [8], an ADN is a type of public distribution network with flexible topology using active DER management, energy storage, and bidirectional customer demand management. There are three key aspects of ADNs:

- Different types of DERs (wind, solar, hydro, etc) and energy storage systems are collected

and converted to Alternating Current(AC) or Direct Current(DC) power by power electronic devices and connected to the main grid via power transformers.

- Information and communication technology (ICT) and automation of devices are installed and commissioned in systems in suitable ways.
- Smart meters installed on customers' side to achieve timely data and information collection and bidirectional operational controls between customers and distribution network/system operators.

In ADNs, peer-to-peer (P2P) energy trading between power consumers and producers can be guaranteed by utilising a flexible management architecture, including active management of DERs, energy storage and bidirectional demand management [9]. P2P energy trading enabled by ICT can assure the integration of demand-side flexibility and the optimal operation of DERs and other network resources while preserving power balance, supply quality and security with precision in seconds [10]. A smart metering system capable of ensuring customers are actively participating in ADNs is required for P2P power trading [11]. Smart meters can report energy consumption figures, trends, and other relevant information for P2P energy trading, such as:

- Current electricity consumption demand of customers.
- The number of contracted power units
- Feed-in tariffs and/or prices per kWh for surplus power
- Total power budget available for trading in the shared network
- Cost of using/renting the power distribution infrastructure
- Contract length and smart contract blockchain proof

- Guarantee power supply for the contracted period and the agreed-upon unit prices

In summary, the ADNs development would improve network controllability and have the ability to provide the flexible management architecture that encouraging P2P electricity market trading.

2.1.1 Service restoration in distribution networks

Service restoration influences human society directly, including industrial production and quality of living. Facing potential extreme natural disasters, the grid can improve its network reliability by using DERs to achieve black start power supply quickly rather than simply cut off the blackout area from distribution network protection [12]. Different from traditional distribution networks where the direction of power flows is just from substations to customers' loads, ADNs have further choices of service restoration by utilising DERs and making the network topology flexible. Therefore, service restoration strategies of ADNs become one of the important Research And Development(R&D) topics. [13].

Development of a self-healing power network to allow resilience and fast recovery of power systems in response to disturbances have been envisaged [14] for future power grids. Various concepts and techniques are used for solving the service restoration problem, for instance: knowledge-based, expert systems [15, 16], heuristic techniques [17], fuzzy logic [18, 19], optimal routing algorithm [20], and multi-agent method [21]. A comparative study is proposed to compare modern heuristic algorithms for service restoration in different distribution systems [22]. In [23, 24], the black start power supply of DERs is considered and a genetic algorithm is applied to solve network configuration problems for service restoration. In short, the above algorithms of service restoration take a long time and the solutions of them can

easily trap in local optima. In [25], a mixed-integer second-order cone programming (MISOCP) formulation is proposed for the service restoration of a distribution network with DERs, considering both PQ and PV models of DERs.

As power electronic technology develops, DC power systems have been applied widely around the world, because of their advantages of high performance and quick responses in power control. In reference [26], the authors consider starting from a DC converter station after main network restoration. In reference [27], the authors looked at the service restoration problem of renewable-powered microgrids in islanded operations due to an unscheduled breakdown event from the main grid. In reference [28], the authors presented a hybrid programming (HP) technique to solve the DC microgrid reconfiguration problem for loss reduction and service restoration.

2.1.2 Three-phase imbalance in distribution networks

Three-phase imbalance commonly happens in around 70% of the UK's low voltage (LV) power distribution networks [29,30]. Financial losses are incurred due to wire losses such as losses in neutral wires [31] and additional network reinforcement investment such as equipment failure caused by network unbalanced operations [32]. The conventional causes of imbalance are uneven load phase-allocations and randomness of single-phase load profiles [33–35]. Recently, the integration of various distributed energy resources (DERs) such as distributed generation (DG), plug-in electric vehicles (PEVs) and energy storage systems (ESSs) brings not only new opportunities but also challenges. For example, unbalanced three-phase voltages are observed more frequently because of increasing single-phase DER installations and uncertainties of renewable power generation outputs [36, 37] and charging/discharging of batteries and electric vehicles. However, the unbalanced voltages can also be caused by other occurrences, e.g., (i)

large single-phase distribution transformer; (ii) open phase of capacitor banks; (iii) open phase on the primary of a three-phase transformer; (iv) unequal transformer tap settings; (v) unequal impedances of the main feeders; (vi) unbalanced ground faults in the power transformers, among others.

As a technique, single-phase loads can be moved from one phase to another when a definite maximum or minimum (or both) demand phase(s) can be found. Demand-side management as a technology from the view of managing load has been used for the above phase-balancing purpose [38]. However, the time variances of load and DG make the imbalance changing between phases. Therefore, over a given period of time, e.g. 24 hours, there are no fixed maximum and minimum load phases. Various techniques are proposed from the angle of managing DGs and loads themselves. Reference [39] optimises hierarchical power oscillations control for DG under unbalanced conditions. In [40], inclusion of voltage-dependency in current-injection based three-phase load flow is investigated and the results are compared with constant-power load model in terms of phase-balancing. Reference [41] proposes a new technique based on Bacterial Foraging with Spiral Dynamic (BF-SD) which is applied for simultaneous optimisation of re-phasing, reconfiguration, and DG placement. In [42], smart distribution feeder was balanced by DG sizing and rephasing strategy simultaneously and the problem is investigated in deterministic and stochastic frameworks. While reference [43] introduced an optimal phase-balancing method, discusses the effect of load modelling on phase balancing studies. From an angle of changing the network itself, reference [44] reports an approach that reduces imbalance by distribution network reconfiguration with tie switches. However, the total switching operational time can be 1 to 100 seconds, by using tie switches to reconfigure the distribution networks [45]. To improve the switching performance, new types of switches with power-electronic devices, such as soft open points (SOPs), designed and installed to replace these traditional tie switches with much shorter response time (20 ms) [46], to provide an alternative

novel solution to flexible distribution networks.

2.2 Review of Soft Open Point and AC/DC Hybrid Network

2.2.1 Soft open point

The SOP concept for the first time was proposed by researchers from Electrical Engineering Department, Imperial College London, indicating that it can promote a substantial increase in DG penetration [47]. At that time, it was called as "soft normally-open points". SOP also has other names like "DC-link" [48–50], "MV direct current (dc) link (MVdc-link)" [51], "Soft Multi-state Open Point (SMOP)" [52], "Back-to-back (B2B) system" [53] and "Loop Balance Controller (LBC)" [54]. There are four basic topologies of SOPs: back-to-back voltage-source converters (B2B VSCs), multi-terminal voltage-source converters (multi-terminal VSCs), unified power flow controller (UPFC), and static synchronous series compensator (SSSC). The SOPs based on multi-terminal VSCs tend to offer greater flexibility to the network than the other three topologies of SOPs when considering a uniform deployment across all networks [55]. Different areas of existing research on SOPs are listed and compared in Table 2.1.

Distribution network planning: In [68,69] researchers independently proposed stochastic planning models with new control strategies or conventional assets such as Demand-Side Response, Coordinated Voltage Control, SOPs and the possibility of active power generation curtailment of the DG units. In [62], the authors formulated a mixed-integer non-linear programming (MINLP) model to optimally determine the locations and energy/power capacities of distributed energy storage systems in ADNs with SOPs. For the same purpose, in [61], considering the long-term operation characteristics of distributed generation, an MINLP is formulated based on the typical operational scenarios generated by Wasserstein distance which can

Table 2.1: Comparison of Existing Research on SOPs

Ref.	Model	Phase	SOP type	Other devices	Objectives
[56]	BFM-SDP	Three	Two-terminal SOP	DGs	Minimize total power losses, voltage and current unbalanced conditions
[57, 58]	Heuristic algorithm	Single	Two-terminal SOP	DGs and tie-switches	Minimize the power loss, load balancing and maximize the DG penetration level
[59]	SOCP	Single	Two-terminal SOP, multi-terminal SOP and two-terminal SOP with ESS	DGs	Improve the DG penetration
[60, 61]	MISOCP	Single	Two-terminal SOP	DGs and tie-switches	Minimize the fixed investment cost of SOP, annual operation cost of SOP and annual cost of losses in distribution system
[62]	MISOCP	Single	Two-terminal SOP	ESS, DG inverters and on load tap changers	Determine the locations and energy / power capacities of distributed ESS
[63]	MISOCP	Single	Two-terminal SOP	DGs, on-load tap changer (OLTC) and switchable capacitor banks (CBs)	Minimize power losses, cost of OLTC and voltage deviation
[64]	Enhanced SOCP with tighten relaxation	Single	Multi-terminal SOP	DGs	Mitigate the feeder load imbalance and reduce power losses
[65]	Robust SOCP	Single	Two-terminal SOP	DGs with uncertainty	Address the uncertainties of photovoltaics (PVs)
[66]	Primal-dual interior-point algorithm	Single	Two-terminal SOP	Tie switches	Maximize of active power of restored loads
[67]	Ant colony algorithm and chaos algorithm	Single	Two-terminal SOP	DGs and tie switches	Minimize the total loss of load DGs curtailment and network losses

compare probability distributions.

Optimisation scheduling: In [57, 58, 60], optimisation problems, distribution network reconfiguration (DNR) and optimal SOP outputs, were formulated simultaneously within a multi-objective framework, exploring the maximum DG penetration level that a distribution network can accommodate before violating the network operational constraints. In [56], the authors propose an optimal operation of SOPs in ADNs under three-phase unbalanced conditions. In [64], the authors proposed a flexible way of interconnection based on a multi-terminal SOP which significantly benefits the operation of ADNs by using a second-order cone program-

ming (SOCP)-based method. In [65], a two-stage adjustable robust optimisation model with operational strategies of SOP is built to tackle the uncertainties of photovoltaics (PV) outputs. In [70], the authors proposed an optimal reactive power control method for distribution systems with SOPs and consider the direct load control (DLC) of thermostatically controlled air-conditioning.

Operation control: The SOP based on direct modular multilevel converter (MMC) is capable of bidirectional power flows between two feeders at any power factors, even when the feeders have different nominal voltages and operate with a phase-shift angle or unbalanced voltages [71]. In [63], the authors considered the cooperation of SOPs and multiple voltage regulation devices and proposed a coordinated real-time voltage and VAR control method based on SOPs for ADNs. The method converts the original nonconvex mixed-integer non-linear optimisation model into an MISOCP model. In [46], the authors develop two control modes for the operations of SOP. Under normal operational condition, the SOP can control real power and compensate reactive power. Under fault conditions, the SOP can effectively isolate fault zones. In [72], the authors used a Jacobian matrix-based sensitivity method to define the operational region of an SOP when the grids/feeders have various load and generation conditions. In [73], the authors propose a decentralised voltage control strategy of SOPs in ADNs.

Fault recovery: In [66], the authors used the primal-dual interior-point algorithm to solve the model of the supply restoration based on SOP to improve the self-healing ability of distribution systems. In [67], the authors proposed a service restoration strategy to restore the black-out for loads by coordinating SOPs and DGs. [74], the authors studied the impact of using SOPs on an existing feeder automation scheme under balanced fault conditions. [75], the authors investigated the dynamic performance of a medium voltage (MV) distribution network with

a connected SOP, under grid-side AC faults. The use of sequence networks is extended to include SOPs, such that conventional asymmetrical fault analysis technique can be used on a distribution network with SOPs.

2.2.2 AC/DC hybrid network

Table 2.2: Comparison of AC and DC in distribution networks

	AC distribution	DC distribution
Transmission efficiency and system losses	Under the same nominal voltage single-phase operation, AC lines can transfer more power with fewer losses than DC lines	Under the same nominal voltage multi-phase operation, DC lines can transfer more power (15%) with fewer losses (2/3) than AC lines
Transmission distance	Limited by reactive power, different voltage level AC line has different power supply radius	Without reactive power limitation, DC lines only transfer active power and power supply radius only depends on the voltage level.
Reliability	Compared with DC distribution, line faults easier influence the external system.	Fewer components, simpler system structure and lower fault rate compared with AC distribution.
Economic benefit	AC lines have higher losses, need more cross-sectional building space, and lower efficiency with DERs connection compared with DC lines.	DC lines have lower losses, need less cross-sectional building space, lower erection height and higher efficiency with DERs connection compared with DC lines.
Decomposition and control	Phase angle difference disturbs the stability of the network operation.	Active power and reactive power can be decomposed in operation.

As power electronic devices develop and an increasing number of DC loads in the distribution network, DC has seen more applications than before because of its good power transition ability, low investment, and friendly connections for DERs and energy storage systems. It is anticipated that in future a growth in DC distribution and changes required for AC distribution, because of taking advantages of both their different technical characters shown in the

Table 2.2. In 2010, the authors from Center for Power Electronics Systems (CPES) of The Bradley Department of Electrical and Computer Engineering proposed a four-layer AC DC hybrid network (including HVAC/HVDC transmission, AC distribution, AC/DC nano-grid, and microgrid), where the overall system cost and reliability could improve [76]. In 2011, NSF FREEDM Systems Center, Raleigh, NC proposed a system structure called “The Future Renewable Electric Energy Delivery and Management (FREEDM)” based on plug-and-play of DERs and distributed energy storage devices [77].

There are also design and applications of AC/DC hybrid or DC distribution networks. RWTH Aachen University started a DC MV distribution network research project in 2015 [78]. This DC project has the following sub-topics for research, including offshore wind power collection, DC MV loop system as the city’s backbone network, 10 kV campus distribution network [79]. In January 2016, ScottishPower Energy Networks started a project, ‘Angle-DC’, which creates a controllable bidirectional MVDC link between the Isle of Anglesey and North Wales by converting existing 33kV AC assets to DC [80,81], as shown in Figure 2.1. In 2018, Guizhou electrical power research institute built a demonstration DC ± 10 kV - 4MVA system with a 3-kilometer DC transmission line and conducts no-load experiments, reactive power experiments, active power experiments, and equipment aging tests [82].

However, AC power is still the main form of the distribution system. It is impractical to replace all existing AC distribution networks with DC solutions at one time. DC current, unlike AC, is uni-directional and the comparison between AC and DC for power transmission has been under discussions with research findings on adapting AC lines for DC power distribution. However, still there are research gaps to be filled until the conversion can be practically implemented. AC/DC power conversion technologies and hybrid systems have been widely used in high voltage transmission [83,84], medium voltage distribution networks [80,85,86]

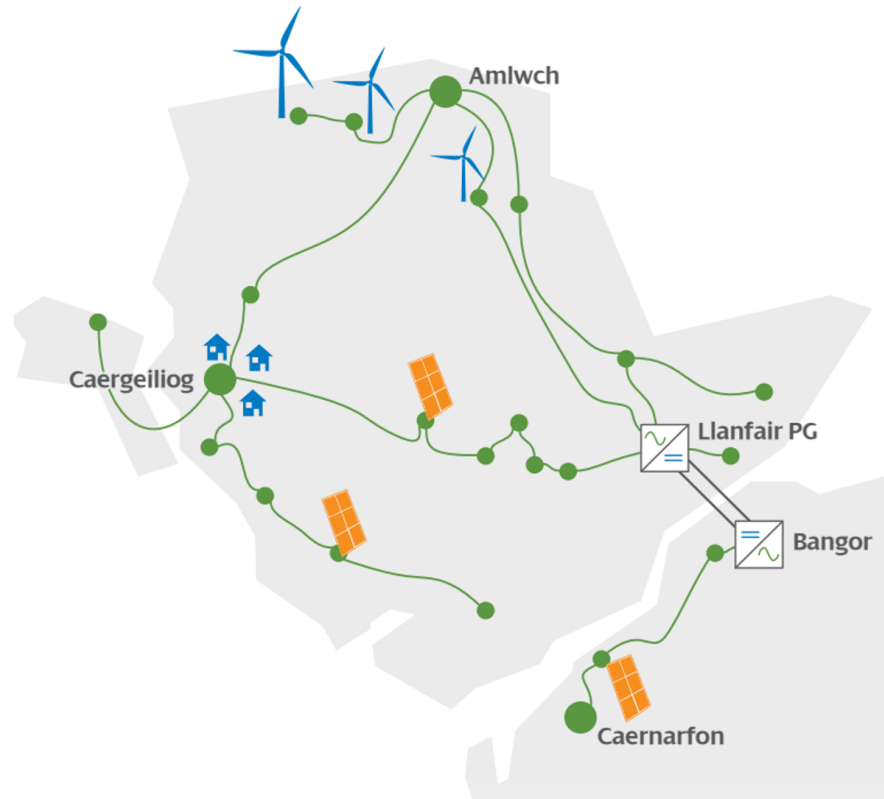


Figure 2.1: Geographical information of Angle-DC between Isle of Anglesey and North Wales [84]

and low voltage microgrids [87, 88]. Especially, various methods to convert existing AC lines for DC have been discussed in reference [89].

Adapting AC lines for DC power distribution to reduce the power imbalance is a direct way especially in three-phase four-wire systems in terms of network configuration. There are three reasons as follows:

- The potential solution of adapting AC lines for DC power distribution is not limited by whether there is a fixed maximum demand phase.
- In some three-phase four-wire LV systems, there are no tie switches available for reconfiguration.

- Compared with SOPs, adapting AC lines for DC power distribution can directly convert unbalanced AC networks into DC networks which have no imbalance problem. SOPs cannot increase the maximum power transfer capacity of each AC line as well.

2.3 Review of Convex Optimisation of Power Flows in ADNs

Convex problems can be classified into a large number of types [90]. The most restrictive one, linear programming problems (LP), can be reduced to quadratic programming (QP), and in turn, a second-order cone programming (SOCP), semidefinite programming (SDP), cone programming (CP), graph form programming (GFP), as shown in Figure 2.2a.

In the view of power system applications, radial networks are specific forms of mesh networks (a virtual wire with zero current). AC single-phase optimal power flow (OPF) problem is a specific form of AC three-phase OPF problem because when currents are balanced in three phases, an AC three-phase OPF problem can be converted into an AC single-phase OPF problem. Direct current optimal power flow (DC OPF) is a specific form of AC single-phase OPF, because compared with AC single-phase OPF, DC OPF does not consider reactive power, as shown in Figure 2.2b.

For ADNs, research of convex optimisation of power flows includes linear DC OPF, single-phase OPF, three-phase OPF, robust control OPF and the exactness of the convex relaxation of OPF.

DC OPF: Although it can instruct economic dispatch, and consider power flows with asset thermal constraints, DC OPF cannot be used for quantifying losses, voltage constraints or reactive power flows [91, 92] in most situations. In addition, DC approximations are more

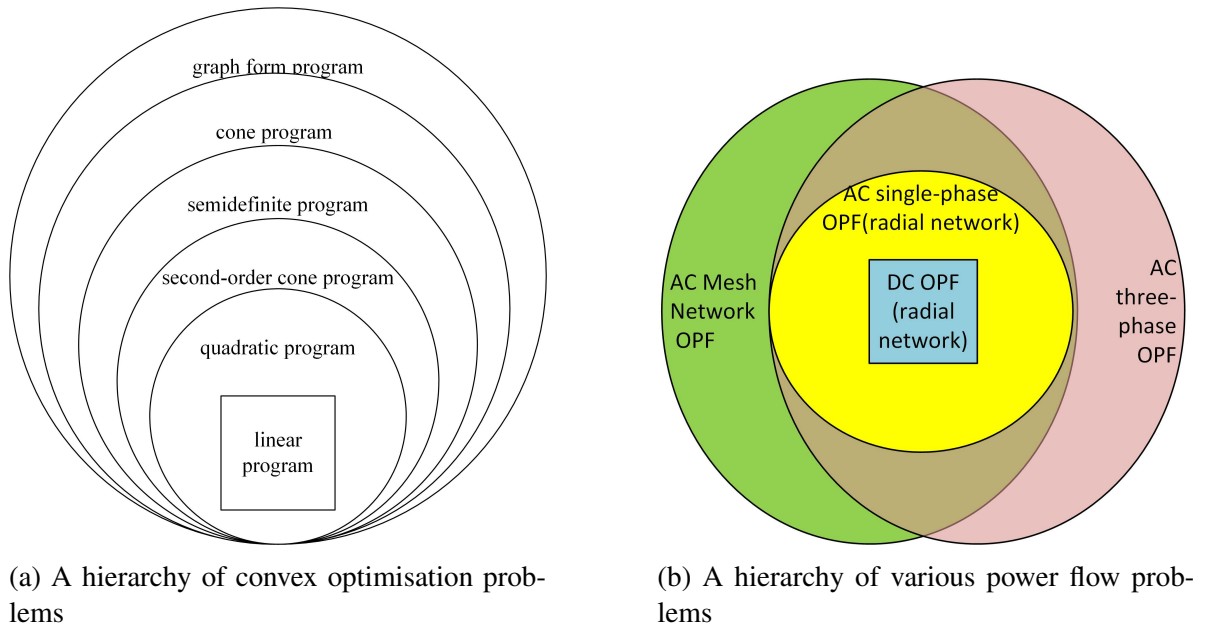


Figure 2.2: A hierarchy of convex optimisation problems and convexity of OPF problems

suitable for the transmission systems than the distribution systems [92]. Progresses have been made in this area: In references [93], the authors explored the current-voltage (I-V) formulation of the power-flow problem and convexified a similar formulation for four-wire unbalanced distribution networks. Piece-wise approximations with integer variables were proposed in references [92, 94–96] by the application of Taylor expansions (or similar) to handle the nonconvexity introduced by the quadratic losses. However, the computational burden is increased due to the increase of data with hundreds and thousands of dimensions. A linearly-constrained and convergence-guaranteed OPF method with reactive power and voltage calculations is proposed in reference [97] but the accuracy of the network model requires further improvement.

Single-phase OPF: In reference [98], the authors formulated the single-phase OPF in the distribution networks as an MISOCP, for which the global optimal solution up to the desired accuracy can be found by using available commercial solvers. The solutions proposed in this reference is proved not singular by the convergence of the Newton-Raphson solving scheme.

Three-phase OPF: The nonconvexity of the single-phase OPF problem is much weaker than that of the three-phase OPF problem [99]. In reference [100], the authors developed a distributed SDP solver for the three-phase OPF problem based on an alternating direction method of multipliers and the Lagrangian relaxation method but with a near-global optimal solution of the relaxed problem. Algorithms proposed in reference [99] guarantee convergence and global optimality when the trace of the regularisation term becomes zero by combining the convex iteration method and the chordal-based conversion technique. In reference [101], the authors presented a convex approximate AC OPF for unbalanced three-phase four-wire distribution networks with energy storage systems, especially when calculating power losses in the neutral wire and for meshed network configuration. References [102, 103] report a three-phase OPF solution which was using the primal-dual interior point method and the three-phase current injection method in rectangular coordinates.

Robust control of OPF and relaxation exactness: Robust control algorithms are designed to deal with various challenges: Load uncertainty – in reference [104], the authors proposed a two-stage robust optimisation model for the distribution network reconfiguration problem with load uncertainty. The model is solved by a column-and-constraint generation algorithm, in which the master problem and sub-problem are transformed into an equivalent MISOCP. Complexity – in reference [105], the authors proposed a quadratic programming model which can deal with the complexity due to the presence of discrete parameters. It showed that the scalability and robustness of the proposed approach are improved or at least for equal quality solutions to the problems. In addition, the exactness of the convex relaxation has been investigated in [106–108].

2.4 Review of P2P Electricity Market Research

Traditionally, distribution network operators (DNOs) set connection charges for exporting and/or importing electricity. Even though now DER owners are allowed for competitive grid connections whilst receiving incentives, their current interactions in the electricity market are only with the grid. In addition, the prices are determined in advance (so-called feed-in tariffs (FiT)) by regulators [109] or suppliers [110]. For example, in the UK, the FiT of wind power is 2.88 p/kWh (pence per kilowatt-hour) when the capacity is between 100 and 1500 kW [111]. Conversely, a standard domestic electricity tariff is 17.493 p/kWh [112]. Recently, replacing FiT, the smart export guarantee (SEG) is launched as an obligation set by the UK government for licensed electricity suppliers to offer a tariff and pay for small-scale low-carbon generations of electricity exported to the National Grid, providing certain criteria are met, which came into force on 1st January 2020 [113]. However, even with the SEG, DER owners can only receive between 2 to 5.6 p/kWh which is decided by suppliers as long as it is not zero. Therefore, under the existing market structure and regulations, market openness and fairness are far from ideal.

To further stimulate DER investments for local energy systems and general market participation, the economic profit margin between standard energy consumption tariff rates and export FiT/SEG should be released. P2P energy trading can directly link consumers with producers for mutual benefits, without intermediators such as aggregators, suppliers [114]. However, P2P trading faces challenges that require radical changes, such as the existing centrally controlled grid, market architecture and regulations of current network connection charge models. Also, the P2P electricity prices should be reflected in an electricity retail market with competition openness.

The following sections summarise existing research and highlight the contributions of this thesis on the P2P electricity market, beyond the state-of-the-art.

From actors' point of view, existing P2P electricity market structures are categorised into three types [115]: 1) community-based markets [116–119], 2) fully decentralised markets [120–122], and 3) 'composite' markets [123–125]. A comparison of these three types of typical P2P market structure in the view of different participants' combinations is listed in Table 2.3 and explained below.

A community-based P2P market is designed for customers and prosumers from microgrids or neighborhoods with common interests and goals that are readily distributed by an aggregator. Authors of [116–119] built up various P2P trading models considering different aspects (e.g. cheating behaviors, blockchain, the uncertainty of PV generation) for different community-based P2P markets. Optimisation algorithms based on alternating direction method of multipliers (ADMM) were proposed for the analysis.

A fully decentralized P2P market is based on the assumption that every participating prosumer can freely trade with others individually without any centralized administration. All transactions between market participants rely on bilateral contracts. In [120–122], every market participant aims to achieve its own optimal objective. A consensus and innovation algorithm was used for linking different participating individuals in the market to find the global optimum based on individual optimum [121, 122].

A 'composite' market can be defined as a combination of community-based and fully decentralized markets. In a market like this, every single prosumer can freely trade with another within a community. After intra-community trading, a community is represented by an aggregator or agent to trade with other communities. In a composite market, prosumers not only

Table 2.3: Comparison of existing designs of three typical types of P2P Market Structure

Paper	Participants	Innovation	Objective
[116]	PV prosumers Energy storage owners	Consider dishonest players	Minimize social cost by energy cooperation
[117, 118]	Energy buildings	Create a building-centric framework / Mismatch of prediction values and actual values	Minimize the cost reduction ratio distribution /Minimize social energy cost; Clear for mutual energy sharing
[119]	Prosumer Microgrid	A penalty mechanism for changing energy sharing profiles	Maximize retailers profit; Minimize prosumer expense
[120]	Individual prosumers	Captures both upstream downstream energy balance and forward market uncertainty	Utility-maximising preferences for real time contracts and forward contracts
[121]	Microgrids with generators, inflexible flexible loads, and storage devices	Achieving global coordination to all the generators	The objective is to determine the settings of the components
[122]	Agents of markets participants	Fully decentralized market with product differentiation	Distributed minimize each agent's expense
[123]	PV prosumers EV	Protect private information by blockchain	Minimize value-at-risk of energy sharing loss
[124]	Community prosumers Aggregator	Introduce community aggregators	Minimize the total social energy cost
[125]	Nanogrid	A hybrid cyber-physical P2P energy sharing framework	Maximize the self-sufficiency; guarantee the stability of ES queues

Paper	Network losses	Algorithm
[116]	Only energy storage's loss	ADMM
[117, 118]	Only energy storage's loss /Power network without congestion and losses	A dynamic best response based algorithm; ADMM
[119]	Transmission losses are neglected in local area	MILP problem
[120]	Losses are not explicitly considered, and need to be accounted for by a separate settlement process	Bilateral contracts
[121]	No description	Consensus + innovations algorithm; ADMM
[122]	Losses are subject to social contracts	Relaxed Consensus + Innovation (RCI)
[123]	The loss of energy distribution is neglected	A relaxation method-based algorithm/Blockchain
[124]	Losses between communities are compensated by the main grid Losses in a community are neglected	A privacy-guaranteed ADMM
[125]	No description	Lyapunov-based algorithm

have fully open-trade options within their community but also are integrated as one actor to have a better bargaining power compared with that of individuals [123]. Prosumers and communities are joining the market in parallel in a composite market [124]. In [125], a small-scale experiment P2P platform with hardware simulation is implemented to prove the potential of applications in the real power systems in future.

However, non-traceable transactions (those who do not consider the paths covered by the electricity) in existing P2P electricity market studies cannot reflect physical power transfers hence asset usage in the physical network. This causes two problems: oversimplified loss allocations and unjustified participants' aggregation without common benefits.

Power flow tracing would also directly address issues including quantifying network constraints and loss allocation in power distribution network. Conventional loss allocation requires separate algorithm, e.g. current-based method [126] where additional decomposition step is required [127].

Specifically, loss allocations in existing studies are either fixedly apportioned to all prosumers with a given percentage of the DERs' output, or simply neglected as 'compensated by the main grid' or 'included in the social costs for all prosumers' [124]. Additionally, communities for P2P energy trading are artificially divided [116–118, 124, 125], resulting in that participants with common benefits may not be classified in the same community. Due to the temporal-spatial randomness of renewable energy outputs and demand profiles in the distribution network, P2P market participants who can be grouped by common benefits (not only from the market but also from physical connections point of view) are dynamically changing as with the continuous power flow variations.

Therefore, a new energy transaction model based on dynamic power flow tracing is proposed in

our study [128], making it possible to bridge the gap between P2P energy trading and network operation (hence fair usage and charges). The dynamic power flow tracing can identify the power transfers truly existing in the physical network and allocate losses by quantifying the power flows reaching load nodes from each source.

Chapter 3

Adaptive Service Restoration Strategy of Distribution Networks with Distributed Energy Resources and Soft Open Points

3.1 Introduction

In this chapter, an adaptive service restoration strategy of distribution networks with DERs and SOPs is proposed, and service restoration is achieved under multiple load levels. This chapter will discuss under the following scenarios with a modified IEEE 33-node test feeder.

- Faults for different durations
- Different service restoration strategies
- Different DER outputs and load levels

The main contributions of this chapter are summarised as follows:

- The influence of faults with different durations on the network with SOP at distribution levels is surveyed. An appropriate optimisation objective function, which includes the minimum weight of the lost load, minimum DER curtailments, and minimum network loss is established. Modelling method of power electronic devices is studied especially for SOPs, DERs, and ESSs during service restoration.
- For a distribution system with SOPs, its service restoration can be achieved by optimising the topology and the outputs of SOPs and DERs simultaneously. Using the second-order cone programming (SOCP) to simplify the solving process of the mixed-integer non-convex programming problem of the model. To formulate the convex MIQP model, the main idea is to convert the non-convex models of branch currents and the currents of SOPs, DERs, ESSs, and loads into linear models, since the objective is quadratic and convex, and other constraints are linear.

3.2 Modelling of Service Restoration Distribution Network with SOPs

3.2.1 Control mode of SOP and the adaptive service restoration strategy

The topology of SOP in this chapter is standard back-to-back voltage-source converters (VSCs) as shown in Figure 3.1.

Table 3.1 gives the control modes of SOP. After the fault-side VSC of the SOP finished close restart and step-up under Vf mode, the distribution network step in service restoration stage.

In the service restoration stage, ESSs and transmission power of SOP are firstly optimised. If the voltage exceeds the upper limit, DER output should be reduced. Finishing the above

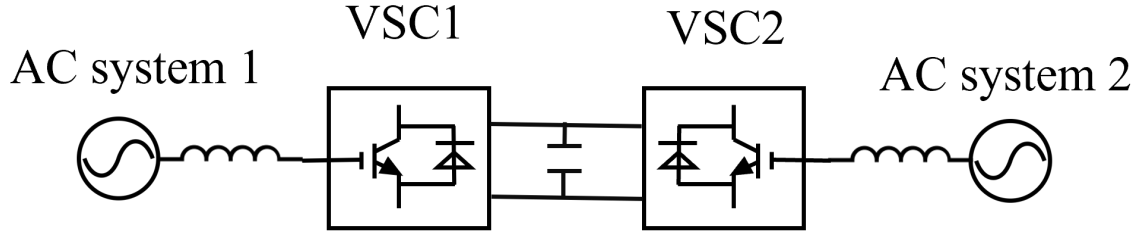


Figure 3.1: Back-to-back VSC-based SOP

Table 3.1: Control modes of VSC-based SOP

Distribution network state		VSC of SOP
Norm operation		PQ mode $V_{dc}Q$ mode
Service restoration	Fault side connect to the system by tie switches	PQ mode (fault side) $V_{dc}Q$ mode (unfaulty side)
	Fault side connect to the system by SOP	Vf mode (fault side) $V_{dc}Q$ mode (unfaulty side)

process, objective function should be calculated. If all lost loads are restored, it proves that the SOP cooperates with ESS so they can adapt to the change to a new operational status of the system. Meanwhile, the distribution network should keep its original topology, and all lost loads are connected to the main grid by SOP. Otherwise, all lost loads cannot be restored. That means tie switches should be operated. Furthermore, SOP, ESSs and tie switches should be optimised at the same time. The control mode of the fault side VSC of the SOP will transfer from Vf to PQ . The flow chart of the adaptive service restoration strategy is shown in Figure 3.2. Control modes of SOP under system fault conditions are shown in Figure 3.3.

3.2.2 Modelling of service restoration of distribution network with SOP

Objective function

In the service restoration, the objective function consists of a total minimum weight of the lost load, minimum DER curtailments, and minimum network loss. Minimum weight of the lost load means fewer customers lose service during the fault. Minimum DER curtailment can improve renewable energy penetration. Minimum network loss can reduce the network operational cost during service restoration. The optimisation variables include the DER power and circuit breakers states.

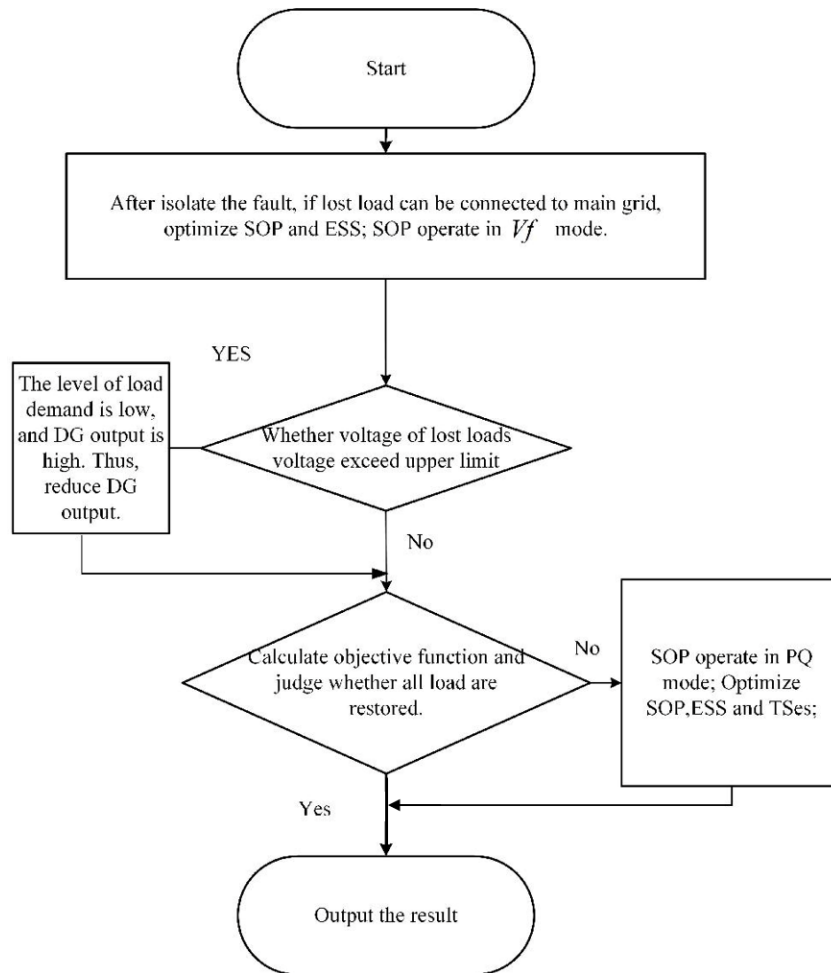


Figure 3.2: Flow chart of the proposed adaptive recovery strategy

$$f_1 = \min \sum_{k=1}^{\Omega_l} \alpha_k P_k \quad (3.1)$$

$$f_2 = \min \sum_{i=1}^{\Omega_d} P_{i,t}^{DER} \quad (3.2)$$

$$f_3 = \min \sum_{t=1}^T \sum_{i,j=1}^{\Omega_b} R_{ij} I_{ij,t}^2 \quad (3.3)$$

where P_k is lost load of node k ; α_k is important degree of node k , loads are divided into 3 levels; Ω_l is a set of power loss loads; $P_{i,t}^{DER}$ is the active power of the DER of node i at time t ; Ω_d is a set of all disconnected DERs; Ω_b is a set of nodes in the distribution network, T is the set of time (total fault time here); R_{ij} is the resistance of branch ij ; $I_{ij,t}$ is the branch current from node i to node j .

The objective function of the original multi-objective problem can be transformed into:

$$f = \min(w_1 f'_1 + w_2 f'_2 + w_3 f'_3) \quad (3.4)$$

where f_1 , f_2 and f_3 are normalised to f'_1 , f'_2 and f'_3 (i.e., the conversion to the interval $[0, 1]$) to eliminate the effect on the optimisation results due to the difference in the magnitude of each target function's value. In real operations, engineers/researchers can set the weight factors considering their various requirements and priorities. The random weight vectors of each target are obtained as follows.

$$[w_1 \ w_2 \ w_3] = [0.7655 \ 0.1600 \ 0.0745] \quad (3.5)$$

Operational constraints

Constraints of SOP: Active and reactive power outputs of SOPs should meet VSC capacity constraints.

$$\begin{cases} P_t^{VSC1} + P_t^{VSC2} = 0 \\ \sqrt{(P_t^{VSCx})^2 + (Q_t^{VSCx})^2} \leq S^{VSCx} \end{cases} \quad (3.6)$$

where P_t^{VSCx} is the active power of VSC x at time t ; Q_t^{VSCx} is the reactive power of VSC x at time t ; S^{VSCx} is the capacity of VSC x .

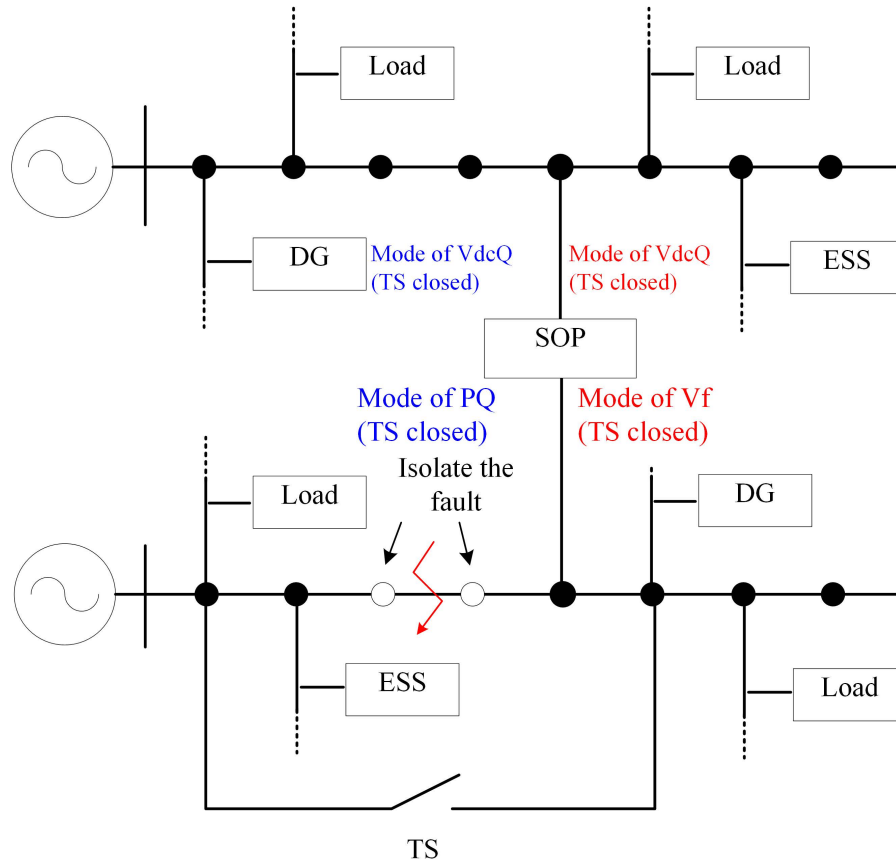


Figure 3.3: Schematic of the control mode of SOP under fault condition

Constraints of energy storage:

$$\left\{ \begin{array}{l} E_{i,t} = E_{i,t-1} + P_{i,t}^{ESS} \\ |P_{i,t}^{ESS,c}| \leq |P_{i,t}^{ESS}| \leq |P_{i,t}^{ESS,d}| \\ E_i^{ESS} SOC_{min} \leq E_{i,t} \leq E_i^{ESS} SOC_{max} \end{array} \right. \quad (3.7)$$

where $P_{i,t}^{ESS}$ is the energy storage charging power or discharging power of node i at time t ; $P_{i,t}^{ESS,c}$ and $P_{i,t}^{ESS,d}$ are the energy storage charging power limit or discharging power limit of node i at time t ; $E_{i,t}$ is the energy storage present state of node i ; E_i^{ESS} is the energy storage capacity of node i ; SOC_{min} and SOC_{max} are the minimum and maximum states of charge.

Power flow constraints:

$$\left\{ \begin{array}{l} \sum_{k \in \psi_i} P_{ik,t} = \sum_{j \in \phi_i} (P_{ji,t} - R_{ji}(I_{ji,t})^2) + P_{i,t} \\ \sum_{k \in \psi_i} Q_{ik,t} = \sum_{j \in \phi_i} (Q_{ji,t} - X_{ji}(I_{ji,t})^2) + Q_{i,t} \end{array} \right. \quad (3.8)$$

$$\left\{ \begin{array}{l} P_{i,t} = P_{i,t}^{DER} + P_{i,t}^{ESS} + P_t^{VSCx} - P_{i,t}^{load} \\ Q_{i,t} = Q_{i,t}^{DER} + Q_{i,t}^{ESS} + Q_t^{VSCx} - Q_{i,t}^{load} \end{array} \right. \quad (3.9)$$

$$(V_{i,t})^2 = (V_{j,t})^2 - 2(R_{ji}P_{ji,t} + X_{ji}Q_{ji,t}) + (R_{ji}^2 + X_{ji}^2)(I_{ji,t})^2 \quad (3.10)$$

where ϕ_i is the set of the head nodes from the system whose terminal node is i ; ψ_i is the set of the terminal nodes from the system whose head node is i ; R_{ji} and X_{ji} are the resistance and reactance of branch ij ; $P_{ji,t}$ and $Q_{ji,t}$ are the active and reactive powers from node j to node i at time t ; $P_{i,t}$ and $Q_{i,t}$ are active and reactive power injections of node i at time t ; $Q_{i,t}^{ESS}$ is the reactive power of the energy storage at node i at time t ; $P_{i,t}^{DER}$ and $Q_{i,t}^{DER}$ are the active and

reactive powers of DER of node i at time t ; P_t^{VSCx} and Q_t^{VSCx} are the active and reactive powers of the SOP at time t ; $P_{i,t}^{load}$ and $Q_{i,t}^{load}$ are the active and reactive powers of the load of node i at time t ; X_{ij} is the reactance of branch ij ; $V_{i,t}$ is the voltage of node i at time t .

Constraints of DER output:

$$\begin{cases} 0 \leq P_{i,t}^{DER} \leq P_{i,t}^{DER,max} \\ 0 \leq Q_{i,t}^{DER} \leq Q_{i,t}^{DER,max} \end{cases} \quad (3.11)$$

where $P_{i,t}^{DER,max}$ and $Q_{i,t}^{DER,max}$ are the maximum active and maximum reactive powers of DER of node i at time t

Voltage constraint:

$$\underline{V}_i \leq V_{i,t} \leq \bar{V}_i \quad (3.12)$$

where \underline{V}_i and \bar{V}_i are the lower and upper voltage limits. In addition, after reconfiguration, the network is still considered as radial.

3.3 Second-Order Cone Transforming

3.3.1 Second-order cone transforming of objectives

The standard form of second-order cone programming model can be formulated as follows:

$$\begin{cases} \min c^T x \\ s.t. Ax = b \\ x \in K \end{cases} \quad (3.13)$$

$$K = \left\{ x \in R^m : 2x_1x_2 \geq \sum_{l=3}^m x_l^2 \quad x_1, x_2 \geq 0 \right\} \quad (3.14)$$

With $(I_{ij,t})^2$ and $(V_{i,t})^2$ replaced by $l_{ij,t}$ and $v_{i,t}$, f_3 in the object can be expressed as follows:

$$f_3 = \min \sum_{t=1}^T \sum_{i,j=1}^B R_{ij} l_{ij,t} \quad (3.15)$$

$$l_{ij,t} = \frac{(P_{ij,t}^2 + Q_{ij,t}^2)}{v_{i,t}} \quad i, j \in \Omega_b \quad (3.16)$$

Equation 3.16 can be further loosed and transformed into the form of SOCP:

$$\| [2P_{ij,t} \quad 2Q_{ij,t} \quad l_{ij,t} - v_{i,t}]^T \|_2 \leq l_{ij,t} + v_{i,t} \quad (3.17)$$

where $\| \dots \|_2$ is the Euclidean norm [129] which is the standard form of the SOCP.

3.3.2 Second-order cone transforming of constraints

The constraint of network reconfiguration in the second-order cone programming model is formulated as follows:

$$\left\{ \begin{array}{ll} \sum \alpha_{ij} = n - n_f & \\ \beta_{ij} + \beta_{ji} = \alpha_{ij} & i, j \in \Omega_b \\ \sum_{j \in N} \beta_{ij} = 1 & \forall i \in \Omega_n / \Omega_{n_f} \end{array} \right. \quad (3.18)$$

where α_{ij} is a Boolean variable, referring to the switch status between node i and node j ; n_f is the number of head nodes; β_{ij} is an auxiliary Boolean variable, and if node i is the parent node of node j , β_{ij} is 1, and if not, β_{ij} is 0; Ω_n is the node set; Ω_{n_f} is the head node. With $(I_{ij,t})^2$ and $(V_{i,t})^2$ replaced by $l_{ij,t}$ and $v_{i,t}$, the constraints of power flow and node voltage as Equations 3.19-3.21. Especially, the Big M Method [129] is employed to reflect the impact of network reconfiguration during the transforming.

$$\begin{cases} \sum_{k \in \Psi_i} P_{ik,t} = \sum_{j \in \Phi_i} (P_{ji,t} - R_{ji}l_{ji,t}) + P_{i,t} \\ \sum_{k \in \Psi_i} Q_{ik,t} = \sum_{j \in \Phi_i} (Q_{ji,t} - X_{ji}l_{ji,t}) + Q_{i,t} \end{cases} \quad (3.19)$$

$$-(1 - \alpha_{ij})M \leq v_{i,t} - v_{j,t} - 2(R_{ji}P_{ji,t} + X_{ji}Q_{ji,t}) + (R_{ji}^2 + X_{ji}^2)l_{ji,t} \leq (1 - \alpha_{ij})M \quad (3.20)$$

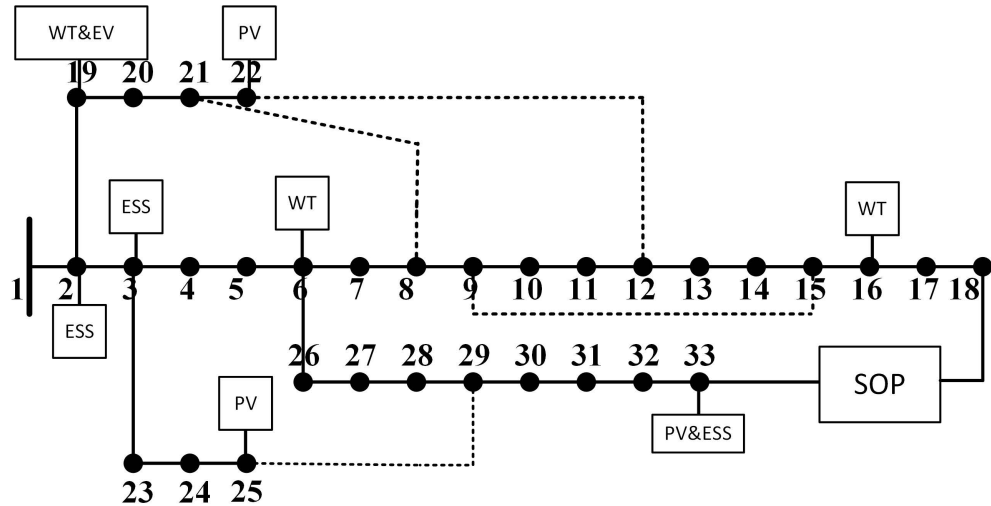
$$\underline{v}_i \leq v_{i,t} \leq \bar{v}_i \quad (3.21)$$

The operation constraints of SOPs can be transformed as follows:

$$\| [P_t^{VSCx}, Q_t^{VSCx}] \|_2 \leq S^{VSCxi} \quad (3.22)$$

3.4 Methodology: Design of the Experiment

In this section, a distribution network as shown in Figure 7.5 is used as a test system to analyze and verify the proposed model and algorithm. The system is an improved IEEE 33-node



* The IEEE 33-node test feeder (12.66kV), created by Baran & Wu, was used to study the impact of distribution network reconfiguration on power losses reduction and load balancing [130].

Figure 3.4: A modified IEEE 33-node test feeder with DERs and SOPs

test feeder with one SOP. The voltage of the substation transformer is 12.66kV. There are 32 normal closed switches and 5 normal open tie switches. The current range of tie switches (8-21,12-22,9-15,25-29) is 100A. The DERs are required to operate with a power factor is 0.95. The total base load is 3715 kW and 2300 MVar. In this modified system, the capacity of the SOP is 300 kVA and replace the original tie-line switch on Line 18–33. The voltage range of all nodes is set to [0.95, 1.05] p.u. The current range of main line (1-18) is 400A. The current range of branch line (19-22,23-25,23-33) is 200A. Priorities of the loads are indicated in Table 3.2. The SOCP program proposed in this chapter is coded by YALMIP [131], and solved by Gurobi [132]. The optimization method proposed is implemented with MATLAB R2019a, and the operating environment is Intel i5-5200 2.2GHz CPU, 8GB RAM. The first design of

Table 3.2: Priorities and controlling types of the loads

Primary load	Second-grade Load	Third-grade Load
2,6,9,13,20,23,26,30,33	The rest	8, 24

the experiment includes photovoltaics (PVs) with four classic scenarios to verify the service restoration result with distribution network reconfiguration.

- In scenario 1, the load level is low and the DER output is low.
- In scenario 2, the load level is low and the DER output is high.
- In scenario 3, the load level is high and the DER output is high.
- In scenario 4, the load level is high and the DER output is low.

Three PVs are installed at nodes 22, 25 and 33 with capacities of 500 kW, 300 kW, and 400 kW, respectively. Three 200 kW wind turbines (WTs) are installed at nodes 6, 16, and 19.

The second design of the experiment test ESSs instillation to verify the service restoration result. Locations and capacities of ESSs are indicated in Table 3.3. The initial state of charge of ESSs is 0.2.

Table 3.3: Locations and capacities of ESSs

Node	2	3	19	33
Power capacity (kW)	120	140	120	280
Energy capacity (kWh)	710	860	720	1700

3.5 Case Studies

3.5.1 Comparison of different scenarios

When a fault happens between Line 7 and Line 8 for one hour. In service restoration, SOP and ESSs should be optimized at first, and then the distribution network reconfiguration will be considered. In Figure 3.5, there are four typical scenarios are used to test the proposed adaptive service strategy, and results are shown in Table 3.4. In scenario 1, load level is low

Table 3.4: Comparison of power recovery results under different scenarios

	Scenario1	Scenario2	Scenario3-1	Scenario3-2	Scenario4-1	Scenario4-2
Active power of lost load (kW)	0	0	359.92	0	477.12	0
Reactive power of lost load (kVar)	0	0	206.62	0	268.17	0
Real output of PV (kW)	179.98	599.92	597.91	598.91	179.35	178.85
Max output of PV (kW)	180	600	600	600	180	180
Real output of WT (kW)	238.24	727.28	790.55	1198.59	359.68	358.79
Max output of WT (kW)	360	1200	1200	1200	360	360
Supplement the reactive power of DER (kVar)	80.41	75.84	90.36	90.76	92.77	90.93
ESSs output (kW)	197.68	197.87	194.27	195.46	196.82	196.25
Transmission active power of SOP (kW)	199.07	67.22	258.83	1.02	271.42	1.05
Supplement the reactive power of SOP (kVar)	341.56	412.3	303.32	586.25	255.57	596.96
Transmission active power of tie switch (kW)	0	0	0	1443.3	0	1475.18
Transmission reactive power of tie switch (kW)	0	0	0	1217.02	0	475.85
Power losses (kW)	34.54	30.85	21.31	20.23	27.59	22.54

* x-1 means without distribution network reconfiguration, x-2 means with distribution network reconfiguration

Table 3.5: DER outputs and loads during the service restoration

Time	1	2	3	4
Load of lines/p.u	0.2	0.7	0.6	1
PV outputs/p.u	1	0.5	1	0.3
WT outputs/p.u	1	0.5	0.2	0.1

and DER output is low, SOP transmit active power and reactive power at same time(199.07 and 341.56 separately). In scenario 2, when load level is low and DER output is high,SOP transmits less active power to the system and more reactive power to the system than scenario 1. Above all, in the first two scenarios, only optimizing SOP can restore all load. Therefore,

Table 3.6: Results of service restoration

	Active power of lost load (kW)	Reactive power of lost load (kVar)	Real output of PV (kW)	Max output of PV (kW)	Real output of WT (kW)	Max output of WT (kW)	Supplement the reactive power of DER (kVar)	Power losses (kW)
Case 1	0	0	1677.7	1680	2157.9	3240	359.35	130.87
Case 2	331.44	190.45	593.16	1680	1187.5	3240	286.72	131.39

there is no need for a network reconfiguration. The SOP should be in Vf mode and supply a reference voltage to lost loads. In scenario 3, the load level is high and the DER output is high. Without distribution network reconfiguration, SOP transmits a considerable number of active power to the system. (258.83 kW)

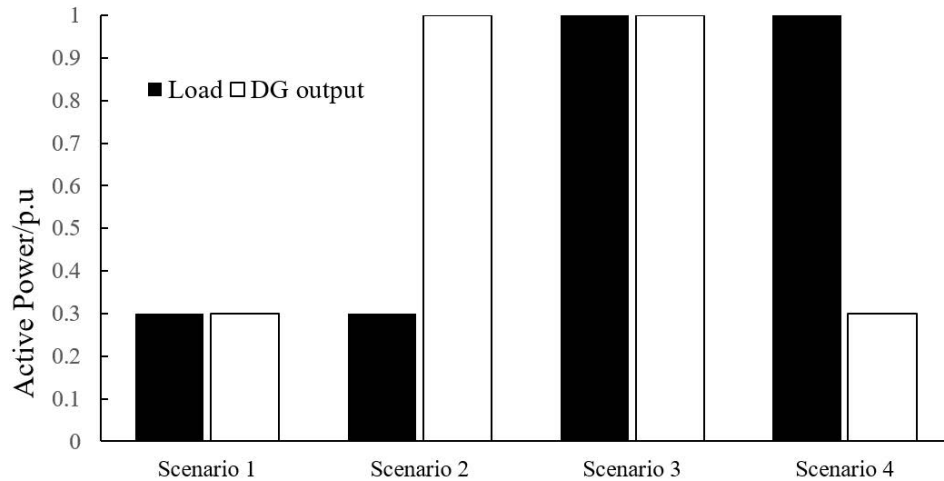


Figure 3.5: Load and DER output levels of the 4 typical scenarios

Therefore, SOP transmits a considerable number of active power to the system. DER power curtailment happens especially the wind power output (790.55kW of 12000kW). At that time, distribution network topology would be optimized. The result shows that tie switches shoulder the responsibility of active power transmission instead of SOP. SOP have extra ability to supply reactive power. The wind power curtailment phenomenon will be reduced. In scenario 4, the load level is high and the DER output is low. Without distribution network reconfiguration, SOP transmits more active power than reactive power.(271.42kW and 255.57kVar). At that

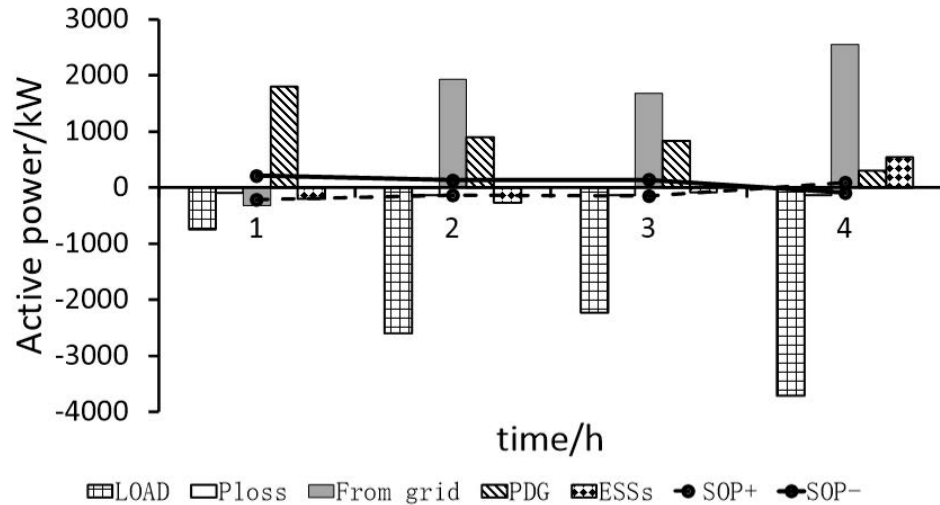


Figure 3.6: Active power balance during service restoration

time, distribution network topology would be optimized. The result shows that tie switches should shoulder the responsibility of active power transmission instead of SOP. SOP have extra ability to supply reactive power. In scenarios 3-2 and 4-2, SOP should be in PQ mode and supply a reference voltage to lost loads.

3.5.2 Comparison of different cases

There are two cases designed to verify the benefits for coordinated optimization of ESSs. When a fault happens between Lines 7 and 8, the outage is to be prolonged for 4 hours. The DER outputs and loads during the service restoration are indicated in Table 3.5.

Case 1: the system is optimized by network reconfiguration, with VSC2 and ESSs.

Case 2: the system is optimized by network reconfiguration and VSC2, without ESSs.

Table 3.6 shows the result of the service restoration. Without ESSs, total restoration power

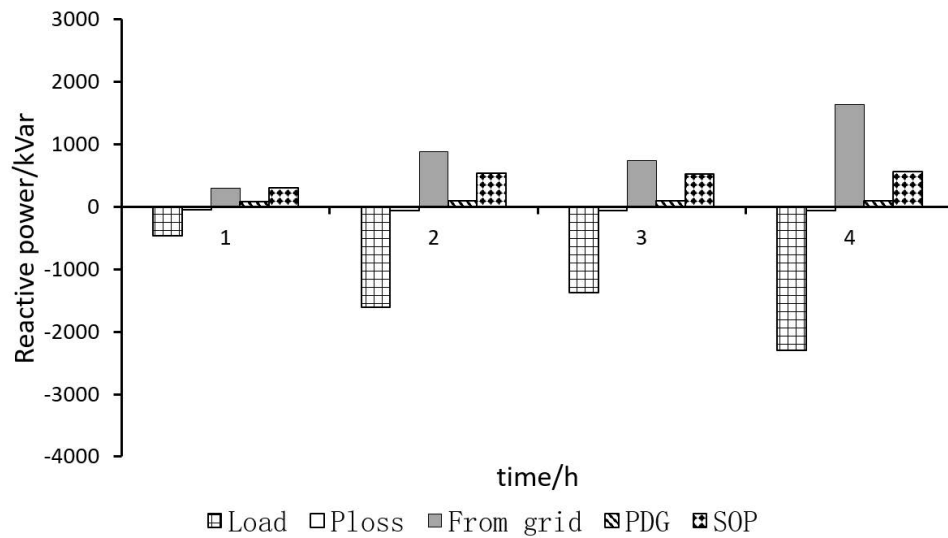


Figure 3.7: Reactive power balance during service restoration

supply of case 2 would significantly decrease compared with case 1. It is worth noticing that DER power curtailment will be reduced in case 1. DERs can also supply more reactive power in case 1.

Figure 3.6 and Figure 3.7 show that after isolating the fault, SOP takes major responsibility to support outage areas' reactive power. It is apparent that it changed to follow the load's demand. With SOPs and ESSs, the lost load can get more energy from the grid. DERs mainly provide active power. And part of it can be shifted by ESSs to the time when the load has a high demand. SOP and grid share the reactive power of loads. Figure 3.8 shows that ESSs were in the charge state at time 1, 2 and 3, and turned to the discharge state at time 4. The reason for this is that ESSs from lines need to supply energy for AC peak loads at time 4.

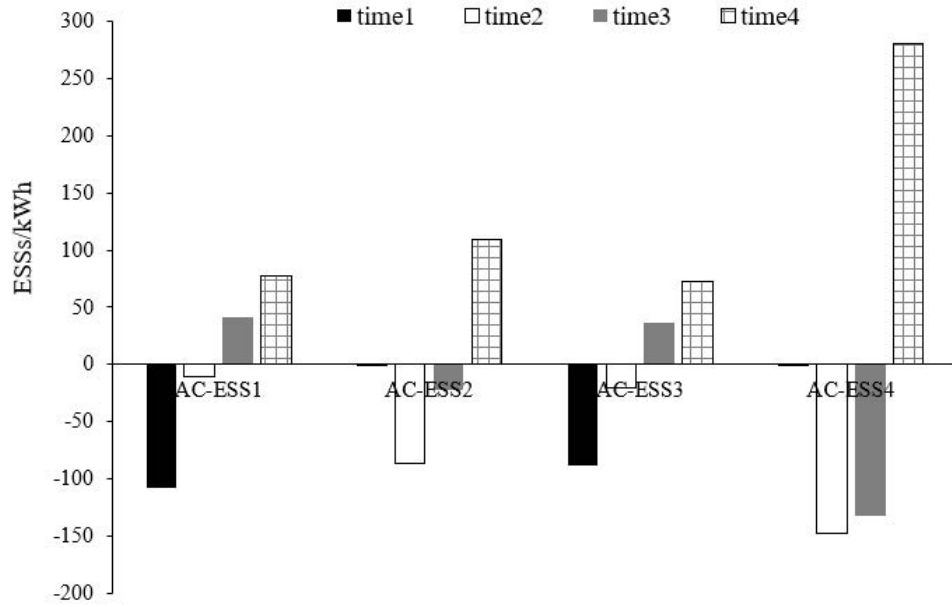


Figure 3.8: Optimal energy dispatch during service restoration

3.6 Conclusion

Considering integrating high levels of various DERs into the grid, this chapter proposes an adaptive service restoration strategy of distribution networks with DERs and SOPs to realise the coordination optimisation of SOPs, ESSs and tie switches. Distribution network scenario classification is described with an analysis of various control models of SOPs. Matching analysis is performed between network scenarios and control models of SOPs. Based on the mixed-integer SOCP, lines and the control devices with different characteristics are proposed. Results show that apart from balancing the supply and demand, the ESSs scheduling along with network reconfiguration enabled by SOPs can be combined to reduce power losses, restore more lost loads to minimise customer interruptions and customer minutes lost.

The limitation of the proposed method is limited to the single-phase system. Meanwhile, the fault reason is also important to be explored. As an example, for the same ten-day period in

2015, a total of 3762 phase regional imbalance daily records were recorded from 2432 distribution transformers (days with outages longer than six hours are recorded as daily records). These daily imbalances cause the fault rate for the local network. For reducing fault rates, SOP in the network should utilize its ability to handle the three-phase imbalance problem.

Chapter 4

A New Phase-Changing Soft Open Point and Impacts on Optimising Unbalanced Power Distribution Networks

4.1 Introduction

To improve the three-phase imbalance, with a solution of network reconfiguration using SOPs, focusing on the optimisation modelling, this chapter proposes an optimised operational strategy for unbalanced ADNs based on SOPs and optimal ESSs dispatch, reducing the three-phase four-wire imbalances while enhancing the operational efficiency of ADNs. The model in this chapter is extended from single-phase from last chapter to three-phase. The contributions of this chapter are summarised as follows:

- The potential of SOPs is explored by a fresh way of connection, i.e. phase power transferring, so-called phase-changing SOP (PC-SOP).
- The benefits of PC-SOPs for unbalanced three-phase four-wire system are further anal-

ysed. A PC-SOP based optimal operational strategy for unbalanced ADNs is proposed considering power losses in the neutral wire.

- The OPF of three-phase four-wire imbalance system with SOPs is mathematically a non-convex nonlinear problem. The original non-convex nonlinear optimisation model is converted into an SOCP formulation, which can be efficiently solved to find the global optimum which can also meet the requirement of efficiency in problem solving.
- Demonstrated by a case study, by optimising the regulation of SOPs, optimal ESSs dispatch and PV curtailment, the reduction of energy losses and effective voltage regulation simultaneously achieved by the proposed approach are significant.

4.2 Unbalanced Three-Phase Optimal Operation Problem Formulation in Three-Phase Four-Wire Distribution Networks

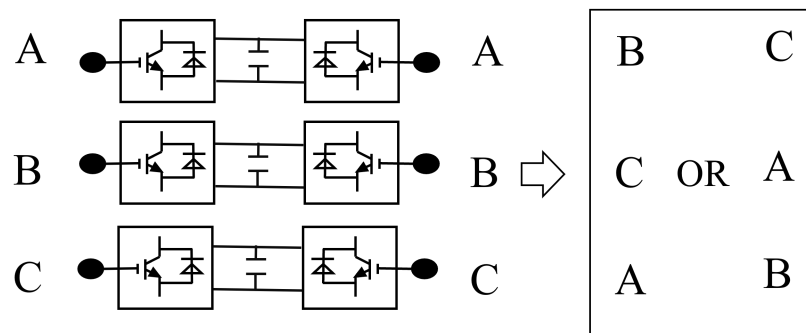


Figure 4.1: The new ways of connection of the SOP (PC-SOP)

Basic principles of SOPs: SOPs are power-electronic devices installed in ADNs to replace tie switches which can accurately and flexibly control power flows [72]. Therefore, ADNs with SOPs can operate with lower cable losses and lower risks caused by frequent switching actions. SOPs have capabilities to transfer active power, supply reactive power and achieve real-time

control of voltage between the connected feeders. B2B VSCs are the most commonly used topology for commercial SOP in medium voltage or low voltage networks. Three-phase active power and reactive power outputs can be controlled independently by SOPs based on the B2B VSC topology. These SOPs operate in a $PQ - V_{dc}Q$ control mode in normal conditions with a certain amount of device losses (the loss index of VSC is 0.00199 [66]). In a balanced system, three-phase feeders would be connected correspondingly (ABC to ABC).

Basic principles of PC-SOPs: However, considering the implementing principle of B2B VSC using a DC link to connect AC feeders, energy is transferred from AC to DC then back to AC. Thus, it is possible that different feeder phases can be connected which is beneficial for unbalanced systems. Energy will be shifted by SOPs from one phase of one feeder to another phase of another feeder.

As the DER outputs and electricity demand have randomness, there is always a mismatch between them. When they are distributed in different feeder phases, networks can achieve a better operating performance when all phases can be indirectly connected by SOPs. Therefore, new ways of connection of three single-phase SOPs, called PC-SOP (ABC to BCA or CAB, marked by the red rectangle in Fig. 4.1) is proposed in this section as shown.

The optimisation process will not affect or be affected by the control scheme and techniques such as various PWM technologies and their current controllers or controlling loops [46]. It is actually one of the advantages of using back-to-back converters, with a ‘decoupling DC-link’, in AC-AC applications from high-power high-voltage, like HVDC tie-links between grids with different frequencies; to lower-power variable-speed, like doubly-fed induction generators for wind turbine power conversion systems; to here, the connection between one unbalanced feeder and another.

The optimisation model of PC-SOPs (using ABC to BCA as an example) is obtained with the following constraints:

PC-SOP active power constraints:

$$\begin{cases} P_t^{VSC1,a} + P_t^{VSC2,c} + P_t^{VSC1,a,loss} + P_t^{VSC2,c,loss} = 0 \\ P_t^{VSC1,b} + P_t^{VSC2,a} + P_t^{VSC1,b,loss} + P_t^{VSC2,a,loss} = 0 \\ P_t^{VSC1,c} + P_t^{VSC2,b} + P_t^{VSC1,c,loss} + P_t^{VSC2,b,loss} = 0 \end{cases} \quad (4.1)$$

$$P_t^{VSCx,\varphi,loss} = \gamma^{VSC} \cdot P_t^{VSCx,\varphi} \quad (4.2)$$

PC-SOP capacity constraint:

$$\sqrt{P_t^{VSCx,\varphi^2} + Q_t^{VSCx,\varphi^2}} \leq S^{VSCx,\varphi^2} \quad (4.3)$$

where $P_t^{VSCx,\varphi}$ is the active power of VSCx at phase φ at time t , $P_t^{VSCx,\varphi,loss}$ is the active power loss of VSCx at phase φ at time t , $Q_t^{VSCx,\varphi}$ is the reactive power of VSCx at phase φ at time t , and $S^{VSCx,\varphi}$ is the capacity of VSCx at phase φ .

Objective function

This section proposes a linear weighted combination of minimum total power losses, the voltage deviation and the voltage unbalance condition:

$$\min f = W_{\alpha} \cdot f^{loss} + W_{\beta} \cdot f^{V,deviation} + W_{\gamma} \cdot f^{VUF} \quad (4.4)$$

where W_{α}, W_{β} and W_{γ} are the wights for each factor and set as equally important (1.0 for each); f^{loss} is the power losses; $f^{V,deviation}$ is the voltage deviation; f^{VUF} is the voltage unbalance condition. Minimum total power loss can reduce the network operational cost during network operation. Minimum voltage deviation can improve the customer-side voltage and power quality. Minimum the voltage unbalance condition can improve the network life and ensure networks operate close to a balanced condition. In addition, in real operations, engineers/researchers can set the weight factors considering their various requirements and priorities. Also, as a future work, recommended weighting factors can be proposed for defined situations, case by case. Each function are formulated as follows:

$$f^{loss} = \text{sum}([I_{branch,real,t}^2 + I_{branch,imag,t}^2] \cdot R) \quad (4.5)$$

$$f^{V,deviation} = \text{sum}(|\vec{V}_t - V_{nominal}|) \quad (4.6)$$

$$f^{VUF} = \text{sum}(VUF_{m,t}) \quad (4.7)$$

where $I_{branch,t}$ is an $l \times 1$ vector containing all branch currents at time t , with their real part $I_{branch,real,t}$ and imaginary part $I_{branch,imag,t}$; R , the vector containing all branch resistances; \vec{V}_t is an $n \times 1$ vector containing voltages at each node at time t ; $VUF_{m,t}$ is the voltage unbalance

factor at bus m at time t ; and $V_{nominal}$ is an $n \times 1$ vector containing nominal voltages at each node.

Three-phase four-wire system operational constraints

Power flow constraints: This branch flow model is proposed for three-phase four-wire networks in [101]. It can be described mathematically with the following constraints. The nodal admittance matrix is the core of calculating power flows following Kirchhoff's Current Law (KCL) [108] in this section.

$$[Y]\vec{V}_t = I_{inj,t} \quad (4.8)$$

where $[Y]$ is the $n \times n$ nodal admittance matrix, $I_{inj,t}$ is the $n \times 1$ vector containing all currents drawn or injected into the network at time t .

The loads, DERs, SOPs and ESSs are modelled as current injections.

$$I_{inj,t}^{load} = \frac{P_{i,t}^{load} - j \cdot Q_{i,t}^{load}}{V_{n,i}^*} \quad (4.9)$$

$$I_{inj,t}^{DER,SOPorESS} = \frac{1}{V_{n,i}^*} (P_{i,t}^{DER,SOPorESS} - j \cdot Q_{i,t}^{DER,SOPorESS}) \quad (4.10)$$

$$I_{inj,t} = sum(I_{inj,t}^{DER,SOPorESS}) - I_{inj,t}^{load} \quad (4.11)$$

where $I_{inj,t}^{load}$ is the current drawn by load at time t ; $P_{i,t}^{load}, Q_{i,t}^{load}$ are the real and reactive load powers at node i at time t ; $P_{i,t}^{DER,SOPorESS}$ are the active powers of DERs, SOPs, or ESSs at node i at time t ; $Q_{i,t}^{DER,SOPorESS}$ are the reactive powers of DERs, SOPs, or ESSs at node i at time t ; $I_{inj,t}^{DER,SOPorESS}$ are the current contribution from DERs, SOPs, or ESSs. Here $V_{n,i}$ (nominal voltage at node i) are used to approximate the $V_{i,t}$ (variable, the voltage at node i at time t), because voltage deviations are relatively small compared with the changes of load, DERs, SOPs or ESSs.

For loss analysis, current sources are preferred for modelling purposes for loads, DERs and ESSs. In practice, although relatively few loads are constant current, a mixture of constant power and constant impedance loads often behaves like a constant current load. Therefore constant current source is a reasonable approximation of a mixture of constant power and constant impedance loads. Moreover, the voltage deviations are small in magnitude compared to the actual voltage values. The accuracy of constant current modelling of loads and DERs have been proved mathematically and practically in [101] with reasonable errors of voltages and currents up to 0.2% and 2%, respectively.

Voltage limits: Each bus voltage can be expressed as a linear combination of the injected currents.

$$V_{i,real,t} = Re([Y_i^*]^{-1}) \cdot I_{inj,real,t} - Im([Y_i^*]^{-1}) \cdot I_{inj,imag,t} \quad (4.12)$$

$$V_{i,real,t} = Re([Y_i^*]^{-1}) \cdot I_{inj,real,t} + Im([Y_i^*]^{-1}) \cdot I_{inj,imag,t} \quad (4.13)$$

$$V_{i,real,t}^2 + V_{i,imag,t}^2 \leq \bar{V}_i^2 \quad (4.14)$$

$$-K_{1A}V_{i,real,t} - K_{2A}V_{i,real,t} \leq -\underline{V}_i, \quad i \in \text{phase } A \quad (4.15)$$

$$-K_{1B}V_{i,real,t} - K_{2B}V_{i,real,t} \leq -\underline{V}_i, \quad i \in \text{phase } B \quad (4.16)$$

$$-K_{1C}V_{i,real,t} - K_{2C}V_{i,real,t} \leq -\underline{V}_i, \quad i \in \text{phase } C \quad (4.17)$$

where $V_{i,real,t}$, $V_{i,real,t}$ are the real part and imaginary part of $V_{i,t}$; \bar{V}_i , \underline{V}_i are the maximum and minimum allowable steady-state voltage magnitudes at node i .

Based on the fact that the approximate voltage angle is known at all phase nodes, the constants $K_{1A}, K_{2A}, K_{1B}, K_{2B}, K_{1C}, K_{2C}$ can be chosen to minimise the weighted average squared approximation error over an angle deviation of ± 10 degrees from the approximate voltage angle [133].

Voltage imbalance constraints:

$$VUF_{m,t} = \frac{V_{m,t}^a + \alpha^2 V_{m,t}^b + \alpha V_{m,t}^c}{V_{m,t}^a + \alpha V_{m,t}^b + \alpha^2 V_{m,t}^c} \approx \frac{V_{m,t}^a + \alpha^2 V_{m,t}^b + \alpha V_{m,t}^c}{V^\varphi} \quad (4.18)$$

$$VUF_{m,t}^2 \leq \overline{VUF}_m^2 \quad (4.19)$$

where $V_{m,t}^\varphi$ is the phase φ voltages at bus m at time t ; α is the phasor rotation operator, $1 \angle 120^\circ$; \overline{VUF}_m is the maximum allowable voltage unbalance factor at bus m .

Current limits: The current through a branch connecting nodes i and j is then:

$$|I_{ij,t}| = \sqrt{(G_{ij}^2 + B_{ij}^2)} \cdot \sqrt{(V_{i,real,t} - V_{j,real,t})^2 + (V_{i,real,t} - V_{j,imag,t})^2} \quad (4.20)$$

and

$$|I_{ij,t}|^2 \leq \bar{I}_{ij}^2 \quad (4.21)$$

where $I_{ij,t}$ is the current of branch connecting nodes i and j at time t ; G_{ij}, B_{ij} are the branch conductance and susceptance respectively; \bar{I}_{ij} is the current limit of the branch connecting nodes i and j [134].

Branch current limits:

$$I_{branch,t} = [M] \vec{V}_t = [M][Y]^{-1} I_{inj,t} \quad (4.22)$$

where $[M]$ is the $l \times n$ connection matrix.

Constraints of energy storage:

$$\left\{ \begin{array}{l} E_{i,t} = E_{i,t-1} + P_{i,t}^{ESS} \\ |P_{i,t}^{ESS,c}| \leq |P_{i,t}^{ESS}| \leq |P_{i,t}^{ESS,d}| \\ E_i^{ESS} SOC_{min} \leq E_{i,t} \leq E_i^{ESS} SOC_{max} \quad i \in phase A, B or C \end{array} \right. \quad (4.23)$$

where $P_{i,t}^{ESS}$ is the energy storage charging power or discharging power at node i at time t ; $P_{i,t}^{ESS,c}, P_{i,t}^{ESS,d}$ are the energy storage charging and discharging power limits at node i at time t ; $E_{i,t}$ is the energy storage present state at node i ; E_i^{ESS} is the energy storage capacity at node i ;

SOC_{min} , SOC_{max} are the minimum and maximum states of charge.

Constraints of DER output:

$$\begin{cases} 0 \leq P_{i,t}^{DER} \leq P_{i,t}^{DER,max} \\ 0 \leq Q_{i,t}^{DER} \leq Q_{i,t}^{DER,max} \end{cases} \quad i \in \text{phase A, B or C} \quad (4.24)$$

where $P_{i,t}^{DER,max}$, $Q_{i,t}^{DER,max}$ are the maximum active and reactive powers of DER at node i at time t .

4.3 Second-Order Cone Transforming and Algorithm Process

The SOP capacity constraint can be transferred into the SOCP model for optimisation:

$$\|[P_t^{VSCx,\varphi}, Q_t^{VSCx,\varphi}]\|_2 \leq S^{VSCx,\varphi} \quad (4.25)$$

where $\|\dots\|_2$ is the Euclidean norm [129] which is the standard form of the SOCP.

Voltage and current limits model can be converted to an SOCP model:

$$\|[V_{i,real,t}, V_{i,real,t}]\|_2 \leq \bar{V}_i \quad (4.26)$$

$$\sqrt{(G_{ij}^2 + B_{ij}^2)} \|[(V_{i,real,t} - V_{j,real,t}), (V_{i,real,t} - V_{j,imag,t})]\|_2 \leq \overline{I_{ij}} \quad (4.27)$$

The detailed procedure of implementing the proposed model and algorithms is shown in Fig. 7.4. After the input of data such as network parameters, load profiles, ESS profiles and PC-SOP locations and sizes, the SOCP problem is relaxed for PC-SOP and the power flow constraints. As ESSs are some of the controllable variables with important initial status, they are assigned with specific constraints. Then the optimisation can be solved as an SOCP OPF problem with power flows and variables considered for a 24-hour simulation period, coded in Gurobi [132].

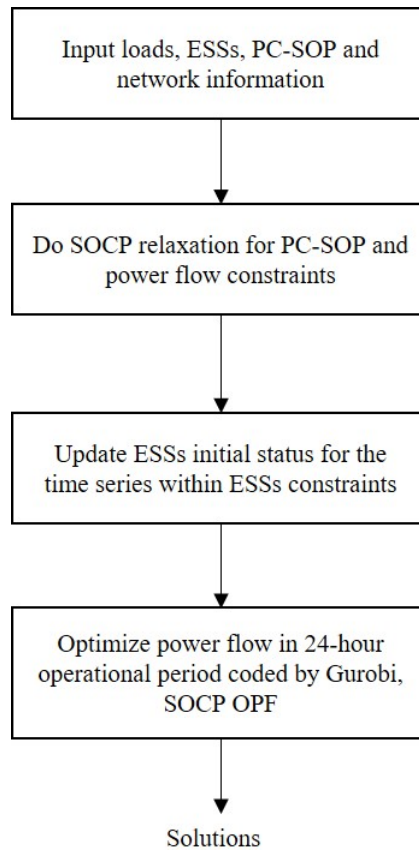
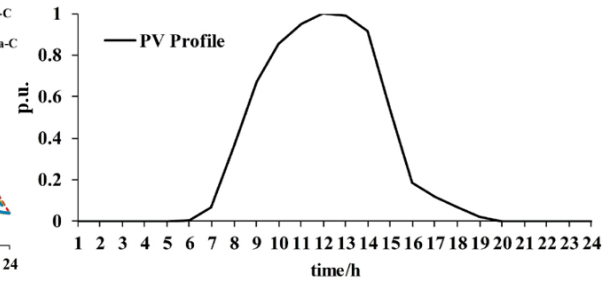
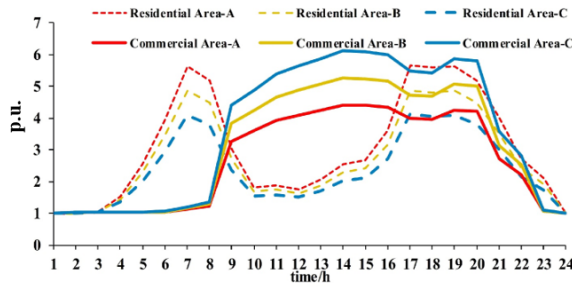
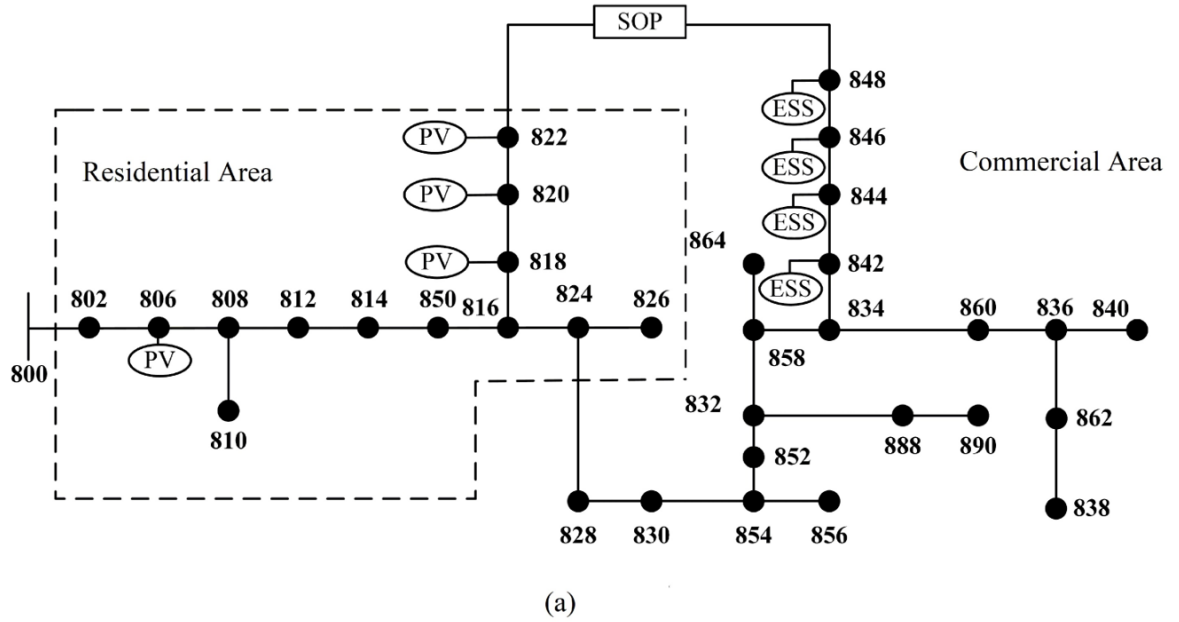


Figure 4.2: Flow chart of the applied solving process with the proposed model and algorithms

4.4 Methodology: Design of the Experiment



* This IEEE 33-node test feeder is an actual feeder located in Arizona, with a nominal voltage of 24.9 kV. It is characterized by long and lightly loaded, two in-line regulators, an in-line transformer for short 4.16 kV section, unbalanced loading, and shunt capacitors [135].

* Load profiles from Standard Load Profile [136]

* PV generation profile from Photovoltaic Solar Panel Energy Generation data [137]

Figure 4.3: (a) The topology of the modified IEEE 33-node test feeder; (b) Residential Area and Commercial Area profiles; (c) Individual PV generation profile

In this section, a modified IEEE 34-node test feeder is used as a test system to analyse and verify the proposed model and a modified IEEE 123-node distribution system is used to verify the scalability of the optimal operation of conventional SOPs on large-scale ADNs with severe unbalanced conditions.

The modified IEEE 34-node test feeder (line voltage 24.9 kV) as shown in Fig. 4.3(a) [138, 139]. Data of the IEEE 34-node test feeder is presented in Tables 4.2 and 4.3. The calculation process of the original fourth-order matrices of four-wire configurations is shown in [140]. To demonstrate the proposed model, the system is modified by removing all regulators and transformers. Single-phase overhead line configurations 302, 303 and 304 are replaced by three-phase overhead line configuration 300. The transformer between 832 and 888 is replaced by a 10 ft 301 configuration. Residential loads are in the dashed-border block, and other loads are commercial. The capacity of the SOP is 100 kVA and they are located between buses 822 and 848. The voltage range of all buses is set to be [0.94, 1.10] as the statutory limits in the UK [141]. The DERs (include PVs and ESSs) are required to operate with a fixed power factor of 0.95. Specifically, the ANSI standard recommends that the electric supply system should be made and function to limit the maximum voltage unbalance to 3% [142]. Four PVs are installed at buses 806 (three-phase, 300 kW), 818 (phase C, 300 kW), 820 (phase C, 600 kW) and 822 (phase C, 600 kW). Four ESSs are installed at buses 842 (three-phase, 100 kW), 844 (phase A, 400 kW), 846 (phase A, 400 kW) and 848 (three-phase, 400 kW). The initial state of charge (SOC) of all ESSs is fixed as 0.5, with a minimum of 0.2 and a maximum of 0.8.

4.5 Case Studies

Table 4.1: Comparison of different connection ways of PC-SOP

	Network Losses (kW/24h)	Neutral wire loss (kW/24h)	Neutral wire loss proportion *	PV curtailment (kW/24h)	Voltage deviation	Three-phase voltage unbalance condition
PC-SOP (BAC)	3527.77	382.86	10.85%	1208.91	+0.50% /-0.60%	1.63%
PC-SOP (CAB)	3509.20	379.34	10.81%	1296.23	+0.50% /-0.60%	1.62%

* Neutral wire loss proportion = Neutral wire loss / Network loss

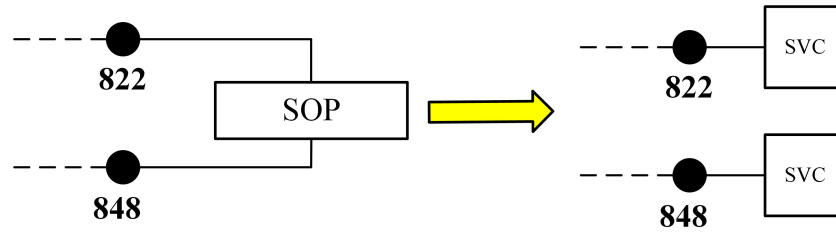


Figure 4.4: The concept of using SVCs to replace the SOP with the same capacity

Table 4.2: Spot loads of the IEEE 34-node test feeder

Node	Ph-1 kW	Ph-1 kVAr	Ph-2 kW	Ph-2 kVAr	Ph-3 kW	Ph-3 kVAr
860	20	16	20	16	20	16
840	9	7	9	7	9	7
844	135	105	135	105	135	105
848	20	16	20	16	20	16
890	150	75	150	75	150	75
830	10	5	10	5	25	10
Total	344	224	344	224	359	229

The SOCP program proposed in this research is coded by YALMIP [131], and solved by Gurobi [132]. The solving process is the primal-dual interior-point method which is a general process of how the solver solves SOCP problem, including: 1) finding the dual SOCP, 2) defining barrier for second-order cone, 3) defining primal-dual potential function, 4) finding strictly feasible initial points, and 5) using primal-dual potential reduction algorithm [129]. The proposed optimisation method is implemented with MATLAB R2019a, and the operating environment is Intel i5-5200 2.2GHz CPU, 8GB RAM. In this chapter, four types of ‘imbalances’ are classified in the test system as shown in Fig. 4.3(b).

- Peak time imbalance for the three phases: Loads in the Residential Area (around hour 7 and around hour 17) and the Commercial Area (hour 9 to hour 21) have different peak hours.
- Total load amount imbalance for the three phases: Loads in phases A, B and C have different total amount for power (456 kW, 418 kW and 429 kW at hour 1). Meanwhile, loads in phase

Table 4.3: Distributed loads of the IEEE 34-node test feeder

Node A	Node B	Ph-1 kW	Ph-1 kVAr	Ph-2 kW	Ph-2 kVAr	Ph-3 kW	Ph-3 kVAr
802	806	0	0	30	15	25	14
808	810	0	0	16	8	0	0
818	820	34	17	0	0	0	0
820	822	135	70	0	0	0	0
816	824	0	0	5	2	0	0
824	826	0	0	40	20	0	0
824	828	0	0	0	0	4	2
828	830	7	3	0	0	0	0
854	856	0	0	4	2	0	0
832	858	7	3	2	1	6	3
858	864	2	1	0	0	0	0
858	834	4	2	15	8	13	7
834	860	16	8	20	10	110	55
860	836	30	15	10	6	42	22
836	840	18	9	22	11	0	0
862	838	0	0	28	14	0	0
842	844	9	5	0	0	0	0
844	846	0	0	25	12	20	11
846	848	0	0	23	11	0	0
Total		262	133	240	120	220	114

A (169 kW) are higher than phase B (72.5 kW) and phase C (27 kW) in the Residential Area at the hour 1. Conversely, loads in phases C (402 kW) are higher than phase A (287 kW) and phase B (345.5 kW) in the Commercial Area at the hour 1. In addition, loads in phase A in the Residential Area and loads in phase C in the Commercial Area are higher than other phases in following hours.

- Location imbalance for different phase loads: Except the highest three load demand at bus 846, loads in phases A, B and C have different power distribution. In phase A, the second highest load demand is close to the middle of the feeder (bus 832). In phase B, loads are distributed evenly. In phase C, the second highest load demand is close to the end of the feeder (bus 864).

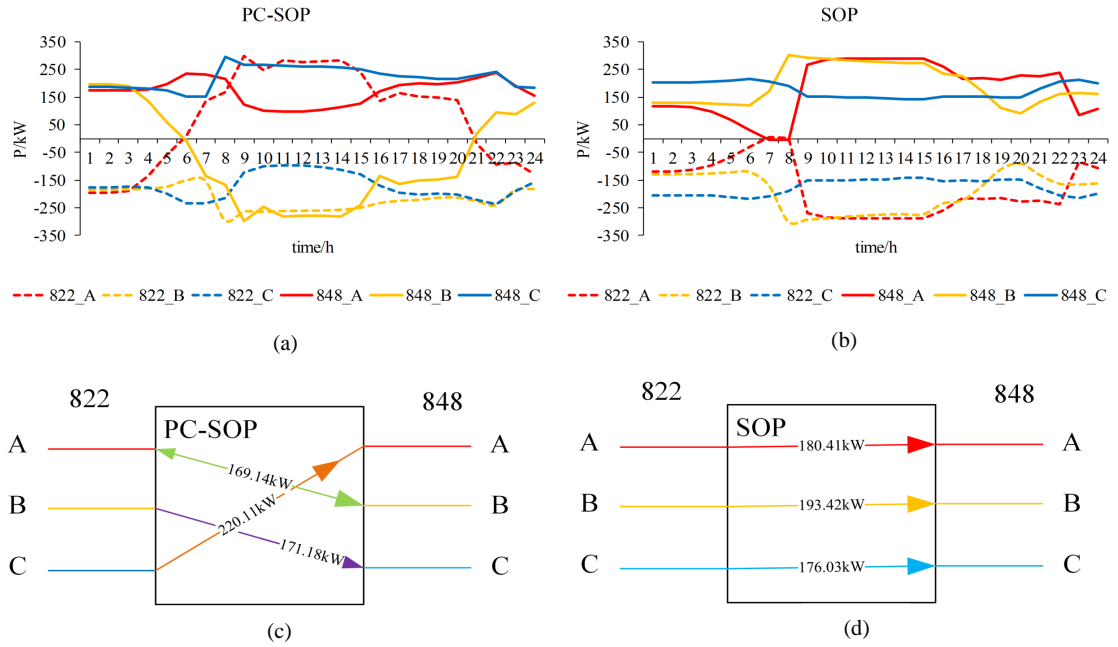


Figure 4.5: (a) PC-SOP active power outcome; (b) SOP active power outcome; (c)PC-SOP average active power outcome; (d) SOP average active power outcome

- Loads and DERs imbalance: In the Residential Area, the total power of phase A is higher than those of phase B and phase C. However, the single-phase PVs are allocated in phase B. In the Commercial Area, the total power of phase C is higher than those of phase A and phase B. However, the single-phase ESSs are allocated in phase B.

Two different connections of PC-SOP are compared with optimisation results in Table 4.1. PC-SOP (ABC to BAC) results in less PV curtailment. In contrast, PC-SOP (ABC to CAB) achieves better network performance in terms of power losses and three-phase voltage unbalance condition. In general, although these PC-SOPs with different ways of connection have individual advantages in the optimisation results, the absolute deviations between them are negligible. Therefore, here we choose the PC-SOP (ABC to BAC) to represent the PC-SOP solution for comparison with other solutions.

Four cases are designed to show the benefits of PC-SOP and coordinated optimisation of PC-

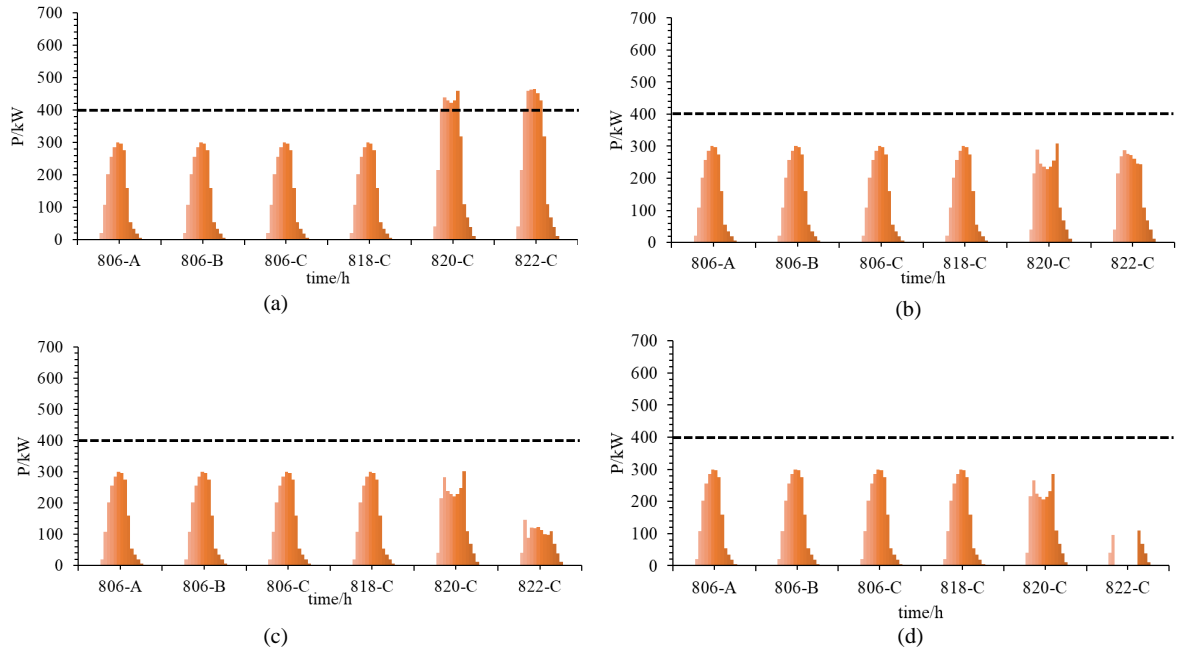


Figure 4.6: Actual PV outputs.

Table 4.4: Optimisation results comparison

	Network Losses (kW/24h)	Neutral wire loss (kW/24h)	Neutral wire loss Proportion	PV curtailment (kW/24h)	Voltage deviation	Three-phase voltage unbalance condition
Case 1	3527.77	382.86	10.86%	1208.91	0.50% /-0.60%	1.63%
Case 2	3723.85	735.67	19.76%	3449.77	+0.50% /-0.62%	2.53%
Case 3	3984.33	681.59	17.11%	4649.51	+0.5% /-0.63%	2.43 %
Case 4	4690.74	990.58	21.12%	5580.13	+0.5% /-0.76%	3.03 %

SOP and ESSs.

Case 1: the system with PC-SOP and ESSs.

Case 2: the system with conventional SOP and ESSs.

Case 3: the system with SVCs and ESSs as shown in Fig. 4.4. (The same capacity SVCs are used to replace SOP.)

Case 4: the system with only ESSs.

The results in Table 6.1 show that the PC-SOP (Case 1) can reduce network losses and PV

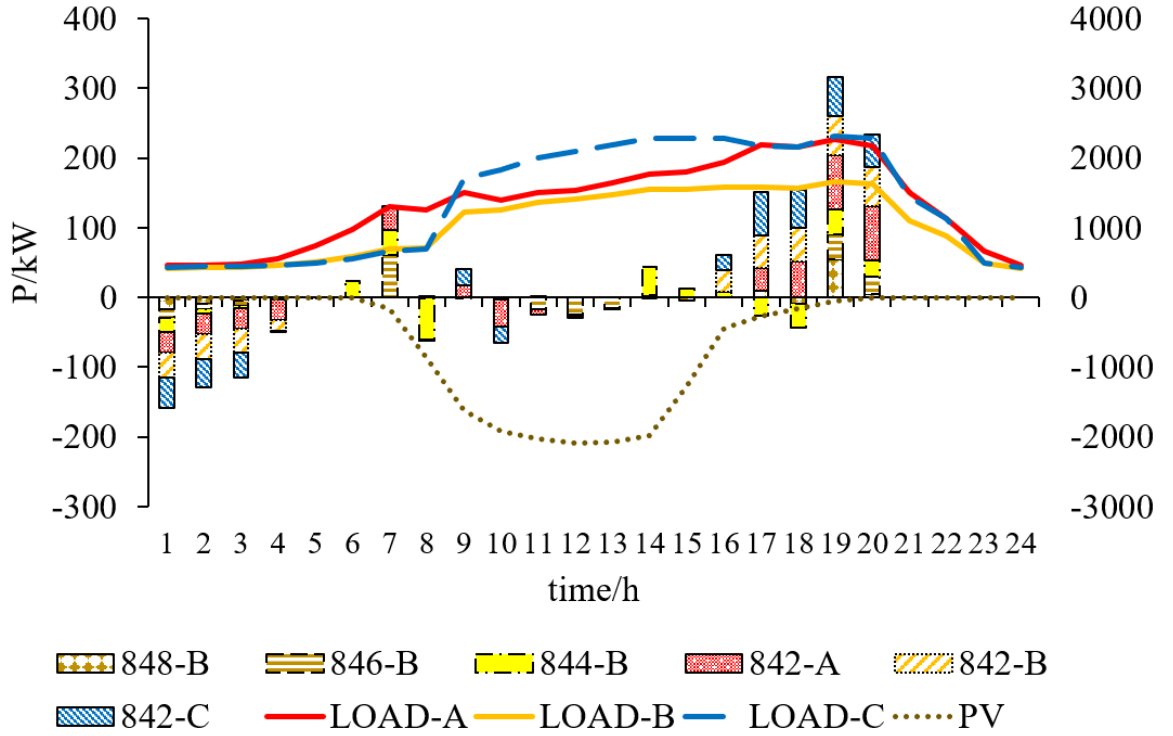


Figure 4.7: ESS output profiles

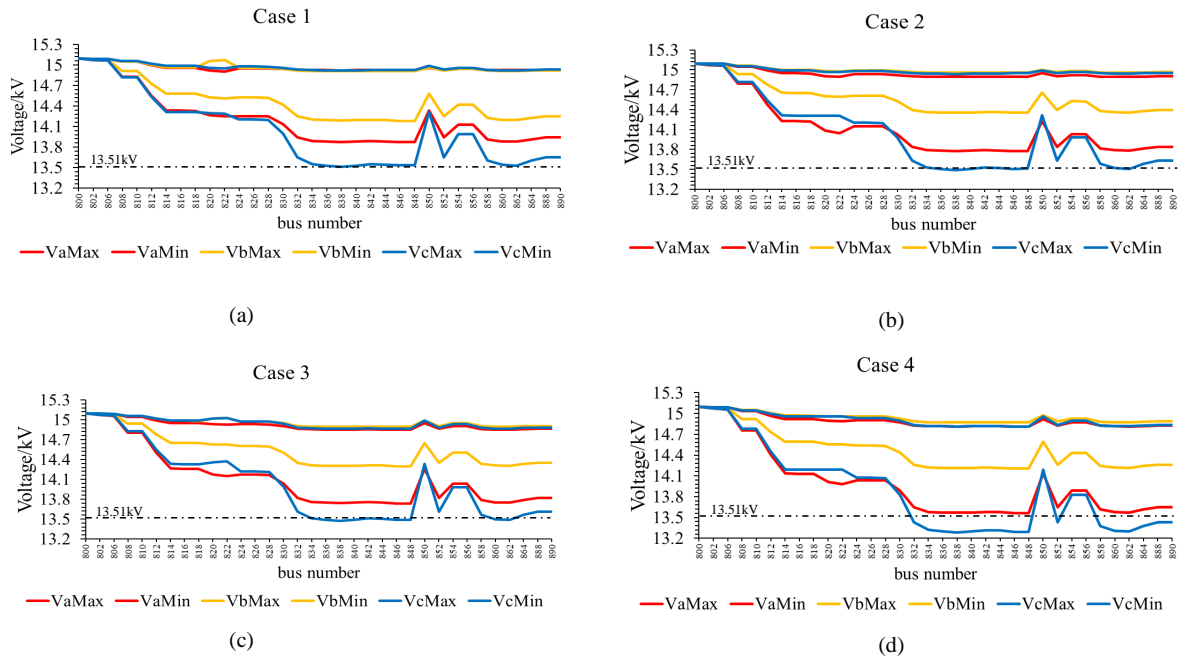


Figure 4.8: The maximum and minimum voltage of three phases - (a) Case 1; (b) Case 2; (c) Case 3; (d) Case 4

curtailment - all network losses, neutral wire losses and PV curtailment are the lowest (3527.77 kW/24h, 382.99 kW/24h and 1208.91 kW/24h respectively). Especially neutral wire loss has the lowest percentage (10.86%) among four cases. Meanwhile, the PC-SOP can considerably reduce voltage deviation and three-phase voltage unbalance condition (+0.50% /-0.60% and 1.63% respectively). In other cases, the minimum value of voltages drop out of constraints [0.94,1.10]. Compared with Case 4, the conventional SOP (Case 2) or SVCs (Case 3) can also reduce network losses and improve PV integration. The PC-SOP helps achieve optimised results and best performance of the distribution network among all four Cases. It is worth noting that the maximum neutral wire current among the four cases is 54.1 A, which is much lower than the normal phases (maximum 236.72A) hence not considered as critical constraints.

This will be discussed in detail from four aspects: 3.1 Active Power Controlled by SOP, 3.2 PV Curtailment and ESSs Utilisation, 3.3 Reactive Power Compensation by SOP and Voltage Profile and 3.4 Algorithm Validation.

4.5.1 Active power controlled by the PC-SOP

The PC-SOP, compared with the conventional SOP, can transfer more power and utilise the network capacity better in unbalanced systems. It can provide links between loads and DERs in different phases, as shown in Fig. 4.5. Differences in transmitted power between the PC-SOP and the SOP are analysed in detail as follows:

- In general, power is transferred from the Residential Area to the Commercial Area because PVs are installed in the Residential Area for both Case 1 and Case 2.
- The operational power of the PC-SOP is greater than that of the SOP. The average active power of the PC-SOP is 186.81 kW. The average active power of the conventional SOP is

183.29 kW.

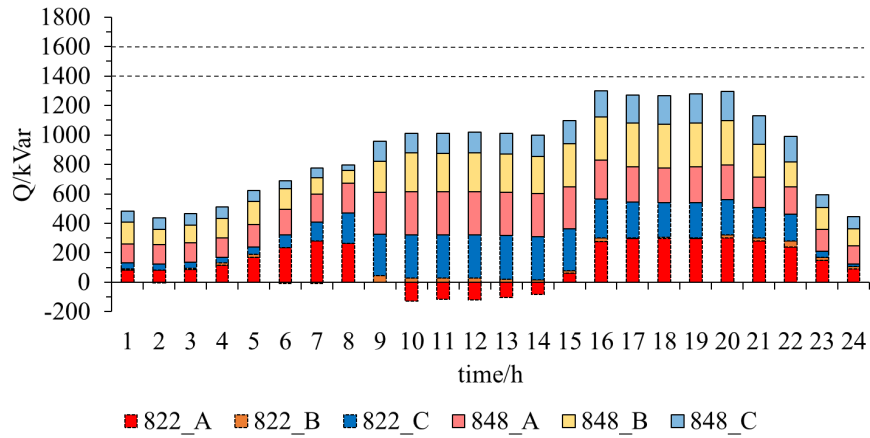
- When the Residential Area loads achieve peak value at hour 7 (especially phase A), the PC-SOP can transfer power from the Commercial Area to the Residential Area while the conventional SOP cannot achieve that. This explains why there is bi-directional power transfer in Case 1 between 822 phase A and 848 phase B (shown as the green arrow in Fig. 4.5(c)).

4.5.2 PV curtailment and ESS utilisation

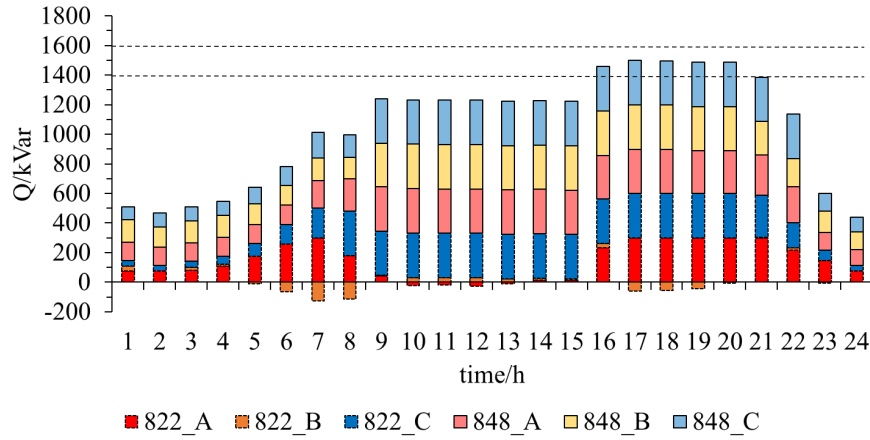
PV Curtailment: in Fig. 4.6, Case 1 shows maximised PV outputs for all installed locations; while Case 4 shows the overall minimal. For three-phase PV 806 and single-phase PV 818, there is nearly no PV curtailment in all four Cases. This is due to that these PVs are on or close to the main system's wire. PVs 820 and 822 hardly generate power which ranges from 0 to 300 kW in Cases 2, 3 and 4. However, the PC-SOP in Case 1 can make the system effectively utilise different phase resources - the outputs of all PVs 820 and 822 in Case 1 exceed 400 kW, because the PC-SOP effectively acts as a bridge to provide a path of power transfer between DERs and loads from different phases (between PVs in phase B and the highest load demand in the Commercial Area in phase C).

ESS Utilisation: ESSs in combination with the PC-SOP can achieve the power regulation by shifting ESS charging or discharging meanwhile the PC-SOP can accomplish the spatial power transfer between different phases by flexibly connecting different phases from adjacent feeders in Fig. 4.7.

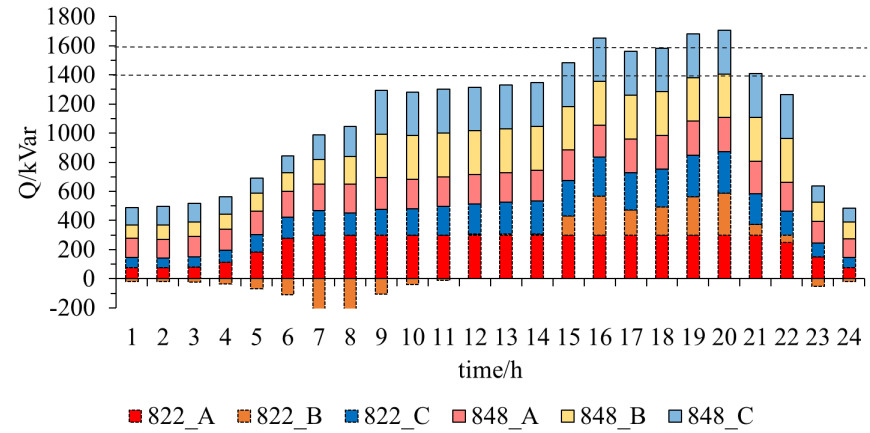
In Period 1 (hour 1 to hour 5), load demand is relatively low and ESSs store energy.



(a)



(b)



(c)

Figure 4.9: Reactive power outcomes - (a) PC-SOP reactive power of Case 1; (b) SOP reactive power of Case 2; (c) SVC reactive power of Case 3

In Period 2 (hour 6 to hour 16), ESSs output power at hour 7 (dashed square 1) because phase A demand is high in the Residential Area. ESSs output power not only in phase A (842-A) but also in phase B (848-B and 844-B). ESSs in phase B are also linked to loads in phase A by the PC-SOP. Because of the PC-SOP, PV's output power in phase B is directly transferred to other phase loads. Therefore, ESSs didn't need to store a lot of energy from hour 8 to hour 16.

In Period 3 (hour 17 to hour 20), ESSs output power is the highest, because PVs stop to output at night when load demands are still high (dashed square 2).

In Period 4 (after hour 20), load demands decrease and ESSs stop outputting power .

4.5.3 Reactive power compensation and voltage profile

Reactive Power Compensation: The PC-SOP can achieve better voltage profiles and reduce three-phase voltage imbalance in Case 1 than those in Cases 2 and 3 with less reactive power support, as shown in Fig. 4.8 and Fig. 4.9. That means the PC-SOP's capacity is better utilised for transferring active power. Meanwhile, the PC-SOP sees less reactive power (maximum output not above 1400 kVar) in the system than SOP (maximum output between 1400 kVar and 1600 kVar) and SVC (maximum output above 1600 kVar). Meanwhile, experimental data illustrates that the system with the PC-SOP can use PVs' reactive power (4414.70 kVar) more than other cases (4056.46 kVar, 2982.98 kVar and 3208.04 kVar). Therefore, systems with the PC-SOP can utilise PVs' reactive power better and leave more capacities for the PC-SOP to transfer active power.

Voltage Profile: In Case 1, no bus voltage is lower than 13.5134 kV (\underline{V}_i , minimum statutory limit of 94%). In Case 2, Case 3 and Case 4, there are six buses, ten buses and sixteen buses whose voltages are lower than 13.5134 kV (\underline{V}_i) during the 24-hour operational period,

respectively. By comparing Case 1 and Case 4 in Fig.4.8, it can be seen that the PC-SOP did not make the operation of any other buses deteriorate. Instead, it improves all bus voltages: not only the voltages at buses 822 and 848 (where the PC-SOP is connected in between) but also, the voltages at other buses (minimum voltage buses over 24 hours, i.e., in Case 4, 832, 834, 836, 838, 840, 842, 844, 846, 848, 852, 858, 860, 862, 864, 888, 890, which are the majority of the Commercial Area buses; the other four buses 828, 830, 854, 856 are the buses close to the Residential Area and their voltages are above 94%). Thus, by connecting the PC-SOP, the transferring of unbalanced power improves voltage performance not only at buses near PC-SOP but also at all other buses, to ensure the system voltages at all buses are always within the statutory limits specified.

4.5.4 Algorithm validation

Algorithm accuracy validation

The computation information of the four cases is shown in Table 4.5. It can be seen that the maximum deviation of convex relaxation converges to the predefined calculation precision (1×10^{-8} p.u.) in around 15 iterations. Thus, the SOCP-based approach calculates distribution system power flow with the PC-SOP with acceptable accuracy. Here, IPOPT (Interior Point OPTimiser) is also used to solve the same instances again to verify the accuracy and efficiency of the proposed method. IPOPT is a software library for large-scale nonlinear optimisation of continuous systems [143]. It can be observed that the proposed method obtains the desirable solution of the flexibility evaluation problem with an improved computational efficiency, compared with the IPOPT package. Because of the convexification and the proper relaxation of the original problem, the SOCP-based method reduces the solving complexity (within 36 seconds) and obtains the solutions with a reasonable accuracy. This creates possibilities for

modelling larger test feeders (e.g. IEEE 8500-node test feeder).

Table 4.5: Computation information of the four cases and performance comparison between the proposed method and IPOPT

Case	Proposed method				IPOPT	
	Iteration steps	Gap (p.u.)	Evaluation index*	Time (s)	Evaluation index*	Time (s)
1	16	1.37E-08	3527.77	34.835	3527.77	368.489
2	17	8.98E-10	3723.85	35.176	3723.86	356.376
3	15	2.76E-09	3984.33	35.850	3984.33	362.182
4	15	4.23E-12	4690.74	27.083	4690.74	256.200

* Evaluation index - total power loss f^{loss} .

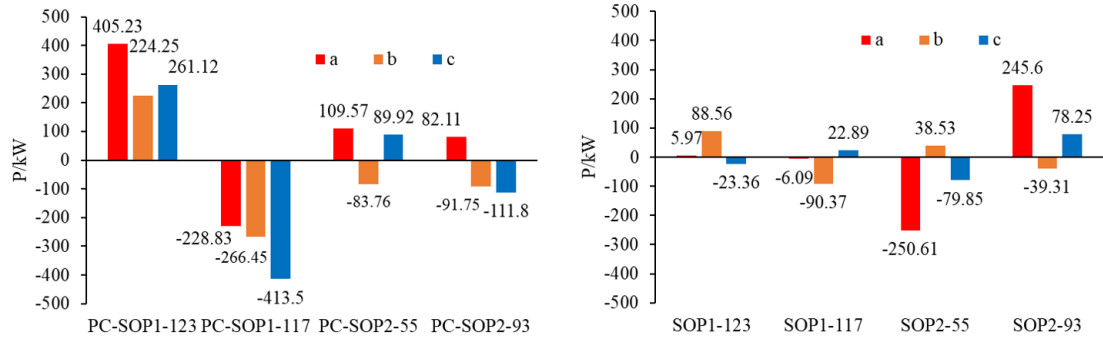
Algorithm scalability validation

In [56], the IEEE 123-node distribution system is used to verify the scalability of the optimal operation of conventional SOPs on large-scale ADNs with severe unbalanced conditions. Results show that regulating the operation of SOPs in ADNs can reduce power losses, mitigate three-phase unbalanced condition and effectively mitigate each phase voltage deviation from the nominal value to improve the voltage profile compared with cases without SOP.

To cross compare the results and benefits, here the proposed PC-SOP is analysed further with the same system, capacities of SOPs, and allocation of PVs. The way of connection under analysis of two PC-SOPs is ABC to CAB. Four scenarios are analysed and compared as fol-

Table 4.6: Optimisation results of the four scenarios with IEEE 123-node test feeder

Scenario	Power losses for three phase (kW)	Power losses for neutral wire (kW)	Three-phase unbalance condition	Voltage deviation	Time (s)	IPOPT	
						Power losses for three-phase (kW)	IPOPT Time (s)
I	93.84	10.66	0.08%	0% /-0.35%	1.54	93.84	14.52
II	67.29	8.32	0.12%	0% /-0.22%	1.44	67.29	13.59
III	80.08	6.47	0.07%	0% /-0.30%	1.33	80.08	12.47
IV	63.93	6.02	0.10%	0% /-0.19%	1.32	63.93	12.47



(a) Three-phase active power outputs of PC-SOP (b) Three-phase active power outputs of SOP

Figure 4.10: Comparison of active power outputs of SOP and PC-SOP

lows:

Scenario I: No PV integration in the system, the unbalanced optimal operation is conducted based on SOPs ('Scenario II' in [56]).

Scenario II: Considering 60 % penetration of PVs, the unbalanced optimal operation is conducted based on SOPs ('Scenario IV' in [56]).

Scenario III: No PV integration in the system, the unbalanced optimal operation is conducted based on PC-SOPs.

Scenario IV: Considering 60 % penetration of PVs, the unbalanced optimal operation is conducted based on PC-SOPs.

Comparison results in Table 4.6 show that, for both scenarios with and without unbalanced DER (PVs), PC-SOP has consistent benefits in all aspects: reducing power losses (i.e. from 93.84 kW to 80.08 kW, and from 67.29 kW to 63.93 kW, respectively), three-phase unbalance condition (from 0.08 % to 0.07 %, and from 0.12 % to 0.10 %) and voltage deviation (from 0.35 % to 0.30 %, and from 0.22 % to 0.19 %), compared with conventional SOP. The reason

in essence is that PC-SOP can transmit more active power and utilise its capacity better than conventional SOP (from below 300kW to up to 400kW), as shown in Fig. 6.5.

In addition, the computation efficiency and robustness of the proposed method are checked again by comparing results with IPOPT in Table 4.6. The simulation speeds of the implementations again are consistently improved compared with IPOPT from minimum 12.47 s to 1.32 s. Moreover, it makes not much difference in simulating different scenarios of SOPs and PC-SOPs.

As shown from the above results and analysis, by optimising the operations of the PC-SOP and ESSs, OPF of the three-phase active and reactive power of the system can be achieved. Unbalanced condition is further improved, and the operational losses are further decreased by the PC-SOP compared with the conventional SOP and SVCs in both the IEEE 34-node and the 123-node test feeders.

4.6 Conclusion

This chapter presents a new way of SOP connections called phase-changing SOP (PC-SOP). An optimised operational strategy based on PC-SOPs is proposed to minimise the operational losses, three-phase imbalances, considering growing penetration levels of DERs for unbalanced three-phase four-wire distribution networks. Compared with conventional SOPs and SVCs, the optimisation results indicate that PC-SOPs significantly reduce unbalanced loading conditions and power losses (especially neutral wire losses) in ADNs. PC-SOP can also make improved use of ESSs in unbalanced systems by transferring power between different phases. Furthermore, the proposed approach can provide support during the planning and installation

stages, with a new solution and concept of PC-SOP, especially when it is required to improve unbalanced loading conditions. For system operators, it can help to achieve a 24-hour optimal plan of ADNs with the addition of flexible and controllable resources such as PC-SOPs, PVs and ESSs in smart distribution systems. For reducing the three-phase four-wire imbalance AC/DC hybrid networks are another solution with flexible DC links worthing discussed.

The limitation of the proposed method is limited to the hourly operation. For three-phase imbalance in ADNs, the coordination and time-response between PC-SOP and other phase transferring techniques require further research, taking into account the robustness of the three-phase imbalance system optimisation and capital investment of power-electronic switches.

Chapter 5

Adapting AC Lines for DC Power Distribution to Reduce the Power Imbalance in Three-Phase Four-Wire Systems

5.1 Introduction

This chapter proposes an optimised operational strategy for AC/DC hybrid networks and optimal ESSs dispatch, reducing the three-phase four-wire imbalances while enhancing the operational efficiency of ADNs. DC networks of AC/DC hybrid networks can seem like a general concept 'SOP' to AC networks. The contributions of this study are summarised as follows:

- The benefits of adapting AC lines for DC power distribution for the unbalanced three-phase four-wire system are analysed. Hybrid AC/DC networks based on optimal operation strategy for unbalanced ADNs is proposed considering power losses in the neutral wire.

- The optimized power flow of AC/DC networks is mathematically a non-convex nonlinear problem. The original non-convex nonlinear optimization model is converted into an SOCP formulation which can be solved with global optimum and high problem-solving efficiency.
- Demonstrated by a case study, by adapting AC lines to DC power distribution and optimizing the regulation of voltage-source converters (VSCs), significant impacts of optimal energy losses and effective voltage regulation are simultaneously achieved by the proposed approach.

5.2 Strategy of Adapting AC Lines for DC Power Distribution

In this research, the process of adapting AC lines to DC power distribution is proposed as shown in Figure 7.4.

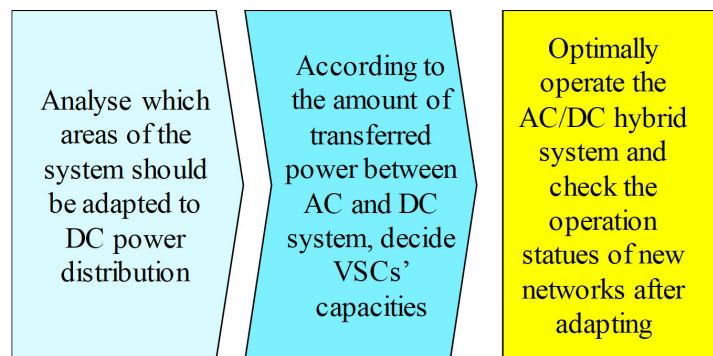


Figure 5.1: The process of adapting AC lines to DC power distribution

There are three principles proposed to locate appropriate lines that should be adapted to DC, as the first step of the process.

- where voltage violation is the most seriously outside the required range;

- where the neutral-wire voltage is the highest;
- where ESSs and DERs are installed, as DC power distribution can increase DER accommodation [89].

VSCs are power electronic devices installed between AC lines and DC lines, as shown in Figure 5.2. Their capacities should be larger than the needs of exchanged power between AC lines and DC lines. The maximum exchanged power is determined by the maximum DER's output or maximum load demand.

$$\sum S^{VSC} \geq \text{Max}(|P^{DER} - P^{Load}|) \quad (5.1)$$

where S^{VSC} is the capacity of VSCs; P^{DER} is DER's active power in the DC system; P^{Load} is loads' active power in the DC system.

The above equation can make sure that extra DERs' output in DC systems can be transferred to AC systems or DC loads can get enough power from AC systems when DC DERs' output cannot meet DC load demand.

After adapting, the voltage of all buses should operate within their ranges and the network performance should be improved.

5.3 Modelling of AC/DC Hybrid Networks with PVs, VSCs and ESSs

1) Modelling of VSCs:

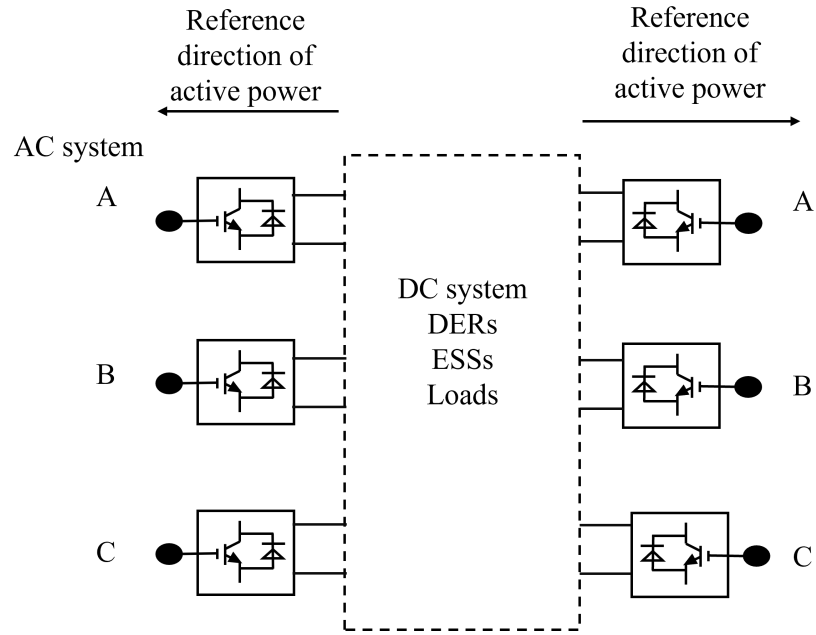


Figure 5.2: AC and DC systems linked by two VSCs

VSC Active Power Constraints:

$$P_{i,t}^{VSCx,\varphi} + P_{j,t}^{VSCx} = 0 \quad i \in \Omega_n \quad j \in \Omega_{nDC} \quad (5.2)$$

where $P_{i,t}^{VSCx,\varphi}$ is VSCx's active power for AC system; $P_{j,t}^{VSCx}$ is VSCx's active power for DC system; φ represents phase A, B or C; n is the number of AC nodes in the network; m is the number of AC buses; $n = 4 \times m$ represents that each AC bus has 4 wires; Ω_{nDC} is the number

of DC nodes in the network. And VSCs' Capacity Constraint for AC system:

$$\sqrt{P_{i,t}^{VSCx,\varphi} + Q_{i,t}^{VSCx,\varphi}} \leq S_i^{VSCx} \quad (5.3)$$

where $Q_{i,t}^{VSCx,\varphi}$ is the reactive power of VSCs at phase φ at node i at time t ; S_i^{VSCx} is the apparent power capacity of VSCx at node i .

2) Objective function:

A multi-objective linear combination is presented with minimum total power losses, the voltage deviation and the voltage unbalance condition. Minimum total power loss can reduce the network operational cost during network operation. Minimum voltage deviation can improve the customer-side voltage and power quality. Minimum the voltage unbalance condition can improve the network life and ensure networks operate close to a balanced condition:

$$\min f = W_\alpha \cdot f^{loss} + W_\beta \cdot f^{V,deviation} + W_\gamma \cdot f^{VUF} \quad (5.4)$$

where W_α, W_β and W_γ are the wight for each factor; the power losses f^{loss} (including AC parts f_{AC}^{loss} and DC part f_{DC}^{loss}); the voltage deviation $f^{V,deviation}$; the voltage unbalance factor f^{VUF} .

Each function is formulated as follows:

$$f^{loss} = f_{AC}^{loss} + f_{DC}^{loss} = [I_{branch,real}^2 + I_{branch,imag}^2] \cdot R + I_{branch,DC}^2 \cdot R_{DC} \quad (5.5)$$

$$f^{V,deviation} = |\vec{V}_t - V_{nominal}| + |\vec{V}_{t,DC} - V_{nominal,DC}| \quad (5.6)$$

$$f^{VUF} = \text{sum}(VUF_m) \quad (5.7)$$

where $I_{branch,real}$ and $I_{branch,imag}$ are the real part and imagine part of I_{branch} ; I_{branch} is an $l \times 1$

vector containing all the AC currents (l is the number of AC branches); $I_{branch,DC}$ is an $l_{DC} \times 1$ vector containing all the DC currents (l_{DC} is the number of DC branches); R is the resistance of AC system; R_{DC} is the resistance of DC system; \vec{V}_t is an $n \times 1$ vector containing the AC voltages at each node at time t ; $\vec{V}_{t,DC}$ is an $n_{DC} \times 1$ vector containing the DC voltages at each node at time t ; VUF_m is the voltage unbalance factor at bus m (only for AC part).

3) Three-phase four-wire system operational constraints:

Power flow constraints: This branch flow model is proposed for three-phase four-wire networks in [101]. It can be described mathematically with the following constraints. The nodal admittance matrix is the core of calculating power flows following Kirchhoff's Current Law (KCL) [108] in this research

$$[Y]\vec{V}_t = I_{inj,t} \quad (5.8)$$

where $[Y]$ is the $n \times n$ nodal admittance matrix, $I_{inj,t}$ is the $n \times 1$ vector containing all currents drawn or injected into the network at time t .

The loads, DERs, SOPs and ESSs are modelled as current injections.

$$I_{inj,t}^{load} = \frac{P_{i,t}^{load} - j \cdot Q_{i,t}^{load}}{V_{n,i}^*} \quad (5.9)$$

$$I_{inj,t}^{DER,SOPorESS} = \frac{1}{V_{n,i}^*} (P_{i,t}^{DER,SOPorESS} - j \cdot Q_{i,t}^{DER,SOPorESS}) \quad (5.10)$$

$$I_{inj,t} = \text{sum}(I_{inj,t}^{DER,SOPorESS}) - I_{inj,t}^{load} \quad (5.11)$$

where $I_{inj,t}^{load}$ is the current drawn by load at time t ; $P_{i,t}^{load}$, $Q_{i,t}^{load}$ are the real and reactive load powers at node i at time t ; $P_{i,t}^{DER,SOPorESS}$ are the active powers of DERs, SOPs, or ESSs at node i at time t ; $Q_{i,t}^{DER,SOPorESS}$ are the reactive powers of DERs, SOPs, or ESSs at node i at time t ; $I_{inj,t}^{DER,SOPorESS}$ are the current contribution from DERs, SOPs, or ESSs. Here $V_{n,i}$

(nominal voltage at node i) are used to approximate the $V_{i,t}$ (variable, the voltage at node i at time t), because voltage deviations are relatively small compared with the changes of load, DERs, SOPs or ESSs. The accuracy of the approximation in assumption has been proved in [101].

Voltage limits: Each bus voltage can be expressed as a linear combination of the injected currents.

$$V_{i,real,t} = Re([Y_i^*]^{-1}) \cdot I_{inj,real,t} - Im([Y_i^*]^{-1}) \cdot I_{inj,imag,t} \quad (5.12)$$

$$V_{i,real,t} = Re([Y_i^*]^{-1}) \cdot I_{inj,real,t} + Im([Y_i^*]^{-1}) \cdot I_{inj,imag,t} \quad (5.13)$$

$$V_{i,real,t}^2 + V_{i,imag,t}^2 \leq \bar{V}_i^2 \quad (5.14)$$

$$-K_{1A}V_{i,real,t} - K_{2A}V_{i,imag,t} \leq -\underline{V}_i, \quad i \in \text{phase A} \quad (5.15)$$

$$-K_{1B}V_{i,real,t} - K_{2B}V_{i,imag,t} \leq -\underline{V}_i, \quad i \in \text{phase B} \quad (5.16)$$

$$-K_{1C}V_{i,real,t} - K_{2C}V_{i,imag,t} \leq -\underline{V}_i, \quad i \in \text{phase C} \quad (5.17)$$

where $V_{i,real,t}, V_{i,imag,t}$ are the real part and imaginary part of $V_{i,t}$; $\bar{V}_i, \underline{V}_i$ are the maximum and minimum allowable steady-state voltage magnitudes at node i .

Based on the fact that the approximate voltage angle is known at all phase nodes, the constants $K_{1A}, K_{2A}, K_{1B}, K_{2B}, K_{1C}, K_{2C}$ can be chosen to minimise the weighted average squared approximation error over an angle deviation of ± 10 degrees from the approximate voltage angle [133].

Voltage imbalance constraints:

$$VUF_{m,t} = \frac{V_{m,t}^a + \alpha^2 V_{m,t}^b + \alpha V_{m,t}^c}{V_{m,t}^a + \alpha V_{m,t}^b + \alpha^2 V_{m,t}^c} \approx \frac{V_{m,t}^a + \alpha^2 V_{m,t}^b + \alpha V_{m,t}^c}{V^\varphi} \quad (5.18)$$

$$VUF_{m,t}^2 \leq \overline{VUF_m}^2 \quad (5.19)$$

where $V_{m,t}^\varphi$ is the phase φ voltages at bus m at time t ; α is the phasor rotation operator, $1 \angle 120^\circ; \overline{VUF}_m$ is the maximum allowable voltage unbalance factor at bus m .

Current limits: The current through a branch connecting nodes i and j is then:

$$|I_{ij,t}| = \sqrt{(G_{ij}^2 + B_{ij}^2)} \cdot \sqrt{(V_{i,real,t} - V_{j,real,t})^2 + (V_{i,real,t} - V_{j,imag,t})^2} \quad (5.20)$$

and
$$|I_{ij,t}|^2 \leq \overline{I}_{ij}^2 \quad (5.21)$$

where $I_{ij,t}$ is the current of branch connecting nodes i and j at time t ; G_{ij}, B_{ij} are the branch conductance and susceptance respectively; \overline{I}_{ij} is the current limit of the branch connecting nodes i and j [134].

Branch current limits:

$$I_{branch,t} = [M] \vec{V}_t = [M][Y]^{-1} I_{inj,t} \quad (5.22)$$

where $[M]$ is the $l \times n$ connection matrix.

4) DC system operational constraints:

$$\sum_{k \in \psi_i} P_{ik,t} = \sum_{j \in \phi_i} (P_{ji,t} - R_{ji}(I_{ji,t})^2) + P_{i,t} \quad (5.23)$$

$$P_{i,t} = P_{i,t}^{DER} + P_{i,t}^{ESS} - P_{i,t}^{VSC} - P_{i,t}^{load} \quad (5.24)$$

$$(V_{i,t})^2 = (V_{j,t})^2 - 2R_{ji}P_{ji,t} + R_{ji}^2 I_{ji,t}^2 \quad (5.25)$$

where ϕ_i is the set of the start nodes from the DC system whose start node is i ; ψ_i is the set of the end nodes from the DC system whose end node is i ; $\phi_i, \psi_i \in \Omega_{nDC}$; R_{ji} is the resistance of

branch ij ; $P_{ji,t}$ is the active power from node j to node i ; $P_{i,t}$ is active power injections of node i ; $P_{i,t}^{ESS}$ is the active power of the energy storage at node i at hour t ; $P_{i,t}^{DER}$ is the active power of DERs of node i at hour t ; $P_{i,t}^{load}$ is the active power of load of node i at hour t ; $V_{i,t}$ is the voltage of node i at hour t .

5) Constraints of energy storage systems and DERs output:

Constraints of energy storage:

$$\left\{ \begin{array}{l} E_{i,t} = E_{i,t-1} + P_{i,t}^{ESS} \\ |P_{i,t}^{ESS,c}| \leq |P_{i,t}^{ESS}| \leq |P_{i,t}^{ESS,d}| \\ E_i^{ESS} SOC_{min} \leq E_{i,t} \leq E_i^{ESS} SOC_{max} \end{array} \quad i \in phaseA, BorC \right. \quad (5.26)$$

where $P_{i,t}^{ESS}$ is the energy storage charging power or discharging power at node i at time t ; $P_{i,t}^{ESS,c}$, $P_{i,t}^{ESS,d}$ are the energy storage charging and discharging power limits at node i at time t ; $E_{i,t}$ is the energy storage present state at node i ; E_i^{ESS} is the energy storage capacity at node i ; SOC_{min} , SOC_{max} are the minimum and maximum states of charge.

Constraints of DER output:

$$\left\{ \begin{array}{l} 0 \leq P_{i,t}^{DER} \leq P_{i,t}^{DER,max} \\ 0 \leq Q_{i,t}^{DER} \leq Q_{i,t}^{DER,max} \end{array} \quad i \in phaseA, BorC \right. \quad (5.27)$$

where $P_{i,t}^{DER,max}$, $Q_{i,t}^{DER,max}$ are the maximum active and reactive powers of DER at node i at time t .

5.4 Second-Order Cone Transforming

The SOCP model of VSC capacity constraint for optimization:

$$\| [P_{i,t}^{VSCx,\phi}, Q_{i,t}^{VSCx,\phi}] \|_2 \leq S_i^{VSCx} \quad (5.28)$$

where $\| \dots \|_2$ is the Euclidean norm [129] which is the standard form of the SOCP.

Voltage and current limits of AC networks model can be converted to an SOCP model:

$$\| [V_{i,real,t}, V_{i,real,t}] \|_2 \leq \bar{V}_i \quad (5.29)$$

$$\sqrt{(G_{ij}^2 + B_{ij}^2)} \| [(V_{i,real,t} - V_{j,real,t}), (V_{i,real,t} - V_{j,imag,t})] \|_2 \leq |\bar{I}_{ij}| \quad (5.30)$$

For DC networks, with $I_{branch,DC}^2$, $(I_{ij,t})^2$ and $(V_{i,t})^2$ replaced by $l_{branch,DC}$, $l_{ij,t}$ and $v_{i,t}$, objects and power flow constraints can be expressed as follows:

$$f_{DC}^{loss} = l_{branch,DC} \cdot R_{DC} \quad (5.31)$$

$$l_{ij,t} = \frac{P_{ij,t}^2}{v_{i,t}} \quad ij \in \Omega_{bDC} \quad i \in \Omega_{nDC} \quad (5.32)$$

$$\sum_{k \in \Psi_i} P_{ik,t} = \sum_{j \in \Phi_i} (P_{ji,t} - R_{ji}(l_{ji,t})) + P_{i,t} \quad (5.33)$$

Equation 5.25 can be further loosed and transformed into the form of SOCP.

$$\| [2P_{ij,t} \quad l_{ij,t} - v_{i,t}]^T \|_2 \leq l_{ij,t} + v_{i,t} \quad (5.34)$$

5.5 Methodology: Design of the Experiment

There are four types of imbalance for the design of the experiment in the test system as shown in Figure 5.3. The loads at all buses are shown in Table 5.1. These types of imbalance cause two major problems shown in Figure 5.4 and Figure 5.5.

- Peak time imbalance from different phases: Loads in phases A, B and C have different peak hours (3h, 11h, 15h).
- Load capacity imbalance for the three phases: Loads in phases A, B and C have different total amounts for power (35.69kW, 42.75kW, 38.14kW).
- Location distribution imbalance from different phases: Loads in phases A, B and C have different power distribution (In phase A, the highest load demand is close to the middle of the feeder (bus 9). In phase B, the highest load demand is close to the beginning of the feeder (bus 1). In phase C, the highest load demand is close to the end of the feeder (bus 14)).
- The imbalance between loads and DER: The total power of phase B is higher than those of phase A and phase C. However, the PVs and ESSs are allocated in phase A.

In this section, a distribution network as shown in Figure 5.3 is used as a test system to analyse and verify the proposed model. The SOCP model with three-phase four-wire system is coded by YALMIP [131] and solved by Gurobi [132] in this research. The simulation of the adapting AC lines for DC power distribution model is carried out using MATLAB R2019a, and the operating environment is Intel i5-5200 2.2GHz CPU, 8GB RAM.

The system is a modified 415V 3-phase 4-wire system in the city centre of Birmingham in

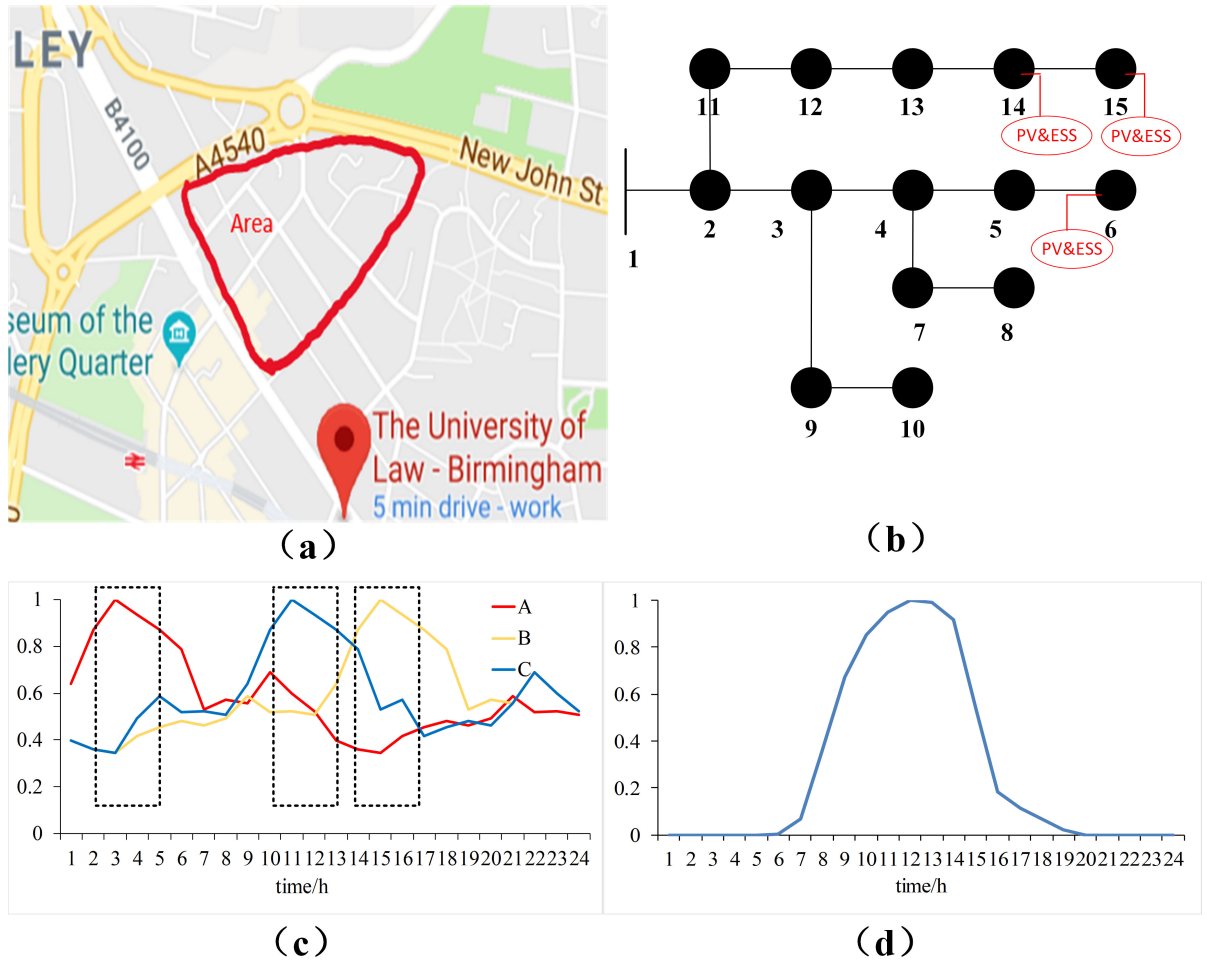
Table 5.1: Active power and reactive power demand at all buses of the test system (Cells in red represent the highest bus load of one phase; Cells in green represent the highest total load among three phases)

Bus number	Pa/kW	Qa/kVA	Pb/kW	Qb/kVA	Pc/kW	Qc/kVA
2	0	0	6.83	2.24	0	0
3	0	0	0	0	0	0
4	4.14	1.37	4.02	1.32	2.84	0.93
5	2.2	0.72	3.3	1.09	1.9	0.62
6	3.31	1.09	0	0	5.09	1.67
7	2.02	0.67	5.51	1.81	2.15	0.71
8	3.68	1.2	4.59	1.51	2.32	0.76
9	5.94	1.95	4.17	1.37	5.29	1.74
10	3.52	1.16	1.93	0.64	2.42	0.79
11	3.35	1.11	3.82	1.25	4.73	1.55
12	0	0	0	0	0	0
13	3	0.99	2.34	0.77	3.42	1.13
14	2.37	0.78	1.13	0.37	5.12	1.69
15	2.18	0.71	5.12	3.98	2.85	0.94
Sum	35.69	11.73	42.75	16.35	38.14	12.54

England in the UK, considering daily load profiles of residential customers and PV profiles. The per-unit voltage range of the system is set to be [0.94, 1.10] as the statutory limits in the UK [144]. The DERs (including PVs and ESSs) are required to operate with a fixed power factor of 0.95. Five PVs are installed at buses 6, 14 and 15 in phase A with a capacity of 10 kW each. Five ESSs are installed at buses 6, 14 and 15 in phase A with a capacity of 5 kW each. All ESSs' initial state of charge (SOC) is default value as 0.5, with a range from 0.2 to 0.8.

5.6 Case Studies

There are two problems caused by four types of imbalance. One is voltage cannot operate with limits. Figure 5.4 shows the minimum voltage drop out of 0.94 (especially bus 6, bus 8 and bus 15).



- * This test feeder is an actual feeder located modified 415V 3-phase 4-wire system in the city centre of Birmingham in England in the UK.
- * Load profiles from Standard Load Profile [136]
- * PV generation profile from Photovoltaic Solar Panel Energy Generation data [137]

Figure 5.3: (a) The map of the area of the modified system; (b) The topology of the test system ;(c) Single-phase load profiles; (d) Individual PV generation profile

Another one is that at hour 12 to 15, the neutral-wire voltage is high especially for bus 6 to bus 8, shown in Figure 5.5. That is mainly because of the load and DER imbalance as mentioned above.

Therefore, buses 6, 8 and 15 are the potential places where installation of new equipment is required to improve the network performance. Considering that PVs and ESSs' positions, buses 6, 14 and 15 and wires between these buses are adapted for DC power distribution (DC

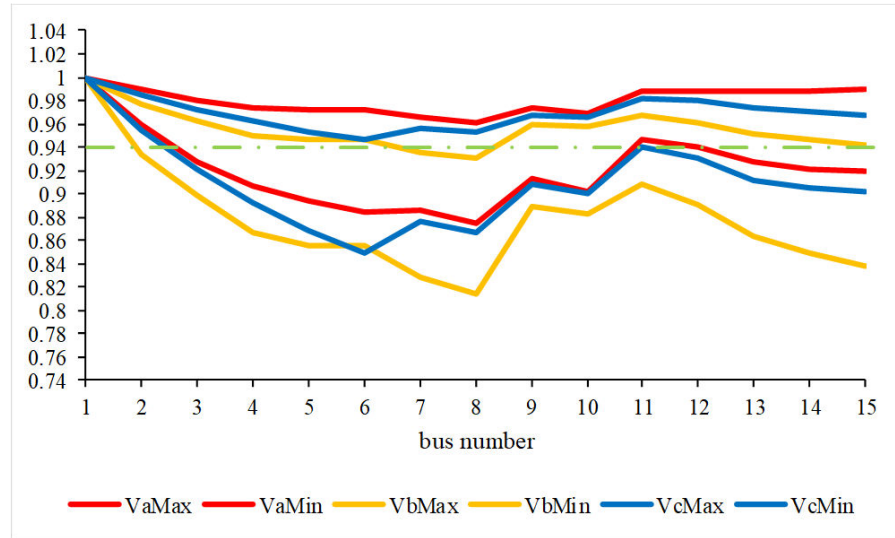


Figure 5.4: The maximum and minimum voltages of three phases of the original network for 24 hours

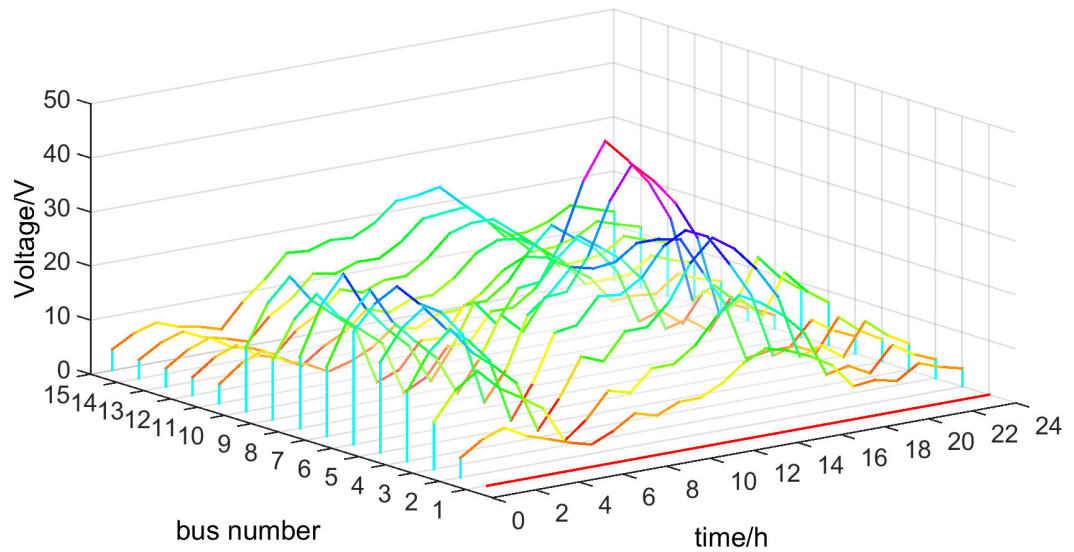


Figure 5.5: The neutral-wire voltage profiles of the original network

solution). The solution proposed in this research considers improvement of both the network performance and DER's integration. Original 415V AC networks are adapted to 400V DC networks [145]. The maximum power gap between PV and Load is 17.37 kW. AC and DC systems are linked by two VSCs whose capacities are 10 kVA. The total capacity of VSCs is 20 kVA is larger than 17.37 kW. The remaining capacity can be utilized to supply reactive

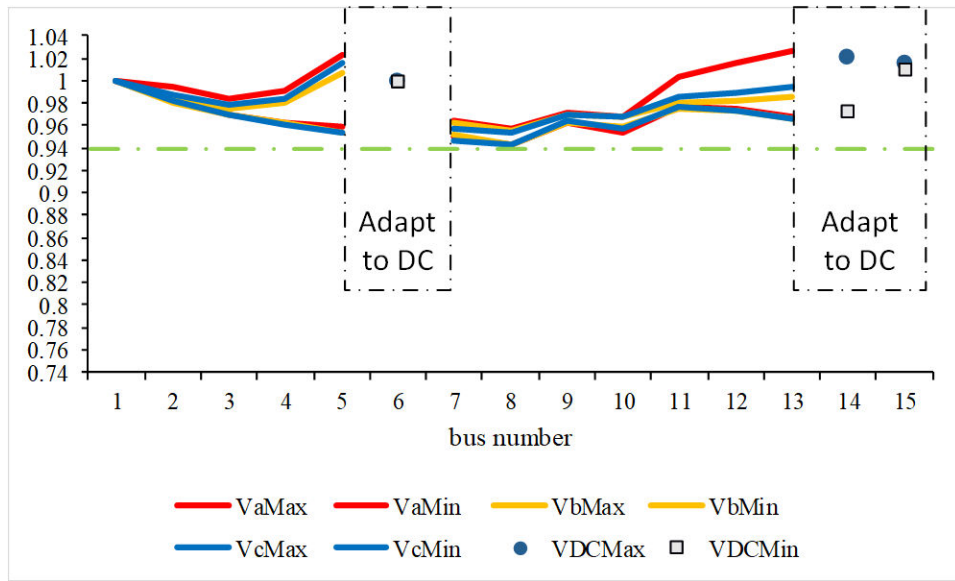


Figure 5.6: The maximum and minimum voltages of three phases for 24 hours after adapting AC lines to DC power distribution

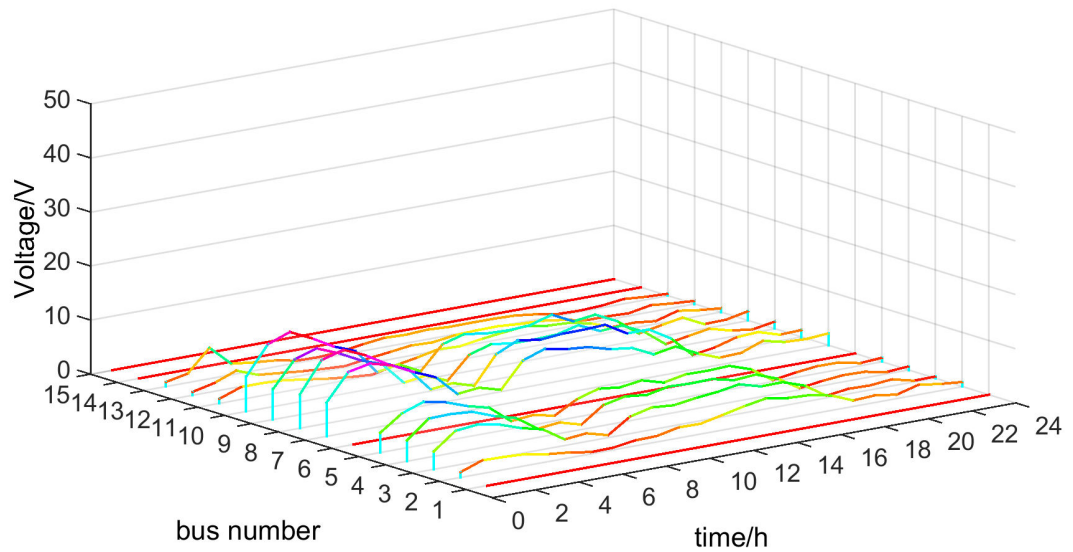


Figure 5.7: The neutral-wire voltage profiles after adapting AC lines to DC power distribution

power. In the control group, a 10 kVA SOP is applied to link bus 6 and bus 15 (SOP solution). These two upgrade solutions proposed in this chapter are shown in Figure 5.8.

The results in Table 5.2 show that adapting AC lines to DC power distribution can reduce

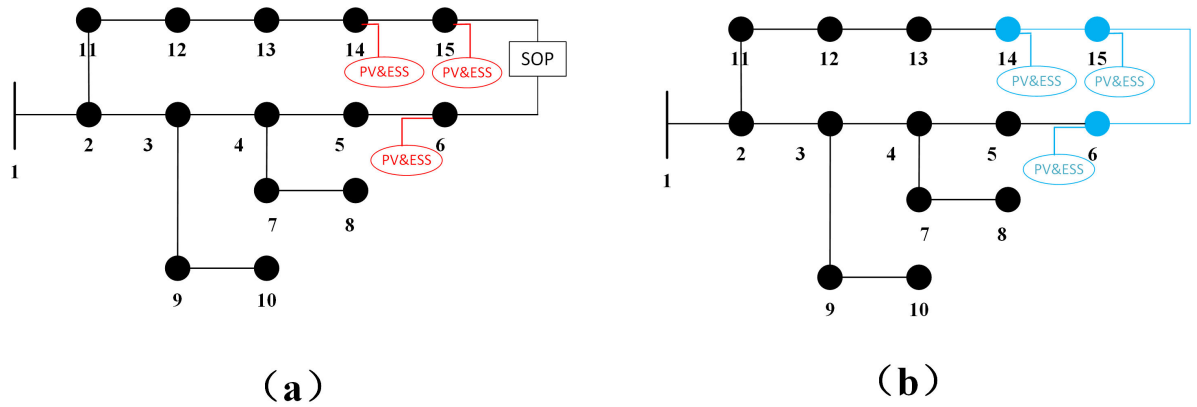


Figure 5.8: (a) Upgrade solution by SOP; (b) Upgrade solution by adapting AC lines to DC power distribution

network losses and voltage deviation and increase PV output - both network losses and average voltage deviation are the lowest (67.76 kW/24h and 2.88% respectively) and PV output is the highest (201.90 kW/24h). Although the SOP solution can also alleviate these issues, the results are not as significant as the DC solution. The ESSs in DC solution can output and input the highest amount of power compared with other two cases (28.13 kW/24h and 23.63 kW/24h respectively). This means that adapting AC lines to DC power distribution can improve the utilization of ESSs in the network.

Table 5.2: Optimization results of network loss, PV output, average voltage deviation and ESSs

	Original network	SOP solution	DC solution
Network loss (kW/24h)	94.53	82.83	67.76
PV output (kW/24h)	136.37	164.8	201.9
Average voltage deviation	6.12%	4.46%	2.88%
Total ESSs output(kW/24h)	9.74	17.14	28.13
Total ESSs input(kW/24h)	5.24	12.64	23.63

All voltages operate within regulated range afterwards. Figure 5.6 shows after adapting AC lines to DC power distribution, the minimum voltage variation of bus 6 and bus 15 can be within $\pm 2\%$. Although bus 8 is not adapted to DC power distribution, the minimum voltage of bus 8 is higher than 0.94.

The maximum neutral-wire voltage drastically drops from 42.81V to 13.23V because of adapting AC lines to DC power distribution. As shown in Figure 5.7, the neutral-wire voltage of bus 6, bus 14 and bus 16 become 0, because DC power distribution is balanced.

5.7 Conclusion

This chapter presents an approach to adapting AC lines to DC power distribution to reduce three-phase imbalance. An operational strategy is also proposed to minimise the operational losses, voltage deviation and maximise DERs' integration for the three-phase four-wire systems. Compared with the AC network and SOP solutions, the optimisation results indicate that adapting AC lines to DC power distribution significantly reduce unbalanced loading and increase ESSs utilisation. Furthermore, it can provide support for network planning a new solution with the new adapting strategy when it is required to improve unbalanced loading stress. For system operators, it can help to achieve a 24-hour optimal plan of AC/DC hybrid system with the addition of flexible and controllable resources such as VSCs, PVs and ESSs in smart power distribution systems. For three-phase imbalance in ADNs, the robustness of AC/DC hybrid system optimisation and capital investment of deploying the adapting strategy require further research.

Meanwhile, for multi-region or single-phase wires connections, two-terminal conventional SOPs and two-terminal DC networks cannot fulfil the demand. As a result, bifurcation PC-SOP and multi-terminal PC-SOP are worthy of investigation.

Chapter 6

Bifurcation Phase-Changing Soft Open Point and Multi-terminal Phase-Changing Soft Open Point SDP Modeling for Imbalance Mitigation in Active Distribution Networks

6.1 Introduction

In this chapter, an optimised operational strategy for unbalanced ADNs based on SOPs is proposed. It enhances the operation efficiency and reduces the three-phase imbalance. Different SOPs' installation strategies focusing on the optimisation modelling are investigated including the previous mentioned two-terminal conventional SOP and two-terminal PC-SOP. For one SOP installed in the system, an SOP with bifurcation connection is investigated. For more than one SOP installed in the system, solutions that using a multi-terminal SOP to replace two

conventional SOPs are investigated.

The contributions of this study can be summarized as follows:

- The potential of SOPs is explored by a new way of connection, i.e. power transferring between phases, so-called phase-changing SOP (PC-SOP).
- The benefits of PC-SOPs, SOPs with bifurcation connection and multi-terminal SOPs for unbalanced three-phase networks are further analyzed. A SOP with bifurcation connection and a multi-terminal PC-SOP based optimal operational strategy for unbalanced ADNs are proposed considering power losses and voltage deviation as a penalty.
- The OPF of three-phase unbalanced networks with SOPs is mathematically a non-convex nonlinear problem. Therefore, here the original non-convex nonlinear optimization model is converted into a symmetrical SDP formulation, which can be solved to find the global optimum with improved computational efficiency.
- In research of SOP with bifurcation connection, one case studies are conducted to optimize the regulations of SOPs and PV curtailment. Compared with other alternative SOP solutions, SOP with bifurcation connection can reduce power losses by between 8.33% and 11.46%.
- In research of multi-terminal SOPs, two case studies are conducted to optimize the regulations of SOPs and PV curtailment. Compared with other alternative SOP solutions, multi-terminal PC-SOP can reduce power losses by between 5.56% and 28.98%.
- In both SOPs with bifurcation connection and multi-terminal SOPs research, there is a significant improvement simultaneously achieving effective voltage regulation.

6.2 Unbalanced Optimal Operation Problem Formulation

SOPs are power-electronic devices that are used to replace tie switches for network reconfiguration and offer further capabilities of accurate and flexible power flow control [72]. SOPs can transfer active power, supply reactive power and achieve real-time control of voltage between the connected feeders. Thereby cable power losses and risks caused by frequent switching actions in ADNs can be reduced.

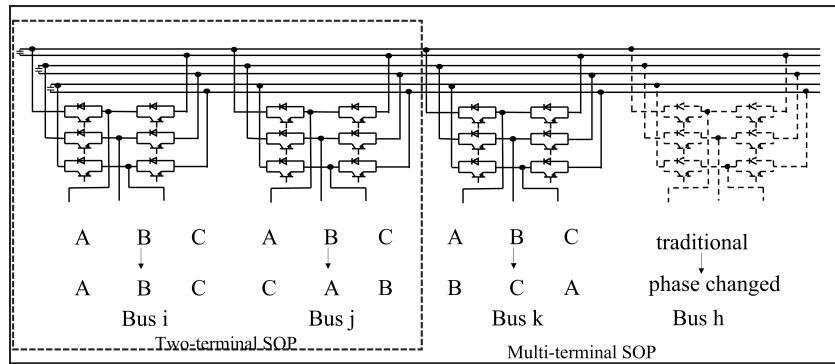


Figure 6.1: Illustration and comparison of different SOPs.

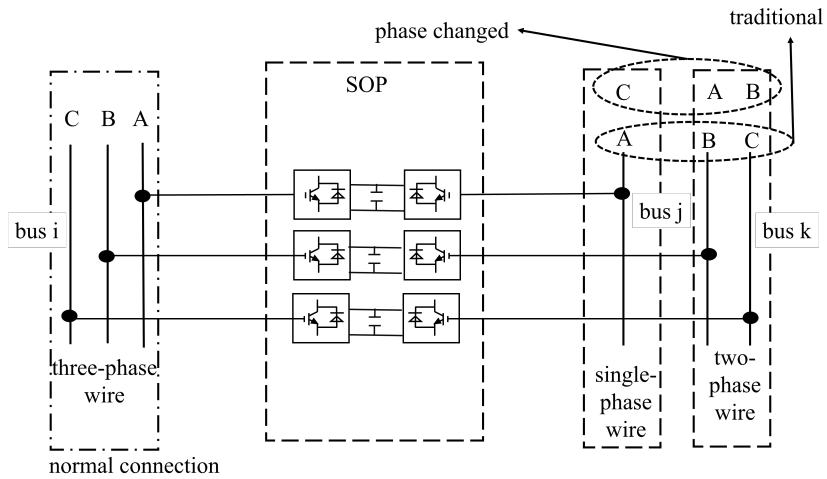


Figure 6.2: Comparison of conventional SOP with PC-SOP and normal connection with bifurcation connection

6.2.1 Principles and Modeling of Different SOPs

Basic principles of two-terminal and multi-terminal conventional SOPs

B2B VSCs are the most commonly used SOP devices. Therefore normally they are used to analyze the optimization model for both the two-terminal [62, 146] and multi-terminal SOPs [64] in steady-state operations. B2B VSCs can control three-phase active power and reactive power outputs independently [56]. One VSC of them operates in $V_{dc}f$ control mode; the other VSC(s) operate in PQ control mode. The loss index of each VSC can be 0.002 [64]. In a balanced system, three-phase feeders would be connected as balanced, i.e. corresponding phases (ABC to ABC) or (ABC to ABC to ABC) as shown in Fig. 6.1.

Two- and multi-terminal PC-SOPs

As the local DG outputs and electricity demand have inherent randomness, there is always a mismatch between them. When they are distributed unevenly in different feeder phases, the whole network can achieve improved operating performances when phases can be indirectly connected by two-terminal PC-SOPs [147] marked by the dotted rectangle in Fig.6.1.

Bifurcation Phase-Changing SOPs

Three-phase systems also have single-phase buses and two-phase buses which may be needed to be connected by SOP, because single-phase buses and two-phase buses are often located in end of line where voltage is worse than buses near the substations or sources. Bus i is a three-phase bus connected with an SOP by a three-phase wire. Bus i and k are single-

phase bus and two-phase bus connected with an SOP by a single-phase wire and two-phase wire separately. Therefore, new ways of connection of two-terminal SOPs, called two-terminal bifurcation SOPs are proposed in this chapter marked by the dotted rectangle in Fig.6.2

New ways of connection of multi-terminal SOPs, called multi-terminal PC-SOPs (ABC to CAB to BCA, as a three-terminal example). In a multi-terminal PC-SOP, three-phase wires can be connected together between at least three buses, which means energy can be transferred amongst three phases of at least three feeders/buses marked by the solid line rectangle in Fig.6.1. Operational constraints are expressed mathematically below.

Two-terminal PC-SOP operational constraints: e.g. ABC to CAB two-terminal PC-SOP

$$\begin{cases} P_t^{VSC1,a} + P_t^{VSC2,c} + P_t^{VSC1,a,loss} + P_t^{VSC2,c,loss} = 0 \\ P_t^{VSC1,b} + P_t^{VSC2,a} + P_t^{VSC1,b,loss} + P_t^{VSC2,a,loss} = 0 \\ P_t^{VSC1,c} + P_t^{VSC2,b} + P_t^{VSC1,c,loss} + P_t^{VSC2,b,loss} = 0 \end{cases} \quad (6.1)$$

Multi-terminal PC-SOP operational constraints: e.g. ABC to CAB to BCA three-terminal PC-SOP

$$\begin{cases} P_t^{VSC1,a} + P_t^{VSC2,c} + P_t^{VSC3,b} + P_t^{VSC1,a,loss} + P_t^{VSC2,c,loss} + P_t^{VSC3,b,loss} = 0 \\ P_t^{VSC1,b} + P_t^{VSC2,a} + P_t^{VSC3,c} + P_t^{VSC1,b,loss} + P_t^{VSC2,a,loss} + P_t^{VSC3,c,loss} = 0 \\ P_t^{VSC1,c} + P_t^{VSC2,b} + P_t^{VSC3,a} + P_t^{VSC1,c,loss} + P_t^{VSC2,b,loss} + P_t^{VSC3,a,loss} = 0 \end{cases} \quad (6.2)$$

PC-SOP capacity and loss constraints:

$$\sqrt{P_t^{VSCx,\varphi^2} + Q_t^{VSCx,\varphi^2}} \leq S^{VSCx^2} \quad (6.3)$$

$$P_t^{VSCx,\varphi,loss} = \gamma^{VSC} \sqrt{P_t^{VSCx,\varphi^2} + Q_t^{VSCx,\varphi^2}} \quad (6.4)$$

where $P_t^{VSCx,\varphi}$ is the active power of VSCx at phase φ at time t , $P_t^{VSCx,\varphi,loss}$ is the active power loss of VSCx at phase φ at time t , $Q_t^{VSCx,\varphi}$ is the reactive power of VSCx at phase φ at time t , and $S^{VSCx,\varphi}$ is the capacity of VSCx at phase φ .

The PC-SOP capacity and loss constraints can be transferred into an SDP model for optimization (\succeq means ‘at least as good as’ in SDP models [129]):

$$\begin{bmatrix} S^{VSCx} & P_t^{VSCx,\varphi} + jQ_t^{VSCx,\varphi} \\ P_t^{VSCx,\varphi} - jQ_t^{VSCx,\varphi} & S^{VSCx} \end{bmatrix} \succeq 0 \quad (6.5)$$

$$\begin{bmatrix} P_t^{VSCx,\varphi,loss} / \gamma^{VSC} & P_t^{VSCx,\varphi} + jQ_t^{VSCx,\varphi} \\ P_t^{VSCx,\varphi} - jQ_t^{VSCx,\varphi} & P_t^{VSCx,\varphi,loss} / \gamma^{VSC} \end{bmatrix} \succeq 0 \quad (6.6)$$

6.2.2 Optimisation Modeling of Three-phase ADNs with PVs, SOPs and Voltage Regulators

Objective function

This work aims to minimise an objective function comprising total power losses and voltage deviation penalties. Minimum total power loss can reduce the network operational cost during network operation. Minimum voltage deviation penalties can improve the customer-side voltage and power quality.

$$\min f = f^{loss} + M \cdot \sum_{t=1}^T \sum_{i=1}^{\Omega_n} (d_{i,t}^+ + d_{i,t}^-)$$

(6.7)

$$f^{loss} = \sum_{t=1}^T \left(\sum_{ij \in \Omega_b} \text{diag}(l_{ij,t} \cdot z_{ij}) + \sum_{\substack{x=1,2,3 \\ \varphi=a,b,c}} P_t^{VSCx,\varphi,loss} \right) \quad (6.8)$$

where z_{ij} is the branch resistance from node i to node j , l_{ij} is the second-order decision variable of current from node i to node j at time t , $d_{i,t}^+$ is the positive penalty variable at node i at time t , and $d_{i,t}^-$ is the negative penalty variable at node i at time t .

Three-phase system operational constraints

Power flow balance constraint at time t :

$$\sum_{ij \in \Omega_b} \text{diag}(S_{ij,t} - z_{ij} l_{ij,t}) + s_{j,t} + y_{j,t} v_{j,t} = \sum_{jk \in \Omega_b} \text{diag}(S_{jk,t}) \quad (6.9)$$

where $S_{ij,t}$ is the second-order decision variable of power from node i to node j at time t , s_i is the nodal injection at node i , i.e. either loads or the net injection of a distributed energy resource, y_i is the nodal shunt capacitance of node i , and $v_{i,t}$ is the second-order decision variable of voltage at node i at time t .

Kirchoff's voltage constraints along line ij at time t :

$$v_{j,t} = v_{i,t} - (S_{ij,t}z_{ij}^H + S_{ij,t}^H z_{ij}) + z_{ij}l_{ij,t}z_{ij}^H \quad i \rightarrow j \quad (6.10)$$

$$\underline{v}_i \leq \text{diag}(v_{i,t}) \leq \bar{v}_i \quad (6.11)$$

$$v_0 = V_0^{ref} (V_0^{ref})^H \quad (6.12)$$

where \bar{v}_i is the upper limit for second-order decision variable of voltage at node i , and \underline{v}_i is the lower limit for second-order decision variable of voltage at node i .

Equation 6.13 expresses the positive semidefinite constraint where positive semidefinite matrix should have rank one, as enforces in Equation 6.14.

$$\begin{bmatrix} v_{i,t} & S_{ij,t} \\ S_{ij,t}^H & l_{ij,t} \end{bmatrix} \succeq 0 \quad i \rightarrow j \quad (6.13)$$

$$\text{rank} \begin{bmatrix} v_{i,t} & S_{ij,t} \\ S_{ij,t}^H & l_{ij,t} \end{bmatrix} = 1 \quad i \rightarrow j \quad (6.14)$$

Node voltage, branch current and related second-order decision variables are defined as:

$$\begin{cases} V_{i,t} = \begin{bmatrix} V_{i,t}^a & V_{i,t}^b & V_{i,t}^c \end{bmatrix} \\ v_{i,t} = V_{i,t} V_{i,t}^H \\ I_{ij,t} = \begin{bmatrix} I_{ij,t}^a & I_{ij,t}^b & I_{ij,t}^c \end{bmatrix} \\ l_{ij,t} = I_{ij,t} I_{ij,t}^H \\ S_{ij} = V_{i,t} I_{ij,t}^H \end{cases} \quad (6.15)$$

Modeling of voltage regulators

Ratios between the primary and secondary voltages are expressed as (Tap^φ is integer between $[-16, 16]$):

$$\begin{aligned} ratio &= \begin{bmatrix} r_t^a & r_t^b & r_t^c \end{bmatrix} \\ V_{sec,t}^T &= \begin{bmatrix} V_{sec,t}^a & V_{sec,t}^b & V_{sec,t}^c \end{bmatrix}^T = \begin{bmatrix} r_t^a V_{pri}^a & r_t^b V_{pri}^b & r_t^c V_{pri}^c \end{bmatrix} \\ r_t^\varphi &= 1 + 0.00625 \cdot Tap^\varphi \quad \exists \varphi = a, b, c \end{aligned} \quad (6.16)$$

The voltages on the two sides of a regulator are linked as follows:

$$v_{sec,t}^{abc} = (v_{i,t} - (S_{reg,t} z_{reg}^H + S_{reg,t}^H z_{reg}) + z_{reg} l_{reg} z_{reg}^H) \cdot ratio \quad (6.17)$$

Converted into symmetrical components, Equation 6.17 becomes:

$$A v_{sec,t}^{012} A^H = A [(v_{i,t}^{012} - (S_{reg,t}^{012} z_{reg}^{012,H} + S_{reg,t}^{012,H} z_{reg}^{012}) + z_{reg}^{012} l_{reg,t} z_{reg}^{012,H})] A^H \cdot ratio \quad (6.18)$$

where $V_{pri,t}^\varphi$ and $V_{sec,t}^\varphi$ are voltages of the regulator's primary side and secondary side at time t . $v_{sec,t}$ is the second-order decision variable of $V_{sec,t}$. $S_{reg,t}$ is the second-order decision variable of power for regulators at time t . z_{reg} is the regulator's resistance. $I_{reg,t}$ is the regulator's branch current vector.

Modeling of loads

Different models of loads are considered in this chapter including constant impedance, constant current and constant power characteristics, also known as ZIP models [148].

Following the input of data such as network parameters, load profiles and SOP locations and sizes, the SDP problem is relaxed for SOP and power flow constraints. Then the optimization can be solved as an SDP OPF problem with power flows and variables considered for a 24-hour simulation period, solved by MOSEK (commercial SDP solver) [149]. If all output voltages are within 0.2% deviation after multiple iterations, the solution achieves convergence and can be the final output. Otherwise the OPF results are used to update data until convergence is achieved.

6.3 Symmetrical SDP Transforming

The symmetrical components transformation reduces the phase coupling in three-phase systems. Voltages in phase components are transformed into symmetrical components as follows:

$$V_{i,t}^{abc} = AV_{i,t}^{012} \quad (6.19)$$

where

$$A = \begin{bmatrix} 1 & 1 & 1 \\ 1 & a^2 & a \\ 1 & a & a^2 \end{bmatrix}, A^H = A^{-1} \quad (6.20)$$

and $a = 1 \angle 120^\circ$. Hence, the three-phase variables in the BFM-SDP method and the impedance parameters are related to the equivalent variables in symmetrical components:

$$\begin{aligned} v_{i,t}^{abc} &= V_{i,t}^{abc} \cdot V_{i,t}^{abc,H} = AV_{i,t}^{012} \cdot (AV_{i,t}^{012})^H = AV_{i,t}^{012} A^H \\ I_{i,t}^{abc} &= AI_{i,t}^{012} A^H \\ S_{i,t}^{abc} &= AS_{i,t}^{012} A^H \\ z_{i,t}^{abc} &= Az_{i,t}^{012} A^{-1} = Az_{i,t}^{012} A^H \\ y_{i,t}^{abc} &= Ay_{i,t}^{012} A^{-1} = Ay_{i,t}^{012} A^H \end{aligned} \quad (6.21)$$

Objective function Equation 6.8 and constraints Equation 6.9 – 6.13 are transformed as follows Equation 6.22 – 6.27. Penalty factors are introduced in voltage constraints Equation 6.28:

$$f^{loss} = \sum_{t=1}^T \left(\sum_{ij \in \Omega_b} \text{diag}(A(l_{ij,t}^{012} z_{ij,t}^{012}) A^H) + \sum_{\substack{x=1,2,3 \\ \varphi=a,b,c}} P_{\varphi,t}^{VSCx,loss} \right) \quad (6.22)$$

$$\sum_{ij \in \Omega_b} \text{diag}(A(S_{ij,t}^{012} - z_{ij,t}^{012} l_{ij,t}^{012}) A^H) + s_{j,t} + y_{j,t}^{012} v_{j,t}^{012} = \sum_{jk \in \Omega_b} \text{diag}(AS_{jk,t}^{012} A^H) \quad (6.23)$$

$$v_{j,t}^{012} = v_{i,t}^{012} - (S_{ij,t}^{012} z_{ij}^{012,H} + S_{ij,t}^{012,H} z_{ij}) + z_{ij}^{012} l_{ij,t}^{012} z_{ij}^{012,H} \quad (6.24)$$

$$\underline{v}_{i,t} \leq \text{diag}(Av_{i,t}^{012}A^H) \leq \overline{v}_{i,t} \quad (6.25)$$

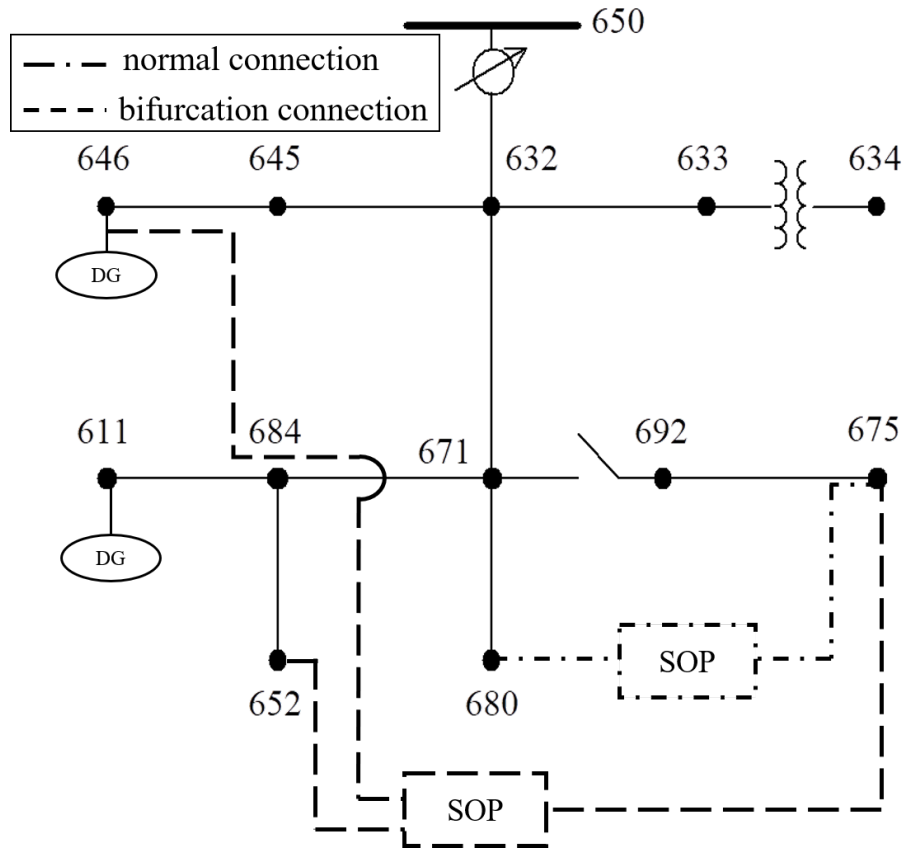
$$v_0^{012} = V_0^{012,ref} (V_0^{012,ref})^H \quad (6.26)$$

$$\begin{bmatrix} v_i^{012} & S_{ij}^{012} \\ S_{ij}^{012,H} & l_{ij}^{012} \end{bmatrix} \succeq 0 \quad i \rightarrow j \quad (6.27)$$

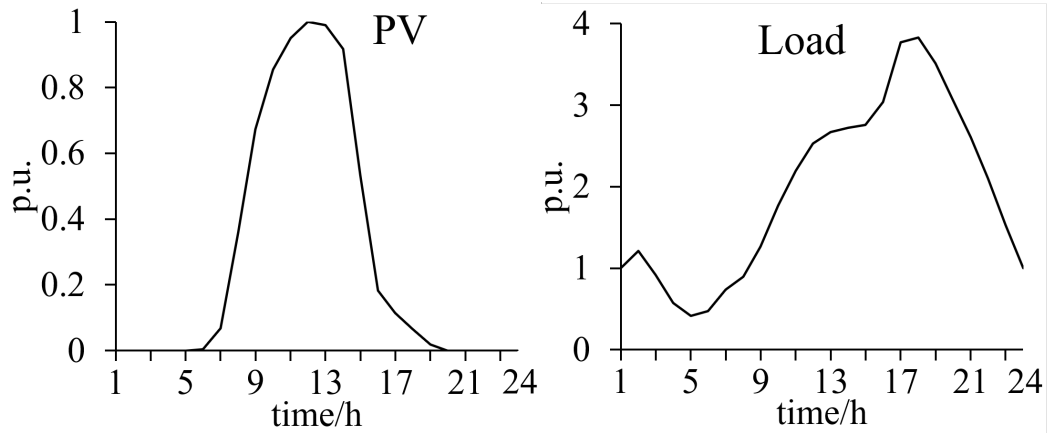
$$\begin{aligned} \text{diag}(Av_{i,t}^{012}A^H) + d_{i,t}^+ &\geq \underline{v}_{i,t}, d_{i,t}^+ \geq 0 \\ \text{diag}(Av_{i,t}^{012}A^H) - d_{i,t}^- &\leq \overline{v}_{i,t}, d_{i,t}^- \geq 0 \end{aligned} \quad (6.28)$$

6.4 Methodology: Design of the Experiment with Bifurcation PC-SOP

In this section, the IEEE 13-node test feeder [139], as shown in Fig. 6.3, is used as the test system to analyze and verify the proposed model. The capacity of the SOP is 500 kVA. It is located between buses 646 (phases B and C), 652 (phase A) and 675 for bifurcation connection, and it is located between buses 675 and 680 for normal connection. There are two 5 MVA DGs located in buses 611 (phase C) and 646 (phases B and C). The voltage range of all buses is set



(a) Topology of the IEEE 13-node test feeder



(b) Individual PV generation and load profiles

- * The IEEE 13-node test feeder is very small and used to test common features of distribution analysis software, operating at 4.16 kV [135].
- * Load profiles from Standard Load Profile [136].
- * PV generation profile from Photovoltaic Solar Panel Energy Generation data [137].

Figure 6.3: Test network with IEEE 13-node topology and profiles.

to be $[0.94, 1.10]$ as the statutory limits in the UK [141].

The SDP program proposed in this research is coded with YALMIP [131], and solved by MOSEK [149]. The operating environment is Intel i7-10850H 2.7GHz CPU, 32GB RAM.

Four cases are designed to show the benefits of PC-SOP with bifurcation connection.

Case 0: the original system

Case 1: the system with conventional SOP.

Case 2: the system with PC-SOP.

Case 3: the system with conventional SOP and bifurcation connection.

Case 4: the system with PC-SOP with bifurcation connection.

6.5 Case Study with Bifurcation PC-SOP

Table 6.1: Optimisation results comparison

	Case 0	Case 1	Case 2	Case 3	Case 4
Objective (MW/24h)	80.53	74.10	74.10	72.59	71.71
Network losses (MW/24h)	49.00	43.73	43.71	40.09	38.70
Penalty function value	0.01	0.01	0.01	0.01	0.01
SOP losses (MW/24h)	\	2.59	2.59	3.05	3.11
SOP transmitted active power (MW/24h)	\	1.29	1.29	7.24	11.00
SOP supplied reactive power (MVar/24h)	\	20.47	20.47	32.25	29.32
PV active power (MW/24h)	83.84	88.04	88.02	86.46	86.01
PV reactive power (MVar/24h)	13.42	11.42	11.42	9.61	9.78
Maximum system imbalance index	0.28	0.27	0.27	0.16	0.16
Voltage deviation	6.72%/ -2.77%	5.61%/ -1.81%	5.61%/ -1.81%	5.62%/ -1.56%	5.61%/ -1.56%

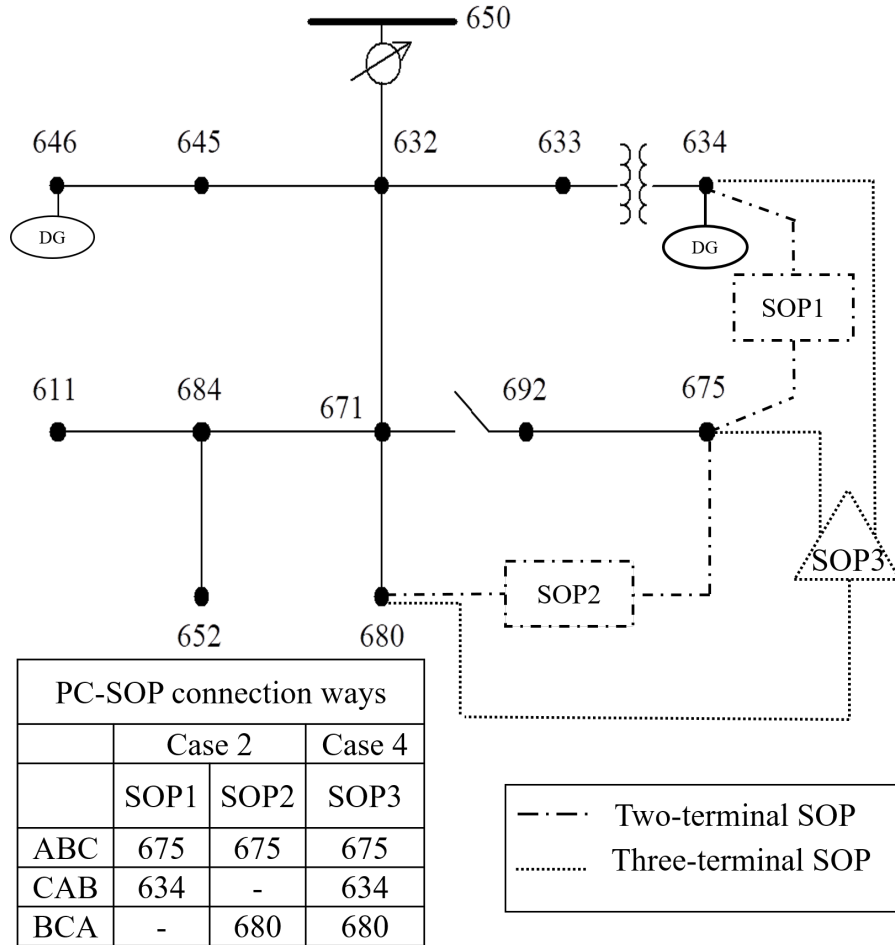
$$\lambda_{UI,sys} = \text{Max}\left(\frac{|V_{i,t}^A + aV_{i,t}^B + a^2V_{i,t}^C|}{|V_{i,t}^A + a^2V_{i,t}^B + aV_{i,t}^C|}\right) \quad (6.29)$$

Maximum system imbalance index for 24 hours can be calculated as Equation 6.29 [56].

The results in Table 6.1 show that the PC-SOP with bifurcation connection achieve the best objective (71.71 MW/24h) with minimum network losses maximum system imbalance index and voltage deviation (38.70 MW/24h, 0.16 and +5.61% /-1.56% respectively). Without SOP, the original system has the highest network losses (49.00 MW/24h), highest maximum system imbalance index (0.28), lowest PV output (83.84 MW/24h) and highest voltage deviation (6.72% / -2.77%) in Case 0. All SOP solutions improve the original networks performance. However, without bifurcation connection, Case 1 and 2 have nearly the same results in all standard, because PC-SOP and SOP cannot effective transmit active power (1.29 MW/24h in Case 1 and 2) and SOP's capacity is mainly used to supply reactive power. With bifurcation connection, single-phase and two-phase nodes 611 and 652 are effectively connected with the three-phase node 675. That makes bifurcation connection transmit more active power than normal connection. PC-SOP solution's advantage is highlighted with higher active power transmission (11.00 MW/24h) compared with conventional SOP (7.24 MW/24h). Although PV output is higher in Cases 1 and 2 (88.04 and 88.02 MW/24h) than Cases 3 and 4 (86.46 and 86.01 MW/24h), network losses, voltage drop in Cases 3 and 4 (40.09 MW/24h & -1.56% and 38.70 MW/24h & -1.56%) are much lower than Cases 1 and 2 (43.73 MW/24h & -1.81% and 43.71 MW/24h & -1.81%). Therefore bifurcation connection can achieve better objective than normal connection considering both network losses and PV curtailment. In addition, PC-SOP can achieve better objective and network performance in bifurcation connection than conventional SOP by comparing Case 3 and Case 4.

6.6 Methodology: Design of the Experiment with Multi-terminal PC-SOP

6.6.1 Design of the experiment with three-terminal PC-SOP



* The IEEE 13-node test feeder is very small and used to test common features of distribution analysis software, operating at 4.16 kV [135].

Figure 6.4: IEEE 13-Node test feeder with three-terminal PC-SOP

In this section, the IEEE 13-node test feeder [139], as shown in Fig. 6.4, is used as the test network to implement and validate the proposed model. The total capacity of the SOP is 2 MVA. It is located between buses 634, 675 and 680. It can be two 1 MVA two-terminal SOPs

(SOP1 and SOP2) or one 2 MVA three-terminal SOP (SOP3). There are two 5 MVA PV installations located at buses 634 (phase B) and 646 (phases B and C). The power factor of PV generation is 0.95. The voltage range of all buses is set to be $[0.94, 1.10]$ as the statutory limits in the UK [141]. The three-phase regulator between buses 650 and 632 is set as $[r_t^a \ r_t^b \ r_t^c] = [1.05 \ 1.0375 \ 1.04375]$, same parameters as the example case in OpenDss.

Five cases are designed to demonstrate the benefits of multi-terminal PC-SOPs. PC-SOP connection ways (including Case 2 and 4) are shown in the table of Fig. 6.4. For Case 2, the connection way of SOP 1 is ABC to CAB and the connection way of SOP 2 is ABC to BCA. Therefore three phases are connected by two PC-SOPs. For Case 4, one three-terminal PC-SOP connects three-phase buses (ABC to CAB to BCA). It has been proved that the absolute deviations between the optimal selection of individual PC-SOP phase connections can be negligible [147].

Case 0: the original network

Case 1: the network with two two-terminal conventional SOPs.

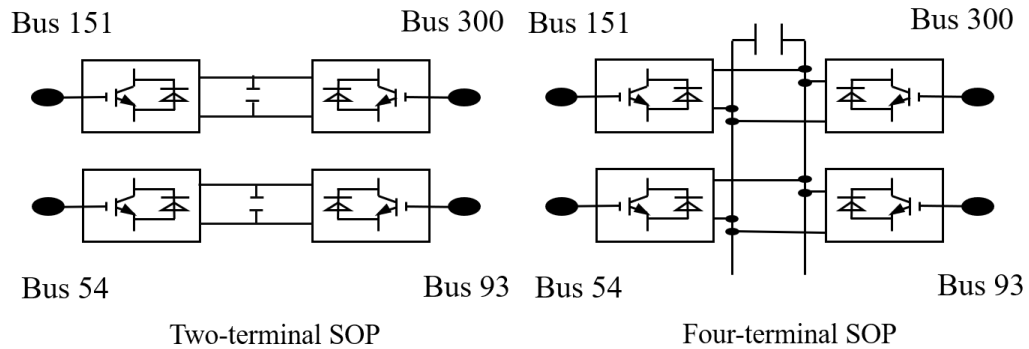
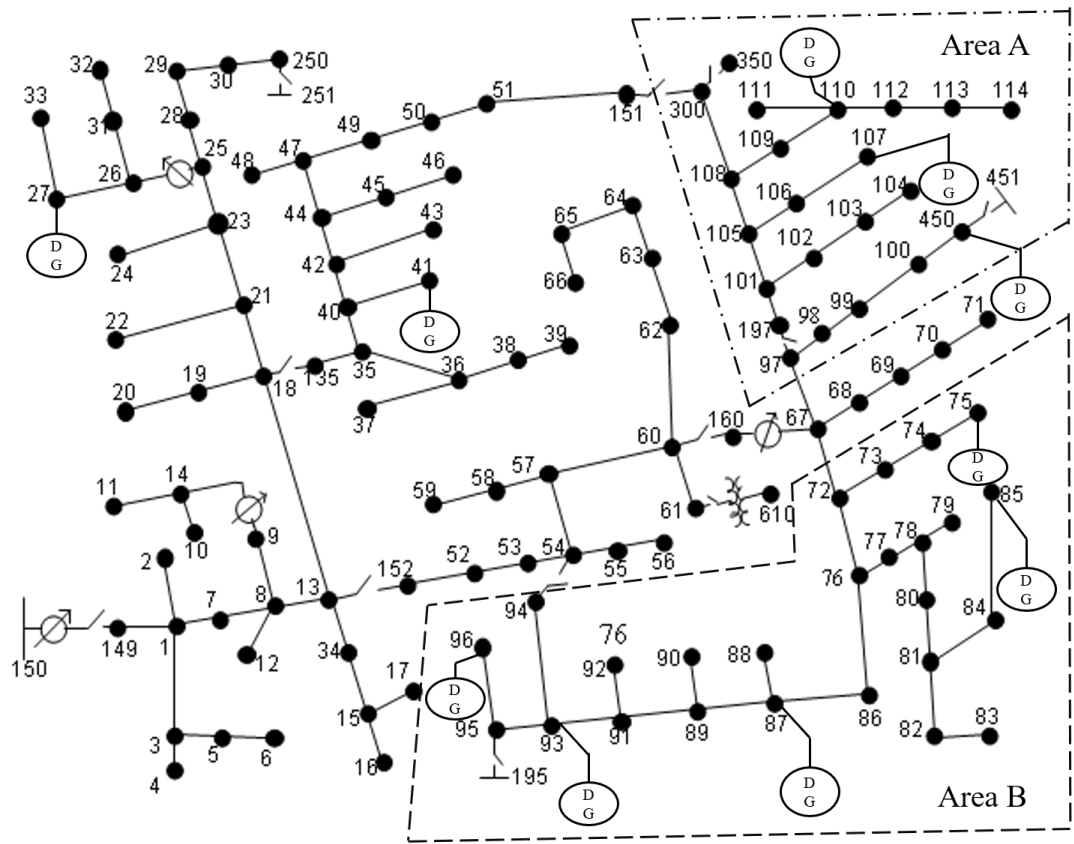
Case 2: the network with two two-terminal PC-SOPs.

Case 3: the network with one three-terminal conventional SOP.

Case 4: the network with one three-terminal PC-SOP.

6.6.2 Design of the experiment with four-terminal PC-SOP

In [56], a modified IEEE 123-node distribution network is used to verify the scalability of the optimal operation of multi-terminal on large-scale ADNs with severe unbalanced conditions. In [147], PC SOP has been proved that it can transmit more active power and utilize its capacity better than conventional SOP.



* The IEEE 123-node test feeder operates at a nominal voltage of 4.16 kV. [135].

Figure 6.5: Test network with IEEE 123-node topology.

However, in the original network, the line segment between bus 93 and 94 is single-phase (A-N), and bus 94 is single-phase [139], as shown in Fig. 6.5. The tie switch between bus 54 and bus 94 is moved to between bus 54 and bus 93 to keep the original line configurations, because bus 93 is three-phase and SOP normally connects with three-phase buses. Other DGs' parameters and total SOP's capacity are the same as the data in [56]. PV generation

and load profiles are the same as shown in Fig. 6.3b. The regulators are set as $[r_t^a \ r_t^b \ r_t^c] = [1.04375 \ 1.04375 \ 1.04375]$ (buses 150 to 149, three-phase regulator), $r_t^a = 0.99375$ (buses 9 to 14, single-phase regulator), $[r_t^a \ r_t^c] = [0 \ 0.99375]$ (buses 25 to 26, two-phase regulator), $[r_t^a \ r_t^b \ r_t^c] = [1.5 \ 1.00625 \ 1.3125]$ (buses 67 to 160, two-phase regulator), same parameters as the example case in OpenDss. The load at bus 610 connected to the secondary is directly connect to the primary bus 61.

Similar to design of the experiment with three-terminal PC-SOP, five cases are designed to show the benefits of multi-terminal PC-SOPs. The difference with Section III-A, is that in this section Cases 3 and 4 aim at proving the benefits of four-terminal SOPs. Meanwhile, an assumption is made that the physical distances between buses 54, 93, 151 and 300 are not too far from each other to be connected with a multi-terminal SOP.

6.7 Case Studies with Multi-terminal PC-SOP

6.7.1 Case Study with three-terminal PC-SOP

$$\lambda_{UI,sys} = \sum_{t=1}^T \sum_{i=1}^{\Omega_n} \left(\frac{|V_{i,t}^A + aV_{i,t}^B + a^2V_{i,t}^C|}{|V_{i,t}^A + a^2V_{i,t}^B + aV_{i,t}^C|} \right) \quad (6.30)$$

Network imbalance index for 24 hours can be calculated as Equation 6.30 [56]. The results in Table 6.2 show that the three-terminal PC-SOP achieves the best objective value (13.30) with minimum network losses, the lowest network imbalance index (11.37 MW/24h and 14.80 respectively). Without SOP, the original network voltages drop out of the low bound (-45.16%). Therefore the penalty function value is the highest (189470.00). That causes the highest network losses (1488.80 MW/24h), the highest network imbalance index (19.58). All SOP solu-

Table 6.2: Optimisation Result Comparison of the IEEE 13-Node Test Feeder Network

	Case 0	Case 1	Case 2	Case 3	Case 4
Objective	189470.00	17.51	15.45	16.09	13.30
Network losses (MW/24h)	1488.80	16.01	13.70	14.52	11.37
Penalty function value	187980.00	0.01	0.01	0.02	0.01
SOP losses (MW/24h)	-	1.49	1.75	1.55	1.92
SOP transmit active power(MW/24h)	-	7.90	17.36	8.81	21.34
SOP supply reactive power(MVAr/24h)	-	69.31	70.32	74.21	75.36
PV active power (MW/24h)	54.15	22.94	29.23	23.54	35.54
PV reactive power (MVar/24h)	15.63	6.01	7.16	6.20	6.67
Network imbalance index	19.58	15.82	15.08	15.92	14.80
Voltage deviation	10%/	6.14%/	6.40%/	10.00%/	10.00%/
	-45.16%	-6.00%	-6.00%	-6.00%	-6.00%

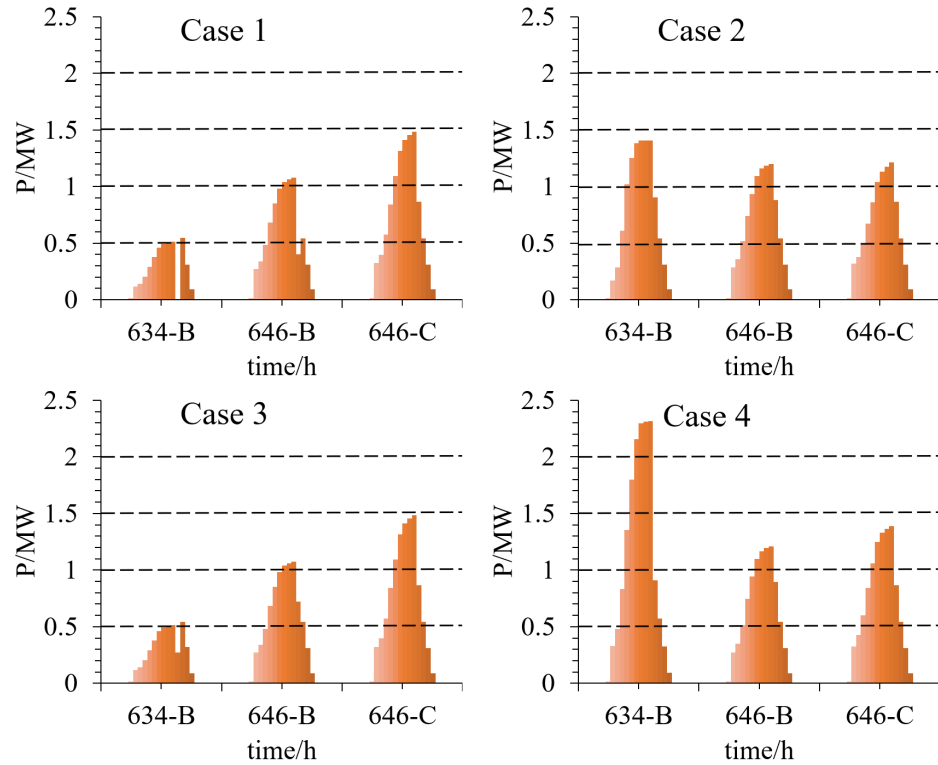


Figure 6.6: Actual PV outputs.

tions improve the original networks performance. The objective value shows phase-changing solution (Case 2, 15.45) and multi-terminal solution (Case 3, 16.09) achieve better perfor-

mance than two-terminal conventional SOPs in Case 1. Both Case 2 (17.36 MW/24h) and Case 3 (8.81 MW/24h) can transmit more active power than Case 1 (7.90 MW/24h). Although PV output is the highest in Cases 0, it can be ignored because system cannot operate within that voltage range. Except Case 0, Case 2, 3, 4 can improve PV output compared with Case 1. Especially, PV active power in Case 4 (35.54 MW/24h) is the highest among Cases 1-4. Therefore both phase changing and multi-terminal solutions for SOPs can achieve better objective values than the normal solution for SOP considering network losses. In addition, the combination solution (Case 4, which combines multi-terminal with phase-changing) can achieve better performance compared with individual solutions.

In Fig. 6.6, Case 4 shows maximized PV outputs for all installation locations; while Case 1 shows the overall minimal among Cases 1-4. For two-phase PV 646, there is nearly the same PV curtailment in all four Cases. This is due to that PV 646 is on the opposite side of SOPs in the network. PV 634 hardly generates power which ranges from 0 to 0.6 kW in Cases 1 and 3. However, the PC-SOP in Case 2 and Case 4 can make the network effectively utilize different phase resources - the outputs of PV 634 in Case 2 exceed 1 MW and PV 634 in Case 4 exceed 2 MW, because the PC-SOP effectively acts as a 'bridge' to provide a path for power transfer between DG and loads from different phases (between PVs in phase B and the load demand in phases A and C). One multi-terminal PC-SOP can be more effective in phase connection than two separate two-terminal PC-SOPs with the same total capacity.

6.7.2 Case Study with four-terminal PC-SOP

The results in Table 6.3 show that the four-terminal PC-SOP achieves the best objective value (9.91) with minimum network losses, the lowest network imbalance index (8.34 MW/24h and

Table 6.3: Optimisation result comparison of the IEEE 123-Node test feeder

	Case 0	Case 1	Case 2	Case 3	Case 4
Objective	80229.00	14.14	13.29	10.33	9.91
Network losses (MW/24h)	66.85	12.90	11.96	8.85	8.34
Penalty function value	80162.00	0.14	0.15	0.13	0.14
SOP losses (MW/24h)	-	1.10	1.18	1.35	1.43
SOP transmit active power(MW/24h)	-	12.45	14.08	19.56	21.84
SOP supply reactive power(MVAr/24h)	-	47.08	48.61	52.30	52.83
PV active power (MW/24h)	4.08	4.71	4.71	4.71	4.71
Network imbalance index	23.05	22.11	15.83	22.99	14.49
Voltage deviation	9.82%/ -13.14%	9.64%/ -6.00%	9.64%/ -6.00%	9.64%/ -6.00%	9.64%/ -6.00%

14.49 respectively). Without SOP, the original network voltages drop below the low bound (-13.14%). Therefore the penalty function value is the highest (80162.00). That causes the highest network losses (66.85 MW/24h), the highest network imbalance index (23.05). All SOP solutions improve the original networks performance. The objective value shows the phase-changed solution (Case 2, 13.29) and the multi-terminal solution (Case 3, 10.33) achieve better performance than two-terminal conventional SOPs in Case 1. However, compared with Section III-A, here the Case 3's objective value is better than the Case 2. Therefore, it proves that both multi-terminal and PC-SOP solutions can improve networks' performance. The multi-terminal solution has the advantage of improving load distribution imbalance in the whole network. While the PC-SOP solution has the advantage of balancing DG and load distributions in different phases.

The multi-terminal PC-SOP, compared with the conventional SOP, two-terminal PC-SOP and multi-terminal SOP, can transfer more power and utilize the network capacity better in un-

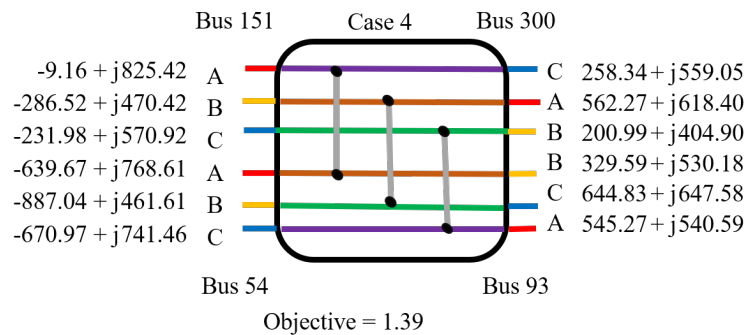
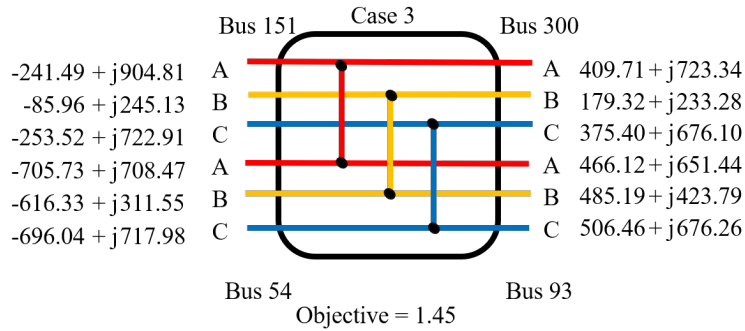
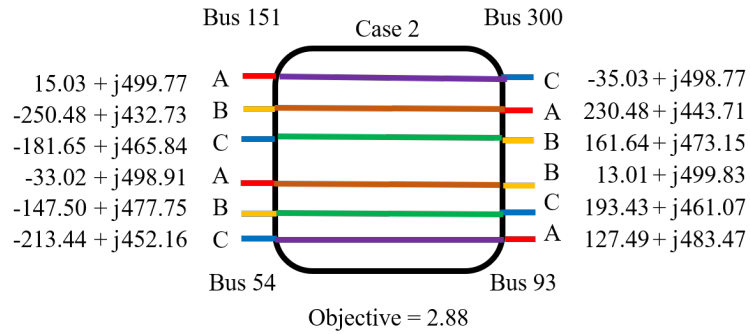
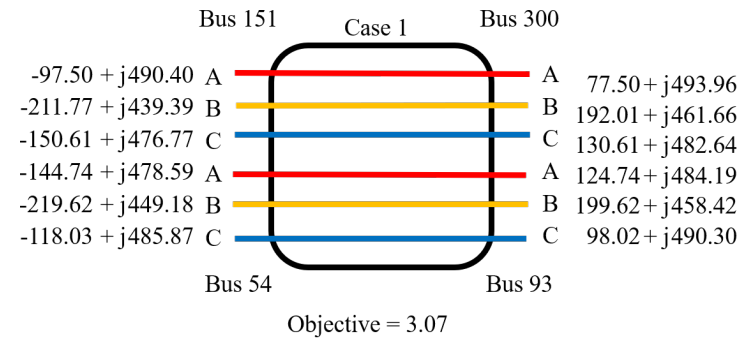


Figure 6.7: SOP power flows outcome (kVA).

balanced networks. As shown in Fig. 6.7, the differences in the transmitted power between different cases at hour 18 (peak load hour) are analyzed in detail as follows:

- In general, power is transferred from the network left side (bus 151 and bus 54) to the network right side (bus 300 and bus 93) because the substation is installed at the left (bus 150).
- The operational power of the multi-terminal PC-SOP is greater than those of the other 3 cases. The average active power of the multi-terminal PC-SOP is 423.55 kW. The average active powers of the other 3 cases are 137.08, 126.85 and 403.70 kW.
- In the Area A (from bus 97 to bus 450), Phase A load is the highest among three phases (Phase A: 688.92 kW, Phase B: 459.28 kW, Phase C: 535.82 kW at hour 18) and in the Area B (bus 72 to bus 96), Phase C load is the highest among three phases (Phase A: 1014.24 kW, Phase B: 1109.92 kW, Phase C: 1186.47 kW at hour 18). In Cases 2 to 4, SOP mainly transmit active power to Phase A at bus 300 and Phase C at bus 93. However, SOP cannot achieve this in Case 1. Meanwhile, the multi-terminal PC-SOP can transmit the highest power (562.27 kW and 644.83 kW). Therefore, Case 4 achieves the minimum objective value (1.39) at hour 18.

6.7.3 Algorithm validation

The computation information of the Case 4 is shown in Table 6.4 to demonstrate the superior numerical stability of the symmetrical SDP over the BFM-SDP. The results obtained with the BSM-SDP OPF and the symmetrical SDP OPF are compared with the OpenDSS benchmark results based on the absolute percentage errors of the voltages. The computation efficiency and robustness of the proposed method is demonstrated by comparing results with the Interior

Point OPTimizer (IPOPT, a software library for large scale nonlinear optimization of continuous systems) [150].

$$Error_v^\phi = \left| \frac{v_{SDP}^\phi - v_{OpenDSS}^\phi}{v_{OpenDSS}^\phi} \right| \times 100\% \quad (6.31)$$

Table 6.4: OPF solution time and voltage error on various test feeders

Test feeder	IEEE 13-Node				IEEE 123-Node			
	Volatge error%			Time(s)	Volatge error%			Time(s)
	Phase A	Phase B	Phase C		Phase A	Phase B	Phase C	
BFM-SDP (Sedumi)	2.103%	1.652%	1.451%	41.72	1.055%	2.422%	1.445%	202.23
BFM-SDP (Mosek)	-	-	-	-	-	-	-	-
Sym.SDP (Sedumi)	0.037%	0.028%	0.026%	39.59	0.014%	0.029%	0.018%	191.91
Sym.SDP (Mosek)	0.036%	0.028%	0.026%	12.53	0.014%	0.029%	0.018%	60.74
IPOPT	0.036%	0.028%	0.026%	116.09	0.014%	0.029%	0.018%	562.77

It is shown that the symmetrical SDP method achieves a voltage error of less than 0.2% which is smaller compared with the BFM-SDP. Based on [148], this research further proves that symmetrical SDP is more accurate and efficient compared with BFM-SDP in networks with multi-terminal SOPs with the SeDuMi (open-source SDP solver) [151] and MOSEK. Owing to the proper relaxation of the original problem with convexification, the symmetrical SDP method reduces the solving complexity (12.53 seconds for IEEE 13-node test feeder and 60.74 seconds for IEEE 123-node test feeder - both for 24-hour network operation) and obtains the solution within a reasonable accuracy. This creates possibilities for modeling larger test feeders (e.g. IEEE 8500-node test feeder). Nodal voltages for the IEEE 13-node test feeder at hour 1 as an example are shown in Table 6.5. When multi-terminal PC-SOP outputs are: Phase A $[0 + j0; 0 + j0; 0 + j0]$ kVA, Phase B $[44.356 + j78.027; -7.388 + j0.842; 13.632 +$

Table 6.5: Nodal voltages for the IEEE 13-node test feeder

Bus	symmetrical SDP			OpenDSS		
	Phase A	Phase B	Phase C	Phase A	Phase B	Phase C
SOURCEBUS	1	1	1	1	1	1
650	0.9999	0.9999	0.9999	1	1	1
RG60	1.0499	1.0374	1.0437	1.0498	1.0374	1.0436
633	1.0131	1.02	1.0087	1.0127	1.0202	1.0084
634	0.9963	1.0035	0.9955	0.9959	1.0037	0.9952
671	0.9893	1.0248	0.9871	0.9885	1.0258	0.9876
645	0	1.0127	1.0087	0	1.0128	1.0084
646	0	1.0109	1.0066	0	1.0111	1.0064
692	0.9893	1.0248	0.9871	0.9885	1.0258	0.9876
675	0.9851	1.0261	0.9868	0.9842	1.0271	0.9873
611	0	0	0.9831	0	0	0.9836
652	0.9818	0	0	0.981	0	0
632	1.0156	1.0219	1.0106	1.0153	1.0221	1.0103
680	0.9893	1.0248	0.9871	0.9885	1.0258	0.9876
684	0.9874	0	0.9851	0.9866	0	0.9856

$j244.930$] kVA and Phase C $[-15.150 + j68.443; -50.163 + j46.362; 4.190 + j44.788]$ kVA, all voltage errors are within 2%.

6.8 Conclusion

This chapter compares different SOP configurations for multiple buses in power distribution networks.

For one SOP situation, this chapter compares different cases of SOP configurations for multi-buses (including single-phase buses and two-phase buses) in power distribution networks. An optimized operational strategy based on various connection ways and the SOP with bifurcation connection is proposed to minimize the operational losses considering the growing penetration levels of DERs for unbalanced three-phase systems. The optimization results indicate that the

PC-SOP and bifurcation connection significantly reduce unbalanced loading conditions and power losses in ADNs. For distribution system operators, it can help to achieve a 24-hour optimal schedule of ADNs with the addition of flexible and controllable resources such as conventional SOPs, PC-SOPs and PVs in smart distribution systems.

For more than one SOP situation, an optimized operational strategy based on various connection ways and a new multi-terminal PC-SOP connection is proposed to minimize the operational losses considering the growing penetration levels of DERs for unbalanced three-phase networks. The optimization results indicate that the multi-terminal and PC-SOP cases significantly reduce unbalanced loading conditions and power losses in ADNs. For distribution network operators, it can help to achieve a 24-hour optimal ADN schedule with the addition of flexible and controllable resources such as conventional SOPs, PC-SOPs and PVs in smart ADNs. From the network side, both PC-SOPs and AC/DC hybrid networks can improve network performance. Research will be conducted on how to improve customer engagement and transfer the benefits of the network to the customer in the next chapter.

One of the limitations of the current study is that transient operational performance has not been carried out with hardware design and simulations which are required for further implementation.

Chapter 7

Power Flow Traceable P2P Electricity Market Segmentation and Pricing

7.1 Introduction

In this chapter, a P2P market architecture based on dynamic power flow tracing which improve market efficiency is proposed after research network operational efficiency improvement in the above chapters. It aims at boosting P2P engagements by improving to a fair market based on transparent energy tracing and pricing. The contributions of this study can be summarised as follows:

- The full potential of P2P market is explored - here ‘cocktail-layered energy market’ is used as an analogy of the market segmentation. Critical points of the different ‘cocktail layers’ for market segmentation are calculated by second-order cone programming.
- The loss function - a combination of an exponential function with a quadratic function, is

designed for different types of DERs based on various market situations in individual market sharing models. The percentage of DER's loss is in direct proportion with its output. Then based on the pricing strategy proposed in this chapter, the market price of a DER should be in inverse proportion with its output. Therefore, the output of a DER to achieve its maximum profit is pursued with a low loss proportion which is closely linked with the loss function in optimal power flows.

- The problem formulation approach is graph-based with nodes and links uniquely defined. Every participant is an optimisation node in the graph connected by link constraints of different optimisation functions. In this way, every participant's benefit is considered, while only price and power flow information is shared in the link constraints to ensure data privacy and security.
- A case study based on the IEEE 33-Node test feeder is conducted to verify the proposed power flow traceable P2P models. In a transparent open P2P market, the followings benefits are achieved: 1) DER owners could maximise their revenue meanwhile have clear information of associated network losses (percentage share of their total output in an individual P2P transaction); 2) consumers could benefit from lower energy costs due to DERs' pricing strategies for being continuously competitive in this market; 3) the power supply quality from the grid can be potentially improved because the proposed market allows market dominance for DERs when they are located close to the tails of the network where voltage drops tend to be a problem.

7.2 Dynamic Power Flow Tracing

7.2.1 Dynamic Power Flow Tracing Model

Distribution Networks Power Flow Tracing (DN-PFT), shown in Figure 7.1, can address the issue of breaking down a specific generator's power injection into constituent pieces that serve different loads, the undergone losses across lines, and enable transparent P2P energy trading [128].

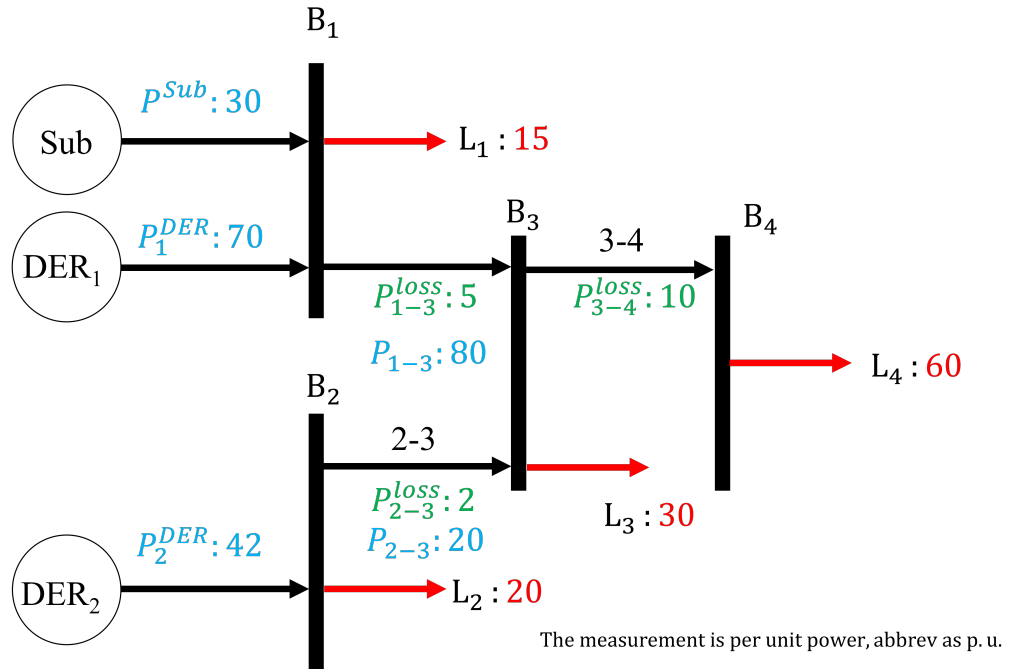


Figure 7.1: Benchmark circuit for demonstrating the DN-PFT energy transaction model.

$$P_g^{DER} = \sum_{j \in \Omega_n} \gamma_{load_j}^{DER_g} \cdot P_j^{load} + \sum_{lk \in \Omega_b} \gamma_{loss_{lk}}^{DER_g} \cdot P_{lk}^{loss} \quad (7.1)$$

where the coefficients $\gamma_{load_j}^{DER_g}$ and $\gamma_{loss_{lk}}^{DER_g}$ represent the proportions of power provided by DER g to load j and losses in line kl . They are calculated by applying the proportional sharing principle directly to each mixing bus, i.e., the bus that receives inputs from several sources

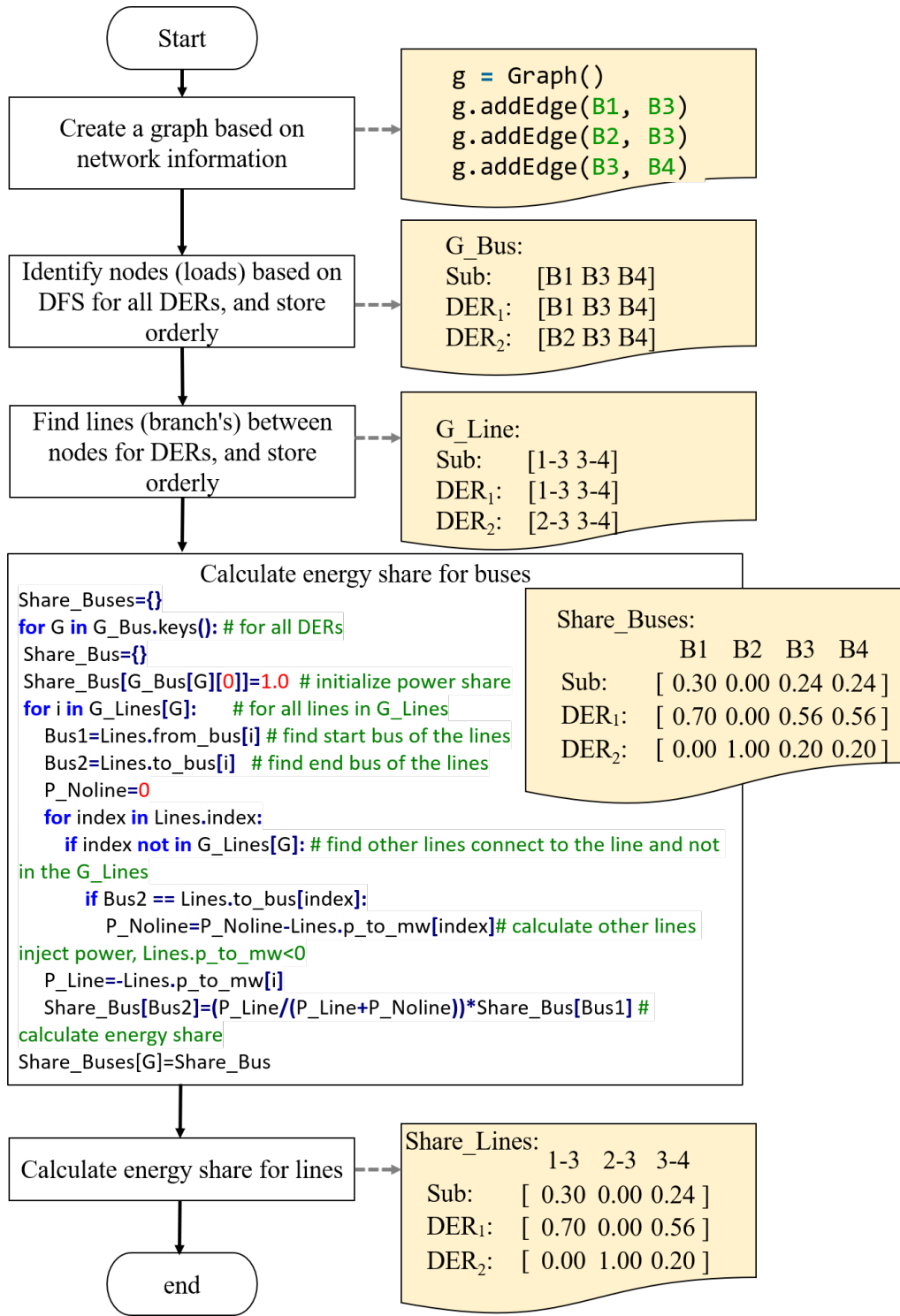


Figure 7.2: Proposed dynamic power flow tracing algorithms based on DFS.

[152]. P_j^{load} is the active power consumption of load j and P_{lk}^{loss} are the losses in line lk .

In Equation 7.2, the power share of a generator DER in the line ij is stated as the ratio of active power arriving from the DER to the total active power injected in the line, multiplied by the power share in line hi , which is likewise powered by the DER. (the power share in lines fed by this DER only, would be 1).

There will only be one path from the DER to the line due to the radial network topology. When applying this equation, it is critical to know which lines are powered by each DER. This computation should begin from the DER and work its way downstream to the loads. Therefore, for each computation, a depth-first search (DFS) for a graph is used to find sets of loads and sets of lines fed by each DER [153]. The DFS technique is used to traverse or explore data structures such as trees and graphs [154]. The algorithm starts from the root node (in this case of a graph, DER buses are used as the root node) and examines each branch as far as feasible before retracing. The fundamental concept is to start at the root or any arbitrary node and mark it, then proceed to the next unmarked node and repeat until there are no more unmarked nodes. Then it goes back and check for any additional unmarked nodes to cross. Finally, the path's nodes are output/printed. The key steps of the DFS are summarised as follows:

- Create a recursive function that takes a visited array and the index of nodes.
- Make the current node a visited node and print it.
- Call the recursive function using an index of the adjacent node after traversing all adjacent and unmarked nodes.

After DFS based power flow direction, the DER's share can be calculated based on the information of the sets of lines and the sets of nodes. A DER's share of power in a load will be the same as the DER's share of power in the last line feeding the load. The share of electric-

ity losses from a DER in a line is approximated to the share of power supplied by the DER through it. The pro-rata losses allocation assumption supports this assertion. As a result, in our model, a DER is responsible for the same share of losses in a line as the DER's share of power served through the line.

$$\begin{aligned}
 \gamma_{ij}^{DER_g} &= \gamma_{hi}^{DER_g} \frac{\Re(V_i \cdot \Sigma(Y_{ig})^* \cdot (V_g)^*)}{P_i} \\
 &= \gamma_{hi}^{DER_g} \frac{\Re(V_i \cdot \Sigma(Y_{ig})^* \cdot (V_g)^*)}{\Re(V_i \cdot \Sigma(Y_{ik})^* \cdot (V_k)^*)} \\
 &= \gamma_{hi}^{DER_g} \frac{\Re(I_i^{DER_g})}{\Re(I_i)}
 \end{aligned} \tag{7.2}$$

where $\gamma_{ij}^{DER_g}$ is the proportion of power of line ij provided by DER at node g ; I_i is the current injected in node i ; $I_i^{DER_g}$ is the current injected in node i from DER at node g .

The principles discussed thus far are depicted in Figure 7.1 as a circuit, where the proportions of power are calculated using Equation 7.2, the result is:

$$\begin{aligned}
 \gamma_{13}^{Sub} &= 30/(30 + 70) = 0.30 \\
 \gamma_{23}^{Sub} &= 0/42 = 0 \\
 \gamma_{34}^{Sub} &= 0.30 \times 80/(80 + 20) = 0.24 \\
 \\
 \gamma_{13}^{DER_1} &= 70/(30 + 70) = 0.70 \\
 \gamma_{23}^{DER_1} &= 0/42 = 0 \\
 \gamma_{34}^{DER_1} &= 0.70 \times 80/(80 + 20) = 0.56 \\
 \\
 \gamma_{13}^{DER_2} &= 0/(30 + 70) = 0 \\
 \gamma_{23}^{DER_2} &= 42/42 = 1.00 \\
 \gamma_{34}^{DER_2} &= 1.00 \times 20/(80 + 20) = 0.20
 \end{aligned} \tag{7.3}$$

The technique presented in Figure 7.2 is used to dynamically track the power flowing at each time step and distribute it across generators. Indices are used to loop the power share assessment in a line from any generator and across all lines.

Determining which lines are powered by a particular generator is a procedure that is aided by power flow calculations at each time step. The lines are checked with the DFS search order. First, each line with outflows is chosen to start from the connecting point for each generator. Then, the node at the end of the line is examined, and lines connecting to them with outflows are chosen once again. This process is repeated until there are no further outflows.

The technique for calculating power shares in loads is identical to that for lines linked to the same bus. The power in load L3 (30, per unit power, abbrev as p.u.) is 24% provided by the substation (7.2 p.u.), 56% provided by DER1 (16.8 p.u.), and 20 % provided by DER 2 (6.0 p.u.). Loads supplied by a specific generator may also be tracked; for example, the substation feeds 30% of L1 (15 p.u., linked to B1 and with the same share as line 1-3), 24% of L3 (30 p.u., connected to B3 and with the same share as line 3-4), and 24% of L4 (60 p.u., connected to B4 and with the same share as line 3-4); Therefore, the substation feeds loads 26.1 p.u. in total. The remaining 3.9 p.u. produced by the substation are for losses in the lines.

7.2.2 Loss Allocation Based on Power Flow Tracing

Considering the energy transaction benchmark circuit depicted in Figure 7.1, which includes the substation, DER 1, and DER 2 that produce 30 p.u., 70 p.u., and 42 p.u., respectively. There are three lines and four loads. Line losses are highlighted in green. The number of energy transactions is 9 which can be easily explained by the number of generators feeding directly the bus where the load is connected (the substation L1, DER 1 L1 in B1 and DER 2

Table 7.1: Transaction Breakdown

	P_{13}^{loss}	P_{23}^{loss}	P_{34}^{loss}	Total losses	Power transferred	
Sub - L1	0.00	0.00	0.00	0.00	4.50	
Sub - L3	0.45	0.00	0.00	0.45	7.20	Sub: 26.10
Sub - L4	1.05	0.00	2.40	3.45	14.40	
DER ₁ - L1	0.00	0.00	0.00	0.00	10.50	
DER ₁ - L3	1.05	0.00	0.00	1.05	16.80	DER ₁ : 60.90
DER ₁ - L4	2.45	0.00	5.60	8.05	33.60	
DER ₂ - L2	0.00	0.00	0.00	0.00	20.00	
DER ₂ - L3	0.00	0.60	0.00	0.60	6.00	DER ₂ : 38.00
DER ₂ - L4	0.00	1.40	2.00	3.40	12.00	

* The measurement is per unit power, abbrev as p.u.

L2 in B2) or powering the line feeding the bus (the substation L3, the substation L4, DER 1 L3, DER 1 L4, DER 2 L3 and DER 2 L4, with the substation, DER 1, and DER 2 feeding B3 with L3 and powering line 3-4 feeding B4 where L4 is connected).

Lines from a particular transaction are traced upstream from the bus to which the load is linked, seeking lines powered by the generator in this transaction. Table 7.1 provides breakdown of the transactions, identifying the lines involved, their loss shares, and the electricity generated that is delivered to the loads. The total losses, which are accounted for DERs, can be calculated using Equation 7.5, where the set comprises all of the lines powered by a DER.

$$P_{loss}^{DERg} = \sum \gamma_{ij}^{DERg} \cdot P_{ij}^{loss} \quad (7.4)$$

$$\begin{aligned}
P_{loss_{ij}}^{DER_g} &= \sum \gamma_{ij}^{DER_g} \cdot P_{ij}^{loss} \cdot \gamma_{ij}^{load_y} \\
\gamma_{ij}^{load_y} &= \gamma_{ik}^{load_y} \cdot \frac{\Re(V_i \cdot \sum(Y_{iy})^* \cdot (V_y)^*)}{P_i} \\
&= \gamma_{ik}^{load_y} \cdot \frac{\Re(V_i \cdot \sum(Y_{iy})^* \cdot (V_y)^*)}{\Re(V_i \cdot \sum(Y_{ik})^* \cdot (V_k)^*)} \\
&= \gamma_{ik}^{load_y} \cdot \frac{\Re(I_i^{load_y})}{\Re(I_i)}
\end{aligned} \tag{7.5}$$

$$P_{loss}^{DER_g} = \sum P_{loss_{ij}}^{DER_g} \tag{7.6}$$

The losses incurred as a result of a certain transaction are provided by Equation 7.5, where the set contains all lines powered by DER at node g participating in the transaction. $\gamma_{ij}^{load_y}$ denotes the power share to load at node y ; $P_{loss}^{DER_g}$ is the active power loss consumption of DER at node g ; $P_{loss_{ij}}^{DER_g}$ is the active power loss consumption of line ij of the DER at node g . Its computation necessitates knowledge of the power share in the next line along the way to the load; hence, this calculation should begin at the load and go upstream to the generator as expressed in Equation 7.6.

7.3 Market Segmentation and Modeling

Based on the previous study on dynamic power flow tracing [128], applications in marketing segmentation and corresponding modeling are explored in this section considering proportional sharing of energy and losses.

7.3.1 Market Segmentation Principle

In the proposed model, the buses/areas towards the grid supply point/sub-station from the point of common-coupling of a DER are called ‘upstream’; whereas, those close to the tails of the network are called ‘downstream’. Considering a case with two DERs (generators) in one feeder from a substation (Sub) in top of Figure 7.3. DER 1 position is used as the reference to partition the network. B and C are wires (cables) upstream. D is the wire downstream. E is a branch wire. For DER 1, once its downstream loads are fully fed by it, surplus power flows against the power flow from the substation. After branch E loads are fed by DER 1, electricity fed by DER 2 could be in reverse flows through the transformer. In addition, how DER 2 can feed to the network depends on power from DER 1.

Under this assumption, DERs located close to the tails of the network have the market dominance - as naturally power flows will follow low impedance routes. This leads to the fact that the market segmentation fully depends on power flow tracing results. For example, DER 1 and DER 2 are shown in Figure 7.3 both have the ability to cover all loads’ needs in the network in the assumption. As DER 1 is located in the tail of the system, DER 1 will take all markets and DER 2 only can sell its power to upper-level substations. This in fact can encourage DERs to be installed within and towards the tails of the network where potential voltage drop issues can be alleviated. The active power market-entry limitation of one generator is obtained by setting the corresponding wire active power as 0. Base on the above, ‘branch market’ is defined as customers being fed by the substation or DERs connected to other branches, when the local DER cannot meet load demand or there is no DER available locally in this branch. For example, by setting the active power of wire B as 0, the active power of DER 1 is its market-entry limitation for the ‘branch market’. If DER 1 wants to get in the ‘branch market’, its active power output should be larger than the above limit. These active power market-entry

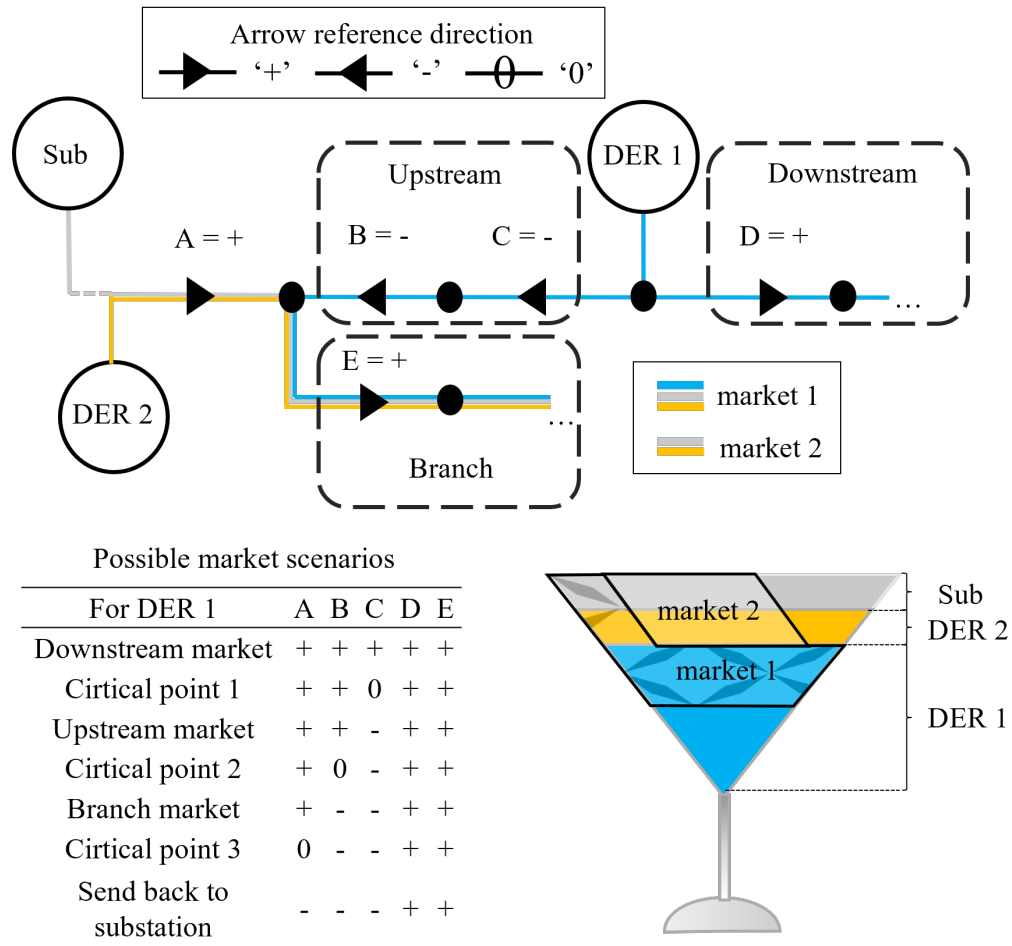


Figure 7.3: Market segmentation based on dynamic power flow tracing.

limitations are named as ‘critical points’ between different markets.

Arrow directions of A, B, C, D and E are active power flow directions. ‘+’ corresponds to flows in the same direction as that radial coming from the substation and ‘-’ corresponds to flows in the opposite direction. ‘0’ means there is no active power flow in this wire. The ‘branch market’ situation is shown in Figure 7.3 as an example, where arrow directions of A, D, E are ‘+’. Arrow directions of B and C are ‘-’. Downstream and upstream loads are fully supplied by DER 1. The flows through wires B (from DER 1) and A (from DER 2 and the substation) converge to wire E. Therefore, the branch market is open for P2P competitions.

Possible market scenarios are listed in the table of Figure 7.3:

- *Downstream market:* Arrow directions of A, B, C, D, E are all '+'. Loads are supplied by DER 1, DER 2 and the substation.
- *Upstream market:* Arrow directions of A, B, D, E are '+'. The arrow direction of C is '-'. Loads in the upstream market are supplied by DER 1, DER 2 and the substation. Meanwhile, DER 1 downstream loads are only supplied by DER 1.
- *Branch market:* as described herein-before.
- *Surplus market:* After market 1 (explained below), loads are supplied by DER 2 and the substation.

Only one area of loads from downstream, upstream and branch can be fed by all of DER 1, DER 2 and the substation. Therefore, only one market of the downstream market, upstream market and branch market can exist at one time, marked as 'market 1'. The surplus market happens with one of the above three markets at the same time, marked as 'market 2'. In this case, network loads are met ('filled') by DER 1, DER 2 and the substation in order.

7.3.2 Market Segmentation Model

These newly defined critical points can be identified with the minimum absolute value of specified branch active power by means of second-order cone programming (SOCP). Critical point 1 means that DER 1 output well matches its downstream loads. Critical point 2 means that DER 1 output can fulfill downstream loads plus upstream loads. Critical point 3 means that DER 1 output plus DER 2 output equal to downstream loads plus upstream loads plus branch load. DER outputs for different critical points, $P_i^{DER,cp}$, can be calculated when the value of specified branch active power is close to 0, e.g. the branch are A, B or C near the bifurcation

branch E or DER 1, as shown in Figure 7.3. An analogy of the market segmentation based on power flow tracing is ‘a layered cocktail’ that has a sequentially filled characteristic, where critical points are similar to the liquid interfaces between different layers in a cocktail.

$$\min |P_{ij}| \quad \forall ij \in \text{branch } A, B \text{ or } C \quad (7.7)$$

Power flow constraints:

$$\left\{ \begin{array}{l} \sum_{ik \in \Omega_b} P_{ik} = \sum_{ij \in \Omega_b} (P_{ji} - R_{ji}(I_{ji})^2) + P_i \\ \sum_{ik \in \Omega_b} Q_{ik} = \sum_{ij \in \Omega_b} (Q_{ji} - X_{ji}(I_{ji})^2) + Q_i \\ P_i = P_i^{DER} - P_i^{load} \\ Q_i = Q_i^{DER} - Q_i^{load} \\ (V_i)^2 = (V_j)^2 - 2(R_{ji}P_{ji} + X_{ji}Q_{ji}) + (R_{ji}^2 + X_{ji}^2)(I_{ji})^2 \\ \underline{V}_i \leq V_i \leq \bar{V}_i \end{array} \right. \quad (7.8)$$

Where Ω_b is the set of all network branches; P_{ji} and Q_{ji} are the active and reactive powers from node j to node i ; P_i and Q_i are active and reactive power injections of node i ; P_i^{DER} and Q_i^{DER} are the active and reactive powers of DER of node i ; P_i^{load} and Q_i^{load} are the active and reactive powers of load of node i ; R_{ij} is the resistance of branch ij ; X_{ij} is the reactance of branch ij ; $V_{i,t}$ is the voltage of node i .

By replacing $(I_{ij})^2$ and $(V_i)^2$ with l_{ij} and v_i , the model of network in the second-order cone programming is formulated as follows:

$$\left\{ \begin{array}{l}
 \sum_{ik \in \Omega_b} P_{ik} = \sum_{ij \in \Omega_b} (P_{ji} - R_{ji} l_{ij}) + P_i \\
 \sum_{ik \in \Omega_b} Q_{ik} = \sum_{ij \in \Omega_b} (Q_{ji} - X_{ji} l_{ij}) + Q_i \\
 P_i = P_i^{DER} - P_i^{load} \\
 Q_i = Q_i^{DER} - Q_i^{load} \\
 v_i = v_j - 2(R_{ji} P_{ji} + X_{ji} Q_{ji}) + (R_{ji}^2 + X_{ji}^2) l_{ij} \\
 \underline{v}_i \leq v_i \leq \bar{v}_i
 \end{array} \right. \quad (7.9)$$

$$l_{ij} = \frac{(P_{ij}^2 + Q_{ij}^2)}{v_{ij}} \quad ij \in \Omega_b \quad (7.10)$$

Equation (7.10) can be further loosened and transformed into the form of SOCP.

$$\|[2P_{ij} \ 2Q_{ij} \ l_{ij} - V_{ij}]^T\|_2 \leq l_{ij} + V_{ij} \quad (7.11)$$

The generation share that a DER can participate within a market is calculated by the following equation:

$$\eta_i^{DER,share} = \frac{P_i^{DER} - P_i^{DER,cp}}{P_i^{DER}} \quad (7.12)$$

where $\eta_i^{DER,share}$ is the market share of DER at node i .

7.3.3 Individual Market Loss Allocation Model

After determining the market segmentation by systematic sampling of P^{DER} , the loss function is defined as the combination of an exponential function and a quadratic function. This definition enables limiting the error within the range of 10^{-3} [155]:

$$f^{loss}(x) = m \cdot \ln(x) + ax^2 + bx + c \quad (7.13)$$

where f^{loss} represents $(1 - P_{loss}^{DER}/P^{DER})$, loads percentage of DER active power output (excluding losses); P_{loss}^{DER}/P^{DER} represents network loss percentage of DER active power output; x represents $P^{DER}/\sum P^{load}$, DER active power percentage of whole networks loads.

When DER active power percentage ($P^{DER}/\sum P^{load}$) increases, the load area transferred by DER increases. Therefore, an DER accounts for more losses in the network as its power is transferred to the loads further than before (P_{loss}^{DER}/P^{DER} increases and f^{loss} decreases).

7.3.4 Individual DER Pricing Strategy Model

Pricing strategy function:

$$\begin{cases} Price^{DER} = Price^{Grid} - \alpha Price^{Grid} \cdot \frac{P^{DER}}{P^{DER,max}} \\ 0 < \alpha \leq 0.5 \end{cases} \quad (7.14)$$

$$-\alpha \cdot \frac{Price^{Grid}}{P^{DER,max}} < 0 \quad (7.15)$$

$$Price^{Grid} - 2\alpha \cdot \frac{Price^{Grid} \cdot P^{DER}}{P^{DER,max}} \geq 0 \quad (7.16)$$

where the DER income function is $Income^{DER} = Price^{DER} \cdot P^{DER}$. By setting the price factor α meeting, 1) the derivative of price function is less than zero, as expressed in Equation (7.15) and 2) the income function is not negative, as expressed in Equation (7.16). It satisfies that the total income increases when DERs increase outputs until their maximum capacities, even though marginal price decreases. It motivates prosumers to increase their DER outputs whilst decreasing their unit price.

7.3.5 Model Implementation

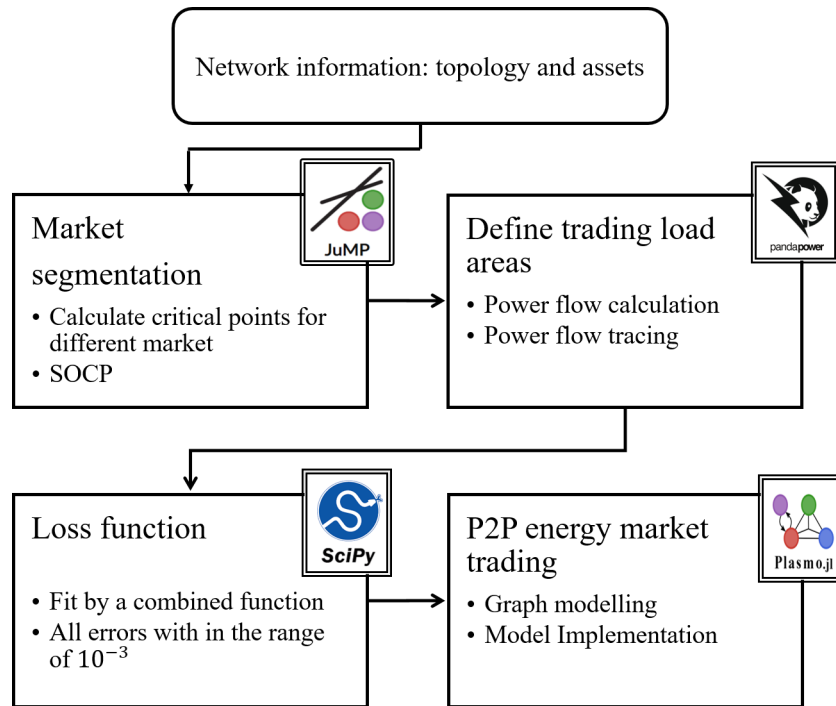


Figure 7.4: Flow chart of the implementation process with the proposed P2P market model, functions and algorithms.

The models described in the previous section within the P2P energy market are implemented

with OptiGraph, built with a set of OptiNodes (each embedding an optimization model with its local variables, constraints, objective function and data) and a set of OptiEdges (each embedding a set of linking constraints) [156]. The OptiGraph as an undirected hypergraph contains the optimization model of interest. The OptiEdges are hyperedges that connect two or more OptiNodes.

OptiNode model for $load_a$

Here a represents a set of loads in market 1 and market 2. The $load_a$'s objective is to minimize its electricity purchase cost.

$$\begin{aligned}
 \min \quad & Price_i^{DER} \cdot P_i^{DER-load_a} + Price^{Grid} \cdot P^{Grid-load_a} \\
 \text{s.t.} \quad & P_i^{DER-load_a} + P^{Grid-load_a} = P_i^{load_a} \\
 & P_i^{DER-load_a}, P^{Grid-load_a} \geq 0
 \end{aligned} \tag{7.17}$$

where $Price^{Grid}$ is the electricity price from the substation; $P_i^{DER-load_a}$ is the active power from DER at node i to $load_a$; $P_i^{Grid-load_a}$ is the active power from substation to $load_a$.

OptiNode model for DER

Each DER's objective is to maximize its total income.

$$\begin{aligned}
\max \quad & Price_i^{DER} \cdot P_i^{DER_{no\,loss}} \\
\text{s.t.} \quad & Price_i^{DER} \leq Price^{Grid} \\
& P_i^{DER} \leq P_i^{DER,max} \\
& P_i^{DER_{no\,loss}} = f^{loss} \left(\frac{P_i^{DER}}{\sum P_i^{load}} \right) \cdot P_i^{DER} \\
& Price_i^{DER} = Price^{Grid} - \alpha Price^{Grid} \cdot \frac{P_i^{DER}}{P_i^{DER,max}} \\
& 0 < \alpha_i \leq 0.5
\end{aligned} \tag{7.18}$$

where $P_i^{DER,max}$ is the maximum active power of DER at node i ; $P_i^{DER_{no\,loss}}$ is active power output from DER at node i except for its accounts for the losses.

OptiEdges for linking constraints

Linking constraints include price linking constraints and power linking constraints.

Price linking constraints: The price provided by DERs equals to the price received by customers.

Power linking constraints: DER outputs in markets equals to all loads in markets.

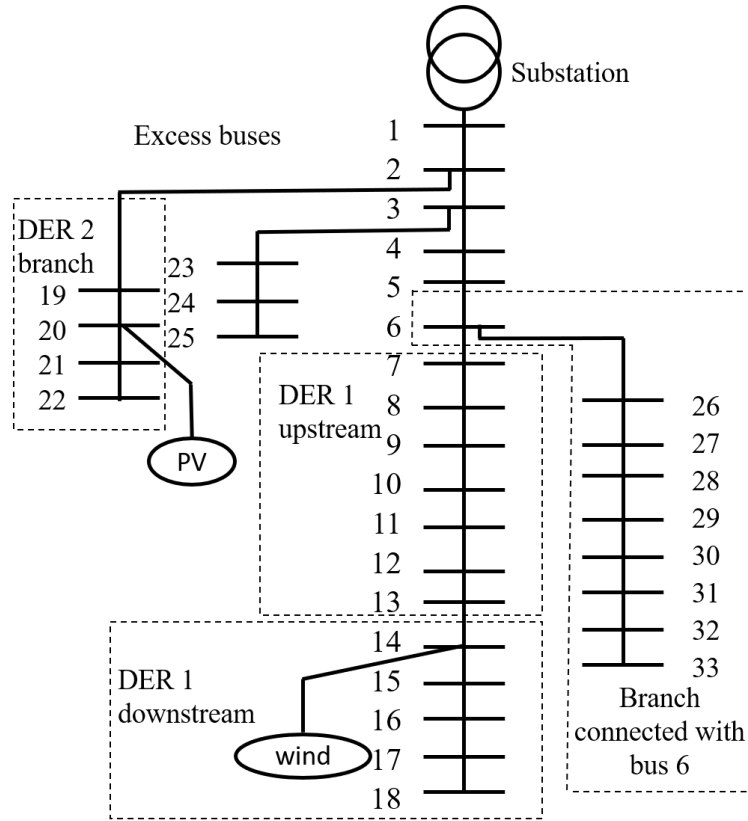
$$P_i^{DER_{no\,loss}} \cdot \eta_i^{DER,share} = \sum P_i^{DER-load_a} \tag{7.19}$$

7.4 Methodology: Design of the Experiment

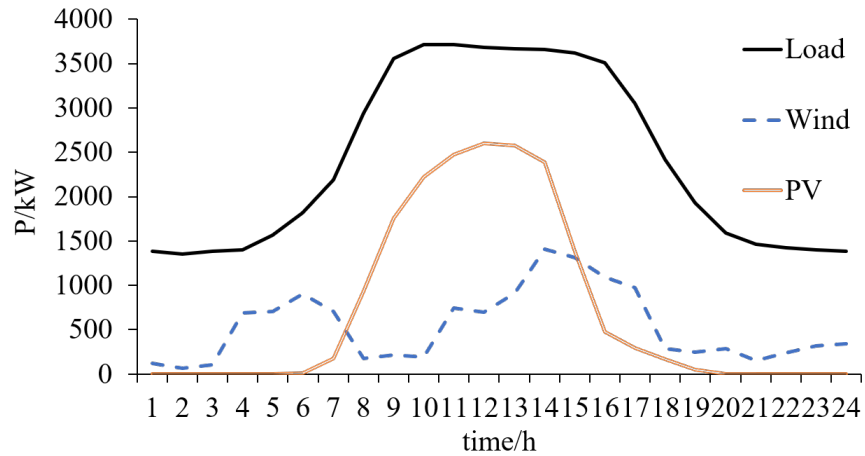
The design of the experiment of implementing the proposed P2P market model and algorithms is shown in Figure 7.4, based on Python and Julia [157].

- *Market Segmentation:* Critical points for different markets are calculated by the SOCP coded with a Julia package, JuMP [158].
- *Defining trading load areas:* The power flow tracing model is based on that published in [128], with power flow calculations obtained by means of the Python package, Pandapower [159].
- *Loss functions:* All loss functions are fitted by the Python package `scipy.optimize.curve_fit` [160] and the error tolerance is set as 10^{-3} .
- *P2P energy market trading:* This is based on graph modeling which is coded with a Julia package, Plasmo [156].

The computing environment used to simulate the proposed model is Intel i7-10850H 2.7GHz CPU, 32GBRAM, Linux (Ubuntu). The IEEE 33-node test feeder, a 12.66kV radial distribution system is used for this case study. The original circuit is modified by installing two DERs: a 2 MVA wind power turbine (DER 1) at bus 14 and a 3 MVA solar photo-voltaic (PV) plant (DER 2) at bus 20. The topology of the circuit is shown in Figure 7.5a. The profiles of DER 1, DER 2 and all the loads are shown in Figure 7.5b.



(a) Topology of the IEEE 33-node test feeder



(b) PV, wind generation and load profiles

- * The IEEE 33-node test feeder (12.66kV), created by Baran & Wu, was used to study the impact of distribution network reconfiguration on power losses reduction and load balancing [130].
- * PV generation profile from Photovoltaic Solar Panel Energy Generation data [137].
- * Wind generation profile from Wind energy in the UK [161].
- * Load profiles from Standard Load Profile [136].

Figure 7.5: IEEE 33-node test feeder and PV, wind generation and load profiles.

7.5 Case Studies

7.5.1 Market Segmentation Result

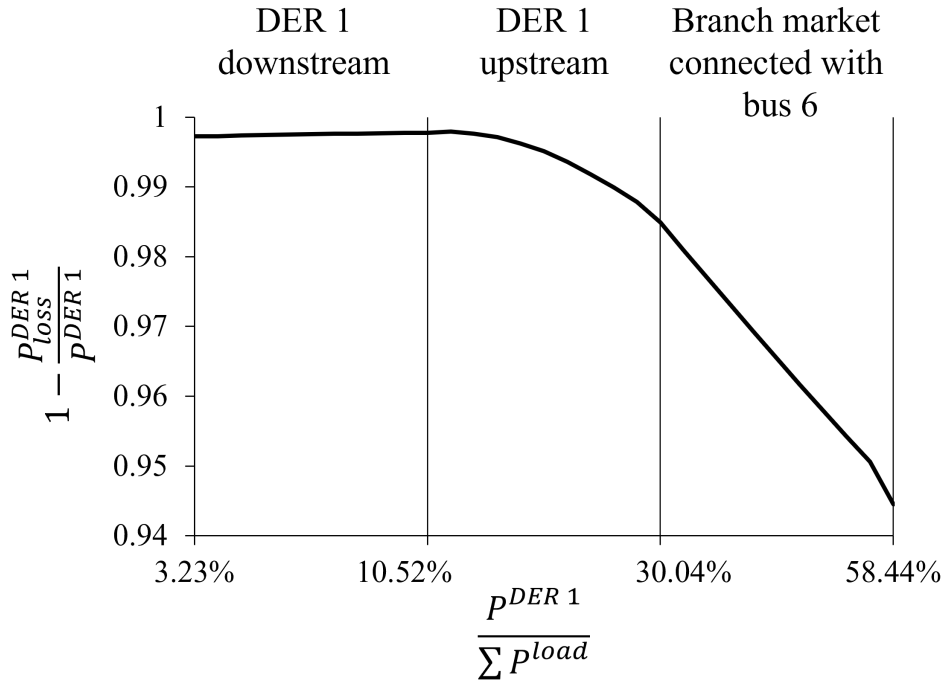
Considering all DERs are under maximum output situation, four load areas are categorized as follows: DER 1 downstream (buses 15 to 18), DER 1 upstream (buses 7 to 13), bus 6 with its branch (bus 6 and buses 26 to 33), and excess buses (buses 1 to 6 and buses 23 to 24), as shown in Figure 7.5a and Table 7.2. Colours are used to visualize different markets in 24 hours.

DER 1 downstream market (including DER 1 downstream loads): From hours 1 to 3, loads are supplied by both substation and DER 1. From hours 8 to 10, loads are supplied by the substation, DER 1 and DER 2.

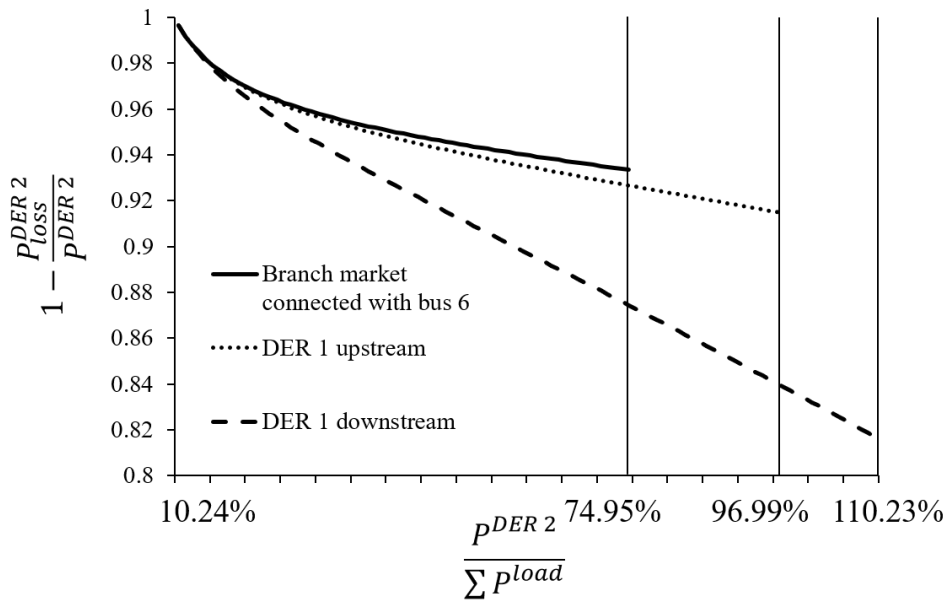
DER 1 upstream market (including DER 1 upstream loads): From hours 11 to 13, loads are supplied by substation, DER 1 and DER 2. From hours 18 to 24, loads are supplied by substation and DER 1.

Branch market connected with bus 6 (including Bus 6 with its branch loads): From hours 4 to 7, loads are supplied by both the substation and DER 1. From hours 14 to 17, loads are supplied by the substation, DER 1, and DER 2.

Surplus market: In hours 6, 7, 18, and 19, there are sporadic markets between DER 2 and substation. These markets are independent of the markets between DER 1 and substation. Therefore, these markets can be ignored considering DER 2 output is small. However, between hour 8 and hour 17, the surplus market at least includes all loads from excess buses and can influence market 1. Therefore, the surplus market is considered during this period.



(a) Loss percentage $(1 - \frac{P_{loss}^{DER1}}{P^{DER1}})$ and DER percentage $(\frac{P^{DER1}}{\sum P^{load}})$ functions of DER 1



(b) Loss percentage $(1 - \frac{P_{loss}^{DER2}}{P^{DER2}})$ and DER percentage $(\frac{P^{DER2}}{\sum P^{load}})$ functions of DER 2

Figure 7.6: Loss functions of DERs in different markets.

Table 7.2: 24-hour power flow tracing results for the IEEE 33-Node test network

		time/h																									
		1	2	3	4	5	6	7	8	9	10	11	12	13	14	15	16	17	18	19	20	21	22	23	24		
Bus number	Excess buses	1	100	100	100	100	100	100	100	100	100	100	100	100	100	100	100	100	100	100	100	100	100	100	100	100	
		2	100	100	100	100	100	100	100	100	110	110	110	110	110	110	110	110	110	110	100	100	100	100	100	100	100
		3	100	100	100	100	100	100	100	100	110	110	110	110	110	110	110	110	110	110	100	100	100	100	100	100	100
	Bus 6	4	100	100	100	100	100	100	100	100	110	110	110	110	110	110	110	110	110	110	100	100	100	100	100	100	100
		5	100	100	100	100	100	100	100	100	110	110	110	110	110	110	110	110	110	110	100	100	100	100	100	100	100
		6	100	100	100	101	101	101	101	101	110	110	110	110	110	110	111	111	111	111	100	100	100	100	100	100	100
	DER 1 upstream	7	100	100	100	001	001	001	001	001	110	110	110	110	110	111	001	001	001	001	100	100	100	100	100	101	101
		8	100	100	100	001	001	001	001	001	110	110	110	111	111	001	001	001	001	001	100	100	100	100	100	101	001
		9	100	100	100	001	001	001	001	001	110	110	110	001	001	001	001	001	001	001	100	100	101	100	101	001	001
	DER 1 downstream	10	100	100	100	001	001	001	001	001	110	110	110	001	001	001	001	001	001	001	100	100	001	100	001	001	001
		11	100	100	100	001	001	001	001	001	110	110	110	001	001	001	001	001	001	001	100	100	001	100	001	001	001
		12	100	100	100	001	001	001	001	001	110	110	110	001	001	001	001	001	001	001	100	101	001	100	001	001	001
	DER 2 branch	13	100	100	100	001	001	001	001	001	110	110	110	001	001	001	001	001	001	001	101	001	001	101	001	001	001
		14	001	001	001	001	001	001	001	001	001	001	001	001	001	001	001	001	001	001	001	001	001	001	001	001	001
		15	101	101	101	001	001	001	001	001	111	111	111	001	001	001	001	001	001	001	001	001	001	001	001	001	001
	Branch connected with bus 6	16	101	101	101	001	001	001	001	001	111	111	111	001	001	001	001	001	001	001	001	001	001	001	001	001	
		17	101	101	101	001	001	001	001	001	111	111	111	001	001	001	001	001	001	001	001	001	001	001	001	001	
		18	101	101	101	001	001	001	001	001	111	111	111	001	001	001	001	001	001	001	001	001	001	001	001	001	001
	Excess buses	19	100	100	100	100	100	100	110	010	010	010	010	010	010	010	010	010	010	010	100	100	100	100	100	100	
		20	100	100	100	100	100	110	010	010	010	010	010	010	010	010	010	010	010	010	100	100	100	100	100	100	
		21	100	100	100	100	100	100	010	010	010	010	010	010	010	010	010	010	010	010	110	110	100	100	100	100	
	Branch connected with bus 6	22	100	100	100	100	100	010	010	010	010	010	010	010	010	010	010	010	010	010	110	110	100	100	100	100	
		23	100	100	100	100	100	100	100	100	110	110	110	110	110	110	110	110	110	110	100	100	100	100	100	100	
		24	100	100	100	100	100	100	100	100	110	110	110	110	110	110	110	110	110	110	100	100	100	100	100	100	
	Excess buses	25	100	100	100	100	100	100	100	100	110	110	110	110	110	110	110	110	110	110	100	100	100	100	100	100	
		26	100	100	100	101	101	101	101	101	110	110	110	110	110	110	111	111	111	111	100	100	100	100	100	100	
		27	100	100	100	101	101	101	101	101	110	110	110	110	110	110	111	111	111	111	100	100	100	100	100	100	
	Branch connected with bus 6	28	100	100	100	101	101	101	101	101	110	110	110	110	110	110	111	111	111	111	100	100	100	100	100	100	
		29	100	100	100	101	101	101	101	101	110	110	110	110	110	110	111	111	111	111	100	100	100	100	100	100	
		30	100	100	100	101	101	101	101	101	110	110	110	110	110	110	111	111	111	111	100	100	100	100	100	100	
	Excess buses	31	100	100	100	101	101	101	101	101	110	110	110	110	110	110	111	111	111	111	100	100	100	100	100	100	
		32	100	100	100	101	101	101	101	101	110	110	110	110	110	110	111	111	111	111	100	100	100	100	100	100	
		33	100	100	100	101	101	101	101	101	110	110	110	110	110	110	111	111	111	111	100	100	100	100	100	100	



If the bus is supplied by the source, the corresponding digit is noted as 1 otherwise 0. E.g., 111 means this bus is supplied by DER 1, DER 2 and substation.

7.5.2 Individual Market Sharing Result

Active power market-entry limitations of DERs are shown in Table 7.3. By setting $P_{ij} \big|_{i=13, j=14}$, $P_{ij} \big|_{i=6, j=7}$, $P_{ij} \big|_{i=5, j=6}$ as 0, active power market-entry upper limitations of the downstream generator can be obtained as 10.52%, 30.04% and 58.44%. 3.23% means DER 1 located in bus 14 can meet the demand of the local load. Based on the DER 1 market $P_{ij} = 0$ condition, by setting $P_{ij} \big|_{i=1, j=2}$ as 0, upper limitations of the downstream generator for different markets can be obtained as 110.23%, 96.99% and 74.95%. 10.24% means DER 2 located in bus 20 can meet the demand of loads from the branch (bus 19 to bus 22).

Table 7.3: Active power market-entry limitations of DERs

	DER 1 downstream	DER 1 upstream	Branch market connected with bus 6
Market bus	15 to 18	7 to 13	6 to 33 and 6
$P_{ij} = 0$ (DER 1 market)	$i = 13, j = 14$	$i = 6, j = 7$	$i = 5, j = 6$
$P_{DER1} / \sum P_{load}$	3.23% ~ 10.52%	10.52% ~ 30.04%	30.04% ~ 58.44%
Power factor (DER 1)	0.85	0.85	0.97
Voltage at DER 1	0.95	1	1.04
$P_{ij} = 0$ (DER 2 market)	$i = 1, j = 2$	$i = 1, j = 2$	$i = 1, j = 2$
$P_{DER2} / \sum P_{load}$	10.24% ~ 110.23%	10.24% ~ 96.99%	10.24% ~ 74.95%
Power factor (DER 2)	0.84	0.85	1
Voltage at DER 2	1.07	1.05	1.03

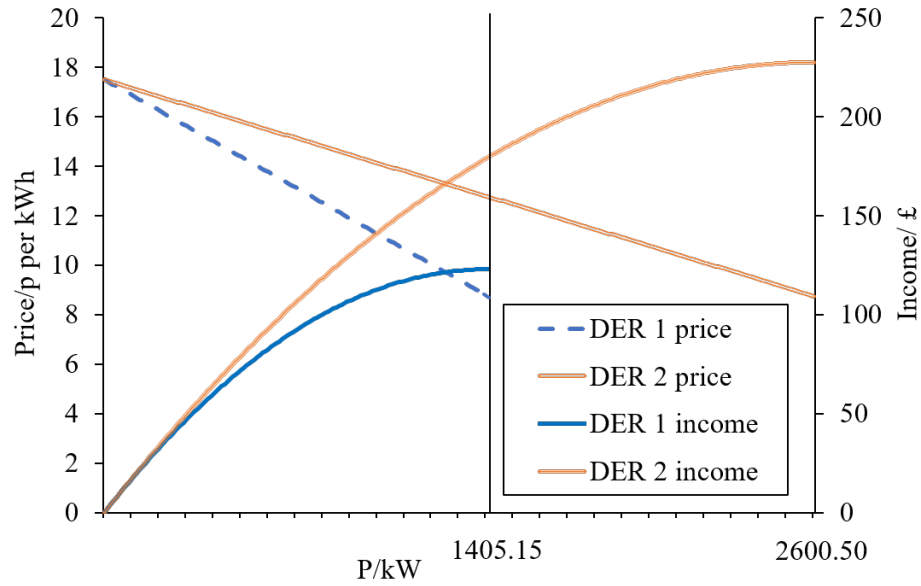


Figure 7.7: Pricing strategy and total income functions of DER 1 and DER 2.

Different loss functions for different DERs in different market situations are shown in Figure 7.6. Fitted loss functions' parameters are shown in Table 7.4 .

For the DER 1 power generator, in the test system, the loss function curve can be divided into three parts: constant (zero deceleration), increasing deceleration, constant deceleration, corresponding to three market situations: DER 1 downstream, DER 1 upstream, and Branch

market.

For DER 2 in the test system, when it can get into more markets, it shares more losses even with the same output because it can transfer power to loads farther away. Therefore, the slope of the loss function of DER 2 can be sorted from the largest to the smallest as: DER 1 downstream > DER 1 upstream > Branch market connected with bus 6.

Table 7.4: Loss Function Parameters

	Loss index of DER 1			Loss index of DER 2		
	DER 1 downstream market	DER 1 upstream market	Branch market connected with bus 6	DER 1 downstream market	DER 1 upstream market	Branch market connected with bus 6
m	0	0	0	-0.0361	-0.0464	-0.0356
a	0	-0.4370	0	-0.0510	-0.0492	0
b	0	0.0937	-0.1376	-0.0312	0.0800	0.0019
c	0.9975	0.9927	1.0220	0.9162	0.8813	0.9100
Error*	1.63E-04	2.71E-04	6.04E-04	3.92E-04	4.10E-04	8.67E-04

* Standard error of the regression.

7.5.3 Market Pricing Results

Individual Prices and DER Outputs

The pricing strategy function is shown in Figure 7.7, with an assumption that $\alpha^{DER1} = \alpha^{DER2} = 0.5$. When DER 1 arrives at its maximum output of 1405.14 kW or DER 2 arrives at its maximum output of 2600.50 kW, they can provide the price of 8.747 p/kWh (pence per kilowatt-hour) as half of the standard electricity tariff of 17.493 p/kWh. However, DERs' price, 8.747 p/kWh, is higher than the feed-in tariff (2.28 p/kWh for DER 1 and 0.33 p/kWh for DER 2 [111]). DERs' prices decrease but total incomes increase with increasing outputs.

Prices for different customers and DERs' output results are shown in Table 7.5. Market 1 is

Table 7.5: P2P Price and DER Output Results

Time h	DER 1 price p/kWh	DER 1 output kWh	DER 1 loss kWh	DER 2 price p/kWh	DER 2 output kWh	DER 2 loss kWh	Market 1 p/kWh	Market 2 p/kWh
1	16.75	119.18	0.30	-	-	-	16.95	-
2	17.07	68.00	0.17	-	-	-	17.39	-
3	16.84	104.95	0.26	-	-	-	17.10	-
4	13.22	686.99	30.90	-	-	-	14.61	-
5	13.12	702.45	27.58	-	-	-	15.20	-
6	11.90	899.17	40.95	-	-	-	13.63	-
7	13.09	706.97	15.62	-	-	-	17.22	-
8	16.42	172.05	0.43	14.35	934.92	53.74	16.17	16.68
9	16.16	214.79	0.53	11.60	1752.47	150.78	15.16	14.87
10	16.33	187.57	0.47	10.02	2221.91	227.05	14.38	13.40
11	12.87	742.79	4.48	9.18	2471.29	342.66	10.77	11.05
12	13.16	696.32	3.62	8.75	2600.50	324.45	10.06	10.02
13	11.81	913.32	10.13	8.86	2566.33	307.03	9.74	8.86
14	8.75	1405.14	42.73	9.48	2383.84	181.07	9.52	9.60
15	9.30	1315.47	36.33	12.84	1382.91	78.09	13.96	15.09
16	10.70	1091.33	22.24	15.90	473.95	8.99	17.21	17.35
17	11.45	970.41	20.80	16.49	297.91	2.21	17.19	17.46
18	15.69	289.05	0.68	-	-	-	17.41	-
19	15.95	248.55	0.62	-	-	-	17.37	-
20	15.71	285.82	1.31	-	-	-	17.05	-
21	16.53	154.55	0.35	-	-	-	17.49	-
22	16.02	236.12	0.89	-	-	-	17.20	-
23	15.50	320.60	2.79	-	-	-	16.69	-
24	15.38	338.73	3.56	-	-	-	16.53	-

p/kWh - British pence per kilowatt-hour.

one of the three markets (DER 1 downstream market, DER 1 upstream market, and Branch market connected with bus 6), which includes buses supplied by DER 1 and the substation all the time and further includes buses supplied by DER 2 between hour 8 and hour 17. Market 2 is the surplus market which only includes buses supplied by DER 2 and substation without DER 1 between hour 8 and hour 17. Price of loads in a market can be calculate by $\sum(P^{DER} * Price^{DER} + P^{Sub} * Price^{Sub}) / P^{load}$. For other loads which are not in a market, their tariffs are determined by their electricity sources.

Table 7.6: Consumers' Cost Reductions and DERs' Income Increases

		£ per day						
		1 to 3	4 to 7	8 to 10	11 to 13	14 to 17	18 to 24	24 hour
DER 14 downstream		0.62	8.90	5.75	18.88	28.32	1.35	9.70
DER 14 upstream		0.00	15.64	14.74	38.48	49.74	2.88	18.27
Branch connected with bus 6		0.00	9.46	21.09	52.28	28.94	0.00	15.57
The rest buses		0.00	0.00	35.73	88.56	33.41	0.00	21.10
DER 20 branch		0.00	0.00	14.06	30.60	9.98	0.00	7.25
Sum		0.62	34.01	91.38	228.81	150.39	4.23	71.89
Wind increase income		14.15	74.89	26.75	79.72	88.07	34.49	50.86
PV increase income		0.00	0.00	165.30	189.84	121.00	0.00	64.56
Sum		14.15	74.89	192.05	269.55	209.07	34.49	115.42

		p per kWh						
		1 to 3	4 to 7	8 to 10	11 to 13	14 to 17	18 to 24	24 hour
DER 14 downstream		0.64	4.68	2.33	4.88	7.51	1.66	3.43
DER 14 upstream		0.00	4.68	2.63	5.66	7.51	1.66	3.48
Branch connected with bus 6		0.00	2.19	2.63	8.02	3.17	0.00	2.22
The rest buses		0.00	0.00	2.63	8.02	2.76	0.00	1.79
DER 20 branch		0.00	0.00	5.68	8.56	3.96	0.00	2.44
Sum		0.64	11.55	15.91	35.13	24.91	3.32	13.37
Wind increase income		14.54	10.00	13.97	10.17	7.37	13.48	11.10
PV increase income		0.00	0.00	10.10	7.46	10.66	0.00	3.97
Sum		14.54	10.00	24.07	17.63	18.03	13.48	15.07

When a DER increases output, its price decreases and the losses it needs to share increase. From hours 1 to 7 and 18 to 24, the market 1 price is higher than the DER 1 price and lower than 17.493 p/kWh. The average output portions in market 1 from hours 8 to 10 are $P^{DER1} : P^{DER2} : P^{Sub} = 33\% : 32\% : 34\%$, and from hours 11 to 13 $P^{DER1} : P^{DER2} : P^{Sub} = 58\% : 32\% : 10\%$. From hours 8 to 13, market 1 price is between DER 1 price and DER 2 price. This is because that after DER 1 supplies its exclusive market, it has sufficient extra energy to supply the market (over one-third).

Meanwhile, the market 1 price is lower than the market 2. The average output portion in market 1 from hours 14 to 18 is $P^{DER1} : P^{DER2} : P^{Sub} = 14\% : 33\% : 53\%$. From hours 14 to 18, DER 1's exclusive market is bigger than the previous two time period include buses 7 to 18, therefore there is not enough DER 1 power to supply the branch market connected with

bus 6 (below 15%). From hours 8 to 17, the market 2 price is higher than the DER 2 price and lower than 17.493 p/kWh.

Customer Total Energy Costs

In total, customers can save £1736.44, $\sum P^{DER} \times (Price^{Sub} - Price^{DER})$. DER 1 and DER 2 can increase income to £ (GBP - British pound sterling) 1264.58 and £1910.79, $\sum P^{DER} \times (Price^{DER} - Price^{feed-intariff})$. Details about budgets saved by customers and increase incomes of DERs are shown in Table 7.6. In general, when customers consume more energy on DERs, they save more money both in total and per unit. When DERs produce more energy, their total incomes increase but per-unit incomes decrease.

Time analysis for the market: From hour 11 to 13, for customers from branch connected with bus 6, excess buses and DER 2 branch, they can most money (52.28, 88.56 and 30.60 average £ per hour & 8.02, 8.02 and 8.56 p/kWh) both in total and per unit. That is because DERs total output is the highest during this period. But from hour 14 to 17, for customers from DER 1 downstream and DER 1 upstream, they can save the most (28.32 and 49.74 average £ per hour & 7.51 and 7.51 p/kWh) both in total and per unit. That is because DER 1 total output is the highest during this period and customers from DER 1 downstream and DER 1 upstream are mainly supplied by DER 1.

Spatial analysis for the market: Customers from the excess buses can save the most amount of money (21.10 £ per hour) for 24 hours because the total demand for them is the highest. Customers from DER 1 upstream can save the most amount of money (3.48 p/kWh) for 24 hours. Firstly, it is because they receive energy from DERs most of the time. Secondly, from hours 11 to 13, they can get a better price than customers from DER 1 upstream, because a

part of their energy is supplied by DER 2.

7.5.4 Modeling Details

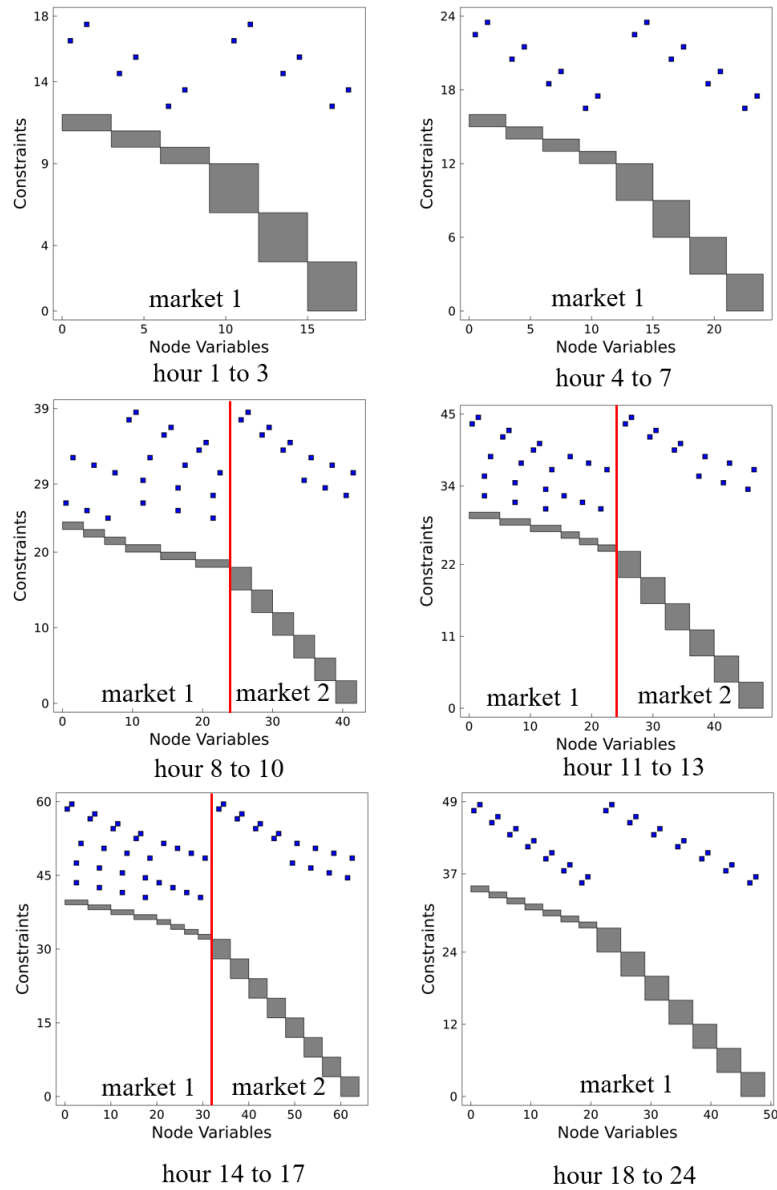


Figure 7.8: Graph matrix of 24-hour market.

The graph matrix generated for the case study is shown in the Figure 7.8, with blocks representing OptiNode and blue marks representing linking constraints that connect their vari-

ables [156]. Blocks' number in one graph equal to hours \times participants' number. For example, hour 1 to 3 has two participants. Therefore, there are 6 blocks.

In hours 8 to 10, hours 11 to 13 and hours 14 to 17, market 1 has more blue marks than market 2. This is due to that market 1 has three participants, DER 1, DER 2 and $load_a$; conversely, market 2 have two participants DER 2 and $load_a$. The number of the link constraints between three participants is more than the that of the link constraints between two participants.

As shown from the above results and analysis, a P2P market based on power flow tracing is designed to unlock potential economic values within local energy systems. Network losses can be clearly traced to DERs and market segmentation links the trading with the usage of the physical power networks. This idea unlocks future work regarding services to the grid provided by prosumers. For example, DERs would take peer-to-peer power supply responsibility for the reliability of the electricity to customers whom they trade with. Both DERs and consumers are encouraged to actively participate in the trading with improved benefits from the P2P market designed in this research.

7.6 Conclusion

This chapter reports work on building a new P2P energy market model supported by dynamic power flow tracing in power distribution networks. An optimised market segmenting strategy based on identifying power transactions is proposed. Graph-based modeling is applied to determine electricity transaction prices and maximise the benefits of both DERs and consumers by quantifying each transaction's usage of the network with allocated losses.

The optimisation results of the proposed model demonstrate opportunities for profits within several markets segmented by power flow tracing, compared with the existing centralised market with unified incentives, for both individual DER owners and consumers. DER owners observe increased revenue (£1264.58 for DER 1 and £1910.79 for DER 2, as shown in the Case Study) compared with traditional FiT; meanwhile consumers see reduced bills (£1736.44, as shown in Case Studies) with lower tariffs.

Nevertheless, ESSs are able to perform a significant role in the development of P2P energy trading in order to both improve efficiency and increase efficiency. In future research, it needs to be examined how ESSs can be used as a mechanism to facilitate P2P energy trading, as well as the relevant modelling methodology. At same time, the network usage charges of all transactions and pricing strategies of DERs would require further research, taking into account the life of equipment/assets, such as transformers, switches and wires, and DERs' capital investment.

Chapter 8

Conclusions and Future Work

8.1 Conclusions

The contributions of this thesis are summarised as follows:

SOPs are power-electronic devices installed in open point positions in distribution networks. When networks operate in a normal condition, SOPs can control active power flows, compensate reactive power, and regulate voltage levels. Meanwhile, when networks operate in an abnormal condition, SOPs can isolate fault zones quickly and restore post-fault loads. In addition, SOPs can balance three-phase loads especially by adopting the PC-SOP proposed in this thesis for a three-phase unbalanced network. By adapting part of the AC network (lines) for DC power distribution, DC lines can be seen as SOPs for the rest AC network. This can provide another solution to reduce three-phase imbalance situations. The followings are concluded from the research on SOPs for power supply service restoration and distribution imbalance mitigation:

- To achieve the optimal coordination of SOPs, ESSs, and tie switches, an adaptive service restoration strategy of distribution networks with DERs and SOPs is proposed. An analysis of several SOP control models is used to describe the classification of different distribution network scenarios. Network circumstances are matched with SOP control models accordingly. The overall problem is solved by the mixed-integer SOCP. Case studies show that, in addition to balancing supply and demand, ESSs scheduling, SOPs controlling and network reconfiguration can be integrated to reduce power losses, restore additional amount of lost loads, and reduce customer interruptions and customer minutes lost.
- A new type of SOP connection known as phase-changing SOP (PC-SOP) is introduced. For unbalanced three-phase four-wire distribution networks, an optimised operating strategy based on PC-SOPs is provided to minimise operational losses, three-phase imbalances, and escalating DER penetration levels. The optimisation results show that PC-SOPs greatly minimise unbalanced loading conditions and power losses (particularly losses in neutral wires) in ADNs compared to conventional SOPs and SVCs. By shifting power across various phases, PC-SOP can also improve the utilisation of ESSs.
- For reducing three-phase imbalance, adapting AC lines to DC power distribution and further PC-SOP solutions (including bifurcation and multi-terminal) are discussed in this thesis. For adapting AC lines to DC power distribution, there are three principles (based on locations of both voltage violations and DC DERs) proposed in this thesis to locate appropriate lines that should be adapted to DC. For further PC-SOP solutions, bifurcation SOPs can connect single-phase buses or two-phase buses, where loads cannot be balanced as the lack of one or two phases, in distribution networks. The multi-terminal solution further improves load distribution spatial imbalance throughout the network based on three-phase loads that have been balanced by PC-SOPs.

With the concept of the “P2P economy” and "sharing economy" development, peer-to-peer (P2P) energy trading emerges as a new energy trading structure, which refers to direct energy trading among consumers and generator owners in distribution networks. P2P energy trading can solve the problem of rising electricity retail prices because of the currently low feed-in tariffs (FiTs).

- A new P2P energy market model is developed based on dynamic power flow tracing in distribution networks. This thesis presents an optimised market segmentation strategy based on recognising power transactions. By measuring each transaction’s network consumption with allocated losses, a graph-based modeling is used to establish electricity transaction prices and maximise the benefits of both DERs and consumers. Multiple markets segmented by power flow tracing can create more opportunities for profits, compared to the existing centralised market with unified incentives, for both individual DER owners and consumers. Compared to typical FiTs, DER owners receive more revenue; meanwhile, customers get lower bills with lower tariffs.

In conclusion, there are three areas that are investigated in this thesis, including service restoration, three-phase balancing and P2P energy trading. Firstly, an adaptive service restoration strategy of distribution networks with DERs and SOPs is proposed to reduce power losses and customer interruptions and restore lost loads. Secondly, PC-SOPs (including two-terminal, bifurcation and multi-terminal) and adapting AC lines to DC power distribution are discussed to reduce the network three-phase imbalance phenomena. Thirdly, a power flow traceable P2P electricity market is designed to achieve direct trading practices between customers and DER owners aiming at improving the benefits for both.

8.2 Future Work

Potential future work is proposed and listed as follows:

- For multi-terminal SOPs or PC-SOPs in a three-phase system, numerous sets of converters need to be coordinated and controlled to ensure voltage and power quality, and circulating current suppression. The service restoration strategy of a three-phase system with multi-terminal SOPs or PC-SOPs is more difficult and complicated than a single-phase system with two-terminal conventional SOPs. Therefore, related AC/DC power-electronic technologies requires further research.
- The technological advantages of PC-SOPs in unbalanced distribution networks were examined in this thesis. An economic evaluation will provide a clear sight of whether PC-SOP deployment is viable compared with conventional SOP considering manufacturing, installation and maintenance costs. Therefore, additional research on the economic analysis of SOPs should be performed. Meanwhile, PC-SOPs' life cycle costs should also be estimated to be compared with conventional SOPs. The ideal number, locations, and capacities of PC-SOPs should be determined with capital and operational costs (CAPEX and OPEX) of PC-SOPs. In addition, the cooperative operation and planning of PC-SOPs and conventional SOPs are worth discussions.
- A thorough investigation of the consequences of ICT infrastructure and its involvement in the deployment of PC-SOPs in future smart grids is necessary. Domestic and certain commercial customers connected to the distribution networks at the LV levels often have single-phase or unbalanced three-phase connections. The ICT infrastructure should be able to detect the imbalance rapidly and deliver detailed information to PC-SOPs.

- In this study, SOPs and PC-SOPs was not taken into account when simulating P2P energy trading. SOPs and PC-SOPs can significantly influence on the power flow distribution results and further power flow tracing results. SOPs and PC-SOPs can improve flexibility for P2P energy trading. One operational strategy of SOPs and PC-SOPs is to transfer energy directly from producers to customers in P2P energy trading. That strategy may conflict with the original aim of SOPs and PC-SOPs to balance power networks. When SOPs and PC-SOPs are introduced to the simulation of P2P electricity markets which is based on chapter 5 work, this scenario should be further investigated.
- In transportation systems, self-driving cars have had the ability to travel between destinations without human operators/drivers. Similarly, artificial intelligence techniques, such as machine learning, could be used to achieve the self-operation (automation) of SOPs or other power electronic devices in the distribution network. Artificial intelligence techniques can also be used to achieve demand-side flexibility and energy trading in the P2P electricity market by predicting future power consumption and generations of prosumers and consumers for technical and/or economic purposes.

Appendix A

IEEE test feeders

IEEE 13-node test feeder

The IEEE 13-node test feeder is used to test common features of distribution analysis software, operating at 4.16 kV. It is characterised by being short, relatively highly loaded, a single voltage regulator at the substation, overhead and underground lines, shunt capacitors, an in-line transformer, and unbalanced loading [135].

Table A1: Regulator data of the IEEE 13-node test feeder

Regulator ID:	1		
Line Segment:	650 - 632		
Location:	50		
Phases:	A - B -C		
Connection:	3-Ph,LG		
Monitoring Phase:	A-B-C		
Bandwidth:	2.0 volts		
PT Ratio:	20		
Primary CT Rating:	700		
Compensator Settings:	Ph-A	Ph-B	Ph-C
R - Setting:	3	3	3
X - Setting:	9	9	9
Voltage Level:	122	122	122

Table A2: Shunt capacitors of the IEEE 13-node test feeder

Node	Ph-A	Ph-B	Ph-C
	kVAr	kVAr	kVAr
675	200	200	200
611			100
Total	200	200	300

Table A3: Line segment data of the IEEE 13-node test feeder

Node A	Node B	Length(ft.)	Config.
632	645	500	603
632	633	500	602
633	634	0	XFM-1
645	646	300	603
650	632	2000	601
684	652	800	607
632	671	2000	601
671	684	300	604
671	680	1000	601
671	692	0	Switch
684	611	300	605
692	675	500	606

Table A4: Overhead line configurations (Config.) of the IEEE 13-node test feeder

Config.	Phasing	Phase	Neutral	Spacing
		ACSR	ACSR	ID
601	B A C N	556,500 26/7	4/0 6/1	500
602	C A B N	4/0 6/1	4/0 6/1	500
603	C B N	1/0	1/0	505
604	A C N	1/0	1/0	505
605	C N	1/0	1/0	510

Table A5: Distributed loads of the IEEE 13-node test feeder

Node A	Node B	Load Model	Ph-1 kW	Ph-1 kVAr	Ph-2 kW	Ph-2 kVAr	Ph-3 kW	Ph-3 kVAr
632	671	Y-PQ	17	10	66	38	117	68

Table A6: Spot loads of the IEEE 13-node test feeder

Node	Load Model	Ph-1 kW	Ph-1 kVAr	Ph-2 kW	Ph-2 kVAr	Ph-3 kW	Ph-3 kVAr
634	Y-PQ	160	110	120	90	120	90
645	Y-PQ	0	0	170	125	0	0
646	D-Z	0	0	230	132	0	0
652	Y-Z	128	86	0	0	0	0
671	D-PQ	385	220	385	220	385	220
675	Y-PQ	485	190	68	60	290	212
692	D-I	0	0	0	0	170	151
611	Y-I	0	0	0	0	170	80
	TOTAL	1158	606	973	627	1135	753

Table A7: Transformer data of the IEEE 13-node test feeder

	kVA	kV-high	kV-low	R - %	X - %
Substation:	5,000	115 - D	4.16 Gr. Y	1	8
XFM -1	500	4.16 - Gr.W	0.48 - Gr.W	1.1	2

Table A8: Underground cable configurations (Config.) of the IEEE 13-node test feeder

Config.	Phasing	Cable	Neutral	Space ID
606	A B C N	250,000 AA, CN	None	515
607	A N	1/0 AA, TS	1/0 Cu	520

Figure 8.1: IEEE 13-node test feeder impedance

Configuration 601:

Z (R +jX) in ohms per mile

0.3465	1.0179	0.1560	0.5017	0.1580	0.4236
		0.3375	1.0478	0.1535	0.3849
				0.3414	1.0348

B in micro Siemens per mile

6.2998	-1.9958	-1.2595			
	5.9597	-0.7417			
		5.6386			

Configuration 602:

Z (R +jX) in ohms per mile

0.7526	1.1814	0.1580	0.4236	0.1560	0.5017
		0.7475	1.1983	0.1535	0.3849
				0.7436	1.2112

B in micro Siemens per mile

5.6990	-1.0817	-1.6905			
	5.1795	-0.6588			
		5.4246			

Configuration 603:

Z (R +jX) in ohms per mile

0.0000	0.0000	0.0000	0.0000	0.0000	0.0000
		1.3294	1.3471	0.2066	0.4591
				1.3238	1.3569

B in micro Siemens per mile

0.0000	0.0000	0.0000			
	4.7097	-0.8999			
		4.6658			

Configuration 604:

Z (R +jX) in ohms per mile

1.3238	1.3569	0.0000	0.0000	0.2066	0.4591
		0.0000	0.0000	0.0000	0.0000
				1.3294	1.3471

B in micro Siemens per mile

4.6658	0.0000	-0.8999			
	0.0000	0.0000			
		4.7097			

Configuration 605:

Z (R +jX) in ohms per mile
 0.0000 0.0000 0.0000 0.0000 0.0000 0.0000
 0.0000 0.0000 0.0000 0.0000
 1.3292 1.3475
 B in micro Siemens per mile
 0.0000 0.0000 0.0000
 0.0000 0.0000
 4.5193

Configuration 606:

Z (R +jX) in ohms per mile
 0.7982 0.4463 0.3192 0.0328 0.2849 -0.0143
 0.7891 0.4041 0.3192 0.0328
 0.7982 0.4463
 B in micro Siemens per mile
 96.8897 0.0000 0.0000
 96.8897 0.0000
 96.8897

Configuration 607:

Z (R +jX) in ohms per mile
 1.3425 0.5124 0.0000 0.0000 0.0000 0.0000
 0.0000 0.0000 0.0000 0.0000
 0.0000 0.0000
 B in micro Siemens per mile
 88.9912 0.0000 0.0000
 0.0000 0.0000
 0.0000

IEEE 34-node test feeder

The IEEE 34-node test feeder is an actual feeder located in Arizona, with a nominal voltage of 24.9 kV. It is characterized by long and lightly loaded, two in-line regulators, an in-line transformer for short 4.16 kV section, unbalanced loading, and shunt capacitors [135].

Table A9: Regulator data of the IEEE 34-node test feeder

Regulator ID: 1				Regulator ID: 2			
Line Segment:	814 - 850			Line Segment:	852 - 832		
Location:	814			Location:	852		
Phases:	A - B -C			Phases:	A - B -C		
Connection:	3-Ph,LG			Connection:	3-Ph,LG		
Monitoring Phase:	A-B-C			Monitoring Phase:	A-B-C		
Bandwidth:	2.0 volts			Bandwidth:	2.0 volts		
PT Ratio:	120			PT Ratio:	120		
Primary CT Rating:	100			Primary CT Rating:	100		
Compensator:	Ph-A	Ph-B	Ph-C	Compensator:	Ph-A	Ph-B	Ph-C
R - Setting:	2.7	2.7	2.7	R - Setting:	2.5	2.5	2.5
X - Setting:	1.6	1.6	1.6	X - Setting:	1.5	1.5	1.5
Voltage Level:	122	122	122	Voltage Level:	124	124	124

Table A10: Shunt capacitors of the IEEE 34-node test feeder

Node	Ph-A	Ph-B	Ph-C
	kVAr	kVAr	kVAr
844	100	100	100
848	150	150	150
Total	250	250	250

Table A11: Transformer data of the IEEE 34-node test feeder

	kVA	kV-high	kV-low	R - %	X - %
Substation:	2500	69 - D	24.9 -Gr. W	1	8
XFM -1	500	24.9 - Gr.W	4.16 - Gr. W	1.9	4.08

Table A12: Line segment data of the IEEE 34-node test feeder

Node A	Node B	Length(ft.)	Config.	Node A	Node B	Length(ft.)	Config.
800	802	2580	300	834	860	2020	301
802	806	1730	300	834	842	280	301
806	808	32230	300	836	840	860	301
808	810	5804	303	836	862	280	301
808	812	37500	300	842	844	1350	301
812	814	29730	300	844	846	3640	301
814	850	10	301	846	848	530	301
816	818	1710	302	850	816	310	301
816	824	10210	301	852	832	10	301
818	820	48150	302	854	856	23330	303
820	822	13740	302	854	852	36830	301
824	826	3030	303	858	864	1620	302
824	828	840	301	858	834	5830	301
828	830	20440	301	860	836	2680	301
830	854	520	301	862	838	4860	304
832	858	4900	301	888	890	10560	300
832	888	0	XFM-1				

Table A13: Overhead line configurations (Config.) of the IEEE 34-node test feeder

Config.	Phasing	Phase	Neutral	Spacing ID
		ACSR	ACSR	
300	B A C N	1/0	1/0	500
301	B A C N	#2 6/1	#2 6/1	500
302	A N	#4 6/1	#4 6/1	510
303	B N	#4 6/1	#4 6/1	510
304	B N	#2 6/1	#2 6/1	510

Table A14: Spot loads of the IEEE 34-node test feeder

Node	Ph-1 kW	Ph-1 kVAr	Ph-2 kW	Ph-2 kVAr	Ph-3 kW	Ph-3 kVAr
860	20	16	20	16	20	16
840	9	7	9	7	9	7
844	135	105	135	105	135	105
848	20	16	20	16	20	16
890	150	75	150	75	150	75
830	10	5	10	5	25	10
Total	344	224	344	224	359	229

Table A15: Distributed loads of the IEEE 34-node test feeder

Node A	Node B	Ph-1 kW	Ph-1 kVAr	Ph-2 kW	Ph-2 kVAr	Ph-3 kW	Ph-3 kVAr
802	806	0	0	30	15	25	14
808	810	0	0	16	8	0	0
818	820	34	17	0	0	0	0
820	822	135	70	0	0	0	0
816	824	0	0	5	2	0	0
824	826	0	0	40	20	0	0
824	828	0	0	0	0	4	2
828	830	7	3	0	0	0	0
854	856	0	0	4	2	0	0
832	858	7	3	2	1	6	3
858	864	2	1	0	0	0	0
858	834	4	2	15	8	13	7
834	860	16	8	20	10	110	55
860	836	30	15	10	6	42	22
836	840	18	9	22	11	0	0
862	838	0	0	28	14	0	0
842	844	9	5	0	0	0	0
844	846	0	0	25	12	20	11
846	848	0	0	23	11	0	0
Total		262	133	240	120	220	114

Figure 8.2: IEEE 34-node test feeder impedance

Configuration 300:

```

      Z (R +jX) in ohms per mile
1.3368  1.3343  0.2101  0.5779  0.2130  0.5015
          1.3238  1.3569  0.2066  0.4591
          1.3294  1.3471
      B in micro Siemens per mile
          5.3350  -1.5313  -0.9943
          5.0979  -0.6212
          4.8880

```

Configuration 301:

```

      Z (R +jX) in ohms per mile
1.9300  1.4115  0.2327  0.6442  0.2359  0.5691
          1.9157  1.4281  0.2288  0.5238
          1.9219  1.4209
      B in micro Siemens per mile
          5.1207  -1.4364  -0.9402
          4.9055  -0.5951
          4.7154

```

Configuration 302:

```

      Z (R +jX) in ohms per mile
2.7995  1.4855  0.0000  0.0000  0.0000  0.0000
          0.0000  0.0000  0.0000  0.0000
          0.0000  0.0000
      B in micro Siemens per mile
          4.2251  0.0000  0.0000
          0.0000  0.0000
          0.0000

```

Configuration 303:

```

      Z (R +jX) in ohms per mile
0.0000  0.0000  0.0000  0.0000  0.0000  0.0000
          2.7995  1.4855  0.0000  0.0000
          0.0000  0.0000
      B in micro Siemens per mile
          0.0000  0.0000  0.0000
          4.2251  0.0000
          0.0000

```

Configuration 304:

```

      Z (R +jX) in ohms per mile
0.0000  0.0000  0.0000  0.0000  0.0000  0.0000
          1.9217  1.4212  0.0000  0.0000
          0.0000  0.0000
      B in micro Siemens per mile
          0.0000  0.0000  0.0000
          4.3637  0.0000
          0.0000

```

IEEE 123-node test feeder

The IEEE 123-node test feeder operates at a nominal voltage of 4.16 kV. While this is not a popular voltage level it does provide voltage drop problems that must be solved with the application of voltage regulators and shunt capacitors. This circuit is characterized by overhead and underground lines, unbalanced loading with constant current, impedance, and power, four voltage regulators, shunt capacitor banks, and multiple switches. This circuit is “well-behaved” with minimal convergence problems [135].

Table A16: Regulator data of the IEEE 123-node test feeder

Regulator ID:	1			Regulator ID:	3		
Line Segment:	150 - 149			Line Segment:	25 - 26		
Location:	150			Location:	25		
Phases:	A-B-C			Phases:	A-C		
Connection:	3-Ph, Wye			Connection:	2-Ph,L-G		
Monitoring Phase:	A			Monitoring Phase:	A & C		
Bandwidth:	2.0 volts			Bandwidth:	1		
PT Ratio:	20			PT Ratio:	20		
Primary CT Rating:	700			Primary CT Rating:	50		
Compensator:	Ph-A	Ph-B	Ph-C	Compenator:	Ph-A	Ph-B	Ph-C
R - Setting:	3	-	-	R - Setting:	0.4	-	0.4
X - Setting:	7.5	-	-	X - Setting:	0.4	-	0.4
Voltage Level:	120	-	-	Voltage Level:	120	-	120
Regulator ID:	2			Regulator ID:	4		
Line Segment:	9 - 14			Line Segment:	160 - 67		
Location:	9			Location:	160		
Phases:	A			Phases:	A-B-C		
Connection:	1-Ph, L-G			Connection:	3-Ph, LG		
Monitoring Phase:	A			Monitoring Phase:	A-B-C		
Bandwidth:	2.0 volts			Bandwidth:	2		
PT Ratio:	20			PT Ratio:	20		
Primary CT Rating:	50			Primary CT Rating:	300		
Compensator:	Ph-A	Ph-B	Ph-C	Compensator:	Ph-A	Ph-B	Ph-C
R - Setting:	0.4	-	-	R - Setting:	0.6	1.4	0.2
X - Setting:	0.4	-	-	X - Setting:	1.3	2.6	1.4
Voltage Level:	120	-	-	Voltage Level:	124	124	124

Table A17: Line segment data of the the IEEE 123-node test feeder

Node A	Node B	Length (ft.)	Config.	Node A	Node B	Length (ft.)	Config.
1	2	175	10	60	61	550	5
1	3	250	11	60	62	250	12
1	7	300	1	62	63	175	12
3	4	200	11	63	64	350	12
3	5	325	11	64	65	425	12
5	6	250	11	65	66	325	12
7	8	200	1	67	68	200	9
8	12	225	10	67	72	275	3
8	9	225	9	67	97	250	3
8	13	300	1	68	69	275	9
9	14	425	9	69	70	325	9
13	34	150	11	70	71	275	9
13	18	825	2	72	73	275	11
14	11	250	9	72	76	200	3
14	10	250	9	73	74	350	11
15	16	375	11	74	75	400	11
15	17	350	11	76	77	400	6
18	19	250	9	76	86	700	3
18	21	300	2	77	78	100	6
19	20	325	9	78	79	225	6
21	22	525	10	78	80	475	6
21	23	250	2	80	81	475	6
23	24	550	11	81	82	250	6
23	25	275	2	81	84	675	11
25	26	350	7	82	83	250	6
25	28	200	2	84	85	475	11
26	27	275	7	86	87	450	6
26	31	225	11	87	88	175	9
27	33	500	9	87	89	275	6
28	29	300	2	89	90	225	10
29	30	350	2	89	91	225	6
30	250	200	2	91	92	300	11
31	32	300	11	91	93	225	6
34	15	100	11	93	94	275	9
35	36	650	8	93	95	300	6
35	40	250	1	95	96	200	10
36	37	300	9	97	98	275	3
36	38	250	10	98	99	550	3
38	39	325	10	99	100	300	3
40	41	325	11	100	450	800	3
40	42	250	1	101	102	225	11
42	43	500	10	101	105	275	3
42	44	200	1	102	103	325	11
44	45	200	9	103	104	700	11
44	47	250	1	105	106	225	10
45	46	300	9	105	108	325	3
47	48	150	4	106	107	575	10
47	49	250	4	108	109	450	9
49	50	250	4	108	300	1000	3
50	51	250	4	109	110	300	9
51	151	500	4	110	111	575	9
52	53	200	1	110	112	125	9
53	54	125	1	112	113	525	9
54	55	275	1	113	114	325	9
54	57	350	3	135	35	375	4
55	56	275	1	149	1	400	1
57	58	250	10	152	52	400	1
57	60	750	3	160	67	350	6
58	59	250	10	197	101	250	3

Table A18: Spot loads of the IEEE 123-node test feeder

Node	Load Model	Ph-1 kW	Ph-1 kVAr	Ph-2 kW	Ph-2 kVAr	Ph-3 kW	Ph-4 kVAr	Node	Load Model	Ph-1 kW	Ph-1 kVAr	Ph-2 kW	Ph-2 kVAr	Ph-3 kW	Ph-4 kVAr
1	Y-PQ	40	20	0	0	0	0	60	Y-PQ	20	10	0	0	0	0
2	Y-PQ	0	0	20	10	0	0	62	Y-Z	0	0	0	0	40	20
4	Y-PR	0	0	0	0	40	20	63	Y-PQ	40	20	0	0	0	0
5	Y-I	0	0	0	0	20	10	64	Y-I	0	0	75	35	0	0
6	Y-Z	0	0	0	0	40	20	65	D-Z	35	25	35	25	70	50
7	Y-PQ	20	10	0	0	0	0	66	Y-PQ	0	0	0	0	75	35
9	Y-PQ	40	20	0	0	0	0	68	Y-PQ	20	10	0	0	0	0
10	Y-I	20	10	0	0	0	0	69	Y-PQ	40	20	0	0	0	0
11	Y-Z	40	20	0	0	0	0	70	Y-PQ	20	10	0	0	0	0
12	Y-PQ	0	0	20	10	0	0	71	Y-PQ	40	20	0	0	0	0
16	Y-PQ	0	0	0	0	40	20	73	Y-PQ	0	0	0	0	40	20
17	Y-PQ	0	0	0	0	20	10	74	Y-Z	0	0	0	0	40	20
19	Y-PQ	40	20	0	0	0	0	75	Y-PQ	0	0	0	0	40	20
20	Y-I	40	20	0	0	0	0	76	D-I	105	80	70	50	70	50
22	Y-Z	0	0	40	20	0	0	77	Y-PQ	0	0	40	20	0	0
24	Y-PQ	0	0	0	0	40	20	79	Y-Z	40	20	0	0	0	0
28	Y-I	40	20	0	0	0	0	80	Y-PQ	0	0	40	20	0	0
29	Y-Z	40	20	0	0	0	0	82	Y-PQ	40	20	0	0	0	0
30	Y-PQ	0	0	0	0	40	20	83	Y-PQ	0	0	0	0	20	10
31	Y-PQ	0	0	0	0	20	10	84	Y-PQ	0	0	0	0	20	10
32	Y-PQ	0	0	0	0	20	10	85	Y-PQ	0	0	0	0	40	20
33	Y-I	40	20	0	0	0	0	86	Y-PQ	0	0	20	10	0	0
34	Y-Z	0	0	0	0	40	20	87	Y-PQ	0	0	40	20	0	0
35	D-PQ	40	20	0	0	0	0	88	Y-PQ	40	20	0	0	0	0
37	Y-Z	40	20	0	0	0	0	90	Y-I	0	0	40	20	0	0
38	Y-I	0	0	20	10	0	0	92	Y-PQ	0	0	0	0	40	20
39	Y-PQ	0	0	20	10	0	0	94	Y-PQ	40	20	0	0	0	0
41	Y-PQ	0	0	0	0	20	10	95	Y-PQ	0	0	20	10	0	0
42	Y-PQ	20	10	0	0	0	0	96	Y-PQ	0	0	20	10	0	0
43	Y-Z	0	0	40	20	0	0	98	Y-PQ	40	20	0	0	0	0
45	Y-I	20	10	0	0	0	0	99	Y-PQ	0	0	40	20	0	0
46	Y-PQ	20	10	0	0	0	0	100	Y-Z	0	0	0	0	40	20
47	Y-I	35	25	35	25	35	25	102	Y-PQ	0	0	0	0	20	10
48	Y-Z	70	50	70	50	70	50	103	Y-PQ	0	0	0	0	40	20
49	Y-PQ	35	25	70	50	35	20	104	Y-PQ	0	0	0	0	40	20
50	Y-PQ	0	0	0	0	40	20	106	Y-PQ	0	0	40	20	0	0
51	Y-PQ	20	10	0	0	0	0	107	Y-PQ	0	0	40	20	0	0
52	Y-PQ	40	20	0	0	0	0	109	Y-PQ	40	20	0	0	0	0
53	Y-PQ	40	20	0	0	0	0	111	Y-PQ	20	10	0	0	0	0
55	Y-Z	20	10	0	0	0	0	112	Y-I	20	10	0	0	0	0
56	Y-PQ	0	0	20	10	0	0	113	Y-Z	40	20	0	0	0	0
58	Y-I	0	0	20	10	0	0	114	Y-PQ	20	10	0	0	0	0
59	Y-PQ	0	0	20	10	0	0	Total		1420	775	915	515	1155	630

Table A19: Overhead line configurations (Config.) of the IEEE 123-node test feeder

Config.	Phasing	Phase Cond.	Neutral Cond.	Spacing
		ACSR	ACSR	ID
1	A B C N	336,400 26/7	4/0 6/1	500
2	C A B N	336,400 26/7	4/0 6/1	500
3	B C A N	336,400 26/7	4/0 6/1	500
4	C B A N	336,400 26/7	4/0 6/1	500
5	B A C N	336,400 26/7	4/0 6/1	500
6	A C B N	336,400 26/7	4/0 6/1	500
7	A C N	336,400 26/7	4/0 6/1	505
8	A B N	336,400 26/7	4/0 6/1	505
9	A N	1/0	1/0	510
10	B N	1/0	1/0	510
11	C N	1/0	1/0	510

Table A20: Transformer data of the IEEE 123-node test feeder

	kVA	kV-high	kV-low	R - %	X - %
Substation	5,000	115 - D	4.16 Gr-W	1	8
XFM - 1	150	4.16 - D	.480 - D	1.27	2.72

Table A21: Underground line configuration (Config.) of the IEEE 123-node test feeder

Config.	Phasing	Cable	Spacing ID
12	A B C	1/0 AA, CN	515

Table A22: Three phase switches of the IEEE 123-node test feeder

Node A	13	18	60	61	97	150	250	450	54	151	300
Node B	152	135	160	610	197	149	251	451	94	300	350
Normal	closed	closed	closed	closed	closed	closed	open	open	open	open	open

Figure 8.3: IEEE 123-node test feeder impedance

Configuration 1:

Z (R +jX) in ohms per mile
 0.4576 1.0780 0.1560 0.5017 0.1535 0.3849
 0.4666 1.0482 0.1580 0.4236
 0.4615 1.0651

B in micro Siemens per mile
 5.6765 -1.8319 -0.6982
 5.9809 -1.1645
 5.3971

Configuration 2:

Z (R +jX) in ohms per mile
 0.4666 1.0482 0.1580 0.4236 0.1560 0.5017
 0.4615 1.0651 0.1535 0.3849
 0.4576 1.0780

B in micro Siemens per mile
 5.9809 -1.1645 -1.8319
 5.3971 -0.6982
 5.6765

Configuration 3:

Z (R +jX) in ohms per mile
 0.4615 1.0651 0.1535 0.3849 0.1580 0.4236
 0.4576 1.0780 0.1560 0.5017
 0.4666 1.0482

B in micro Siemens per mile
 5.3971 -0.6982 -1.1645
 5.6765 -1.8319
 5.9809

Configuration 4:

Z (R +jX) in ohms per mile
 0.4615 1.0651 0.1580 0.4236 0.1535 0.3849
 0.4666 1.0482 0.1560 0.5017
 0.4576 1.0780

B in micro Siemens per mile
 5.3971 -1.1645 -0.6982
 5.9809 -1.8319
 5.6765

Configuration 5:

Z (R +jX) in ohms per mile
 0.4666 1.0482 0.1560 0.5017 0.1580 0.4236
 0.4576 1.0780 0.1535 0.3849
 0.4615 1.0651

B in micro Siemens per mile
 5.9809 -1.8319 -1.1645
 5.6765 -0.6982
 5.3971

Configuration 6:

Z (R +jX) in ohms per mile
 0.4576 1.0780 0.1535 0.3849 0.1560 0.5017
 0.4615 1.0651 0.1580 0.4236
 0.4666 1.0482

B in micro Siemens per mile
 5.6765 -0.6982 -1.8319
 5.3971 -1.1645
 5.9809

Configuration 7:

Z (R +jX) in ohms per mile
 0.4576 1.0780 0.0000 0.0000 0.1535 0.3849
 0.0000 0.0000 0.0000 0.0000
 0.4615 1.0651

B in micro Siemens per mile
 5.1154 0.0000 -1.0549
 0.0000 0.0000
 5.1704

Configuration 8:

Z (R +jX) in ohms per mile
 0.4576 1.0780 0.1535 0.3849 0.0000 0.0000
 0.4615 1.0651 0.0000 0.0000
 0.0000 0.0000

B in micro Siemens per mile
 5.1154 -1.0549 0.0000
 5.1704 0.0000
 0.0000

Configuration 9:

Z (R +jX) in ohms per mile
 1.3292 1.3475 0.0000 0.0000 0.0000 0.0000
 0.0000 0.0000 0.0000 0.0000
 0.0000 0.0000

B in micro Siemens per mile
 4.5193 0.0000 0.0000
 0.0000 0.0000
 0.0000

Configuration 10:

Z (R +jX) in ohms per mile
 0.0000 0.0000 0.0000 0.0000 0.0000 0.0000
 1.3292 1.3475 0.0000 0.0000
 0.0000 0.0000

B in micro Siemens per mile
 0.0000 0.0000 0.0000
 4.5193 0.0000
 0.0000

Configuration 11:

Z (R +jX) in ohms per mile
 0.0000 0.0000 0.0000 0.0000 0.0000 0.0000
 0.0000 0.0000 0.0000 0.0000
 1.3292 1.3475

B in micro Siemens per mile
 0.0000 0.0000 0.0000
 0.0000 0.0000
 4.5193

Configuration 12:

Z (R +jX) in ohms per mile
 1.5209 0.7521 0.5198 0.2775 0.4924 0.2157
 1.5329 0.7162 0.5198 0.2775
 1.5209 0.7521

B in micro Siemens per mile
 67.2242 0.0000 0.0000
 67.2242 0.0000
 67.2242

IEEE 33-node test feeder

The IEEE 33-node test feeder system , created by Baran & Wu, was used to study the impact of distribution network reconfiguration on power losses reduction and load balancing [130].

Table A23: IEEE 33-node test feeder

Brach	Bus A	Bus B	R	X	P	Q
1	1	1	0.0922	0.047	100	60
2	1	1	0.493	0.2511	90	40
3	1	1	0.366	0.1864	120	80
4	1	1	0.3811	0.1941	60	30
5	1	1	0.819	0.707	60	20
6	1	1	0.1872	0.6188	200	100
7	1	1	0.7114	0.2351	200	100
8	1	1	1.03	0.74	60	20
9	1	1	1.044	0.74	60	20
10	1	1	0.1966	0.065	45	30
11	1	1	0.3744	0.1238	60	35
12	1	1	1.468	1.155	60	35
13	1	1	0.5416	0.7129	120	80
14	1	1	0.591	0.526	60	10
15	1	1	0.7463	0.545	60	20
16	1	1	1.289	1.721	60	20
17	1	1	0.372	0.574	90	40
18	1	1	0.164	0.1565	90	40
19	1	1	1.5042	1.3554	90	40
20	1	1	0.4095	0.4784	90	40
21	1	1	0.7089	0.9373	90	40
22	1	1	0.4512	0.3083	90	50
23	1	1	0.898	0.7091	420	200
24	1	1	0.896	0.7011	420	200
25	1	1	0.203	0.1034	60	25
26	1	1	0.2842	0.1447	60	25
27	1	1	1.059	0.9337	60	20
28	1	1	0.8042	0.7006	120	70
29	1	1	0.5075	0.2585	200	600
30	1	1	0.9744	0.963	150	70
31	1	1	0.3105	0.3619	210	100
32	1	1	0.341	0.5362	60	40

Appendix B

PC-SOP operation result

Table B1 shows the active power of the SOP and PC-SOP in Figure 4.5 in Chapter 3.

Table B1: SOP and PC-SOP active power outcome (kW)

time/h	SOP						PC-SOP					
	822_A	822_B	822_C	848_A	848_B	848_C	822_A	822_B	822_C	848_A	848_B	848_C
1	-117.62	-129.08	-204.23	117.62	129.08	204.23	-195.01	-185.14	-175.10	175.10	195.01	185.14
2	-117.63	-128.85	-204.23	117.63	128.85	204.23	-194.92	-185.18	-175.03	175.03	194.92	185.18
3	-112.12	-127.87	-203.88	112.12	127.87	203.88	-188.92	-184.20	-174.64	174.64	188.92	184.20
4	-97.44	-125.87	-205.87	97.44	125.87	205.87	-134.83	-181.40	-177.65	177.65	134.83	181.40
5	-67.53	-121.90	-210.48	67.53	121.90	210.48	-59.57	-174.28	-197.26	197.26	59.57	174.28
6	-29.36	-121.09	-216.64	29.36	121.09	216.64	8.64	-151.65	-233.50	233.50	-8.64	151.65
7	3.75	-169.78	-207.41	-3.75	169.78	207.41	135.68	-153.19	-232.41	232.41	-135.68	153.19
8	3.24	-300.00	-190.46	-3.24	300.00	190.46	168.51	-296.15	-215.31	215.31	-168.51	296.15
9	-267.77	-293.17	-150.68	267.77	293.17	150.68	298.71	-265.02	-121.48	121.48	-298.71	265.02
10	-284.66	-288.98	-152.13	284.66	288.98	152.13	247.52	-265.38	-99.63	99.63	-247.52	265.38
11	-287.52	-282.29	-149.60	287.52	282.29	149.60	282.86	-262.66	-98.16	98.16	-282.86	262.66
12	-289.47	-278.24	-148.91	289.47	278.24	148.91	277.16	-261.53	-97.24	97.24	-277.16	261.53
13	-289.56	-274.54	-146.76	289.56	274.54	146.76	278.63	-260.46	-102.35	102.35	-278.63	260.46
14	-287.94	-273.41	-141.89	287.94	273.41	141.89	282.44	-258.15	-111.98	111.98	-282.44	258.15
15	-287.51	-273.49	-141.68	287.51	273.49	141.68	240.27	-250.48	-127.28	127.28	-240.27	250.48
16	-259.79	-234.62	-153.04	259.79	234.62	153.04	134.52	-233.91	-169.78	169.78	-134.52	233.91
17	-214.83	-223.62	-152.04	214.83	223.62	152.04	163.41	-225.50	-194.25	194.25	-163.41	225.50
18	-217.99	-172.35	-153.19	217.99	172.35	153.19	151.95	-222.18	-200.58	200.58	-151.95	222.18
19	-213.47	-110.57	-147.29	213.47	110.57	147.29	148.38	-214.27	-197.50	197.50	-148.38	214.27
20	-226.99	-90.49	-148.45	226.99	90.49	148.45	137.49	-214.21	-202.19	202.19	-137.49	214.21
21	-223.53	-131.42	-178.89	223.53	131.42	178.89	-18.46	-226.60	-220.14	220.14	18.46	226.60
22	-237.04	-162.82	-205.29	237.04	162.82	205.29	-94.84	-241.66	-238.24	238.24	94.84	241.66
23	-85.22	-165.77	-213.59	85.22	165.77	213.59	-86.61	-187.07	-190.40	190.40	86.61	187.07
24	-107.92	-161.75	-198.13	107.92	161.75	198.13	-129.91	-182.46	-156.23	156.23	129.91	182.46

Table B2 shows the active power of the ESS in Figure 4.7 in Chapter 3.

Table B2: ESS active power outcome (kW)

time/h	848-B	846-B	844-B	842-A	842-B	842-C	LOAD-A	LOAD-B	LOAD-C	PV
1	-16.40	-12.64	-20.08	-30.38	-35.49	-43.22	456.00	418.00	429.00	0.00
2	-8.61	-7.86	-6.79	-30.05	-34.62	-41.45	464.02	426.02	442.76	0.00
3	-4.99	-6.55	-3.13	-29.96	-34.45	-35.25	474.93	430.28	447.21	0.00
4	0.00	-2.95	0.00	-29.60	-15.44	-0.08	556.98	454.48	463.99	0.00
5	0.00	0.00	0.00	0.00	0.00	0.00	734.94	507.11	500.64	0.00
6	0.00	0.00	23.78	0.00	0.00	0.00	975.58	580.56	555.11	-8.33
7	0.53	60.00	36.22	31.99	0.00	0.00	1306.86	699.04	667.33	-164.03
8	-0.53	0.00	-60.00	-0.33	0.00	0.00	1257.37	704.71	700.65	-862.83
9	0.00	0.00	0.00	16.93	0.39	22.90	1509.71	1222.11	1701.48	-1617.36
10	0.00	-2.17	0.00	-39.35	-0.39	-22.90	1398.63	1260.32	1830.88	-1923.93
11	0.00	-17.25	0.00	-7.08	0.20	0.24	1510.35	1364.55	2006.46	-2033.06
12	0.00	-24.66	0.00	-2.16	-0.20	-0.23	1541.00	1411.05	2093.00	-2085.92
13	0.00	-15.92	0.00	-0.01	-0.01	-0.01	1642.15	1474.73	2186.19	-2069.20
14	3.94	0.00	40.31	0.00	0.00	0.00	1774.79	1547.73	2285.91	-1986.93
15	-3.94	0.00	12.19	0.00	0.00	0.00	1795.19	1551.34	2284.92	-1276.29
16	0.00	0.00	7.51	0.00	32.28	21.20	1934.62	1580.65	2288.09	-437.41
17	9.47	0.01	-25.90	32.13	48.04	61.70	2186.83	1577.87	2174.24	-274.94
18	-9.47	0.00	-34.10	52.42	47.05	54.73	2164.58	1564.78	2155.71	-156.74
19	54.64	35.19	36.17	77.94	56.87	55.32	2265.83	1658.73	2313.74	-45.82
20	5.36	24.80	23.83	77.51	55.76	47.05	2177.23	1625.26	2279.91	0.00
21	0.00	0.00	0.00	0.00	0.00	0.00	1510.68	1101.44	1442.49	0.00
22	0.00	0.00	0.00	0.00	0.00	0.00	1133.51	882.17	1133.91	0.00
23	0.00	0.00	0.00	0.00	0.00	0.00	665.23	492.58	499.34	0.00
24	0.00	0.00	0.00	0.00	0.00	0.00	456.00	418.00	429.00	0.00

Table B3, B4, B5 and B6 show the voltage profile data of four cases in Figure 4.8 in Chapter 3.

Table B3: The maximum and minimum voltage of three phases of Case 1 (kV)

Bus Number	VaMax	VaMin	VbMax	VbMin	VcMax	VcMin
800	15.09	15.09	15.09	15.09	15.09	15.09
802	15.09	15.08	15.09	15.08	15.09	15.07
806	15.09	15.06	15.09	15.07	15.09	15.06
808	15.05	14.83	15.05	14.91	15.06	14.82
810	15.05	14.83	15.05	14.91	15.06	14.82
812	15.00	14.55	15.00	14.73	15.02	14.54
814	14.96	14.33	14.97	14.58	14.99	14.31
816	14.96	14.33	14.96	14.58	14.99	14.31
818	14.96	14.33	14.96	14.58	14.98	14.31
820	14.92	14.27	15.06	14.52	14.96	14.29
822	14.91	14.25	15.07	14.51	14.95	14.29
824	14.95	14.25	14.96	14.53	14.98	14.21
826	14.95	14.25	14.96	14.52	14.98	14.21
828	14.95	14.25	14.96	14.52	14.98	14.20
830	14.94	14.13	14.94	14.42	14.96	13.99
832	14.93	13.94	14.92	14.25	14.93	13.65
834	14.93	13.89	14.91	14.20	14.92	13.55
836	14.92	13.88	14.91	14.20	14.92	13.53
838	14.92	13.87	14.91	14.19	14.92	13.51
840	14.92	13.88	14.91	14.20	14.92	13.53
842	14.93	13.89	14.91	14.20	14.92	13.55
844	14.93	13.88	14.91	14.20	14.92	13.55
846	14.93	13.87	14.91	14.18	14.92	13.53
848	14.93	13.87	14.91	14.18	14.93	13.53
850	14.96	14.33	14.97	14.58	14.99	14.31
852	14.93	13.94	14.92	14.25	14.93	13.65
854	14.94	14.13	14.94	14.42	14.96	13.99
856	14.94	14.13	14.94	14.42	14.96	13.99
858	14.93	13.91	14.92	14.23	14.93	13.60
860	14.92	13.88	14.91	14.20	14.92	13.54
862	14.92	13.88	14.91	14.19	14.92	13.53
864	14.93	13.91	14.92	14.23	14.93	13.60
888	14.93	13.94	14.92	14.25	14.93	13.65
890	14.93	13.94	14.92	14.25	14.93	13.65

Table B4: The maximum and minimum voltage of three phases of Case 2 (kV)

Bus number	VaMax	VaMin	VbMax	VbMin	VcMax	VcMin
800	15.09	15.09	15.09	15.09	15.09	15.09
802	15.09	15.07	15.09	15.08	15.09	15.08
806	15.09	15.06	15.09	15.08	15.09	15.06
808	15.04	14.79	15.06	14.94	15.06	14.82
810	15.04	14.79	15.06	14.94	15.06	14.82
812	14.99	14.48	15.03	14.78	15.02	14.54
814	14.95	14.23	15.00	14.65	14.99	14.31
816	14.95	14.23	15.00	14.65	14.99	14.31
818	14.95	14.22	15.00	14.65	14.99	14.31
820	14.91	14.09	14.98	14.60	14.97	14.31
822	14.90	14.05	14.98	14.59	14.96	14.31
824	14.94	14.15	14.99	14.61	14.98	14.20
826	14.94	14.15	14.99	14.61	14.98	14.20
828	14.94	14.15	14.99	14.61	14.98	14.19
830	14.92	14.03	14.98	14.53	14.97	13.98
832	14.90	13.84	14.96	14.40	14.95	13.63
834	14.90	13.79	14.96	14.36	14.95	13.53
836	14.89	13.78	14.96	14.36	14.94	13.51
838	14.89	13.78	14.96	14.35	14.94	13.49
840	14.89	13.78	14.96	14.36	14.94	13.51
842	14.90	13.79	14.96	14.36	14.95	13.53
844	14.90	13.79	14.96	14.36	14.95	13.52
846	14.90	13.78	14.96	14.35	14.95	13.51
848	14.90	13.78	14.96	14.36	14.95	13.51
850	14.95	14.23	15.00	14.65	14.99	14.31
852	14.90	13.84	14.96	14.40	14.95	13.63
854	14.92	14.03	14.98	14.53	14.97	13.98
856	14.92	14.03	14.98	14.53	14.97	13.98
858	14.90	13.82	14.96	14.38	14.95	13.58
860	14.90	13.79	14.96	14.36	14.94	13.52
862	14.89	13.78	14.96	14.36	14.94	13.51
864	14.90	13.82	14.96	14.38	14.95	13.58
888	14.90	13.84	14.96	14.40	14.95	13.63
890	14.90	13.84	14.96	14.40	14.95	13.63

Table B5: The maximum and minimum voltage of three phases of Case 3 (kV)

Bus number	VaMax	VaMin	VbMax	VbMin	VcMax	VcMin
800	15.09	15.09	15.09	15.09	15.09	15.09
802	15.09	15.07	15.09	15.08	15.09	15.08
806	15.09	15.06	15.09	15.08	15.09	15.06
808	15.04	14.80	15.06	14.94	15.06	14.83
810	15.04	14.80	15.06	14.94	15.06	14.83
812	14.99	14.50	15.02	14.78	15.02	14.55
814	14.95	14.26	14.98	14.65	14.99	14.33
816	14.95	14.26	14.98	14.65	14.99	14.33
818	14.95	14.25	14.98	14.65	14.99	14.33
820	14.93	14.17	15.02	14.63	15.02	14.36
822	14.93	14.15	15.02	14.62	15.03	14.37
824	14.93	14.17	14.97	14.60	14.97	14.22
826	14.93	14.17	14.97	14.60	14.97	14.22
828	14.93	14.17	14.97	14.60	14.97	14.21
830	14.91	14.04	14.95	14.51	14.94	13.99
832	14.87	13.82	14.91	14.35	14.88	13.61
834	14.85	13.76	14.90	14.31	14.87	13.51
836	14.85	13.75	14.90	14.31	14.87	13.49
838	14.85	13.74	14.90	14.30	14.86	13.47
840	14.85	13.75	14.90	14.31	14.87	13.49
842	14.85	13.75	14.90	14.31	14.87	13.51
844	14.85	13.75	14.90	14.31	14.87	13.50
846	14.85	13.74	14.89	14.30	14.87	13.49
848	14.85	13.74	14.89	14.30	14.87	13.49
850	14.95	14.26	14.98	14.65	14.99	14.33
852	14.87	13.82	14.91	14.35	14.88	13.61
854	14.91	14.03	14.95	14.50	14.94	13.98
856	14.91	14.03	14.95	14.50	14.94	13.98
858	14.86	13.79	14.90	14.33	14.88	13.56
860	14.85	13.75	14.90	14.31	14.87	13.50
862	14.85	13.75	14.90	14.31	14.86	13.49
864	14.86	13.79	14.90	14.33	14.88	13.56
888	14.87	13.82	14.91	14.35	14.88	13.61
890	14.87	13.82	14.91	14.35	14.88	13.61

Table B6: The maximum and minimum voltage of three phases of Case 4 (kV)

Bus number	VaMax	VaMin	VbMax	VbMin	VcMax	VcMin
800	15.09	15.09	15.09	15.09	15.09	15.09
802	15.09	15.07	15.09	15.08	15.09	15.07
806	15.09	15.06	15.09	15.07	15.09	15.06
808	15.03	14.76	15.05	14.92	15.05	14.78
810	15.03	14.76	15.05	14.92	15.05	14.78
812	14.97	14.41	15.01	14.74	15.00	14.45
814	14.92	14.13	14.97	14.59	14.96	14.19
816	14.92	14.13	14.97	14.59	14.96	14.19
818	14.92	14.13	14.97	14.59	14.96	14.19
820	14.90	14.01	14.96	14.56	14.96	14.19
822	14.89	13.98	14.96	14.55	14.96	14.19
824	14.90	14.04	14.96	14.54	14.94	14.07
826	14.90	14.04	14.96	14.54	14.94	14.07
828	14.90	14.03	14.96	14.53	14.94	14.06
830	14.87	13.89	14.93	14.44	14.90	13.83
832	14.83	13.65	14.89	14.26	14.84	13.43
834	14.82	13.58	14.88	14.22	14.82	13.32
836	14.82	13.57	14.88	14.22	14.82	13.30
838	14.81	13.57	14.87	14.21	14.81	13.28
840	14.82	13.57	14.88	14.22	14.82	13.30
842	14.82	13.58	14.88	14.22	14.82	13.32
844	14.82	13.58	14.88	14.22	14.82	13.31
846	14.81	13.56	14.87	14.21	14.82	13.29
848	14.81	13.56	14.87	14.21	14.82	13.29
850	14.92	14.13	14.97	14.59	14.96	14.19
852	14.83	13.65	14.89	14.26	14.84	13.43
854	14.87	13.89	14.93	14.43	14.90	13.82
856	14.87	13.89	14.93	14.43	14.90	13.82
858	14.82	13.62	14.88	14.24	14.83	13.38
860	14.82	13.58	14.88	14.22	14.82	13.31
862	14.82	13.57	14.88	14.22	14.82	13.30
864	14.82	13.61	14.88	14.24	14.83	13.38
888	14.83	13.65	14.89	14.26	14.84	13.43
890	14.83	13.65	14.89	14.26	14.84	13.43

Table B7 show 24-hour three-terminal PC-SOP active power outcome in Chapter 5.

Table B7: Three-terminal PC-SOP active power outcome (kW)

time/h	1	2	3	4	5	6	7	8
Bus 680A	0.00	0.00	0.00	0.00	0.00	0.00	0.00	0.00
Bus 680B	0.00	0.00	0.00	0.00	0.00	0.00	0.00	0.00
Bus 680C	0.00	0.00	0.00	0.00	0.00	0.00	0.00	0.00
Bus 675A	44.36	70.07	32.73	0.08	0.05	0.14	217.54	339.51
Bus 675B	-7.39	-21.16	-4.53	-0.09	-0.05	-0.10	-6.76	-15.03
Bus 675C	13.63	30.14	8.30	0.01	0.00	0.01	-3.95	-0.35
Bus 634A	-15.15	-32.94	-9.38	-0.02	-0.01	-0.02	-0.56	-6.81
Bus 634B	-50.16	-79.51	-37.25	-0.09	-0.06	-0.16	-218.57	-342.44
Bus 634C	4.19	15.07	2.31	0.08	0.04	0.08	2.27	7.52
time/h	9	10	11	12	13	14	15	16
Bus 680A	0.00	0.00	0.00	0.00	0.00	0.00	0.00	0.00
Bus 680B	0.00	0.00	0.00	0.00	0.00	0.00	0.00	0.00
Bus 680C	0.00	0.00	0.00	0.00	0.00	0.00	0.00	0.00
Bus 675A	618.80	1039.02	1400.93	1686.13	1800.49	1800.24	1798.54	951.30
Bus 675B	-54.35	-120.46	-169.10	-205.79	-220.74	-226.37	-229.75	-253.77
Bus 675C	26.24	69.05	106.17	135.53	147.08	145.87	144.73	153.80
Bus 634A	-40.23	-95.68	-144.68	-183.65	-199.14	-198.36	-197.43	-189.11
Bus 634B	-626.86	-1055.18	-1424.68	-1716.40	-1833.60	-1834.82	-1834.02	-1000.64
Bus 634C	39.33	93.97	132.56	161.21	172.89	178.21	181.44	209.94
time/h	17	18	19	20	21	22	23	24
Bus 680A	0.00	0.00	0.00	0.00	0.00	0.00	0.00	0.00
Bus 680B	0.00	0.00	0.00	0.00	0.00	0.00	0.00	0.00
Bus 680C	0.00	0.00	0.00	0.00	0.00	0.00	0.00	0.00
Bus 675A	1057.06	896.45	780.91	419.63	216.15	160.82	101.45	44.36
Bus 675B	-310.77	-196.02	-330.40	-441.76	-180.32	-116.96	-53.66	-7.39
Bus 675C	344.60	326.95	379.51	305.12	147.61	95.45	54.37	13.63
Bus 634A	-407.33	-402.18	-440.32	-338.88	-166.53	-107.35	-59.65	-15.15
Bus 634B	-1125.33	-966.69	-847.39	-480.10	-259.40	-188.61	-116.79	-50.16
Bus 634C	230.77	116.01	252.31	386.41	145.29	95.23	42.66	4.19

Table B8 show 24-hour Four-terminal PC-SOP active power outcome in Figure 6.7 in Chapter

5.

Table B8: Four-terminal PC-SOP active power outcome (kW)

time/h	1	2	3	4	5	6	7	8
Bus 151 A	-0.72	-7.56	-0.09	0.01	0.00	0.01	0.09	9.53
Bus 151 B	-9.00	-24.90	-2.83	-0.07	-0.01	-0.07	-0.89	-0.10
Bus 151 C	-20.94	-30.80	-15.38	-0.07	-0.01	-0.07	-2.73	-12.03
Bus 300 A	42.06	75.95	26.93	0.15	0.03	0.14	4.39	48.39
Bus 300 B	-0.09	0.04	-0.05	-0.02	-0.01	-0.04	-0.29	-5.50
Bus 300 C	0.38	6.21	0.03	-0.01	0.00	0.00	-0.05	0.01
Bus 54 A	-0.07	-0.66	-0.01	0.00	0.00	0.00	0.06	0.08
Bus 54 B	-35.96	-68.19	-25.81	-0.10	-0.02	-0.10	-3.71	-51.30
Bus 54 C	-5.81	-25.82	-1.39	-0.08	-0.02	-0.07	-1.37	-29.68
Bus 93 A	25.97	54.20	16.33	0.16	0.03	0.16	4.27	45.96
Bus 93 B	0.04	0.48	0.00	-0.01	0.00	-0.02	-0.13	-10.11
Bus 93 C	0.19	11.33	0.02	0.01	0.00	0.01	-0.08	-0.04
time/h	9	10	11	12	13	14	15	16
Bus 151 A	68.94	88.95	92.79	101.62	103.27	97.58	67.53	56.24
Bus 151 B	-1.32	-17.55	-20.07	-20.79	-22.37	-27.57	-53.02	-82.91
Bus 151 C	-10.47	-28.65	-38.87	-43.32	-44.67	-46.06	-51.97	-58.69
Bus 300 A	101.99	167.49	220.96	273.48	299.44	315.64	351.85	449.66
Bus 300 B	-18.39	-9.58	-8.50	-0.18	8.67	19.29	69.37	147.50
Bus 300 C	9.75	37.25	55.23	74.27	85.02	91.87	120.12	183.59
Bus 54 A	1.76	14.36	1.72	-44.43	-78.47	-115.81	-255.71	-512.93
Bus 54 B	-110.33	-196.71	-303.24	-411.69	-466.36	-502.45	-586.02	-795.77
Bus 54 C	-107.37	-206.58	-294.54	-377.69	-417.15	-436.61	-475.59	-626.71
Bus 93 A	130.72	232.39	323.78	398.37	428.33	437.84	430.93	500.42
Bus 93 B	-83.89	-147.79	-162.45	-150.04	-131.16	-96.77	40.42	234.19
Bus 93 C	1.94	30.72	78.42	128.18	155.33	178.82	248.94	381.38
time/h	17	18	19	20	21	22	23	24
Bus 151 A	5.44	-9.16	14.73	44.94	22.42	2.78	-9.81	-0.72
Bus 151 B	-257.03	-286.52	-199.63	-101.26	-85.75	-69.45	-44.26	-9.00
Bus 151 C	-208.78	-231.98	-150.49	-63.61	-59.86	-54.06	-41.45	-20.94
Bus 300 A	555.87	562.27	531.08	474.27	364.32	244.81	123.92	42.06
Bus 300 B	189.50	200.99	179.78	169.32	112.28	53.01	5.04	-0.09
Bus 300 C	256.24	258.34	238.86	202.36	141.26	80.98	25.36	0.38
Bus 54 A	-628.01	-639.67	-640.41	-620.08	-436.30	-245.87	-61.78	-0.07
Bus 54 B	-886.30	-887.04	-887.69	-850.61	-634.19	-397.65	-162.22	-35.96
Bus 54 C	-671.93	-670.97	-668.41	-659.03	-478.62	-287.43	-100.31	-5.81
Bus 93 A	636.38	644.83	589.71	512.32	395.95	269.35	129.05	25.97
Bus 93 B	308.18	329.59	335.14	330.24	241.66	143.24	39.73	0.04
Bus 93 C	523.24	545.27	497.67	427.96	317.71	197.01	70.43	0.19

Appendix C

Flow tracing result

Table C1 shows the detailed load proportion from each generation includes DERs and substation, of Table 7.2 in Chapter 6.

Table C1: 24-hour power flow tracing results of load proportion

time/h	Power flow tracing result for 24 hours Generation: {Bus number: load proportion}
1	DER 1: {13: 1.0, 14: 0.74, 15: 0.74, 16: 0.74, 17: 0.74} Substation: {0: 1.0, 1: 1.0, 2: 1.0, 18: 1.0, 3: 1.0, 22: 1.0, 4: 1.0, 5: 1.0, 25: 1.0, 6: 1.0, 26: 1.0, 27: 1.0, 28: 1.0, 29: 1.0, 30: 1.0, 31: 1.0, 32: 1.0, 7: 1.0, 8: 1.0, 9: 1.0, 10: 1.0, 11: 1.0, 12: 1.0, 13: 0.0, 14: 0.26, 15: 0.26, 16: 0.26, 17: 0.26, 23: 1.0, 24: 1.0, 19: 1.0, 20: 1.0, 21: 1.0}
2	DER 1: {13: 1.0, 14: 0.25, 15: 0.25, 16: 0.25, 17: 0.25} Substation: {0: 1.0, 1: 1.0, 2: 1.0, 18: 1.0, 3: 1.0, 22: 1.0, 4: 1.0, 5: 1.0, 25: 1.0, 6: 1.0, 26: 1.0, 27: 1.0, 28: 1.0, 29: 1.0, 30: 1.0, 31: 1.0, 32: 1.0, 7: 1.0, 8: 1.0, 9: 1.0, 10: 1.0, 11: 1.0, 12: 1.0, 13: 0.0, 14: 0.75, 15: 0.75, 16: 0.75, 17: 0.75, 23: 1.0, 24: 1.0, 19: 1.0, 20: 1.0, 21: 1.0}
3	DER 1: {13: 1.0, 14: 0.6, 15: 0.6, 16: 0.6, 17: 0.6} Substation: {0: 1.0, 1: 1.0, 2: 1.0, 18: 1.0, 3: 1.0, 22: 1.0, 4: 1.0, 5: 1.0, 25: 1.0, 6: 1.0, 26: 1.0, 27: 1.0, 28: 1.0, 29: 1.0, 30: 1.0, 31: 1.0, 32: 1.0, 7: 1.0, 8: 1.0, 9: 1.0, 10: 1.0, 11: 1.0, 12: 1.0, 13: 0.0, 14: 0.4, 15: 0.4, 16: 0.4, 17: 0.4, 23: 1.0, 24: 1.0, 19: 1.0, 20: 1.0, 21: 1.0}
4	DER 1: {13: 1.0, 12: 1.0, 14: 1.0, 11: 1.0, 10: 1.0, 9: 1.0, 8: 1.0, 7: 1.0, 6: 1.0, 5: 0.72, 25: 0.72, 26: 0.72, 27: 0.72, 28: 0.72, 29: 0.72, 30: 0.72, 31: 0.72, 32: 0.72, 15: 1.0, 16: 1.0, 17: 1.0} 2: {0: 1.0, 1: 1.0, 2: 1.0, 18: 1.0, 3: 1.0, 22: 1.0, 4: 1.0, 5: 0.28, 25: 0.28, 26: 0.28, 27: 0.28, 28: 0.28, 29: 0.28, 30: 0.28, 31: 0.28, 32: 0.28, 23: 1.0, 24: 1.0, 19: 1.0, 20: 1.0, 21: 1.0}
5	DER 1: {13: 1.0, 12: 1.0, 14: 1.0, 11: 1.0, 10: 1.0, 9: 1.0, 8: 1.0, 7: 1.0, 6: 1.0, 5: 0.57, 25: 0.57, 26: 0.57, 27: 0.57, 28: 0.57, 29: 0.57, 30: 0.57, 31: 0.57, 32: 0.57, 15: 1.0, 16: 1.0, 17: 1.0} Substation: {0: 1.0, 1: 1.0, 2: 1.0, 18: 1.0, 3: 1.0, 22: 1.0, 4: 1.0, 5: 0.43, 25: 0.43, 26: 0.43, 27: 0.43, 28: 0.43, 29: 0.43, 30: 0.43, 31: 0.43, 32: 0.43, 23: 1.0, 24: 1.0, 19: 1.0, 20: 1.0, 21: 1.0}

6	DER 1: {13: 1.0, 12: 1.0, 14: 1.0, 11: 1.0, 10: 1.0, 9: 1.0, 8: 1.0, 7: 1.0, 6: 1.0, 5: 0.73, 25: 0.73, 26: 0.73, 27: 0.73, 28: 0.73, 29: 0.73, 30: 0.73, 31: 0.73, 32: 0.73, 15: 1.0, 16: 1.0, 17: 1.0} DER 2: {19: 0.2} Substation: {0: 1.0, 1: 1.0, 2: 1.0, 18: 1.0, 3: 1.0, 22: 1.0, 4: 1.0, 5: 0.27, 25: 0.27, 26: 0.27, 27: 0.27, 28: 0.27, 29: 0.27, 30: 0.27, 31: 0.27, 32: 0.27, 23: 1.0, 24: 1.0, 19: 0.8, 20: 1.0, 21: 1.0}
7	DER 1: {13: 1.0, 12: 1.0, 14: 1.0, 11: 1.0, 10: 1.0, 9: 1.0, 8: 1.0, 7: 1.0, 6: 1.0, 5: 0.11, 25: 0.11, 26: 0.11, 27: 0.11, 28: 0.11, 29: 0.11, 30: 0.11, 31: 0.11, 32: 0.11, 15: 1.0, 16: 1.0, 17: 1.0} DER 2: {19: 1.0, 18: 0.35, 20: 1.0, 21: 1.0} Substation: {0: 1.0, 1: 1.0, 2: 1.0, 18: 0.65, 3: 1.0, 22: 1.0, 4: 1.0, 5: 0.89, 25: 0.89, 26: 0.89, 27: 0.89, 28: 0.89, 29: 0.89, 30: 0.89, 31: 0.89, 32: 0.89, 23: 1.0, 24: 1.0}
8	DER 1: {13: 1.0, 14: 0.36, 15: 0.36, 16: 0.36, 17: 0.36}, DER 2: {19: 1.0, 18: 1.0, 20: 1.0, 1: 0.25, 2: 0.25, 3: 0.25, 22: 0.25, 4: 0.25, 5: 0.25, 25: 0.25, 6: 0.25, 26: 0.25, 27: 0.25, 28: 0.25, 29: 0.25, 30: 0.25, 31: 0.25, 32: 0.25, 7: 0.25, 8: 0.25, 9: 0.25, 10: 0.25, 11: 0.25, 12: 0.25, 13: 0.0, 14: 0.16, 15: 0.16, 16: 0.16, 17: 0.16, 23: 0.25, 24: 0.25, 21: 1.0} Substation: {0: 1.0, 1: 0.75, 2: 0.75, 3: 0.75, 22: 0.75, 4: 0.75, 5: 0.75, 25: 0.75, 6: 0.75, 26: 0.75, 27: 0.75, 28: 0.75, 29: 0.75, 30: 0.75, 31: 0.75, 32: 0.75, 7: 0.75, 8: 0.75, 9: 0.75, 10: 0.75, 11: 0.75, 12: 0.75, 13: 0.0, 14: 0.48, 15: 0.48, 16: 0.48, 17: 0.48, 23: 0.75, 24: 0.75}
9	DER 1: {13: 1.0, 14: 0.38, 15: 0.38, 16: 0.38, 17: 0.38}, DER 2: {19: 1.0, 18: 1.0, 20: 1.0, 1: 0.44, 2: 0.44, 3: 0.44, 22: 0.44, 4: 0.44, 5: 0.44, 25: 0.44, 6: 0.44, 26: 0.44, 27: 0.44, 28: 0.44, 29: 0.44, 30: 0.44, 31: 0.44, 32: 0.44, 7: 0.44, 8: 0.44, 9: 0.44, 10: 0.44, 11: 0.44, 12: 0.44, 13: 0.0, 14: 0.27, 15: 0.27, 16: 0.27, 17: 0.27, 23: 0.44, 24: 0.44, 21: 1.0} Substation: {0: 1.0, 1: 0.56, 2: 0.56, 3: 0.56, 22: 0.56, 4: 0.56, 5: 0.56, 25: 0.56, 6: 0.56, 26: 0.56, 27: 0.56, 28: 0.56, 29: 0.56, 30: 0.56, 31: 0.56, 32: 0.56, 7: 0.56, 8: 0.56, 9: 0.56, 10: 0.56, 11: 0.56, 12: 0.56, 13: 0.0, 14: 0.34, 15: 0.34, 16: 0.34, 17: 0.34, 23: 0.56, 24: 0.56}
10	DER 1: {13: 1.0, 14: 0.25, 15: 0.25, 16: 0.25, 17: 0.25} DER 2: {19: 1.0, 18: 1.0, 20: 1.0, 1: 0.54, 2: 0.54, 3: 0.54, 22: 0.54, 4: 0.54, 5: 0.54, 25: 0.54, 6: 0.54, 26: 0.54, 27: 0.54, 28: 0.54, 29: 0.54, 30: 0.54, 31: 0.54, 32: 0.54, 7: 0.54, 8: 0.54, 9: 0.54, 10: 0.54, 11: 0.54, 12: 0.54, 13: 0.0, 14: 0.41, 15: 0.41, 16: 0.41, 17: 0.41, 23: 0.54, 24: 0.54, 21: 1.0} Substation: {0: 1.0, 1: 0.46, 2: 0.46, 3: 0.46, 22: 0.46, 4: 0.46, 5: 0.46, 25: 0.46, 6: 0.46, 26: 0.46, 27: 0.46, 28: 0.46, 29: 0.46, 30: 0.46, 31: 0.46, 32: 0.46, 7: 0.46, 8: 0.46, 9: 0.46, 10: 0.46, 11: 0.46, 12: 0.46, 13: 0.0, 14: 0.34, 15: 0.34, 16: 0.34, 17: 0.34, 23: 0.46, 24: 0.46}
11	DER 1: {13: 1.0, 12: 1.0, 14: 1.0, 11: 1.0, 10: 1.0, 9: 1.0, 8: 1.0, 7: 0.32, 15: 1.0, 16: 1.0, 17: 1.0} DER 2: {19: 1.0, 18: 1.0, 20: 1.0, 1: 0.75, 2: 0.75, 3: 0.75, 22: 0.75, 4: 0.75, 5: 0.75, 25: 0.75, 6: 0.75, 26: 0.75, 27: 0.75, 28: 0.75, 29: 0.75, 30: 0.75, 31: 0.75, 32: 0.75, 7: 0.51, 23: 0.75, 24: 0.75, 21: 1.0} Substation: {0: 1.0, 1: 0.25, 2: 0.25, 3: 0.25, 22: 0.25, 4: 0.25, 5: 0.25, 25: 0.25, 6: 0.25, 26: 0.25, 27: 0.25, 28: 0.25, 29: 0.25, 30: 0.25, 31: 0.25, 32: 0.25, 7: 0.17, 23: 0.25, 24: 0.25}

12	DER 1: {13: 1.0, 12: 1.0, 14: 1.0, 11: 1.0, 10: 1.0, 9: 1.0, 8: 1.0, 7: 0.12, 15: 1.0, 16: 1.0, 17: 1.0} DER 2: {19: 1.0, 18: 1.0, 20: 1.0, 1: 0.79, 2: 0.79, 3: 0.79, 22: 0.79, 4: 0.79, 5: 0.79, 25: 0.79, 6: 0.79, 26: 0.79, 27: 0.79, 28: 0.79, 29: 0.79, 30: 0.79, 31: 0.79, 32: 0.79, 7: 0.7, 23: 0.79, 24: 0.79, 21: 1.0} Substation: {0: 1.0, 1: 0.21, 2: 0.21, 3: 0.21, 22: 0.21, 4: 0.21, 5: 0.21, 25: 0.21, 6: 0.21, 26: 0.21, 27: 0.21, 28: 0.21, 29: 0.21, 30: 0.21, 31: 0.21, 32: 0.21, 7: 0.18, 23: 0.21, 24: 0.21}
13	DER 1: {13: 1.0, 12: 1.0, 14: 1.0, 11: 1.0, 10: 1.0, 9: 1.0, 8: 1.0, 7: 1.0, 6: 0.21, 15: 1.0, 16: 1.0, 17: 1.0} DER 2: {19: 1.0, 18: 1.0, 20: 1.0, 1: 0.86, 2: 0.86, 3: 0.86, 22: 0.86, 4: 0.86, 5: 0.86, 25: 0.86, 6: 0.68, 26: 0.86, 27: 0.86, 28: 0.86, 29: 0.86, 30: 0.86, 31: 0.86, 32: 0.86, 23: 0.86, 24: 0.86, 21: 1.0} Substation: {0: 1.0, 1: 0.14, 2: 0.14, 3: 0.14, 22: 0.14, 4: 0.14, 5: 0.14, 25: 0.14, 6: 0.11, 26: 0.14, 27: 0.14, 28: 0.14, 29: 0.14, 30: 0.14, 31: 0.14, 32: 0.14, 23: 0.14, 24: 0.14}
14	DER 1: {13: 1.0, 12: 1.0, 14: 1.0, 11: 1.0, 10: 1.0, 9: 1.0, 8: 1.0, 7: 1.0, 6: 1.0, 5: 0.31, 25: 0.31, 26: 0.31, 27: 0.31, 28: 0.31, 29: 0.31, 30: 0.31, 31: 0.31, 32: 0.31, 15: 1.0, 16: 1.0, 17: 1.0} DER 2: {19: 1.0, 18: 1.0, 20: 1.0, 1: 0.98, 2: 0.98, 3: 0.98, 22: 0.98, 4: 0.98, 5: 0.68, 25: 0.68, 26: 0.68, 27: 0.68, 28: 0.68, 29: 0.68, 30: 0.68, 31: 0.68, 32: 0.68, 23: 0.98, 24: 0.98, 21: 1.0} Substation: {0: 1.0, 1: 0.02, 2: 0.02, 3: 0.02, 22: 0.02, 4: 0.02, 5: 0.01, 25: 0.01, 26: 0.01, 27: 0.01, 28: 0.01, 29: 0.01, 30: 0.01, 31: 0.01, 32: 0.01, 23: 0.02, 24: 0.02}
15	DER 1: {13: 1.0, 12: 1.0, 14: 1.0, 11: 1.0, 10: 1.0, 9: 1.0, 8: 1.0, 7: 1.0, 6: 1.0, 5: 0.24, 25: 0.24, 26: 0.24, 27: 0.24, 28: 0.24, 29: 0.24, 30: 0.24, 31: 0.24, 32: 0.24, 15: 1.0, 16: 1.0, 17: 1.0} DER 2: {19: 1.0, 18: 1.0, 20: 1.0, 1: 0.5, 2: 0.5, 3: 0.5, 22: 0.5, 4: 0.5, 5: 0.38, 25: 0.38, 26: 0.38, 27: 0.38, 28: 0.38, 29: 0.38, 30: 0.38, 31: 0.38, 32: 0.38, 23: 0.5, 24: 0.5, 21: 1.0} Substation: {0: 1.0, 1: 0.5, 2: 0.5, 3: 0.5, 22: 0.5, 4: 0.5, 5: 0.38, 25: 0.38, 26: 0.38, 27: 0.38, 28: 0.38, 29: 0.38, 30: 0.38, 31: 0.38, 32: 0.38, 23: 0.5, 24: 0.5}
16	DER 1: {13: 1.0, 12: 1.0, 14: 1.0, 11: 1.0, 10: 1.0, 9: 1.0, 8: 1.0, 7: 1.0, 6: 1.0, 5: 0.06, 25: 0.06, 26: 0.06, 27: 0.06, 28: 0.06, 29: 0.06, 30: 0.06, 31: 0.06, 32: 0.06, 15: 1.0, 16: 1.0, 17: 1.0} DER 2: {19: 1.0, 18: 1.0, 20: 1.0, 1: 0.06, 2: 0.06, 3: 0.06, 22: 0.06, 4: 0.06, 5: 0.06, 25: 0.06, 26: 0.06, 27: 0.06, 28: 0.06, 29: 0.06, 30: 0.06, 31: 0.06, 32: 0.06, 23: 0.06, 24: 0.06, 21: 1.0} Substation: {0: 1.0, 1: 0.94, 2: 0.94, 3: 0.94, 22: 0.94, 4: 0.94, 5: 0.88, 25: 0.88, 26: 0.88, 27: 0.88, 28: 0.88, 29: 0.88, 30: 0.88, 31: 0.88, 32: 0.88, 23: 0.94, 24: 0.94}
17	DER 1: {13: 1.0, 12: 1.0, 14: 1.0, 11: 1.0, 10: 1.0, 9: 1.0, 8: 1.0, 7: 1.0, 6: 1.0, 5: 0.09, 25: 0.09, 26: 0.09, 27: 0.09, 28: 0.09, 29: 0.09, 30: 0.09, 31: 0.09, 32: 0.09, 15: 1.0, 16: 1.0, 17: 1.0} DER 2: {19: 1.0, 18: 1.0, 20: 1.0, 1: 0.0, 2: 0.0, 3: 0.0, 22: 0.0, 4: 0.0, 5: 0.0, 25: 0.0, 26: 0.0, 27: 0.0, 28: 0.0, 29: 0.0, 30: 0.0, 31: 0.0, 32: 0.0, 23: 0.0, 24: 0.0, 21: 1.0} Substation: {0: 1.0, 1: 1.0, 2: 1.0, 3: 1.0, 22: 1.0, 4: 1.0, 5: 0.91, 25: 0.91, 26: 0.91, 27: 0.91, 28: 0.91, 29: 0.91, 30: 0.91, 31: 0.91, 32: 0.91, 23: 1.0, 24: 1.0}
18	DER 1: {13: 1.0, 12: 0.89, 14: 1.0, 15: 1.0, 16: 1.0, 17: 1.0} DER 2: {19: 1.0, 20: 0.95, 21: 0.95} Substation: {0: 1.0, 1: 1.0, 2: 1.0, 18: 1.0, 3: 1.0, 22: 1.0, 4: 1.0, 5: 1.0, 25: 1.0, 6: 1.0, 26: 1.0, 27: 1.0, 28: 1.0, 29: 1.0, 30: 1.0, 31: 1.0, 32: 1.0, 7: 1.0, 8: 1.0, 9: 1.0, 10: 1.0, 11: 1.0, 12: 0.11, 23: 1.0, 24: 1.0, 19: 0.0, 20: 0.05, 21: 0.05}

19	DER 1: {13: 1.0, 12: 1.0, 14: 1.0, 11: 0.45, 15: 1.0, 16: 1.0, 17: 1.0} DER 2: {19: 1.0, 20: 0.03, 21: 0.03} Substation: {0: 1.0, 1: 1.0, 2: 1.0, 18: 1.0, 3: 1.0, 22: 1.0, 4: 1.0, 5: 1.0, 25: 1.0, 6: 1.0, 26: 1.0, 27: 1.0, 28: 1.0, 29: 1.0, 30: 1.0, 31: 1.0, 32: 1.0, 7: 1.0, 8: 1.0, 9: 1.0, 10: 1.0, 11: 0.55, 23: 1.0, 24: 1.0, 19: 0.0, 20: 0.97, 21: 0.97}
20	DER 1: {13: 1.0, 12: 1.0, 14: 1.0, 11: 1.0, 10: 1.0, 9: 1.0, 8: 0.88, 15: 1.0, 16: 1.0, 17: 1.0} Substation: {0: 1.0, 1: 1.0, 2: 1.0, 18: 1.0, 3: 1.0, 22: 1.0, 4: 1.0, 5: 1.0, 25: 1.0, 6: 1.0, 26: 1.0, 27: 1.0, 28: 1.0, 29: 1.0, 30: 1.0, 31: 1.0, 32: 1.0, 7: 1.0, 8: 0.12, 23: 1.0, 24: 1.0, 19: 1.0, 20: 1.0, 21: 1.0}
21	DER 1: {13: 1.0, 12: 0.02, 14: 1.0, 15: 1.0, 16: 1.0, 17: 1.0} Substation: {0: 1.0, 1: 1.0, 2: 1.0, 18: 1.0, 3: 1.0, 22: 1.0, 4: 1.0, 5: 1.0, 25: 1.0, 6: 1.0, 26: 1.0, 27: 1.0, 28: 1.0, 29: 1.0, 30: 1.0, 31: 1.0, 32: 1.0, 7: 1.0, 8: 1.0, 9: 1.0, 10: 1.0, 11: 1.0, 12: 0.98, 23: 1.0, 24: 1.0, 19: 1.0, 20: 1.0, 21: 1.0}
22	DER 1: {13: 1.0, 12: 1.0, 14: 1.0, 11: 1.0, 10: 1.0, 9: 1.0, 8: 0.01, 15: 1.0, 16: 1.0, 17: 1.0} Substation: {0: 1.0, 1: 1.0, 2: 1.0, 18: 1.0, 3: 1.0, 22: 1.0, 4: 1.0, 5: 1.0, 25: 1.0, 6: 1.0, 26: 1.0, 27: 1.0, 28: 1.0, 29: 1.0, 30: 1.0, 31: 1.0, 32: 1.0, 7: 1.0, 8: 0.99, 23: 1.0, 24: 1.0, 19: 1.0, 20: 1.0, 21: 1.0}
23	DER 1: {13: 1.0, 12: 1.0, 14: 1.0, 11: 1.0, 10: 1.0, 9: 1.0, 8: 1.0, 7: 0.86, 15: 1.0, 16: 1.0, 17: 1.0} Substation: {0: 1.0, 1: 1.0, 2: 1.0, 18: 1.0, 3: 1.0, 22: 1.0, 4: 1.0, 5: 1.0, 25: 1.0, 6: 1.0, 26: 1.0, 27: 1.0, 28: 1.0, 29: 1.0, 30: 1.0, 31: 1.0, 32: 1.0, 7: 0.14, 23: 1.0, 24: 1.0, 19: 1.0, 20: 1.0, 21: 1.0}
24	DER 1: {13: 1.0, 12: 1.0, 14: 1.0, 11: 1.0, 10: 1.0, 9: 1.0, 8: 1.0, 7: 1.0, 6: 0.15, 15: 1.0, 16: 1.0, 17: 1.0} Substation: {0: 1.0, 1: 1.0, 2: 1.0, 18: 1.0, 3: 1.0, 22: 1.0, 4: 1.0, 5: 1.0, 25: 1.0, 6: 0.85, 26: 1.0, 27: 1.0, 28: 1.0, 29: 1.0, 30: 1.0, 31: 1.0, 32: 1.0, 23: 1.0, 24: 1.0, 19: 1.0, 20: 1.0, 21: 1.0}

Bibliography

- [1] R. Ding, C. Q. Kang, T. Zhou, X. Chen, and X. Li, “Analysis and prospect on technical approaches for low carbon power grid,” *Power Syst Technol*, vol. 35, no. 10, pp. 1–8, 2011.
- [2] N. Brinkel, M. Gerritsma, T. AlSkaif, I. Lampropoulos, A. van Voorden, H. Fidler, and W. van Sark, “Impact of rapid pv fluctuations on power quality in the low-voltage grid and mitigation strategies using electric vehicles,” *International Journal of Electrical Power & Energy Systems*, vol. 118, p. 105741, 2020.
- [3] S. Hashemi and J. Østergaard, “Methods and strategies for overvoltage prevention in low voltage distribution systems with pv,” *IET Renewable power generation*, vol. 11, no. 2, pp. 205–214, 2016.
- [4] T. Ackermann, J. R. Abbad, I. M. Dudurych, I. Erlich, H. Holttinen, J. R. Kristoffersen, and P. E. Sorensen, “European balancing act,” *IEEE Power and Energy Magazine*, vol. 5, no. 6, pp. 90–103, 2007.
- [5] A. Korbik, S. D. J. Mcarthur, G. W. Ault, G. M. Burt, and J. R. Mcdonald, “Enabling active distribution networks through decentralised autonomous network management,”

- in *CIREN 2005 - 18th International Conference and Exhibition on Electricity Distribution*, pp. 1–5, 2005.
- [6] L. F. Ochoa, C. J. Dent, and G. P. Harrison, “Distribution network capacity assessment: Variable dg and active networks,” *IEEE Transactions on Power Systems*, vol. 25, no. 1, pp. 87–95, 2010.
- [7] S. Liew and G. Strbac, “Maximising penetration of wind generation in existing distribution networks,” *IEE Proceedings-Generation, Transmission and Distribution*, vol. 149, no. 3, pp. 256–262, 2002.
- [8] C. D’Adamo, C. Abbey, A. Baitech, A. Norsk, B. Matjila, B. Buchholz, D. Moneta, E. Navarro, F. G. L. Pilo, F. Hassan, *et al.*, “Development and operation of active distribution networks,” 2011.
- [9] W. Zhong, S. Xie, K. Xie, Q. Yang, and L. Xie, “Cooperative p2p energy trading in active distribution networks: An milp-based nash bargaining solution,” *IEEE Transactions on Smart Grid*, vol. 12, no. 2, pp. 1264–1276, 2021.
- [10] A. Pouttu, J. Haapola, P. Ahokangas, Y. Xu, M. Kopsakangas-Savolainen, E. Porras, J. Matamoros, C. Kalalas, J. Alonso-Zarate, F. D. Gallego, J. M. Martín, G. Deconinck, H. Almasalma, S. Clayes, J. Wu, M. Cheng, F. Li, Z. Zhang, D. Rivas, and S. Casado, “P2P model for distributed energy trading, grid control and ICT for local smart grids,” in *2017 European Conference on Networks and Communications (EuCNC)*, pp. 1–6, 2017.
- [11] C. Sigl, A. Faschingbauer, A. Berl, J. Geyer, R. Vohnout, and M. Prokỳšek, “The role of smart meters in p2p energy trading in the low voltage grid,” 2018.

- [12] Y. Xu, C. Liu, K. P. Schneider, F. K. Tuffner, and D. T. Ton, "Microgrids for service restoration to critical load in a resilient distribution system," *IEEE Transactions on Smart Grid*, vol. 9, no. 1, pp. 426–437, 2018.
- [13] T. T. H. Pham, Y. Besanger, and N. Hadjsaid, "New challenges in power system restoration with large scale of dispersed generation insertion," *IEEE Transactions on Power Systems*, vol. 24, no. 1, pp. 398–406, 2009.
- [14] Office of Electric Transmission and Distribution, United State Department of Energy, "Grid 2030: A national vision for electricity's second 100 years," 2003.
- [15] C.-C. Liu, S. J. Lee, and S. Venkata, "An expert system operational aid for restoration and loss reduction of distribution systems," *IEEE Transactions on Power Systems*, vol. 3, no. 2, pp. 619–626, 1988.
- [16] M.-S. Tsai, "Development of an object-oriented service restoration expert system with load variations," *IEEE Transactions on Power Systems*, vol. 23, no. 1, pp. 219–225, 2008.
- [17] S. Toune, H. Fudo, T. Genji, Y. Fukuyama, and Y. Nakanishi, "Comparative study of modern heuristic algorithms to service restoration in distribution systems," *IEEE Transactions on Power Delivery*, vol. 17, no. 1, pp. 173–181, 2002.
- [18] H.-C. Kuo and Y.-Y. Hsu, "Distribution system load estimation and service restoration using a fuzzy set approach," *IEEE Transactions on Power delivery*, vol. 8, no. 4, pp. 1950–1957, 1993.
- [19] Y.-Y. Hsu and H.-C. Kuo, "A heuristic based fuzzy reasoning approach for distribution system service restoration," *IEEE Transactions on Power Delivery*, vol. 9, no. 2, pp. 948–953, 1994.

- [20] J.-R. Shin, B.-S. Kim, J.-B. Park, and K. Y. Lee, "A new optimal routing algorithm for loss minimization and voltage stability improvement in radial power systems," *IEEE Transactions on Power Systems*, vol. 22, no. 2, pp. 648–657, 2007.
- [21] J. M. Solanki, S. Khushalani, and N. N. Schulz, "A multi-agent solution to distribution systems restoration," *IEEE Transactions on Power systems*, vol. 22, no. 3, pp. 1026–1034, 2007.
- [22] S. Toune, H. Fudo, T. Genji, Y. Fukuyama, and Y. Nakanishi, "Comparative study of modern heuristic algorithms to service restoration in distribution systems," in *2002 IEEE Power Engineering Society Winter Meeting. Conference Proceedings (Cat. No.02CH37309)*, vol. 2, pp. 787 vol.2–, 2002.
- [23] F. Shariatzadeh, C. Vellaithurai, S. Biswas, R. Zamora, and A. Srivastava, "Real time implementation of intelligent reconfiguration algorithm for microgrid," in *2014 IEEE PES T D Conference and Exposition*, pp. 1–1, 2014.
- [24] J. Mendoza, R. López, D. Morales, E. Lopez, P. Dessante, and R. Moraga, "Minimal loss reconfiguration using genetic algorithms with restricted population and addressed operators: real application," *IEEE Transactions on Power Systems*, vol. 21, no. 2, pp. 948–954, 2006.
- [25] Y. Li, J. Xiao, C. Chen, Y. Tan, and Y. Cao, "Service restoration model with mixed-integer second-order cone programming for distribution network with distributed generations," *IEEE Transactions on Smart Grid*, vol. 10, no. 4, pp. 4138–4150, 2019.
- [26] J. Zhou, Y. Su, and X. Wang, "The role of yunnan guangdong±800 kv dc project in csg black-start and recovery process," *Southern Power System Technology*, vol. 4, no. 4, pp. 48–51, 2010.

- [27] B. Zhao, X. Dong, and J. Bornemann, "Service restoration for a renewable-powered microgrid in unscheduled island mode," *IEEE Transactions on Smart Grid*, vol. 6, no. 3, pp. 1128–1136, 2014.
- [28] T.-C. Ou, W.-M. Lin, C.-H. Huang, and F.-S. Cheng, "A hybrid programming for distribution reconfiguration of dc microgrid," in *2009 IEEE PES/IAS Conference on Sustainable Alternative Energy (SAE)*, pp. 1–7, IEEE, 2009.
- [29] K. Ma, R. Li, and F. Li, "Utility-scale estimation of additional reinforcement cost from three-phase imbalance considering thermal constraints," *IEEE Transactions on Power Systems*, vol. 32, no. 5, pp. 3912–3923, 2017.
- [30] W. Kong, K. Ma, and Q. Wu, "Three-phase power imbalance decomposition into systematic imbalance and random imbalance," *IEEE Transactions on Power Systems*, vol. 33, no. 3, pp. 3001–3012, 2018.
- [31] E. Distribution, S. Losses, and N.-t. Overview, "Electricity Distribution Systems Losses Non-Technical Overview A paper prepared for Ofgem by Sohn Associates Limited," 2006.
- [32] K. Ma, R. Li, and F. Li, "Quantification of additional asset reinforcement cost from 3-phase imbalance," *IEEE Transactions on Power Systems*, vol. 31, no. 4, pp. 2885–2891, 2016.
- [33] M. W. Siti, D. V. Nicolae, A. A. Jimoh, and A. Ukil, "Reconfiguration and load balancing in the lv and mv distribution networks for optimal performance," *IEEE Transactions on Power Delivery*, vol. 22, no. 4, pp. 2534–2540, 2007.

- [34] S. Yan, S. Tan, C. Lee, B. Chaudhuri, and S. Y. R. Hui, "Electric springs for reducing power imbalance in three-phase power systems," *IEEE Transactions on Power Electronics*, vol. 30, no. 7, pp. 3601–3609, 2015.
- [35] G. Mokryani, A. Majumdar, and B. C. Pal, "Probabilistic method for the operation of three-phase unbalanced active distribution networks," *IET Renewable Power Generation*, vol. 10, no. 7, pp. 944–954, 2016.
- [36] T. Xu, J. Pan, Y. Jiang, H. Hou, and Y. Li, "The effect of three-phase voltage imbalance at pcc on solar panel output power," *Procedia Computer Science*, vol. 52, pp. 1218 – 1224, 2015.
- [37] J. Aramizu and J. C. Vieira, "Analysis of PV generation impacts on voltage imbalance and on voltage regulation in distribution networks," *IEEE Power and Energy Society General Meeting*, pp. 1–5, 2013.
- [38] P. Lico, M. Marinelli, K. Knezović, and S. Grillo, "Phase balancing by means of electric vehicles single-phase connection shifting in a low voltage danish grid," in *2015 50th International Universities Power Engineering Conference (UPEC)*, pp. 1–5, 2015.
- [39] P. Jin, Y. Li, G. Li, Z. Chen, and X. Zhai, "Optimized hierarchical power oscillations control for distributed generation under unbalanced conditions," *Applied energy*, vol. 194, pp. 343–352, 2017.
- [40] D. Singh, R. K. Misra, and S. Mishra, "Distribution system feeder re-phasing considering voltage-dependency of loads," *International Journal of Electrical Power & Energy Systems*, vol. 76, pp. 107–119, 2016.

- [41] M. R. Kaveh, R.-A. Hooshmand, and S. M. Madani, "Simultaneous optimization of re-phasing, reconfiguration and dg placement in distribution networks using bf-sd algorithm," *Applied Soft Computing*, vol. 62, pp. 1044–1055, 2018.
- [42] S. Soltani, M. Rashidinejad, and A. Abdollahi, "Stochastic multiobjective distribution systems phase balancing considering distributed energy resources," *IEEE Systems Journal*, vol. 12, no. 3, pp. 2866–2877, 2017.
- [43] S. Eftekhari and M. O. Sadegh, "The effect of load modelling on phase balancing in distribution networks using search harmony algorithm.," *International Journal of Electrical & Computer Engineering (2088-8708)*, vol. 9, no. 3, 2019.
- [44] V. Borozan, D. Rajicic, and R. Ackovski, "Minimum loss reconfiguration of unbalanced distribution networks," *IEEE Transactions on Power Delivery*, vol. 12, no. 1, pp. 435–442, 1997.
- [45] ABB, "Working with the Trip Characteristic Curves of ABB SACE Low Voltage Circuit-Breakers," *Technical Application Guide*, 2001.
- [46] W. Cao, J. Wu, N. Jenkins, C. Wang, and T. Green, "Operating principle of soft open points for electrical distribution network operation," *Applied Energy*, vol. 164, pp. 245–257, 2016.
- [47] J. M. Bloemink and T. C. Green, "Increasing distributed generation penetration using soft normally-open points," in *IEEE PES General Meeting*, pp. 1–8, 2010.
- [48] C. Tang, Y. Chen, Y. Chen, and Y. Chang, "Dc-link voltage control strategy for three-phase back-to-back active power conditioners," *IEEE Transactions on Industrial Electronics*, vol. 62, no. 10, pp. 6306–6316, 2015.

- [49] E. Romero-Ramos, A. Gomez-Exposito, A. Marano-Marcolini, J. Maza-Ortega, and J. Martinez-Ramos, "Assessing the loadability of active distribution networks in the presence of dc controllable links," *IET generation, transmission & distribution*, vol. 5, no. 11, pp. 1105–1113, 2011.
- [50] J. Maza-Ortega, A. Gomez-Exposito, M. Barragan-Villarejo, E. Romero-Ramos, and A. Marano-Marcolini, "Voltage source converter-based topologies to further integrate renewable energy sources in distribution systems," *IET Renewable Power Generation*, vol. 6, no. 6, pp. 435–445, 2012.
- [51] A. Aithal and J. Wu, "Operation and performance of a medium-voltage dc link," *CIREN-Open Access Proceedings Journal*, vol. 2017, no. 1, pp. 1355–1358, 2017.
- [52] J. Song, Y. Zhang, Z. Gao, C. Cao, Z. Wang, and F. Xu, "Research on topology and control technology of soft multi-state open point with fault isolation capability," in *2018 China International Conference on Electricity Distribution (CICED)*, pp. 1467–1473, IEEE, 2018.
- [53] H. Akagi and R. Kitada, "Control and design of a modular multilevel cascade btb system using bidirectional isolated dc/dc converters," *IEEE Transactions on Power Electronics*, vol. 26, no. 9, pp. 2457–2464, 2011.
- [54] N. Okada, M. Takasaki, H. Sakai, and S. Katoh, "Development of a 6.6 kv-1 mva transformerless loop balance controller," in *2007 IEEE Power Electronics Specialists Conference*, pp. 1087–1091, IEEE, 2007.
- [55] J. M. Bloemink and T. C. Green, "Benefits of distribution-level power electronics for supporting distributed generation growth," *IEEE Transactions on Power Delivery*, vol. 28, no. 2, pp. 911–919, 2013.

- [56] P. Li, H. Ji, C. Wang, J. Zhao, G. Song, F. Ding, and J. Wu, "Optimal operation of soft open points in active distribution networks under three-phase unbalanced conditions," *IEEE Transactions on Smart Grid*, vol. 10, no. 1, pp. 380–391, 2019.
- [57] Q. Qi, J. Wu, L. Zhang, and M. Cheng, "Multi-objective optimization of electrical distribution network operation considering reconfiguration and soft open points," *Energy Procedia*, vol. 103, pp. 141 – 146, 2016. Renewable Energy Integration with Mini/Microgrid – Proceedings of REM2016.
- [58] Q. Qi and J. Wu, "Increasing distributed generation penetration using network reconfiguration and soft open points," *Energy Procedia*, vol. 105, pp. 2169 – 2174, 2017. 8th International Conference on Applied Energy, ICAE2016, 8-11 October 2016, Beijing, China.
- [59] H. Ji, C. Wang, P. Li, J. Zhao, G. Song, and J. Wu, "Quantified flexibility evaluation of soft open points to improve distributed generator penetration in active distribution networks based on difference-of-convex programming," *Applied Energy*, vol. 218, pp. 338 – 348, 2018.
- [60] C. Wang, G. Song, P. Li, H. Ji, J. Zhao, and J. Wu, "Optimal configuration of soft open point for active distribution network based on mixed-integer second-order cone programming," *Energy Procedia*, vol. 103, pp. 70 – 75, 2016. Renewable Energy Integration with Mini/Microgrid – Proceedings of REM2016.
- [61] C. Wang, G. Song, P. Li, H. Ji, J. Zhao, and J. Wu, "Optimal siting and sizing of soft open points in active electrical distribution networks," *Applied Energy*, vol. 189, pp. 301 – 309, 2017.

- [62] L. Bai, T. Jiang, F. Li, H. Chen, and X. Li, "Distributed energy storage planning in soft open point based active distribution networks incorporating network reconfiguration and dg reactive power capability," *Applied Energy*, vol. 210, pp. 1082 – 1091, 2018.
- [63] P. Li, H. Ji, C. Wang, J. Zhao, G. Song, F. Ding, and J. Wu, "Coordinated control method of voltage and reactive power for active distribution networks based on soft open point," *IEEE Transactions on Sustainable Energy*, vol. 8, no. 4, pp. 1430–1442, 2017.
- [64] H. Ji, C. Wang, P. Li, J. Zhao, G. Song, F. Ding, and J. Wu, "An enhanced socp-based method for feeder load balancing using the multi-terminal soft open point in active distribution networks," *Applied Energy*, vol. 208, pp. 986 – 995, 2017.
- [65] H. Ji, C. Wang, P. Li, F. Ding, and J. Wu, "Robust operation of soft open points in active distribution networks with high penetration of photovoltaic integration," *IEEE Transactions on Sustainable Energy*, vol. 10, no. 1, pp. 280–289, 2019.
- [66] P. Li, G. Song, H. Ji, J. Zhao, C. Wang, and J. Wu, "A supply restoration method of distribution system based on Soft Open Point," *IEEE PES Innovative Smart Grid Technologies Conference Europe*, pp. 535–539, 2016.
- [67] C. Lou, X. Zhang, P. Cong, B. Zhang, and W. Tang, "Service restoration strategy of active distribution network with soft open points," *Automation of Electric Power Systems*, vol. 42, no. 1, pp. 23–31, 2018.
- [68] S. Giannelos, I. Konstantelos, and G. Strbac, "Stochastic optimisation-based valuation of smart grid options under firm DG contracts," *2016 IEEE International Energy Conference, ENERGYCON 2016*, 2016.

- [69] I. Konstantelos, S. Giannelos, and G. Strbac, "Strategic valuation of smart grid technology options in distribution networks," *IEEE Transactions on Power Systems*, vol. 32, no. 2, pp. 1293–1303, 2017.
- [70] Q. Wang, J. Liao, Y. Su, C. Lei, T. Wang, and N. Zhou, "An optimal reactive power control method for distribution network with soft normally-open points and controlled air-conditioning loads," *International Journal of Electrical Power Energy Systems*, vol. 103, pp. 421 – 430, 2018.
- [71] J. Pereda and T. C. Green, "Direct modular multilevel converter with six branches for flexible distribution networks," *IEEE Transactions on Power Delivery*, vol. 31, no. 4, pp. 1728–1737, 2016.
- [72] C. Long, J. Wu, L. Thomas, and N. Jenkins, "Optimal operation of soft open points in medium voltage electrical distribution networks with distributed generation," *Applied Energy*, vol. 184, pp. 427 – 437, 2016.
- [73] H. Ji, H. Yu, G. Song, P. Li, C. Wang, and J. Wu, "A decentralized voltage control strategy of soft open points in active distribution networks," *Energy Procedia*, vol. 159, pp. 412–417, 2019.
- [74] A. Aithal, C. Long, W. Cao, J. Wu, and C. E. Ugalde-Loo, "Impact of soft open point on feeder automation," *2016 IEEE International Energy Conference, ENERGYCON 2016*, 2016.
- [75] A. Aithal, G. Li, J. Wu, and J. Yu, "Performance of an electrical distribution network with soft open point during a grid side ac fault," *Applied Energy*, vol. 227, pp. 262 – 272, 2018. Transformative Innovations for a Sustainable Future – Part III.

- [76] D. Boroyevich, I. Cvetković, D. Dong, R. Burgos, F. Wang, and F. Lee, “Future electronic power distribution systems a contemplative view,” in *2010 12th International Conference on Optimization of Electrical and Electronic Equipment*, pp. 1369–1380, 2010.
- [77] A. Q. Huang, M. L. Crow, G. T. Heydt, J. P. Zheng, and S. J. Dale, “The future renewable electric energy delivery and management (freedm) system: The energy internet,” *Proceedings of the IEEE*, vol. 99, no. 1, pp. 133–148, 2011.
- [78] M. Stieneker, J. Butz, S. Rabiee, H. Stagge, and R. W. D. Doncker, “Medium-voltage dc research grid aachen,” in *International ETG Congress 2015; Die Energiewende - Blueprints for the new energy age*, pp. 1–7, 2015.
- [79] F. Mura and R. W. De Doncker, “Design aspects of a medium-voltage direct current (mvdc) grid for a university campus,” in *8th International Conference on Power Electronics - ECCE Asia*, pp. 2359–2366, 2011.
- [80] J. Yu, K. Smith, M. Urizarbarrena, N. MacLeod, R. Bryans, and A. Moon, “Initial designs for the angle dc project; converting existing ac cable and overhead line into dc operation,” 2017.
- [81] S. E. Networks, “Brochure – Year 1 Project Summary (ANGLE-DC).” https://www.spenergynetworks.co.uk/pages/angle_dc.aspx. Accessed: 2021-05-05.
- [82] Y. Xu, Z. Tan, L. Guo, X. Li, and D. Huang, “Design scheme of flexible dc power distribution system in guizhou power grid,” *Distrib. Utilization*, vol. 35, no. 1, pp. 34–39, 2018.

- [83] U. Straumann and C. M. Franck, “Ion-flow field calculations of ac/dc hybrid transmission lines,” *IEEE Transactions on Power Delivery*, vol. 28, no. 1, pp. 294–302, 2012.
- [84] M. De Prada, C. Corchero, O. Gomis-Bellmunt, A. Sumper, *et al.*, “Hybrid ac-dc offshore wind power plant topology: optimal design,” *IEEE Transactions on Power Systems*, vol. 30, no. 4, pp. 1868–1876, 2014.
- [85] H. M. Ahmed, A. B. Eltantawy, and M. M. Salama, “A planning approach for the network configuration of ac-dc hybrid distribution systems,” *IEEE Transactions on Smart Grid*, vol. 9, no. 3, pp. 2203–2213, 2016.
- [86] A. Eajal, M. F. Shaaban, K. Ponnambalam, and E. El-Saadany, “Stochastic centralized dispatch scheme for ac/dc hybrid smart distribution systems,” *IEEE Transactions on Sustainable Energy*, vol. 7, no. 3, pp. 1046–1059, 2016.
- [87] F. Nejabatkhah and Y. W. Li, “Overview of power management strategies of hybrid ac/dc microgrid,” *IEEE Transactions on Power Electronics*, vol. 30, pp. 7072–7089, Dec 2015.
- [88] T. Ma, M. H. Cintuglu, and O. Mohammed, “Control of hybrid ac/dc microgrid involving energy storage, renewable energy and pulsed loads,” in *2015 IEEE Industry Applications Society Annual Meeting*, pp. 1–8, IEEE, 2015.
- [89] L. Zhang, J. Liang, W. Tang, G. Li, Y. Cai, and W. Sheng, “Converting ac distribution lines to dc to increase transfer capacities and dg penetration,” *IEEE Transactions on Smart Grid*, vol. 10, no. 2, pp. 1477–1487, 2018.
- [90] A. Agrawal, R. Verschueren, S. Diamond, and S. Boyd, “A rewriting system for convex optimization problems,” *Journal of Control and Decision*, vol. 5, no. 1, pp. 42–60, 2018.

- [91] J. Sun and L. Tesfatsion, "DC Optimal Power Flow Formulation and Solution Using QuadProgJ," *ISU Economics Working Paper No. 06014*, no. March 1, pp. 1–62, 2010.
- [92] C. Coffrin and P. Van Hentenryck, "A linear-programming approximation of AC power flows," *INFORMS Journal on Computing*, vol. 26, no. 4, pp. 718–734, 2014.
- [93] A. Castillo, P. Lipka, J. Watson, S. S. Oren, and R. P. O'Neill, "A successive linear programming approach to solving the iv-acopf," *IEEE Transactions on Power Systems*, vol. 31, no. 4, pp. 2752–2763, 2016.
- [94] J. F. Franco, M. J. Rider, M. Lavorato, and R. Romero, "A set of linear equations to calculate the steady-state operation of an electrical distribution system," *2011 IEEE PES Conference on Innovative Smart Grid Technologies Latin America SGT LA 2011 - Conference Proceedings*, pp. 1–5, 2011.
- [95] T. Akbari and M. Tavakoli Bina, "Linear approximated formulation of ac optimal power flow using binary discretisation," *IET Generation, Transmission Distribution*, vol. 10, no. 5, pp. 1117–1123, 2016.
- [96] H. Yuan, F. Li, Y. Wei, and J. Zhu, "Novel linearized power flow and linearized opf models for active distribution networks with application in distribution lmp," *IEEE Transactions on Smart Grid*, vol. 9, no. 1, pp. 438–448, 2018.
- [97] Z. Yang, H. Zhong, A. Bose, T. Zheng, Q. Xia, and C. Kang, "A linearized opf model with reactive power and voltage magnitude: A pathway to improve the mw-only dc opf," *IEEE Transactions on Power Systems*, vol. 33, no. 2, pp. 1734–1745, 2018.
- [98] R. A. Jabr, "Exploiting sparsity in sdp relaxations of the opf problem," *IEEE Transactions on Power Systems*, vol. 27, no. 2, pp. 1138–1139, 2012.

- [99] W. Wang and N. Yu, "Chordal conversion based convex iteration algorithm for three-phase optimal power flow problems," *IEEE Transactions on Power Systems*, vol. 33, no. 2, pp. 1603–1613, 2018.
- [100] E. Dall'Anese, H. Zhu, and G. B. Giannakis, "Distributed optimal power flow for smart microgrids," *IEEE Transactions on Smart Grid*, vol. 4, no. 3, pp. 1464–1475, 2013.
- [101] J. D. Watson, N. R. Watson, and I. Lestas, "Optimized dispatch of energy storage systems in unbalanced distribution networks," *IEEE Transactions on Sustainable Energy*, vol. 9, no. 2, pp. 639–650, 2018.
- [102] L. R. Araujo, D. Penido, S. Carneiro, and J. L. R. Pereira, "A three-phase optimal power-flow algorithm to mitigate voltage unbalance," *IEEE transactions on power delivery*, vol. 28, no. 4, pp. 2394–2402, 2013.
- [103] L. R. Araujo, D. R. R. Penido, and F. de Alcântara Vieira, "A multiphase optimal power flow algorithm for unbalanced distribution systems," *International Journal of Electrical Power & Energy Systems*, vol. 53, pp. 632–642, 2013.
- [104] C. Lee, C. Liu, S. Mehrotra, and Z. Bie, "Robust distribution network reconfiguration," *IEEE Transactions on Smart Grid*, vol. 6, no. 2, pp. 836–842, 2015.
- [105] J. F. Franco, L. F. Ochoa, and R. Romero, "Ac opf for smart distribution networks: An efficient and robust quadratic approach," *IEEE Transactions on Smart Grid*, vol. 9, no. 5, pp. 4613–4623, 2018.
- [106] S. H. Low, "Convex relaxation of optimal power flow - Part i: Formulations and equivalence," *IEEE Transactions on Control of Network Systems*, vol. 1, no. 1, pp. 15–27, 2014.

- [107] L. Gan, N. Li, U. Topcu, and S. H. Low, “Exact convex relaxation of optimal power flow in radial networks,” *IEEE Transactions on Automatic Control*, vol. 60, no. 1, pp. 72–87, 2015.
- [108] M. Nick, R. Cherkaoui, J. L. Boudec, and M. Paolone, “An exact convex formulation of the optimal power flow in radial distribution networks including transverse components,” *IEEE Transactions on Automatic Control*, vol. 63, no. 3, pp. 682–697, 2018.
- [109] L.-C. Ye, J. F. Rodrigues, and H. X. Lin, “Analysis of feed-in tariff policies for solar photovoltaic in china 2011–2016,” *Applied Energy*, vol. 203, pp. 496–505, 2017.
- [110] R. Cherrington, V. Goodship, A. Longfield, and K. Kirwan, “The feed-in tariff in the uk: A case study focus on domestic photovoltaic systems,” *Renewable Energy*, vol. 50, pp. 421–426, 2013.
- [111] Ofgem, “Feed-in tariff (fit): Tariff table 1 april 2021, Publication date: 28 January 2021.” <https://www.ofgem.gov.uk/publications-and-updates/feed-tariff-fit-tariff-table-1-april-2021>. Accessed: 2021-05-05.
- [112] British Gas, “Our tariffs.” <http://www.britishgas.co.uk>. Accessed: 2021-05-05.
- [113] Ofgem, “About the smart export guarantee (seg).” <https://www.ofgem.gov.uk/environmental-programmes/smart-export-guarantee-seg/about-smart-export-guarantee-seg>. Accessed: 2021-05-05.
- [114] Y. Parag and B. K. Sovacool, “Electricity market design for the prosumer era,” *Nature energy*, vol. 1, no. 4, pp. 1–6, 2016.

- [115] W. Tushar, T. K. Saha, C. Yuen, D. Smith, and H. V. Poor, "Peer-to-peer trading in electricity networks: An overview," *IEEE Transactions on Smart Grid*, vol. 11, no. 4, pp. 3185–3200, 2020.
- [116] S. Cui, Y.-W. Wang, Y. Shi, and J.-W. Xiao, "Community energy cooperation with the presence of cheating behaviors," *IEEE Transactions on Smart Grid*, vol. 12, no. 1, pp. 561–573, 2021.
- [117] S. Cui, Y.-W. Wang, Y. Shi, and J.-W. Xiao, "A new and fair peer-to-peer energy sharing framework for energy buildings," *IEEE Transactions on Smart Grid*, vol. 11, no. 5, pp. 3817–3826, 2020.
- [118] S. Cui, Y.-W. Wang, and J.-W. Xiao, "Peer-to-peer energy sharing among smart energy buildings by distributed transaction," *IEEE Transactions on Smart Grid*, vol. 10, no. 6, pp. 6491–6501, 2019.
- [119] S. Cui, Y.-W. Wang, J.-W. Xiao, and N. Liu, "A two-stage robust energy sharing management for prosumer microgrid," *IEEE Transactions on Industrial Informatics*, vol. 15, no. 5, pp. 2741–2752, 2019.
- [120] T. Morstyn, A. Teytelboym, and M. D. Mcculloch, "Bilateral contract networks for peer-to-peer energy trading," *IEEE Transactions on Smart Grid*, vol. 10, no. 2, pp. 2026–2035, 2019.
- [121] G. Hug, S. Kar, and C. Wu, "Consensus + innovations approach for distributed multiagent coordination in a microgrid," *IEEE Transactions on Smart Grid*, vol. 6, no. 4, pp. 1893–1903, 2015.

- [122] E. Sorin, L. Bobo, and P. Pinson, “Consensus-based approach to peer-to-peer electricity markets with product differentiation,” *IEEE Transactions on Power Systems*, vol. 34, no. 2, pp. 994–1004, 2019.
- [123] S. Cui, Y.-W. Wang, C. Li, and J.-W. Xiao, “Prosumer community: A risk aversion energy sharing model,” *IEEE Transactions on Sustainable Energy*, vol. 11, no. 2, pp. 828–838, 2020.
- [124] S. Cui, Y.-W. Wang, Y. Shi, and J.-W. Xiao, “An efficient peer-to-peer energy-sharing framework for numerous community prosumers,” *IEEE Transactions on Industrial Informatics*, vol. 16, no. 12, pp. 7402–7412, 2020.
- [125] N. Liu *et al.*, “Online energy sharing for nanogrid clusters: A lyapunov optimization approach,” *IEEE Transactions on Smart Grid*, vol. 9, no. 5, pp. 4624–4636, 2018.
- [126] P. Kumar, N. Gupta, K. R. Niazi, and A. Swarnkar, “A circuit theory-based loss allocation method for active distribution systems,” *IEEE Transactions on Smart Grid*, vol. 10, no. 1, pp. 1005–1012, 2019.
- [127] M. Usman, M. Coppo, F. Bignucolo, R. Turri, and A. Cerretti, “Multi-phase losses allocation method for active distribution networks based on branch current decomposition,” *IEEE Transactions on Power Systems*, vol. 34, no. 5, pp. 3605–3615, 2019.
- [128] E. Vega-Fuentes, J. Yang, C. Lou, and N. K. Meena, “Transaction-oriented dynamic power flow tracing for distribution networks—definition and implementation in GIS environment,” *IEEE Transactions on Smart Grid*, vol. 12, no. 2, pp. 1303–1313, 2021.
- [129] S. Boyd and L. Vandenberghe, *Convex optimization*. Cambridge university press, 2004.

- [130] M. Baran and F. Wu, "Network reconfiguration in distribution systems for loss reduction and load balancing," *IEEE Transactions on Power Delivery*, vol. 4, no. 2, pp. 1401–1407, 1989.
- [131] J. Lofberg, "Yalmip: A toolbox for modeling and optimization in matlab," in *2004 IEEE international conference on robotics and automation (IEEE Cat. No. 04CH37508)*, pp. 284–289, IEEE, 2004.
- [132] B. Bixby, "The gurobi optimizer," 2011.
- [133] P. Pillay and M. Manyage, "Definitions of voltage unbalance," *IEEE Power Engineering Review*, vol. 21, no. 5, pp. 50–51, 2001.
- [134] H. B. Funmilayo, J. A. Silva, and K. L. Butler-Purry, "Overcurrent protection for the ieee 34-node radial test feeder," *IEEE Transactions on Power Delivery*, vol. 27, no. 2, pp. 459–468, 2012.
- [135] I. PES, "Ieee pes amps dsas test feeder working group." <https://site.ieee.org/pes-testfeeders/resources/>. Accessed: 2021-05-05.
- [136] R. M. D. S. (RMDS), "Standard load profiles." <https://rmdservice.com/standard-load-profiles/>. Accessed: 2021-05-07.
- [137] U. P. Network, "Photovoltaic (pv) solar panel energy generation data." <https://data.london.gov.uk/dataset>. Accessed: 2021-05-07.
- [138] K. Schneider, B. Mather, B. Pal, C.-W. Ten, G. Shirek, H. Zhu, J. Fuller, J. Pereira, L. Ochoa, L. De Araujo, *et al.*, "Analytic considerations and design basis for the ieee distribution test feeders," *IEEE Transactions on power systems*, vol. 33, no. 3, pp. 3181–3188, 2017.

- [139] W. H. Kersting, "Radial distribution test feeders," *IEEE Transactions on Power Systems*, vol. 6, no. 3, pp. 975–985, 1991.
- [140] W. H. Kersting, *Distribution system modeling and analysis*. CRC press, 2006.
- [141] A. Smith, "Electricity safety, quality and continuity regulations 2002.," *Lighting Journal*, vol. 68, no. 2, pp. 35–36, 2003.
- [142] G. M. Bhutto, B. Bak-Jensen, P. Mahat, and C. Cecati, "Mitigation of unbalanced voltage sags and voltage unbalance in cigre low voltage distribution network," *Energy and Power Engineering*, vol. 5, no. 9, p. 551, 2013.
- [143] L. T. Biegler and V. M. Zavala, "Large-scale nonlinear programming using ipopt: An integrating framework for enterprise-wide dynamic optimization," *Computers & Chemical Engineering*, vol. 33, no. 3, pp. 575–582, 2009.
- [144] C. Lou, J. Yang, T. Li, and E. Vega-Fuentes, "New phase-changing soft open point and impacts on optimising unbalanced power distribution networks," *IET Generation, Transmission & Distribution*, vol. 14, no. 23, pp. 5685–5696, 2020.
- [145] M. S. Carmeli, D. Forlani, S. Grillo, R. Pinetti, E. Ragaini, and E. Tironi, "A stabilization method for dc networks with constant-power loads," in *2012 IEEE International Energy Conference and Exhibition (ENERGYCON)*, pp. 617–622, IEEE, 2012.
- [146] W. Cao, J. Wu, N. Jenkins, C. Wang, and T. Green, "Benefits analysis of soft open points for electrical distribution network operation," *Applied Energy*, vol. 165, pp. 36–47, 2016.
- [147] C. Lou, J. Yang, T. Li, and E. Vega-Fuentes, "New phase-changing soft open point and impacts on optimising unbalanced power distribution networks," *IET Generation, Transmission Distribution*, vol. 14, no. 23, pp. 5685–5696, 2020.

- [148] Z. Wang, D. S. Kirschen, and B. Zhang, “Accurate semidefinite programming models for optimal power flow in distribution systems,” *arXiv preprint arXiv:1711.07853*, 2017.
- [149] M. ApS, *The MOSEK optimization toolbox for MATLAB manual. Version 9.0.*, 2019.
- [150] A. Wächter and L. T. Biegler, “On the implementation of an interior-point filter line-search algorithm for large-scale nonlinear programming,” *Mathematical programming*, vol. 106, no. 1, pp. 25–57, 2006.
- [151] J. F. Sturm, “Using sedumi 1.02, a matlab toolbox for optimization over symmetric cones,” *Optimization methods and software*, vol. 11, no. 1-4, pp. 625–653, 1999.
- [152] J. Bialek, “Tracing the flow of electricity,” *IEEE Proceedings-Generation, Transmission and Distribution*, vol. 143, no. 4, pp. 313–320, 1996.
- [153] R. Tarjan, “Depth-first search and linear graph algorithms,” *SIAM journal on computing*, vol. 1, no. 2, pp. 146–160, 1972.
- [154] GeeksforGeeks, “Depth First Search or DFS for a Graph.” <https://www.geeksforgeeks.org/depth-first-search-or-dfs-for-a-graph/>. Accessed: 2021-06-05.
- [155] D. N. McCloskey and S. T. Ziliak, “The standard error of regressions,” *Journal of economic literature*, vol. 34, no. 1, pp. 97–114, 1996.
- [156] J. Jalving, S. Shin, and V. M. Zavala, “A graph-based modeling abstraction for optimization: Concepts and implementation in plasm.jl,” 2020.
- [157] J. Bezanson, A. Edelman, S. Karpinski, and V. B. Shah, “Julia: A fresh approach to numerical computing,” *SIAM review*, vol. 59, no. 1, pp. 65–98, 2017.

- [158] I. Dunning, J. Huchette, and M. Lubin, “Jump: A modeling language for mathematical optimization,” *SIAM review*, vol. 59, no. 2, pp. 295–320, 2017.
- [159] L. Thurner, A. Scheidler, F. Schäfer, J.-H. Menke, J. Dollichon, F. Meier, S. Meinecke, and M. Braun, “Pandapower—an open-source python tool for convenient modeling, analysis, and optimization of electric power systems,” *IEEE Transactions on Power Systems*, vol. 33, no. 6, pp. 6510–6521, 2018.
- [160] P. Virtanen *et al.*, “Scipy 1.0: fundamental algorithms for scientific computing in python,” *Nature methods*, vol. 17, no. 3, pp. 261–272, 2020.
- [161] O. for National Statistics, “Wind energy in the uk.” <https://www.ons.gov.uk/economy/environmentalaccounts>. Accessed: 2021-07-07.

Publications

Under-review Articles

- [1] Chengwei Lou, Jin Yang, Eduardo Vega-Fuentes, Nand K. Meena, 'Power Flow Traceable P2P Electricity Market Segmentation and Pricing'. *Applied Energy*

Published Articles in Journal

- [1] Lou, Chengwei, Jin Yang, Yue Zhou, Eduardo Vega-Fuentes, Nand K. Meena, and Liang Min. "Multi-terminal phase-changing soft open point SDP modeling for imbalance mitigation in active distribution networks." *International Journal of Electrical Power Energy Systems* 142 (2022): 108228.
- [2] Lou, Chengwei, Jin Yang, Tianrui Li, and Eduardo Vega-Fuentes. "New phase-changing soft open point and impacts on optimising unbalanced power distribution networks." *IET Generation, Transmission & Distribution* 14, no. 23 (2020): 5685-5696.
- [3] Vega-Fuentes, Eduardo, Jin Yang, Chengwei Lou, and Nand K. Meena. "Transaction-oriented dynamic power flow tracing for distribution networks—Definition and imple-

mentation in GIS environment." *IEEE Transactions on Smart Grid* 12, no. 2 (2020): 1303-1313.

- [4] Cong, Pengwei, Zechun Hu, Wei Tang, Chengwei Lou, and Lu Zhang. "Optimal allocation of soft open points in active distribution network with high penetration of renewable energy generations." *IET Generation, Transmission & Distribution* 14, no. 26 (2020): 6732-6740.

Published Articles in Conference Proceeding

- [1] Chengwei Lou, Jin Yang, Lu Zhang: 'Adapting AC Lines for DC Power Distribution to Reduce the Power Imbalance in Three-Phase Four-Wire Systems'. Proc. of the 15th international conference on AC and DC Power Transmission, China, July 2020.
- [2] Chengwei Lou, Jin Yang: 'Adaptive Service Restoration Strategy of Distribution Networks with Distributed Energy Resources and Soft Open Points'. Proc. of the 25th International Conference on Electricity Distribution (CIRED 2019), Madrid, Spain, 3-6 June 2019.
- [3] Nand K. Meena, Jin Yang, Eduardo Vega-Fuentes, Chengwei Lou, 'Strategic Deployment of Low-Carbon Microgrids Considering Carbon Policies and Green City Goals'. Proc. of international Conference on Applied Energy 2019, Västerås, Sweden, Aug 12-15, 2019.